Chapter 6: Carbon and Biogeochemical Cycles

Coordinating Lead Authors: Philippe Ciais (France), Christopher Sabine (USA)

Lead Authors: Govindswamy Bala (India), Laurent Bopp (France), Victor Brovkin (Germany), Josep Canadell (Australia), Abha Chhabra (India), Ruth DeFries (USA), Jim Galloway (USA), Martin Heimann (Germany), Christopher Jones (UK), Corinne Le Quéré (UK), Ranga Myneni (USA), Shilong Piao (China), Peter Thornton (USA)

Contributing Authors: George Hurtt (US), Guido van der Werf (Netherlands), Nicolas Gruber (Switzerland), Taro Takahashi (USA), Samar Khatiwala (USA), Jan Willem Erisman (NL), Gregg Marland (USA), Ralph Keeling (USA), Stephen Piper (USA), Andy Ridgwell (UK), Jerome Chappellaz (France), Andreas Schmittner (USA), Jed Kaplan (Switzerland), Fortunat Joos (Switzerland), Johann Jungclaus (Germany), David Archer (USA), Peter Cox (UK), Pierre Friedlingstein (UK), Yiqi Luo (USA), Paul Hanson (USA), Richard Norby (USA), Edward Schuur (USA), Eugenie Euskirchen (USA), Cory Cleveland (USA), David McGuire (USA), Elena Shevliakova (USA), Soenke Zaehle (Germany), Detlef van Vuuren (Netherlands), Stephen Sitch (UK), Nicolas Metzl (France), Andrew Lenton (Australia), James Orr (France), Oliver Andrews (UK), Alberto Borges (Belgium), Gordon Bonan (USA), Damon Mathews (Canada), Kenneth Caldeira (USA), Carolien Kroeze (Netherlands), Julia Pongratz (USA), Ayako Abe-Ouchi (Japan), Rita Wania (Canada), Charlie Koven (USA), Ben Booth (UK), Long Cao (USA), Stephen Hunter (UK), Silvia Kloster (Germany), Spencer Liddicoat (UK), Atul Jain (USA), Vivek Arora (Canada), Benjamin Stocker (Switzerland), Kees Klein Goldewijk (Netherlands), Jo House (UK), Jerry Tjiputra (Norway), Scott Doney (USA), Richard A. Houghton (USA), Geun-Ha Park (USA), Peter A. Raymond (USA), Frank J. Dentener (Italy), Jean-Francois Larmarque (USA), C. Roedenbeck (Germany), P. Peylin (France), F. Chevallier (France), R. Law (USA), P. Rayner (Australia), S. Gourdji (USA), A. Jacobson (USA), W. Peters (USA), P. Patra (Japan), K. Gurney (USA), Y. Niwa (Japan), Elizabeth Holland (USA), Stephen Sitch (UK), Anders Ahlström (Sweden), Ben Poulter (France) and Mark R. Lomas (UK), Keith Lassey (New Zealand), Ning Zeng (USA), Sander Houweling, (TN), Philippe Bousquet, (France), Stefanie Kirschke (France), Marielle Saunois (France), Lori Bruhwiler (USA), Vaishali Naik (USA), Apostolos Voulgarakis (USA), Renato Spahni (Switzerland), Bruno Ringeval (France), Joe Melton (Switzerland)

Review Editors: Christoph Heinze (Norway), Pieter Tans (USA), Steven Wofsy (USA)

Date of Draft: 16 December 2011

Notes: TSU Compiled Version

Table of Contents

Executive Summary

The radiative properties of the atmosphere are strongly influenced by the abundance of the long-lived greenhouse gases carbon dioxide (CO_2), methane (CH_4) and nitrous oxide (N_2O). The concentrations of these gases have increased since the beginning of the Industrial Revolution around 1750, by a factor 1.4 for CO_2, 2.5 for CH_4, and 1.2 for N_2O. With a very high level of confidence, the concentration increase of these greenhouse gases is caused by anthropogenic emissions. Superimposed on the concentration increase are modulations induced by natural biogeochemical processes.

Human activities use fossil fuel carbon to produce energy, a process that emits CO_2 to the atmosphere. Fossil fuel emissions were 9.1 PgC in 2011 and increasing, equivalent to over 1% of the atmospheric CO_2 content. In addition to fossil fuel burning, land use change emits CO_2 to the atmosphere contributing about an additional 1 PgC in recent years. The human caused release of CO_2 to the atmosphere is absorbed partly by the ocean, and partly by the land biosphere, where it can be stored in the vegetation and soils. The additional CO_2 entering into the surface ocean causes ocean acidification, while it gets slowly mixed into the deep waters. On centennial to millennial time scales, it will react with ocean carbonate sediments and dissolve them. On geological time scales of 10,000 years or longer, rock weathering will further remove the additional CO_2.

The global cycle of atmospheric methane (CH_4) is a small loop of the global carbon cycle. But CH_4 is a much more -potent greenhouse gas than CO_2, and interacts with tropospheric photochemistry. Among the global surface emissions of CH_4, one can distinguish natural sources from wetland ecosystems, termites, wildfires, recently re-appraised geological emanations, and anthropogenic sources from natural gas and oil industry, coal mining, landfills, and agriculture (livestock and rice paddies). The main sink of CH_4 is the chemical reaction with OH radicals in the atmosphere, a small sink in the soils and by reactive chlorine in the marine boundary layer.

In the pre-human world, creation of reactive nitrogen (comprising all nitrogen species other than atmospheric N_2) from atmospheric N_2 occurred primarily through two processes: lightning and biological nitrogen fixation, with the latter being by far the most important. At equilibrium, this reactive N did not accumulate in environmental reservoirs, but was converted back to atmospheric N_2 by microbial denitrification processes. Today, the creation of reactive nitrogen increases every year on a global basis because of anthropogenic activities. The dominant processes are the manufacture of N-fertilizers and NH_3 for industrial feedstocks. However, fossil fuel energy consumption also produces increasing amounts of reactive nitrogen, which is exacerbated by the growing prevalence of biofuels. The addition of more reactive nitrogen to the environment by human activities, also induces more N_2O emissions. These N_2O emissions are caused by microbial nitrification in presence of oxygen, and by microbial denitrification in environments where oxygen is scarce, in soils (cropland soils enriched in fertilizer N, and other soils), as well as in wetlands, rivers, estuaries and the ocean. In addition, there is a small source of N_2O from industry and fossil fuel combustion.

Glacial-interglacial changes in CO_2

The 90 ppm increase in atmospheric CO_2 between glacial and interglacial conditions were mainly caused by ocean outgassing of CO_2 in response to physical changes in the ocean, with significant contributions from changes in biological fertilisation by iron deposition and carbonate chemistry. In parallel, carbon storage on land increased from glacial to inter-glacial. Models of reduced complexity can simulate magnitude and phasing of glacial-interglacial CO_2 changes, while complex full-scale coupled carbon cycle climate models currently cannot account for the entire magnitude of the changes in atmospheric CO_2 during glaciations. Uncertainties in reconstructing glacial conditions and deficiencies in understanding some of the primary controls on the partitioning of carbon between surface and deep ocean waters prevent an unambiguous interpretation of low glacial CO_2.

Holocene changes in CO_2 and CH_4

Available studies suggest that a combination of natural marine and terrestrial processes, with an additional contribution from late Holocene agricultural activity, is consistent both in magnitude and timing with the reconstructed Holocene CO_2 evolution. The contribution of early anthropogenic land use and land cover change is not sufficient to explain the reconstructed 20 ppm CO_2 increase both with respect to the timing of the emissions and their magnitude. However, it could explain the CH_4 increase during the last 4,000 years.

Last millennium changes in CO_2 and CH_4

Causes for variations of CO_2 during the last Millennium, especially for the CO_2 drop by 5 to 8 ppm around year 1600, have not yet been identified. Responses of the global carbon cycle to climate cooling due to reduced solar irradiance or to volcanic eruptions as well as forest regrowth as a consequence of a war or plague induced reduction in world population have been hypothesized to explain these variations. Climatic and anthropogenic forcing are proposed to explain variability in the atmospheric CH_4 during the last millennium, but the confidence in these mechanisms is low.

CO_2 emissions and their fate since 1750

CO_2 emissions from fossil fuel combustion and cement production released 365 ± 22 PgC to the atmosphere between 1750 and 2010, while deforestation and other land use change activities released an additional 151 ± 51 PgC. Of these 516 ± 56 Pg C, 238 ± 7 PgC have accumulated in the atmosphere resulting into the observed increase of atmospheric CO_2 concentration from 278 ± 3 ppm in 1750 to 389.8 ppm at the end of 2010. The remaining amount of anthropogenic carbon has been redistributed in the various reservoirs of the global carbon cycle, namely in the oceans and in terrestrial ecosystems – the carbon "sinks". The transfer of CO_2 between the atmosphere and the sea has led to the storage of 154 ± 20 Pg of additional "anthropogenic" C in the ocean since 1750. Terrestrial ecosystems have accumulated 124 ± 59 Pg of anthropogenic C during the same period, more than compensating the cumulative C losses from land use change (mainly deforestation) since 1750. The gain of carbon by terrestrial ecosystems is estimated to take place mainly through the uptake of CO_2 by enhanced photosynthesis at higher CO_2 levels and N deposition, longer growing seasons in high latitudes, and the expansion and recovery of forests from past land use. These processes vary regionally.

The global budget of anthropogenic CO_2 over the past decade (2000–2009)

Average fossil fuel and cement manufacturing emissions were 7.7 ± 0.5 PgC yr^{-1} in the decade 2000–2009 with an average growth rate of 2.9% yr^{-1}. This rate of increase of fossil fuel emissions is higher than during the 1990's (1.0% yr^{-1}). Emissions from land use change over the same decade are dominated by tropical deforestation, and are estimated at 0.9 ± 0.5 PgC yr^{-1}, with possibly a small decrease from the 1990s due to lower reported forest loss during this decade. Atmospheric CO_2 concentrations grew by 4.0 ± 0.2 PgC yr^{-1} in the 2000s. The estimated mean ocean and land CO_2 sinks are 2.3 ± 0.5 PgC yr^{-1} and 2.3 ± 0.9 PgC yr^{-1}, respectively for 2000–2009.

Historical and recent changes in atmospheric CH_4

Since preindustrial times, the concentration of CH_4 increased by a factor 2.5, from ca. 730 ppb by 1750 to 1790 ppb by the end of 2009. The global growth rate of CH_4 has decreased from 12 ± 2 ppb yr^{-1} during 1983–1989, down to 2 ± 4 ppb yr^{-1} during the years 2000–2009, causing nearly-stable annual global CH_4 concentrations between 1999 and 2006. The reasons for this near stabilization are still debated but different lines of evidence include: reduced emissions from the gas industry in the countries of the former Soviet union, reduced global fossil fuel related emissions, compensation between increasing anthropogenic emissions and decreasing wetland emissions, reduced emissions from rice paddies, and changes in OH concentrations. Since 2007, atmospheric CH_4 is increasing again. A possible cause relies on positive trends in tropical wetland emissions with some contribution of northern high latitudes in 2007, due to anomalies of precipitation and temperature in these regions.

The global budget of CH_4 over the past decade: emissions and sinks

Regional CH_4 sources at the surface the globe are biogenic (64–76%; wetlands, ruminants, landfills, waste, termites), thermogenic (19–30%; oil, gas and coal extraction, transportation and use, and natural geological sources), or pyrogenic (4–6%; wildfires, biomass burning and biofuels) in origin. The single most dominant CH_4 source for annual magnitude and interannual variations is CH_4 emissions from natural wetlands, from the tropics and high northern latitudes (range of 174-280 Tg CH_4 yr^{-1} for 2000–2009). Overall for 2000–2009, from an ensemble of process-based models and inventories, anthropogenic CH_4 sources range between 235 and 338 Tg CH_4 yr^{-1} including ruminant animals, sewage and waste, fossil fuel related emissions, and rice-paddies agriculture. Anthropogenic emissions are found to be of the same order as natural sources (244–368 Tg CH_4 yr^{-1}). Methane is mainly destroyed in the atmosphere by reaction with OH radicals. The different approaches agree now that OH changes remained within 5% in the period 2000–2009. Atmospheric-based estimates of methane emissions and sinks, using data assimilation techniques, provide more narrow ranges

for global emissions (518–550) and global sinks for the years 20000s, with a domination of anthropogenic emissions over natural ones.

Future projections of the coupled carbon-climate system during the 21st century
There is no evidence yet that the carbon cycle - climate feedback is systematically different between the "new" coupled carbon cycle climate models used in the AR5 (called the CMIP5 models) and the "old" AR4 models (called the C4MIP models). The new CMIP5 models consistently estimate a positive feedback, i.e., reduced natural sinks or increased natural CO_2 sources in response to future climate change. In particular, carbon sinks in tropical land ecosystems are vulnerable to climate change. Land-use, land-use change and land management is emerging as a key driver of the future terrestrial carbon cycle, modulating both emissions and sinks, but this human induced process is not consistently represented in coupled carbon cycle climate models, causing a significant source of uncertainty in future projections of atmospheric CO_2 and climate.

A key update since AR4 is the introduction of nutrient dynamics in some land carbon models, in particular the limitations on plant growth imposed by nitrogen availability. Models including the nitrogen cycle predict a significantly lower uptake of anthropogenic CO_2 in land ecosystems than the C4MIP model mean. These nutrient-enabled models also predict that this effect is partly offset by direct stimulation of growth due to airborne nitrogen deposition, and increased nutrient availability due to warming. In all cases, the net effect is a smaller predicted land sink for a given trajectory of anthropogenic CO_2 emissions.

Future projections of ocean acidification and ocean deoxygenation during the 21st century
Mult-model projections show large 21st century decreases in pH and carbonate ion concentrations (CO_3^{2-}) throughout the world oceans for high-emissions scenarios. Aragonite undersaturation in surface waters is reached within decades in the Southern Ocean as highlighted in AR4, but new studies show that undersaturation occurs sooner and is more intense in the Arctic. Most recent projections under AR5 mitigation scenarios illustrate that limiting the atmospheric CO_2 will greatly influence the level of ocean acidification that will be experienced.

Multi-model projections show large 21st century decreases in oceanic dissolved oxygen caused by enhanced stratification and warming, and mainly located in the sub-surface mid-latitude oceans. There is however no consensus on the future evolution of the volume of hypoxic and suboxic waters, due to the large uncertainties in potential biogeochemical effects and in the evolution of tropical ocean dynamics.

Future evolution of the coupled carbon-climate system beyond the 21st century
Ocean and land ecosystems will continue to respond to climate change and atmospheric CO_2 increases created during the 21st century, even for centuries after any stabilization. Ocean acidification will continue inexorably in the future, with surface waters becoming corrosive to aragonite shells even before the end of the 21st century. Committed land ecosystem carbon cycle changes, i.e., induced changes in CO_2 sources and sinks, will manifest themselves further beyond the end of the 21st century. In addition, there is medium confidence that large areas of permafrost will experience thawing, but uncertainty over the magnitude frozen carbon losses through CO_2 or CH_4 emissions to the atmosphere are large. The thawing of frozen carbon stores constitutes a positive feedback that is missing in current coupled carbon-climate models projections.

Future evolution of natural CH_4 sources
Future methane emissions from natural sources will be affected by climate change, but there is limited confidence in quantitative projections of these changes. Models and ecosystem warming experiments show agreement that wetland emissions will increase per unit area in a warmer climate, but wetland areal extent may increase or decrease depending on regional changes in temperature and precipitation affecting wetland hydrology. Estimates of the future release of CH_4 from gas hydrates in response to seafloor warming are poorly constrained, but could lead to significant emissions. However, the global release of CH_4 from hydrates to the atmosphere is likely to be low due to the under-saturated state of the ocean, long-ventilation time of the ocean, and slow propagation of warming through the seafloor.

Carbon dioxide removal methods
Several methods have been proposed to remove CO_2 from the atmosphere in the future. They are categorized as "Carbon Dioxide Removal (CDR)" methods under a broad class of proposals to moderate future climate

change. Examples are afforestation/reforestation, carbon sequestration in soils, biomass energy and carbon capture and storage, ocean fertilization, accelerated weathering and direct air capture of CO_2. The CDR induced extra carbon storage over land would be in organic form, but storage in oceans and geological formations would be in inorganic forms. To have a discernable climate effect, CDR schemes should be able to remove several Petagrams of carbon each year from the atmosphere over several decades in this century.

Carbon dioxide removal methods uncertainties

Scientific considerations for evaluating CDR methods include their storage capacity, the permanence of the storage and potential adverse side effects, and the so called “rebound effect”: When carbon is stored in a reservoir, the concentration gradient between the atmosphere and carbon reservoirs is reduced and thereby the subsequent rate of removal of CO_2 from the atmosphere. The effects of CDR methods are in general slow on account of long time scales required by relevant carbon cycle processes, and thus may not present an option for rapid mitigation of climate change during the next century. The maximum physical potentials may not be achievable in real world because of other constraints, such as competing demands for land. However, if implemented on larger scales and for enough time, CDR methods could potentially make a contribution in reducing atmospheric CO_2. The level of scientific knowledge upon which CDR methods can be evaluated is low, and uncertainties are very large.

Carbon dioxide removal methods side effects

The side effects from CDR methods are highly uncertain. On land, removal of atmospheric CO_2 would lead to a temporary acceleration in global water cycle. Massive changes in forest area will also have climate consequences by altering the surface energy budget. Over the oceans, enhanced biological production may enhance the utilization of nitrogen and phosphate nutrients, causing a decrease in production "downstream" from fertilized regions. Enhanced ocean biological production could acidify the deep ocean, and lead to expand regions with low oxygen concentration, increased production of N_2O and CH_4, possible disruptions to marine ecosystems and disturbance to regional carbon cycle.

6.1 Introduction

The radiative properties of the atmosphere are strongly influenced by the abundance of long-lived greenhouse gases (LLGHGs), including carbon dioxide (CO_2), methane (CH_4) and nitrous oxide (N_2O). The concentrations of these gases have substantially increased over the last 200 years caused primarily by direct and indirect anthropogenic emissions (see Chapter 2). LLGHGs represent a part of the atmospheric branches of the natural global biogeochemical cycles, which describe the flows and transformations of the major elements (C, N, P, O, S, etc.) between the different components of the Earth system (atmosphere, ocean, land, lithosphere) by physical, chemical and biological processes. Since these processes are themselves also dependent on the prevailing environment and climate, changes in the latter can also modify the concentrations of the LLGHGs as witnessed, e.g., during the glacial cycles (see Chapter 5).

6.1.1 Global Carbon Cycle Overview

6.1.1.1 CO_2 Cycle

CO_2 represents a component of the atmospheric branch of the global carbon cycle. The global carbon cycle can be viewed as a series of reservoirs of carbon in the Earth system, which are connected by exchange fluxes. Principally one can distinguish two domains in the global carbon cycle: (1) A fast domain with large exchange fluxes and relatively rapid reservoir turnovers, which consists of carbon in the atmosphere, the ocean and on land in living vegetation and soils. Reservoir turnover times, defined as reservoir content divided by the exchange flux, range from a few years for the atmosphere, to decades, centuries up to a few millennia for the various carbon reservoirs of the land vegetation and soil and the various domains in the ocean. (2) A second, slow domain consists of the huge carbon stores in rocks and sediments, which exchange carbon with the fast domain through volcanism, erosion and sediment formation on the sea floor. Geological turnover times of the reservoirs of the slow domain are 10,000 years or longer. On time scales of the anthropogenic interference with the global carbon cycle, the slow domain can be assumed to be at steady state. Exchange fluxes between the slow and the fast domain are relatively small (<1 PgC yr^{-1}) and can be assumed approximately constant in time (volcanism, sedimentation), although erosion and river fluxes may have been modified by changes in land use (Raymond and Cole, 2003).

During the Holocene prior to the industrial revolution, also the fast domain has been close to steady state as witnessed by the relatively small variations of atmospheric CO_2 recorded in ice cores (see Section 6.2). A schematic of the global carbon cycle with focus on the fast domain is shown in Figure 6.1. The numbers represent the estimated current pool sizes in PgC, and the magnitude of the different exchange fluxes in PgC yr^{-1} averaged over the time period 2000–2009.

[INSERT FIGURE 6.1 HERE]

Figure 6.1: Simplified schematic of the global carbon cycle. Numbers represent reservoir sizes (in PgC), resp. carbon exchange fluxes (in PgC yr^{-1}), representing average conditions over the 2000–2009 time period.

In the atmosphere, CO_2 is the dominant carbon bearing trace gas with a current concentration of approximately 390 ppm (January 2011), which corresponds to 828 PgC. Additional trace gases include carbon monoxide (CO) and (CH_4) (~ 2 PgC each), and still smaller amounts of hydrocarbons and other chemical compounds.

On land, carbon is contained in organic compounds in vegetation (350–550 PgC, (Prentice et al., 2001) and in soils (1500–2400 PgC, (Batjes, 1996), with an additional carbon amount in wetlands (200–450 PgC) and stored in loess permafrost (~1500 PgC, (Tarnocai et al., 2009). Atmospheric CO_2 is taken up by plants through photosynthesis (123 ± 8 PgC yr^{-1}, (Beer et al., 2010) cycled through plant tissue, detritus and soil carbon and subsequently released back into the atmosphere by autotrophic and heterotrophic respiration and additional disturbance processes (e.g., harvest, or fire) on a multitude of time scales. Photosynthesis by the vegetation in the northern extra tropical hemisphere causes the characteristic seesaw seasonal pattern in atmospheric CO_2 (Figure 6.3).

The oceanic carbon reservoir (~3800 PgC) consists predominantly of dissolved inorganic carbon (DIC): carbonic acid, bicarbonate and carbonate ions, which are tightly coupled via ocean chemistry. Marine organisms, primarily phyto-, zooplankton and other microorganisms, represent a small carbon pool (~3

PgC), which is turned over very rapidly in days to a few weeks. Photosynthesis by phytoplankton in the ocean surface layer extracts inorganic carbon, which subsequently is transformed through the marine food chain and finally respired back to DIC by microbes through heterotrophic respiration. After death of the organisms, some of the organic carbon sinks to deeper waters and is remineralized there to inorganic carbon. This process creates a natural concentration gradient of DIC between deeper layers and the surface ocean. Upwelling deeper waters are therefore supersaturated with carbon and release this in the form of CO_2 back to the atmosphere, which, on annual average is then taken up elsewhere by photosynthesis in nutrient rich ocean areas. This natural cycle, termed "marine biological pump", is limited primarily by radiation and the prevailing nutrients (phosphate and nitrate). A second natural oceanic carbon cycle, the "marine carbonate pump" is generated by the formation of calcareous shells of certain oceanic microorganisms in the surface ocean which, after sinking to depth are mostly dissolved and transformed back into bicarbonate and calcium ions. Paradoxically, this cycle operates counter the marine biological pump: in the formation of calcareous shells bicarbonate is split into carbonate and dissolved CO_2, while the reverse takes place during shell dissolution at depth. Only a small fraction (~0.2 PgC yr^{-1}) of the carbon exported by biological processes from the surface reaches the sea floor and is stored in sediments for millennia and longer. A third marine carbon cycle exists due to the fact that the solubility of CO_2 is higher in colder than in warmer waters. This "solubility pump" effectively extracts CO_2 from the atmosphere in colder regions and releases it back to the atmosphere in warmer surface waters.

6.1.1.2 CH_4 Cycle

The global cycle of atmospheric methane (CH_4) represents a small loop of the global carbon cycle. However, because of the stronger radiative properties per molecule of CH_4 compared to CO_2 (Chapter 8), its interactions with photochemistry and its particular source-sink processes, it effectively represents an independent biogeochemical cycle, which is only loosely coupled to the carbon cycle.

Sources of CH_4 are either non-biogenic, including (1) natural emissions from geological sources (see pages from geothermal vents and volcanoes) and natural fires, and (2) anthropogenic emissions from fossil fuel mining or incomplete burning of fossil fuels and biomass (Figure 6.2). A second category consists of biogenic sources including (1) the natural emissions from wetlands, oceans and termites as well as (2) the anthropogenic sources from rice agriculture, livestock, landfills and waste treatment. In general, biogenic CH_4 is produced from organic matter under anoxic conditions by fermentation processes of methanogenic microbes (Conrad, 1996). CH_4 is removed from the atmosphere by photochemistry (reaction with the OH radical to CO and subsequently to CO_2). Atmospheric CH_4 is also removed in the stratosphere by the ozone chemistry and at the surface by oxidation in dry soils.

[INSERT FIGURE 6.2 HERE]

Figure 6.2: Schematic of the global cycle of CH_4. Numbers represent fluxes in $TgCH_4$ yr^{-1} estimated for the time period 2000–2009 (see Section 6.3.). Green arrows denote natural fluxes, red arrows anthropogenic fluxes.

A very large additional pool (1500–7000 PgC,(Archer, 2007) of CH_4 exists in the form of frozen hydrates deposits in permafrost soils, shallow Arctic ocean sediments and on the slopes of continental shelves. These hydrates of biogenic origin are stable under suitable conditions of low temperature and high pressure. Warming or changes in pressure, e.g., due to lowering sea-level could render some of these hydrates unstable with a potential release of CH_4 to the atmosphere. Emissions from melting hydrates have been documented over the East Siberian shelf (Shakhova et al., 2010), however, the estimated magnitude of these fluxes is relatively minor (5–10 TgC yr^{-1}). It is also not clear if recent Arctic Ocean warming triggered these emissions or if they are a relict of the long-term warming trend since the last glaciation. Most of the hydrates are located at depth in soils and ocean sediments, which will be reached by current anthropogenic warming only on millennial time scales. Hence CH_4 emissions from this hydrate pool will manifest itself as chronic seepages, potentially providing an amplifying effect similar to other terrestrial biogeochemical feedbacks (Archer, 2007).

6.1.2 Anthropogenic Perturbation

6.1.2.1 Carbon Cycle

Since the beginning of the industrial revolution, human activities by burning of fossil fuels (coal, oil and gas) have release large amounts of carbon dioxide into the atmosphere (Boden et al., 2011; Rotty, 1983). The amount released can be estimated for the recent decades from statistics of fossil fuel use quite accurately (~5%). Estimates for the time period prior to 1950 are less certain (Rotty, 1983). Total emissions over the industrial period 1750–2008 amount to approximately 340 PgC. This also includes an additional small anthropogenic source of CO_2 caused by the production of cement.

The second major anthropogenic perturbation of the global carbon cycle has been caused by changes in land use and land management, which are accompanied by changes in land carbon storage. In particular deforestation for procurement of land for agricultural or pasture is inevitably associated with a loss of terrestrial carbon. Estimation of this carbon source to the atmosphere requires knowledge of changes in land area as well as estimates of the carbon stored per area prior and after the land use change transition. In addition, longer term effects, such as degradation of soils after land use conversion have to be taken into account as well. Since preindustrial times, anthropogenic land use changes have been massive: Today, already 35% of all ice-free land areas are used for agriculture and pasture (Foley et al., 2007) and total CO_2 emissions from land use changes are estimated at approximately 152 PgC (Houghton, 2010) (see Table 6.2).

The almost exponentially increasing anthropogenic emissions are clearly the cause of the observed increases in atmospheric CO_2. Since most of the emissions take place in the industrialized countries north of the equator, on annual average stations in the northern hemisphere show slightly higher concentrations than stations in the southern hemisphere, as witnessed by the observations from Mauna Loa, Hawaii, and the South Pole (Figure 6.3). The annually averaged concentration difference between the two stations follows extremely well the estimated difference in emissions between the hemispheres (Fan et al., 1999; Keeling et al., 1989a; Tans et al., 1989). CO_2 from fossil fuels and from the land biosphere is depleted in the $^{13}C/^{12}C$ stable isotope ratio, which induces a decreasing trend in the atmospheric $^{13}C/^{12}C$ ratio of the CO_2 concentration as well as on annual average slightly lower $^{13}C/^{12}C$ values in the northern hemisphere (Figure 6.3). Because fossil fuel CO_2 is devoid of radiocarbon (^{14}C), reconstructions of the $^{14}C/C$ isotopic ratio of atmospheric CO_2 from tree rings prior to the nuclear weapon tests also show a declining trend (Levin et al., 2010; Stuiver and Quay, 1981). An additional indication of the anthropogenic influence on atmospheric CO_2 is provided by the declining atmospheric O_2 content (see Figure 6.3 and Section 6.1.3.2).

[INSERT FIGURE 6.3 HERE]

Figure 6.3: Atmospheric concentration of CO_2, oxygen, $^{13}C/^{12}C$ stable isotope ratio in CO_2, CH_4 and N_2O recorded over the last decades at representative stations in the northern (solid lines) and the southern (dashed lines) hemisphere. (a: CO_2 from Mauna Loa and South Pole (Keeling et al., 2005), O_2 from Alert and Cape Grim (http://scrippso2.ucsd.edu/ right axes), b: $^{13}C/^{12}C$: Mauna Loa, South Pole (Keeling et al., 2005), c: CH_4 from Mauna Loa and South Pole (Dlugokencky et al., 2010), d: N_2O from Adrigole and Cape Grim (Prinn et al., 2000).

6.1.2.2 CH_4 Cycle

Throughout the Holocene, atmospheric CH_4 levels varied only moderately (up to 50 ppb) around 700 ppb, indicating a close balance between natural emissions and sinks (see Section 6.2.3.2). During this time the dominant natural source of CH_4 were the wetlands and changes in their geographical extent and climate variations have caused the small variations seen in the ice core record, see Figure 6.6 [references]. After 1800 CH_4 levels rose almost exponentially similar to CO_2, reaching 1650 ppb in 1985. Since then the atmospheric growth of CH_4 has been declining to nearly zero in the early 2000s. Over the last few years atmospheric CH_4 has been growing again, although it is not clear if this reflects a real trend or natural variability.

As with CO_2 there is ample evidence that the atmospheric CH_4 rise during the industrial epoch has been caused by anthropogenic activities. The massive expansion of cattle grazing [number and reference needed], the emissions from fossil fuel mining and the expansion of rice agriculture are the dominant anthropogenic sources which contribute presently more than 75% of the total emissions. The fossil contribution can be estimated from measurements of ^{14}C in CH_4 (Etiope et al., 2008; Lassey et al., 2007; Wahlen et al., 1989). It can also be estimated from ice core measurements of ethane (C_2H_6), which is dominantly emitted from fossil fuel mining in relatively well known amounts relative to CH_4 (Aydin et al., 2011a). The observed north-south gradient in CH_4 provides a powerful indication of the anthropogenic emissions, which are predominantly located in the northern hemisphere (see Figure 6.3 and Figure 6.10).

6.1.3 Connections Between Carbon and Other Biogeochemical Cycles

6.1.3.1 Global Nitrogen Cycle including N_2O

In most terrestrial and oceanic ecosystems, reactive nitrogen (Nr, comprising all nitrogen species other than molecular atmospheric N_2, such as NH_3 and NO_x) constitutes a limiting element for growth, hence the cycles of nitrogen and carbon are closely coupled. In the pre-human world, creation of Nr from N_2 occurred primarily through two processes, lightning and biological nitrogen fixation (BNF). Nr did not accumulate in environmental reservoirs because microbial N fixation and denitrification processes were approximately equal (Ayres et al., 1994). This is no longer the case. Nr is now accumulating in the environment on all spatial scales—local, regional, and global. During the last few decades, production of Nr by humans has been greater than production from all natural terrestrial systems (Galloway et al., 1995). The global increase in Nr production has three main causes: (1) widespread cultivation of legumes, rice, and other crops that promote conversion of N_2 to organic N through BNF; (2) combustion of fossil fuels, which converts both atmospheric N_2 and fossil N to reactive NO_x; and (3) the Haber-Bosch process, which converts nonreactive N_2 to reactive NH_3 to sustain food production and some industrial activities.

On a global basis, the anthropogenic sources of new Nr formed from N_2 are about equal to the Nr formed by BNF in continents and the ocean. For continents, anthropogenic sources are about twice that of natural sources (Figure 6.4). The emission of Nr to the atmosphere by NH_3 and NO_x emissions is driven by agriculture and fossil fuel combustion, respectively. There is a net transfer of Nr from the continental atmosphere to the marine atmosphere, resulting in N deposition to the ocean that is greater than by riverine discharge. The connection between the nitrogen and carbon cycles are discussed in Box 6.1.

[START BOX 6.1 HERE]

Box 6.1: Nitrogen Cycle and Nitrogen Carbon Cycle Feedbacks

In the pre-human world, biological nitrogen fixation was the dominant means by which new reactive nitrogen (Nr, defined as all N species except N_2) was made available to living organisms. The total amount of Nr that circulated naturally among various compartments of the atmosphere and the biosphere of the Earth was quite small. Thus, the biodiversity and intricate webs of relationships found in nature evolved as a result of intensive competition among many different life forms – most of them evolving under N-limited conditions. During the last 18th and 19th centuries, human involvement with N began with discovery of N as an element, the discovery of fundamental microbial processes that transform Nr from one species to another (e.g., biological nitrogen fixation, nitrification, denitrification), and importance of Nr as a nutrient. It was this latter discovery that led to the development of the Haber-Bosch process (synthesis of NH_3 from its elements) in the early 20th century. By the end of the 20th century and continuing into the 21st century, human creation of Nr (Haber-Bosch process, fossil fuel combustion, legume cultivation) dominated Nr creation relative to natural processes (biological nitrogen fixation, lightning) on a global basis. This dominance has profound impacts on human health, ecosystem health and the radiation balance of the earth.

The time-course of Nr production from 1850 to 2005 illustrates both the rate and magnitude of change (Box 6.1, Figure 1). By about the mid-1970s, human systems became more important than natural systems in creating Nr. Currently food production accounts for ~75% of the Nr created by humans, with fossil fuel combustion and industrial uses accounting for ~13% each.

[INSERT BOX 6.1, FIGURE 1 HERE]

Box 6.1, Figure 1: World population (blue line) and reactive creation by the fossil fuel burning (orange line), from legumes (red line) and by the Haber-Bosch process (green line), over the last 160 years.

Of all the questions that could be asked about this, three that are the most relevant to this document are: what is the fate of the anthropogenic Nr?; what are the impacts on humans and ecosystems?; what are the connections to climate change?

With respect to its fate, of this Nr is released to the environment—combustion sources immediately, food production sources within about a year, and industrial sources immediately to years, depending on the use. Once released, the Nr is transported, transformed, and stored. Large amounts are injected into the atmosphere and to coastal systems (Figure 6.1.3). A portion is converted back to N_2 but this amount is uncertain and is one of the most critical questions concerning the human influence on the nitrogen cycle today.

With respect to impacts, they are both positive and negative. The overwhelming positive response is the production of food. The Haber-Bosch process is responsible for providing the nitrogen that helps produce the food for most of the world. However, since most of the Nr created by humans enters that unmanaged environment, the critical question is what are the consequences? They range from local, regional and global and include and increase in tropospheric ozone and atmospheric particles, acidification of the atmosphere, soils and fresh waters, over fertilization of unmanaged forests, grasslands, coastal waters, open ocean, decrease in stratospheric ozone, and direct and indirect contributions to climate change. All of these can have negative impacts on ecosystems and people. A unique characteristic of the impacts of Nr is that the impacts are linked through nitrogen's biogeochemical cycle. Referred to as the 'nitrogen-cascade', essentially once a molecule of N_2 is split and the nitrogen atoms become reactive (e.g., NH_3, NO_x), any given nitrogen atom can contribute to all of the impacts noted above in sequence (Box 6.1, Figure 2). The only way of terminating the N-cascade is to convert Nr back to N_2.

[INSERT BOX 6.1, FIGURE 2 HERE]

Box 6.1, Figure 2: Nitrogen cycle interactions with terrestrial and aquatic ecosystems.

The third question, direct and indirect impacts of Nr on climate change are summarize here and detailed in other areas of the report.

The most important direct links between Nr and climate include 1) N_2O formation, 2) ground level O_3 formation from NO_x, and 3) aerosol formation affecting radiative forcing. The first two have warming effects; the last can have a warming or a cooling effect. The most important indirect links between Nr and climate include: 1) alteration of the biospheric CO_2 sink due to increased supply of Nr, 2) excess Nr deposition either increasing or reducing ecosystem productivity and so C-sequestration, 3) changes in ecosystem CH_4 production and consumption due to Nr deposition to wetlands, 4) changes in CH_4 production and emission from ruminants, 5) O_3 formed in the troposphere as a result of NOx and VOC emissions reduces plant productivity, and therefore reduces CO_2 uptake from the atmosphere, 6) O_3 effects on atmospheric OH radical concentrations and thus atmospheric lifetime of atmospheric CH_4 (Erisman et al., 2011)

It is important to note, that because of the nitrogen cascade, the creation of any molecule of Nr from N_2, at any location, has the potential to climate change, either directly or indirectly. This potential exists until the Nr is converted back to N_2.

[END BOX 6.1 HERE]

[INSERT FIGURE 6.4 HERE]

Figure 6.4: Global nitrogen cycle. In the top panel, the upper part shows the flows of reactive Nitrogen species, the lower part the processes by which atmospheric molecular nitrogen is converted to reactive nitrogen species. The bottom panel shows a schematic of the global cycle of N_2O. Blue arrows are natural, red arrows anthropogenic fluxes, and yellow arrows represent fluxes with an anthropogenic and natural component. BNF: biological nitrogen fixation. Units: TgN yr^{-1}.

6.1.3.2 Oxygen Cycle

The cycle of atmospheric molecular oxygen is tightly coupled to the fast component of the global carbon cycle. The burning of fossil fuels requires oxygen with clearly defined amounts depending on fuel type. As a consequence of the anthropogenic perturbation, atmospheric O_2 levels are decreasing, which has been observed over the last 20 years by accurate O_2 measurements (Keeling and Shertz, 1992; Manning and Keeling, 2006). This provides independent evidence that the rising CO_2 is not caused by volcanic emissions

or by a warming ocean, but must be due to an oxidation process. The oxygen measurements furthermore also show the north-south concentration gradient as expected from the stronger fossil fuel consumption in the northern hemisphere (Keeling et al., 1996).

On land, during photosynthesis and respiration, O_2 and CO_2 are exchanged in well-defined stoichiometric ratios. However, with respect to exchanges with the ocean O_2 behaves quite differently from CO_2, since compared to the atmosphere only a small amount of O_2 is dissolved in the ocean. This is which is different with CO_2, which contains a much larger ocean inventory due to the carbonate chemistry. This different behaviour of the two gases with respect to ocean exchange provides a powerful method to independently assess the partitioning of the uptake of CO_2 by land and oceans (Manning and Keeling, 2006).

6.1.4 Outline of Chapter 6

The material in the following sections is organized as follows: Section 6.2 assesses the present understanding of the mechanisms responsible for the variations of the three major biogeochemical trace gases CO_2, CH_4 and N_2O in the past, emphasizing glacial-interglacial changes, variations during the Holocene since the last glaciation and their variability over the last millennium. Section 6.3 focuses on the fossil fuel era since 1750 addressing the major source and sink processes and their variability in space and time. This information is then used to critically evaluate the simulation models of the biogeochemical cycles, including their sensitivity to changes in atmospheric composition and climate. Section 6.4 assesses future projections of carbon and other biogeochemical cycles computed with off-line and coupled climate-carbon cycle models. This includes a quantitative assessment of sign and magnitude of the various feedback mechanisms as represented in current models, as well as additional processes that might become important in the future, but which are not yet fully described in current biogeochemical models. The final Section 6.5 addresses the effects of deliberate carbon dioxide removal methods and solar radiation management on the carbon cycle.

6.2 Variations before the Fossil Fuel Era

6.2.1 Introduction. Why are past GHG changes relevant for the future climate?

Numerous mechanisms responsible for atmospheric GHG changes in the past will operate in the future climate as well. Past archives of GHG and climate changes provide therefore powerful constraints for biogeochemical models applied for projections of GHG concentration in the future.

6.2.2 Glacial – Interglacial GHG Changes

6.2.2.1 Key Processes Contributing to the Low Glacial GHG Concentrations

6.2.2.1.1 Main glacial-interglacial CO_2 drivers

Ice cores recovered from the Antarctic ice cap reveal that the concentration of atmospheric CO_2 at the height of the Last Glacial Maximum (LGM) around 20 thousand years ago (20 ka) was about one third lower than during the subsequent interglacial (Holocene) period (Delmas et al., 1980; Monnin et al., 2001; Neftel et al., 1982). Longer (to 800 ka) records exhibit similar features, with CO_2 values of ~180–200 ppm during glacial intervals (Luthi et al., 2008), although prior to around 400 ka, interglacial CO_2 values were 240–260 ppm rather than 270–290 ppm subsequently.

A variety of proxy reconstructions as well as conceptual, 'box', Intermediate Complexity (EMIC), but also complex Earth System (ESM) Models have been used to test hypotheses for the cause of lower LGM atmospheric CO_2 concentrations. The ways in which the global carbon cycle operated at the LGM and their relative implications for CO_2 can be broken down by individual drivers (Figure 6.5). It should be recognized however that this breaking down is somewhat artificial, as many of the components may combine non-linearly (Bouttes et al., 2011), preventing a simple linear sum of the component parts. Only well-established individual drivers are quantified (Figure 6.5), and discussed below.

Reduced terrestrial carbon storage. The d13C record of ocean waters as preserved in benthic foraminiferal shells has been used to infer that the terrestrial carbon storage was substantially reduced in glacial times. Estimates of land carbon loss at the LGM range from a few hundreds to 1000 PgC (e.g., Bird et al., 1996).

Recent dynamic vegetation model simulations tend to favor values at the higher end (~800 PgC) (Kaplan et al., 2002; Otto et al., 2002) and indicate a larger role for the physiological effects of low CO_2 on photosynthesis at the LGM than that of climate-induced biome shifts (Prentice and Harrison, 2009).

Lower ocean temperatures. Reconstructions of sea-surface temperatures during the LGM suggest that the global ocean was on average 3–5°C cooler compared to the Holocene). Because the solubility of CO_2 scales inversely with temperature (Zeebe and Wolf-Gladrow, 2001), a colder glacial ocean will hold more carbon. However, uncertainties in reconstructing of pattern of ocean temperature change, particularly in the tropics (Archer et al., 2000; Waelbroeck et al., 2009), together with problems in transforming this pattern to the resolution of (particularly box) models in light of the non-linear nature of the CO_2-temperature relationship (Ridgwell, 2001), creates a ~24 pm spread in CO_2 estimates, although it can be noted that most 3-D OGCM projections cluster more tightly.

Lower global sea level, increased ocean salinity and alkalinity. Changes in ocean volume also induces a well understood effect on CO_2 solubility, with LGM sea-level about ~120 m lower than today. This impacts the ocean carbon cycle in three distinct ways. First, higher LGM ocean surface salinity induces a ~6 ppm decrease in atmospheric CO_2 (Bopp et al., 2003). Second, total dissolved carbon and alkalinity become more concentrated in equal proportions, which has the effect of driving atmospheric CO_2 higher. Finally, decreasing the ambient hydrostatic pressure at the ocean floor with lower sea-level promotes the preservation of $CaCO_3$ in sediments and hence on the longer-term (~2–8 kyr (Archer et al., 2000; Ridgwell and Hargreaves, 2007)) provides an additional alkalinity influence on CO_2.

Ocean circulation. Potential changes in global circulation that promotes the retention of dissolved carbon in the deep ocean have increasingly become the focus on recent work on the glacial-interglacial CO_2 problem. That ocean circulation likely plays a key role in low glacial CO_2 is exemplified by the tight coupling between deep ocean temperatures and atmospheric CO2 (Shackleton, 2000). Evidence from bore hole sites (Adkins et al., 2002) and from surface ocean data in polar regions (Jaccard et al., 2005) show that the glacial ocean was highly stratified compared to interglacial conditions and may have hold a larger store of carbon during glacial times. However, conflicting hypotheses exist on the drivers of increasing ocean stratification, e.g., northward shift and weakening of SH westerly winds (Toggweiler et al., 2006), reduced air-sea buyancy fluxes (Watson and Garabato, 2006), massive brine rejections (Bouttes et al., 2011). Ocean carbon cycles models have projected circulation-induced CO_2 changes that range from 3 ppm (Bopp et al., 2003) to 57 ppm (Toggweiler, 1999).

Aeolian iron fertilization. Both marine and terrestrial sediment records indicate higher rates of deposition of dust and hence Fe supply at the LGM (Mahowald et al., 2006), implying Fe fertilization of marine productivity and lower glacial CO_2 (Martin, 1990). However, despite models generally employ similar reconstructions of glacial dust fluxes (i.e., Mahowald et al., 1999; Mahowald et al., 2006), there is considerable model-model disagreement in the associated CO_2 change. OGCM-based Fe cycle models tend to cluster at the lower end (e.g., Archer et al., 2000; Bopp et al., 2003), with box models (e.g., Watson et al., 2000) or EMICs (e.g., Brovkin et al., 2007) at the higher end although not always (Parekh et al., 2008). An alternative view comes from inferences drawn from the timing and magnitude of changes in dust and CO_2 in ice cores (Rothlisberger et al., 2004), assigning a 20 ppm limit for Southern Ocean Fe fertilization, and 8 ppm in the North Pacific.

Increased sea-ice extent. A long-standing hypothesis is of increased LGM sea-ice cover acting as a barrier to air-sea gas exchange and hence reduces the 'leakage' of CO_2 during winter months to the glacial atmosphere (Broecker and Peng, 1986). However, concurrent changes in ocean circulation and biological productivity complicate the estimation of the CO_2 impact (Kurahashi-Nakamura et al., 2007). Despite this, excepting an idealized box model projection (Stephens and Keeling, 2000), models are relative consistent in projecting a small (increase) in CO_2.

Other glacial CO_2 drivers. A number of further aspects of altered climate and biogeochemistry at the LGM are also likely to have affected atmospheric CO_2. Reduced bacterial metabolic rates (Matsumoto, 2007), reduction in coral reefs growth and other forms of shallow water $CaCO_3$ accumulation (Berger, 1982), increase glacial supply of dissolved Si (required by diatoms to form frustules) (Harrison, 2000), changes in net global weathering rates have (Berner, 1992), but also 'carbonate compensation' (Ridgwell and Zeebe,

2005), 'silica leakage' (Matsumoto et al., 2002), and changes to the $CaCO_3$ to organic matter 'rain ratio' to the sediments (Archer and Maierreimer, 1994), will act to amplify or diminish the CO_2 effect of many of the above drivers.

Summary. All the major glacial CO_2 drivers (Figure 6.5) are likely to have already been identified. However, significant uncertainties in reconstructing glacial boundary conditions plus deficiencies in fully understanding some of the primary controls on carbon storage in the ocean and in the land exist. This uncertainty prevents an unambiguous interpretation of the causes of low glacial CO_2. Assessment of the balance of mechanisms at prior deglacial transitions or glacial inceptions will likely provide additional insights into the drivers of low glacial CO_2. As iron cycling (Parekh et al., 2006) and organic matter remineralization (Matsumoto, 2007) are likely sensitive to climate change in general, improved understanding drawn from the glacial-interglacial cycles will help constrain the magnitude of future ocean feedbacks on atmospheric CO_2.

[INSERT FIGURE 6.5 HERE]

Figure 6.5: Carbon dioxide concentrations changes from late Holocene to the LGM (left) and from late Holocene to early/mid Holocene (7 ka) (right). Filled black circles represent individual model-based estimates for individual ocean, land, geological or human drivers. Solid color bars represent expert judgment (to the nearest 5 ppm) rather than a formal statistical average. References for the different model assessment used for the glacial drivers are as per (Kohfeld and Ridgwell, 2009) with excluded model projections in grey. References for the different model assessment used for the holocene drivers are 1. (Joos et al., 2004), 2. (Brovkin et al., 2008), 3. (Kleinen et al., 2010), 4. (Broecker et al., 1999), 5. (Ridgwell et al., 2003), 6. (Brovkin et al., 2002), 7. Shurgers et al. (2006), 8. (Kleinen et al., 2010), 9. (Yu, 2011), 10. (Kleinen et al., 2011), 11. (Ruddiman, 2003, 2007), 12. (Strassmann et al., 2008), 13. (Olofsson and Hickler, 2008), 14. (Pongratz et al., 2009), 15. (Kaplan et al., 2011), 16. (Lemmen, 2009), 17. (Stocker et al., 2011) and 18. (Roth and Joos, submitted).

6.2.2.1.2 Glacial CH_4 and N_2O

Polar ice core analyses have shown that the atmospheric mixing ratios of CH_4 and N_2O were much lower under glacial conditions compared with interglacial ones. Their reconstructed history encompasses the last 800,000 years (Loulergue et al., 2008; Schilt et al., 2010a). Glacial CH_4 mixing ratios are in the 350–400 ppbv range during the 8 glacial maxima covered so far. This is about half the levels observed during interglacial conditions. The Last Glacial Maximum N_2O mixing ratio amounts to 202 ± 8 ppbv, compared to the Early Holocene levels of about 270 ppbv (Fluckiger et al., 1999).

CH_4 and N_2O isotopic ratio measurements in polar ice provide additional constraints on the mechanisms responsible for their temporal changes. N_2O isotopes have only been used to investigate the causes of in-situ production in ice (Sowers, 2001). δD and ^{14}C of CH_4 have shown that catastrophic methane hydrate degassing events were unlikely causing last deglaciation CH_4 increases (Bock et al., 2010; Petrenko et al., 2009; Sowers, 2006). $\delta^{13}C$ and δD of CH_4 combined with interpolar gradient changes suggest that most of the methane doubling during the last deglaciation results from the development of boreal wetlands, a stronger source from tropical wetlands and an increase residence time due to a reduced oxidative capacity of the atmosphere (Fischer et al., 2008). The biomass burning source would have little changed on the same time scale, whereas this CH_4 source experienced large fluctuations over the last millennium (Mischler et al., 2009; Wang et al., 2010b).

Several modeling studies (Kaplan et al., 2006; Valdes et al., 2005) have addressed the mechanisms behind methane variations on glacial-interglacial time-scales. Tropical temperature influencing tropical wetlands and global vegetation are found to be the dominant controls for global CH_4 emissions and atmospheric concentrations (Konijnendijk et al., 2011).

6.2.2.2 Processes Controlling Changes in GHG During Abrupt Glacial Events

Greenhouse gases (CO_2, CH_4 and N_2O) reveal sharp millennial-scale changes in the course of glaciations, associated with the so-called Dansgaard/Oeschger (DO) climatic events. But their amplitude, shape and timing differ. CO_2 concentrations varied by about 20 ppm, increasing during cold (stadial) events in Greenland, attaining a maximum around the time of the rapid warming in Greenland, which lasted about 1000 years and decreased afterward (Ahn and Brook, 2008). CO_2 co-varied roughly with Antarctic temperatures. Methane and N_2O showed rapid transitions following Greenland temperatures with little or no

lag. DO CH_4 changes are in the 50–200 ppbv range (Fluckiger et al., 2004) and are in phase with Greenland warmings at decadal time scale (Huber et al., 2006). DO N_2O fluctuations can reach glacial-interglacial amplitudes, and for the warmest and longest DO events, N_2O starts to increase several centuries before Greenland temperature and CH_4 (Schilt et al., 2010b).

However, conflicting hypotheses exist on the drivers of these changes. Some model simulations suggest that both CO_2 and N_2O fluctuations can be explained by changes in the Atlantic meridional overturning ocean circulation (Schmittner and Galbraith, 2008), CO_2 variations being mainly caused by changes in the efficiency of the biological pump which affects deep ocean carbon storage (Bouttes et al., 2011), whereas N_2O variations would be due to changes in productivity and oxygen concentrations in the shallow subsurface ocean (Jaccard and Galbraith, accepted). Other studies however suggest that CO_2 fluctuations can be explained by changes in the land carbon storage (Bozbiyik et al., 2011; Menviel et al., 2008), and that terrestrial processes would have to explain most of N2O changes (Goldstein et al., 2003).

6.2.3 GHG Changes over the Holocene (last 11,000 years)

6.2.3.1 Understanding Processes Underlying Holocene CO_2 Changes

The evolution of the well-mixed atmospheric GHGs (carbon dioxide, methane, and N_2O) during the Holocene, a recent interglacial period continuing for about 11 ka, is known with high certainty from ice core analyses (Figure 6.6). A decrease in atmospheric CO_2 of about 7 ppm from 11 to 8 ka was followed by a 20 ppm CO_2 increase until the onset of the industrial period (Elsig et al., 2009; Indermuhle et al., 1999; Monnin et al., 2004). These variations in atmospheric CO_2 over the eleven thousands of years preceding the onset of industrialization are more than a factor of five smaller than the CO_2 increase over the past 200 years. Despite of small scale, the mechanisms of interglacial CO_2 changes are essential for understanding a role of natural forcings in CO_2 dynamics.

[INSERT FIGURE 6.6 HERE]

Figure 6.6: Variations of CO_2, CH_4, and N_2O concentrations during the Holocene. The data are for Antarctic ice cores (EPICA Dome C (Fluckiger et al., 2002; Monnin et al., 2004) (triangles); Law Dome, (MacFarling-Meure et al., 2006) circles), and for Greenland ice core (GRIP (Blunier et al., 1995), squares). Lines are for 200-year moving average.

Since the IPCC AR4 release, mechanisms underlying a 20 ppm CO_2 increase between 7 ka and the industrial period were a matter of intensive debate. During 3 interglacial periods prior to the Holocene, CO_2 was not increasing, and this led to a hypothesis that anthropogenic CO_2 emissions associated with landuse were a main driver of the Holocene CO_2 changes (Ruddiman, 2003, 2007). Recent ice core CO_2 data (Siegenthaler et al., 2005b) reveals that during MIS11, an interglacial period about 400-420 ka, CO_2 was increasing similar to the Holocene period. Drivers of atmospheric CO_2 changes during the Holocene are divided into oceanic and land-based processes (Figure 6.5).

6.2.3.1.1 Oceanic processes

With high certainty, the change in oceanic carbonate chemistry state explains the CO_2 growth through the Holocene. Proposed mechanisms include: (i) a shift of oceanic carbonate sedimentation from a deep sea to the shallow waters and excessive accumulation of CaCO3 on shelves including coral reef growth (Kleinen et al., 2010; Ridgwell et al., 2003); (ii) a carbonate compensation to release of carbon from the deep ocean during deglaciation and buildup of terrestrial biosphere in the early Holocene (Broecker et al., 1999; Elsig et al., 2009; Joos et al., 2004; Menviel and Joos, submitted). The proxies for the carbonate ion concentration in the deep sea (Yu et al., 2010) and increased dissolution of carbonate sediments in the deep tropical Pacific (Anderson et al., 2008) support the hypothesis of oceanic source of carbon for the atmosphere during the Holocene. Changes in SSTs over the last 7 ka (Kim et al., 2004) could drive atmospheric CO_2 slightly lower (Brovkin et al., 2008) or higher (Menviel and Joos, submitted) but with high certainty SST-driven CO2 change is a minor contribution to the Holocene CO_2 growth.

6.2.3.1.2 Terrestrial processes: ice-core evidence

δ^{13} of atmospheric CO_2 trapped in the ice cores is a reliable proxy for changes in terrestrial biospheric carbon pools during interglacial periods. The inverse calculations yield an increase in terrestrial carbon stocks of

about 300 GtC between 11 and 5 ka BP and small overall terrestrial changes in the millennia thereafter (Elsig et al., 2009).

6.2.3.1.3 Natural terrestrial processes

After 7 ka, increasing atmospheric CO_2 concentrations stimulated gross primary productivity of terrestrial vegetation resulting in increases in carbon storage. Modelling studies suggest that CO_2 fertilization represent substantial land sink of carbon (>100 GtC) on Holocene timescales (Joos et al., 2004; Kaplan et al., 2002; Kleinen et al., 2010). Orbitally forced climate variability, including the intensification and decline of the Afro-Asian monsoon and the mid-Holocene warming of the high-latitudes of the northern hemisphere resulted in continental-scale changes in vegetation distribution and terrestrial carbon. These changes are expected to have been small (Brovkin et al., 2002; Schurgers et al., 2006). The Holocene evolution of carbon in peatlands has been reconstructed globally, suggesting a land carbon uptake of several hundred GtC, although uncertainties remain and recent estimates of the current carbon stock in boreal peats differ by about a factor of two (Kleinen et al., 2011; Tarnocai et al., 2009; Yu, 2011). Changes in the rate of carbon emissions from volcanoes (Huybers and Langmuir, 2009; Roth and Joos, submitted) is another uncertainty in the Holocene carbon budget.

6.2.3.1.4 Landuse

Global syntheses of the observational paleoecological and archaeological records for Holocene landuse are not currently available (Gaillard et al., 2010). Available global reconstructions of anthropogenic land use and land cover change (LULCC) prior to the last millennium currently extrapolate the relationship of the land cover change and population density from a single region and specific time period to the entire globe and Holocene (Kaplan et al., 2011) or extrapolate the changes of per-capita land requirements occurring with agro-technological progress over time from single regions to changes in all regions of the world (Goldewijk et al., 2011). Because of regional differences in land use systems and uncertainty in historical population estimates the confidence in spatially explicit LULCC reconstructions is low.

Some recent studies focused on reconstructing LULCC while making very simple assumptions regarding patterns of both terrestrial carbon storage and the effect of land use on carbon (Lemmen, 2009; Olofsson and Hickler, 2008), while others relied on more sophisticated terrestrial biosphere models to simulate carbon storage and loss (Pongratz et al., 2009; Stocker et al., 2011; Strassmann et al., 2008). The conclusion of the above studies was that cumulative Holocene carbon emissions as a result of preindustrial LULCC were not large enough (~50–150 Pg) to have had an influence on Holocene CO_2 concentrations. Recent study by (Kaplan et al., 2011) suggested that these attempts represented significant underestimates and that more than 350 Pg C could have been released as a result of LULCC between 8 ka and AD 1850.

6.2.3.1.5 Human impacts on Holocene biomass burning

In addition to clearing of forests for crop and pasture, biomass burning by preindustrial humans has been hypothesized as sources of both CO_2 and CH_4 over the Holocene. Studies that synthesized charcoal records from lake and bog sediments initially suggested that there could be large-scale correlations between burning activity and atmospheric CO_2 (Carcaillet et al., 2002), though this hypothesis was largely discounted by two later global syntheses that used similar methods and concluded that fire activity followed climate variability (Marlon et al., 2008; Power et al., 2008). In contrast, regional syntheses of charcoal and other paleo-evidence of biomass burning suggest fire is closely related to the dynamics of human societies (McWethy et al., 2009; Nevle and Bird, 2008; Nevle et al., 2011).

6.2.3.2 Holocene CH_4 and N_2O Drivers

The Holocene atmospheric CH_4 dynamics has a minimum around 5 ka and a later rise by about 100 ppb (Figure 6.6). Major Holocene agricultural developments, in particular wet rice cultivation and widespread domestication of ruminants, have been seen as an explanation for the Late Holocene CH_4 rise (Ruddiman, 2007). The most recent syntheses of archaeological data point to an increasing anthropogenic CH_4 source from domesticated ruminants after 5 ka and from rice cultivation after 4 ka (Fuller et al., 2011; Ruddiman, 2007). The modelling support for either natural or anthropogenic explanation of the Late Holocene CH_4 rise is equivocal. A study (Kaplan et al., 2006) suggested that a part of this rise could be explained by anthropogenic sources. Wetland CH_4 models driven by simulated climate changes are able (Singarayer et al., 2011) or unable (Konijnendijk et al., 2011) to simulate Late Holocene methane rise. Additionally to the

wetland CH_4 source, long-term trends in biomass burning have been invoked to explain the CH_4 record (Ferretti et al., 2005; Marlon et al., 2008).

No studies are known about mechanisms of Holocene N_2O changes.

6.2.4 GHG Changes over the Last Millennium

6.2.4.1 Mechanisms which led to the CO_2 drop around year 1600

High resolution records of ice cores reveals that atmospheric CO_2 during the last millennium varied with a drop in atmospheric CO_2 concentration by about 7-10 ppm around year 1600 and a CO_2 recovery during the 17th century (Ahn et al., submitted), in progress; (Siegenthaler et al., 2005a; Trudinger et al., 2002), **Figure 6.7**). The CO_2 decrease during the 17th century was used to evaluate a strength of atmospheric CO_2 sensitivity to changes in global temperature (Cox and Jones, 2008; Frank et al., 2010; Scheffer et al., 2006) which depends on the choice of global temperature reconstructions.

[INSERT FIGURE 6.7 HERE]

Figure 6.7: Variations of CO_2, CH_4, and N_2O during 900–1900 AD. The data are for Antarctic ice cores: (Etheridge et al., 1996; MacFarling-Meure et al., 2006), circles; West Antractic Ice Sheet (Ahn et al., submitted; Mitchell et al., 2011), triangles; Dronning Maud Land (Siegenthaler et al., 2005a), squares. Lines are for 30-year moving average.

One of possible explanations of atmospheric CO_2 drop around yr 1600 is a response of carbon cycle to the cooling caused by reduced solar irradiance during Maunder minimum. However, simulations of EMICs (Brovkin et al., 2004; Gerber et al., 2003) and comprehensive ESMs (Jungclaus et al., 2010) suggest that this forcing is not sufficient to obtain a CO_2 drop of observed amplitude. The CO_2 drop could be also caused by a climate cooling in response to volcanic eruptions. Another hypothesis calls for a link between CO_2 and epidemics and wars and associated reforestation of abandoned lands, especially in central America. Here, results are scenario dependent. Simulations by (Pongratz et al., 2011) does not show any drop in CO_2, while results by (Kaplan et al., 2011) suggest a considerable increase in land carbon storage during late 16th - early 17th century. Low resolution of pollen records available for central America does not allow to support or falsify these model conclusions.

Ensemble simulations over the last 1200 years have been conducted using a comprehensive ESM including a fully-interactive carbon-cycle (Jungclaus et al., 2010). For the two ensemble simulations using a lower and higher estimate for the multi-centennial variations of the solar irradiance, the sensitivity of atmospheric CO_2 concentration to Northern Hemisphere temperature changes is diagnosed as 2.7 and 4.4 ppm K^{-1}, respectively. This sensitivity falls within the range of 1.7–21.4 ppm K^{-1} of a recent reconstruction-based assessment (Frank et al., 2010), though at its lower end.

6.2.4.2 Mechanisms Controlling CH_4 and N_2O

High resolution ice core records reveal a CH_4 drop in the late 16th century by about 20 ppb (MacFarling-Meure et al., 2006; Mitchell et al., 2011). Correlations between variations in CH_4 and temperature in 15–16th centuries suggest that climate change affected CH_4 emissions during this time period. Changes in anthropogenic CH_4 emissions during times of war and plague likely contributes to variability in atmospheric CH_4 concentration, although cannot explain all variability (Mitchell et al., 2011).

No studies are known about mechanisms of N_2O changes for the last Millennium.

6.3 Evolution of Biogeochemical Cycles in the Fossil Fuel Era

6.3.1 CO_2 Emissions and their Fate Since 1750

Prior to the Industrial Revolution, defined in the following to begin by 1750, the concentration of atmospheric CO_2 fluctuated between 170 and 300 ppm for at least 2.1 million years (Honisch et al., 2009; Luthi et al., 2008; Petit et al., 1999; see Section 6.2). Between 1750 and 2011, the combustion of fossil fuels (coal, gas, oil, and gas flaring) and the production of cement have released 365 ± 22 PgC to the atmosphere

(Boden et al., 2011), with an additional 151 ± 51 PgC due to land conversion, mainly deforestation (Table 6.1**;** see Section 6.3.2 for data sources). This carbon is called anthropogenic carbon.

Table 6.1: Global CO_2 budget, cumulated since the Industrial revolution (1750) and averaged over the past three decades.

	1850–2011 PgC	1980–1989 PgC yr^{-1}	1990–1999 PgC yr^{-1}	2000–2009 PgC yr^{-1}
Atmospheric increase[a]:	238 ± 7	3.4 ± 0.3	3.1 ± 0.2	4.0 ± 0.2
Fossil fuel combustion and cement production[b]:	365 ± 22	5.5 ± 0.3	6.4 ± 0.4	7.7 ± 0.5
Ocean-to-atmosphere flux[c]:	154 ± 20	–2.0 ± 0.5	–2.2 ± 0.4	–2.3 ± 0.5
Land-to-atmosphere flux:				
Land Use Change[d]	151 ± 51	1.3 ± 0.5	1.3 ± 0.5	0.9 ± 0.5
Residual terrestrial sink[e]:	124 ± 59	–1.4 ± 0.8	–2.4 ± 0.8	–2.3 ± 0.9

Notes:
(a) Data from Thomas Conway and Pieter Tans, NOAA/ESRL (www.esrl.noaa.gov/gmd/ccgg/trends/).
(b) CO_2 emissions are estimated by the Carbon Dioxide Information Analysis Center (CDIAC) based on UN energy statistics for fossil fuel combustion and US Geological Survey for cement production (Boden et al., 2011).
(c) Averaged from existing global estimates (see text for the mean values and Table 6.5 for the decadal trends).
(d) Land Use Change (LUC) CO_2 emissions are averaged from existing global estimates (see text and Table 6.10).
(e) Estimated as the sum of the other terms, assuming the errors are independent and added quadratically.

Of the 516 ± 56 Pg of anthropogenic C emitted to the atmosphere by human activities, less than half have accumulated in the atmosphere (238 ± 7 PgC), resulting in the current atmospheric CO_2 concentration of 389.8 ppm by year 2010 (Conway and Tans, 2011). The remaining anthropogenic C has been absorbed by the oceans and in terrestrial ecosystems – the carbon "sinks" (Figure 6.8). The CO_2 emissions and the speed at which C is being transferred from the atmosphere to the ocean and terrestrial pools drives the growth rate of atmospheric CO_2, which directly leads to changes in the Earth's radiative forcing.

[INSERT FIGURE 6.8 HERE]
Figure 6.8: Sources and sinks fluxes (PgC yr^{-1}) for all main flux component of the global CO_2 budget from 1750 to 2010. CO_2 emissions are estimated by the Carbon Dioxide Information Analysis Center (CDIAC) based on UN energy statistics for fossil fuel combustion and US Geological Survey for cement production (Boden et al., 2011). CO_2 emissions from deforestation and other land use change prior to 1960 are from the average of three estimates (Pongratz et al., 2009; Shevliakova et al., 2009; van Minnen et al., 2009) for 1750–1959 and from (Friedlingstein et al., 2010) from 1960. The atmospheric CO_2 growth rate prior to 1960 is based on a spline fit to ice core observations (Etheridge et al., 1996; Friedli et al., 1986; Neftel et al., 1982) and a synthesis of atmospheric observations from 1960 (Conway and Tans, 2011)The fit to ice core does not capture the large interannual variability in atmospheric CO_2 and is represented with a dash line on the figure. The ocean CO_2 sink prior to 1960 is from (Khatiwala et al., 2009) and a combination of model and observations from 1960 updated (LeQuere et al., 2009).

The transfer of CO_2 between the atmosphere and the oceans is driven by the differential partial pressure between these two compartments. This transfer has led to the storage of 154 ± 20 Pg of anthropogenic C into the ocean since the beginning of the Industrial Revolution (updated from (Sabine et al., 2004); see Section 6.3.2.4.3). Given the high solubility of CO_2 and the under-saturated state of the oceans, the ocean sink will continue to remove atmospheric CO_2 until the entire ocean has re-equilibrated with the higher atmospheric CO_2 (see Box 6.2).

[START BOX 6.2 HERE]

Box 6.2: CO_2 Residence Time

The concept of a mean characteristic lifetime for fossil fuel CO_2 is misleading because uptake of the CO_2 is driven by several processes operating on very different time scales. Because CO_2 is released to the atmosphere, the atmosphere contains more CO_2 than it would in a steady state with the ocean and the land biosphere, and this imbalance drives uptake into those reservoirs. If CO_2 emissions stopped, the atmospheric concentration is expected to approach equilibrium on a time scale of several centuries, with most of released CO_2 winding up in form of dissolved inorganic carbon in the ocean (the ocean invasion phase, see figure below). In the atmosphere / ocean/ land biosphere steady state, the airborne fraction of the CO_2 slug is expected to be 15–40%, depending on the amount of carbon released (Archer et al., 2009b), which depletes the carbonate buffer system of the ocean.

In a second stage, the pH of the ocean will be restored by the $CaCO_3$ cycle, replenishing the buffer capacity of the ocean and further drawing down atmospheric CO_2 as it seeks a balance between $CaCO_3$ sedimentation and terrestrial weathering. This neutralization stage has a time scale of 3–7 thousand years, and pulls the airborne fraction down to 10–25% of original CO_2 pulse after about 10,000 years (Archer and Brovkin, 2008; Lenton and Britton, 2006; Montenegro et al., 2007; Ridgwell and Hargreaves, 2007; Tyrrell et al., 2007).

The rest of the fossil fuel CO_2 will be removed from the atmosphere by silicate weathering, a slow process of CO_2 reaction with CaO of igneous rocks. This geological process takes up to several hundred thousand years (e.g., (Walker and Kasting, 1992)).

Main chemical reactions of fossil fuel CO_2 removal:

Seawater buffer (ocean invasion) $CO_2 + CO_3 = + H_2O$ <-> $2\ HCO_3-$ (dissolved in the ocean)
Reaction with calcium carbonate, $CaCO_3$ $CO_2 + CaCO_3 + H_2O$ -> $2\ HCO_3-$ (ocean)
Silicate weathering (reaction with igneous rocks) $CO_2 + CaSiO_3$ -> $CaCO_3 + SiO_2$ (ocean sediments)

[INSERT BOX 6.2, FIGURE 1 HERE]

Box 6.2, Figure 1: A fraction of emitted CO_2 remaining in the atmosphere in case of total CO_2 emissions of 100 (blue), 1,000 (red), and 5,000 GtC (black line) released at once in year 0. The graph shows results of the CLIMBER model (Archer et al., 2009b) extended up to 50 thousand years. Arrows indicate a sequence of natural processes of CO_2 removal operating on different time scales. Note that higher CO_2 emissions lead to higher airborne CO_2 fraction due to reduced carbonate buffer capacity of the ocean and positive climate-carbon cycle feedback.

[END BOX 6.2 HERE]

Terrestrial ecosystems have accumulated 124 ± 59 Pg of anthropogenic C during the same period, largely compensating the C losses from deforestation since 1750, mainly through the uptake of CO_2 by enhanced photosynthesis at higher CO_2 levels and N deposition, longer growing seasons in high latitudes, and the expansion and thickening of forests in temperate regions. This increased is inferred by mass balance as the difference between emissions and measured atmospheric and oceanic storage increase (Table 6.1).

6.3.2 Global CO_2 Budget

The anthropogenic CO_2 budget calculations are improved from those of the Fourth Assessment Report (AR4) (Denman et al., 2007). Revised data on the rates of land conversion from country statistics processed by the FAO (FAO, 2010) provides a more robust estimate of the land use change flux (Friedlingstein et al., 2010). In addition, a new global compilation of forest inventory data, based upon 100,000s of individual forest measurements, provides an independent estimate of the amount of carbon that has been gained by forests over the past two decades, albeit with very scarce data for tropical forest (Pan et al., 2011). The net air-sea CO_2 flux climatology established from repeated shipboard measurements was updated with a new global dataset of 3 million measurements of surface water pCO_2 (Takahashi et al., 2009), 2 million more observations than of the previous estimate. For both ocean and land regions, a continuing use of multiple constrains with atmospheric inversions (top down approaches) and ground-based observations and modeling (bottom up approaches) provides coarse scale consistent checks on the estimates for a number of regions (Ciais et al., 2010; McGuire et al., 2009; Piao et al., 2009b). The global anthropogenic CO_2 budget estimated from a range of observations and methods accounts for most of the trends in the CO_2 sinks, and a large part

of the observed variability (LeQuere et al., 2009; Sitch et al., 2008), although unaccounted interannual variability of up to 2 PgC yr^{-1} still remain to be explained (Section 6.3.2.5.1), and is largely driven by tropical latitudes as inferred from atmospheric CO_2 inversions (Figure 6.9).

[INSERT FIGURE 6.9 HERE]

Figure 6.9: The interannual variability of surface CO_2 fluxes from inversions of the TRANSCOM project for the period of 1990–2008. The ensemble of inversion results contains up to 17-atmospheric inversion models. The ensemble mean is bounded by the 1 sigma inter-model spread in ocean-atmosphere (blue) and land-atmosphere (green) CO_2 fluxes (PgC yr^{-1}) grouped into large latitude bands, and over the globe. For each flux and each region, the CO_2 flux anomalies were obtained by subtracting the long term mean flux from each inversion and removing the seasonal signal. Grey shaded regions indicate El Niño episodes, and the back bars indicate the cooling period following the Mt. Pinatubo eruption. A positive flux means a larger than normal source of CO_2 to the atmosphere (or a smaller CO_2 sink).

6.3.2.1 Emissions from Fossil Fuel Combustion and Industrial Processes

Global CO_2 emissions from the combustion of fossil fuels (coal, oil, natural gas) are determined from national energy consumption statistics and converted to emissions by fuel type (Marland and Rotty, 1984). Estimated errors for the annual global emissions are on the order of ±5% (±1 standard deviation), increasing to ±7% for recent decades where a larger fraction of the global emissions originate from emerging economies, where energy statistics are more uncertain (Gregg et al., 2008). CO_2 emissions from cement production were 4% of the total emissions during 2000–2009, compared to 3% in the 1990s. Additional emissions from gas flaring represent <1% of the global emissions.

Global CO_2 emissions from fossil fuel combustion and cement production were 7.7 ± 0.5 PgC yr^{-1} on average in the decade 2000–2009, 6.4 ± 0.4 PgC yr^{-1} during 1990–1999, and 5.5 ± 0.3 PgC yr^{-1} during 1980–1989 (Table 6.1). Global fossil fuel emissions increased by 2.9% yr^{-1} on average during the decade 2000-2009 compared to 1.0% yr^{-1} in the 1990s and 1.9% yr^{-1} in the 1980s. The increased growth since 2000 was caused primarily by rising use of coal for energy production in emerging economies and the growth in global wealth (Raupach et al., 2007); Figure 6.10). The global financial crisis in 2008–2009 induced only a small decrease in global emissions in 2009 (1.3 %), with the return to a high annual growth rate of 5.9% and record high in emissions of 9.1 PgC in 2010 (Peters et al., 2011).

[INSERT FIGURE 6.10 HERE]

Figure 6.10: CO_2 emissions from fossil fuel combustion and cement production by fuel type (PgC yr^{-1}). CO_2 emissions are estimated by the Carbon Dioxide Information Analysis Center (CDIAC) based on UN energy statistics for fossil fuel combustion and US Geological Survey for cement production (Boden et al., 2011).

6.3.2.2 Emissions from Land Use Change

CO_2 is also emitted to the atmosphere by deforestation and other land use activities. Clearing land for agriculture and other land use releases CO_2, often through combustion, and decomposition of dead plant material and soil organic matter. Regrowth of forest can partially compensate for emissions by taking up carbon from the atmosphere if trees are replanted or grow on abandoned agricultural lands. Logging and other forms of biomass removal emit CO_2 when wood products reach the end of their lifetime (e.g., through combustion or decaying in landfills). Approaches to estimate CO_2 fluxes from land use fall into three categories: (1) a so called “bookkeeping” method that tracks carbon in living vegetation, dead plant material, wood products and soils with cultivation, harvesting and reforestation using country-level reports on changes in forest area (Houghton, 2003); (2) process-based terrestrial ecosystem models that simulate carbon exchanges between vegetation, soil, and atmosphere using spatially-explicit data on land use change (see references in Table 6.2) and (3) detailed regional analysis based on satellite data estimate changes in forest area combined with abovementioned bookkeeping models or estimates of biomass loss with land use change, and subsequent decomposition of soil organic matter (Achard et al., 2004; DeFries et al., 2002). The bookkeeping method is based on land cover change and biomass data, but includes only simple process dynamics as decay and regrowth rates. Process-based models include more extensive process dynamics, but generate their own biomass and soil carbon that may differ from observations. Satellite-based estimates are data-rich but generally focus on the tropics only, and do not explicitly include CO_2 emissions that result from deforestation prior to their starting period and thus can underestimate CO_2 emissions by 13–62% depending on the starting year and decade (Ramankutty et al., 2006). Advances in estimating carbon emissions from

fire and separate accounting of deforestation-related fire emissions from other types of fires (van der Werf et al., 2010) provide additional information on interannual variability not available in AR4. None of the available estimates include emissions from peatland drainage, which have been estimated at 0.30 PgC yr^{-1} over 1997–2006 (van der Werf et al., 2009).

Table 6.2: Estimates of land to atmosphere emissions from land use changes (Pg yr^{-1}). Positive values indicate carbon losses from land ecosystems.

	Land Use Database[h]	Climate	1980–1989 GtC yr^{-1}	1990–1999 GtC yr^{-1}	2000–2009 GtC yr^{-1}
Satellite-based Methods (tropics only)					
(Achard et al., 2002)	Landsat	observed		0.64 ± 0.21[a]	
(DeFries et al., 2002)	AVHRR	observed	0.6 (0.3–0.8)	0.9 (0.5–1.4)	
(van der Werf et al., 2010)	GFED	observed			0.83
Bookeeping Method (global) [a]					
(Friedlingstein et al., 2010)	FAO-2010	no variability	1.4 ± 0.5[d]	1.5 ± 0.5[d]	1.1 ± 0.5[d]
Process Models (global) [b]					
(Shevliakova et al., 2009)	HYDE	no variability	1.1	1.1	
(Shevliakova et al., 2009)	SAGE	no variability	1.4	1.3	
(Piao et al., 2009a)		observed	1.0		
(vanMinnen et al., 2009)	HYDE	no variability	1.3	1.3	
(vanMinnen et al., 2009)	HYDE+pastures	no variability	1.6	1.6	
updated from (vanMinnen et al., 2009)	HYDE	no variability	1.2	1.1	1.1[c]
(Strassmann et al., 2008)	HYDE	no variability	1.3	1.3	
updated from (Stocker et al., 2011)	HYDE	no variability	1.4	0.9	0.6
(Yang et al., 2010)	SAGE	observed	1.2	1.0	0.8[c]
(Yang et al., 2010)	FAO-2005	observed	1.7	1.4	
updated from (Yang et al., 2010)	HYDE	observed	1.7	0.9	0.9
updated from (Arora and Boer, 2010)	HYDE crop	averaged[e]	0.5[e]	0.5[e]	0.5[e]
Average of process models[f]			1.3 ± 0.2	1.1 ± 0.2	0.8 ± 0.2
Global average[g]			1.3 ± 0.5	1.3 ± 0.5	0.9 ± 0.5

Notes:
(a) Based on observed land cover change and observed vegetation biomass, but with limited process dynamics.
(b) Based on observed land cover change but modeled vegetation biomass, with more explicit vegetation dynamics.
(c) 2000–2005 only.
(d) Uncertainty from sensitivity study presented in (Houghton, 2005), excluding the older 1981 data. It includes an assessment of uncertainty associated with the rate of deforestation and with the vegetation biomass.
(e) The large variability produced by the calculation method is removed for comparison with other studies by averaging the flux over the three decades.
(f) Average of all estimates. The uncertainty represents ±1 Mean Absolute Deviation from the mean.
(g) Average of the global methods. The uncertainty is assumed independent and added quadratically.
(h) References for the databases used: GFED (van der Werf et al., 2009); HYDE (Goldewijk et al., 2011), SAGE (Ramankutty and Foley, 1999).

Global CO_2 emissions from land use change are estimated at 1.3 ± 0.5, 1.3 ± 0.5, and 0.9 ± 0.5 PgC yr^{-1} for the 1980s, 1990s, and 2000s, respectively (Table 6.2). The lower emissions reported in the 2000s compared to the 1990s is within the error bar of the data and methods, though it is corroborated by satellite monitoring which also reported a decrease in deforestation in the Brazilian Amazon for the latter part of this decade

(Nepstad et al., 2009) and in tropical Asia relative to the 1990s (Hansen et al., 2009). 54 percent of the emissions originated from the tropics in the 1980s on average across methods, a share that increased to 67% in the 1990s and 74% in the 2000s. However the range of estimates is large and estimates from the bookkeeping method and process models do not agree in the extra tropics (Table 6.3).

Table 6.3: Estimates of land to atmosphere emissions from land use changes (PgC yr^{-1}) for decadal periods from 1980s to 2000s. Positive values indicate carbon losses from land ecosystems. Uncertainties are reported as ±1 standard deviation. Numbers in parentheses are ranges in uncertainty provided in some studies. Tropical Americas include all Central and South American countries. Tropical Asia includes the middle East, India and surrounding countries, Indonesia and Papua New Guinea. East Asia includes China, Japan, Mongolia and Korea.

	Tropical Americas	Africa	Tropical Asia	North America	Eurasia	East Asia	Oceania
2000s							
(van der Werf et al., 2010)[a,b]	0.33	0.15	0.35				
(DeFries and Rosenzweig, 2010)[c]	0.46	0.08	0.36				
(Friedlingstein et al., 2010)	0.48	0.31[e]	0.25	0.01	–0.07[d]	0.01[e]	
(vanMinnen et al., 2009)[a]	0.50	0.15	0.16	0.09	0.08	0.13	0.01
(Stocker et al., 2011)[a]	0.19	0.18	0.21	0.019	–0.067	0.12	0.011
(Yang et al., 2010)[a]	0.11	–0.10	0.19	0.25	0.27	0.13[d]	0.02
Average	0.35 ± 0.14	0.13 ± 0.09	0.25 ± 0.07	0.09 ± 0.08	0.05 ± 0.12	0.10 ± 0.04	0.01 ± 0.00
1990s							
(DeFries et al., 2002)	0.5 (0.2–0.7)	0.1 (0.1–0.2)	0.4 (0.2–0.6)				
(Achard et al., 2004)	0.3 (0.3–0.4)	0.2 (0.1–0.2)	0.4 (0.3–0.5)				
(Friedlingstein et al., 2010)	0.67	0.32[e]	0.45	0.05	–0.04	0.05[e]	
(vanMinnen et al., 2009)[a]	0.42	0.12	0.15	0.08	0.08	0.25	0.01
(Stocker et al., 2011)[a]	0.30	0.14	0.19	–0.072	0.11	0.27	0.002
(Yang et al., 2010)[a]	0.16	–0.16	0.22	0.25	0.32	0.16[d]	–0.01
Average	0.37 ± 0.14	0.12 ± 0.12	0.28 ± 0.11	0.08 ± 0.09	0.12 ± 0.10	0.18 ± 0.08	0.01 ± 0.01
1980s							
(DeFries et al., 2002)	0.4 (0.2–0.5)	0.1 (0.08–0.14)	0.2 (01–0.3)				
(Friedlingstein et al., 2010)	0.79	0.22[e]	0.32	0.04	0.00	0.07[e]	
(vanMinnen et al., 2009)[a]	0.36	0.15	0.17	0.07	0.07	0.40	0.00
(Stocker et al., 2011)[a]	0.44	0.16	0.25	0.085	0.11	0.40	0.009
(Yang et al., 2010)[a]	0.21	–0.16	0.27	0.27	0.57	0.54[d]	–0.01
Average	0.44 ± 0.10	0.09 ± 0.13	0.12 ± 0.04	0.12 ± 0.08	0.19 ± 0.19	0.34 ± 0.11	0.01 ± 0.01

Notes:
(a) Updated results.
(b) Based on estimates of carbon emissions from deforestation and degradation fires, including peat carbon emissions. Estimates were doubled to account for emissions other than fire including respiration of leftover plant materials and soil carbon following deforestation following (Olivier et al., 2005). Estimates include peat fires and oxidation. If peat fires are excluded, estimate in tropical Asia is 0.23 and Pan-tropical total 0.71.
(c) CO_2 estimates were summed for dry and humid tropical forests, converted to C and normalized to annual values. Estimates are based on satellite-derived deforestation area (Hansen et al., 2010), and assume 0.6 fraction of biomass emitted with deforestation. Estimates do not include carbon uptake by regrowth. Estimates cover emissions from 2000–2005.
(d) Includes China only.
(e) East Asia and Oceania are averaged in one region. The flux is split in two equally for computing the average; North Africa and the Middle East are combined with Eurasia.

[INSERT FIGURE 6.11 HERE]

Figure 6.11: CO2 emissions from land use change from a range of methods (PgC yr–1). Estimates are from (Friedlingstein et al., 2010), thick black, (Pongratz et al., 2009), thin black, (Shevliakova et al., 2009), HYDE data: cyan full, SAGE data: cyan dotted, (vanMinnen et al., 2009), updated HYDE: green full, HYDE data: green dotted, HYDE with pastures: green dashed, (Piao et al., 2008), blue, (Strassmann et al., 2008), red dotted, (Stocker et al., 2011), red, (Yang et al., 2010) updated HYDE: purple full; FAO data: purple dash; SAGE data: purple dotted).

The estimates shown in Figure 6.11 are the net CO_2 emissions from land use change, which includes (1) the CO_2 emitted during deforestation and other land use change, (2) CO_2 emitted in the years after deforestation from soils and litter decomposition, (3) CO_2 uptake from secondary forest regrowth on abandoned lands and reforestation, and (4) other land use processes such as logging and wood harvesting. (Pan et al., 2011) estimated gross emissions from tropical deforestation, sum of terms (1) and (2) above, at 3.0 ± 0.5 PgC yr^{-1} for the 1990s and 2.8 ± 0.5 PgC yr^{-1} for the 2000s. Thus the gross emissions caused by deforestation are about double the net emissions because of the presence of a large regrowth compensating half of the deforestation fluxes.

The uncertainties in land use CO_2 emissions reduced from AR4's range of 0.5 to 2.7 PgC yr^{-1} for the 1990s to ±0.5 PgC yr^{-1} in this assessment because of improved accuracy of land cover change incorporating satellite data, a the larger number of independent methods to quantify emissions and the consistency of the reported results (Table 6.2). In particular, the FAO forests area loss were revised downwards in 2010 following improvements in data coverage, for instance over Indonesia were new data were introduced and the Amazon where higher resolution satellite data were used (FAO, 2010).

Over the 1750–2011 time period, CO_2 emissions of 151 ± 51 PgC can be estimated using the recent land use fluxes of 25 ± 6 PgC during 1980–2010 (Table 6.1) and the average of the three publications that have estimated land use emissions during 1750–1980: (Pongratz et al., 2009) - 111 PgC, (vanMinnen et al., 2009) - 119 PgC, and (Shevliakova et al., 2009) - 222 PgC. The CO_2 flux from land use has been dominated by deforestation and other land use change in the high latitudes prior to 1980s, and in the tropics since approximately 1980, largely from deforestation in tropical America and Asia with smaller contributions from tropical Africa.

6.3.2.3 Atmospheric CO_2 Concentration Growth Rate

Since preindustrial times (1750), the concentration of CO_2 in the atmosphere increased by 40%, from 278 ± 3 ppm to 388.5 ± 0.1 ppm in 2010 year (Figure 6.12), (MacFarling-Meure et al., 2006), corresponding to an increase in CO_2 of 238 ± 7 PgC in the atmosphere. Atmospheric CO_2 grew at a rate of 3.4 ± 0.3 PgC yr^{-1} in the 1980s, 3.1 ± 0.2 PgC yr^{-1} in the 1990s, and 4.0 ± 0.2 PgC yr^{-1} in the 2000s (Conway and Tans, 2011): NOAA/ESRL (www.esrl.noaa.gov/gmd/ccgg/trends/). The rise of atmospheric CO_2 is established with a very small uncertainty from measurements of CO_2 trapped in air bubbles in ice cores between 1750 and 1957 e.g., (Etheridge et al., 1996), and from highly precise atmospheric CO_2 concentration measurements after that date (Keeling et al., 1976).

[INSERT FIGURE 6.12 HERE]

Figure 6.12: Atmospheric concentration history over the last 260 years determined from air enclosed in ice cores, firn air and direct atmospheric measurements (MacFarling-Meure et al., 2006).

There is ample evidence that the atmospheric increase is caused by the anthropogenic emissions of CO_2 because of the corresponding measured increases in the abundance of $^{14}CO_2$ (before nuclear bomb testing) isotopes (Lassey et al., 2007) and the small decrease in molecular oxygen (O_2) in the atmosphere (Manning and Keeling, 2006), all of which are affected by fossil fuel combustion in known proportions (Figure 6.1). Furthermore, the CO_2 concentration in the atmosphere increases faster in the Northern hemisphere compared to the Southern hemisphere (see Section 6.1), a signal which tracks the increasing fossil CO_2 emissions in the northern hemisphere (Fan et al., 1999; Keeling et al., 1989b; Tans et al., 1989).

The ice core record of atmospheric CO_2 concentration during the past century also exhibits some interesting features, which can be related to climate induced-changes in the carbon cycle. Most conspicuous is the time

interval from about 1940 until the early 1960's, during which the concentration increase of CO_2 (also CH_4 and N_2O) stalled (MacFarling-Meure et al., 2006), possibly caused by slightly decreasing temperatures over land in the northern hemisphere (Rafelski et al., 2009).

There is substantial evidence (e.g., from ^{13}C carbon isotopes, (Keeling et al., 2005) that source/sink processes on land generate most of the interannual variability in the atmospheric CO_2 growth rate (Figure 6.12; Section 6.3.2.5). The Hovmöller diagram suggests that the strong positive anomalies of the CO_2 growth rate in El Niño years (e.g., 1987/1988 and 1997/1998) originated in tropical latitudes, while the anomalies in 2003 and 2005 originated in northern midlatitudes, maybe reflecting the European heat wave in 2003 (Ciais et al., 2010).

[INSERT FIGURE 6.13 HERE]

Figure 6.13: Top panel: Global average atmospheric CO_2 growth rate; symbols: annual means (Keeling et al., 2005); (Conway et al., 1994). Bottom panel: Atmospheric growth rate of CO_2 as a function of latitude determined from the GLOBALVIEW data product, representative for the marine boundary layer (Masarie and Tans, 1995).

6.3.2.4 Ocean Sinks

6.3.2.4.1 Global ocean sink

The estimate of the mean anthropogenic ocean CO_2 sink from AR4 (2.2 ± 0.4 PgC yr^{-1}) is unchanged and confirmed by a variety of contemporary estimates ranging from 1.8 to 2.4 Pg C yr^{-1} for the 1990s (see summary in (Gruber et al., 2009)). The uptake of anthropogenic CO_2 by the oceans is primarily a response to increasing CO_2 in the atmosphere and is limited primarily by the rate at which anthropogenic CO_2 is transported from the ocean surface into the ocean interior (Gloor et al., 2010). However, this anthropogenic uptake occurs on top of a very active natural carbon cycle. Recent trends in the climate system, such as ocean warming, changes in ocean circulation, and changes in marine ecosystems and biogeochemical cycles can affect both the anthropogenic uptake as well as the natural carbon cycle. Since AR4, much progress has been made to quantify the rate of change of the net ocean CO_2 sink in the past decades, including both the response of the oceans to increasing CO_2 in the atmosphere, and its response to climate change and variability.

Observations show that to a first order, surface ocean partial pressure of CO_2 (pCO_2) has been increasing generally at about the same rate as the atmosphere when averaged over large regions over the past two to three decades (McKinley et al., 2011; Takahashi et al., 2009). However, analyses of regional observations highlighted substantial regional and temporal variations around this trend, with surface ocean pCO_2 increasing at the same rate or faster than atmospheric CO_2 (thus a constant or weakening sink for anthropogenic CO_2) between about 1990 and 2005 in the North Atlantic (Schuster et al., 2009), and between 1981 and 2004 in the western equatorial Pacific (Feely et al., 2006) and Southern Ocean (LeQuere et al., 2007). By contrast, pCO_2 appears to have increased at a slower rate than atmospheric CO_2 (thus a CO_2 growing sink) in the North Pacific Ocean (Takahashi et al., 2006).

The difference in decadal rates of uptake of anthropogenic CO_2 by the oceans was estimated with an ensemble of five estimates using various methods giving an uptake of 2.0 ± 0.5 PgC yr^{-1} for the 1980s and 2.3 ± 0.5 PgC yr^{-1} for 2000–2009 (Table 6.4). Methods used are of different nature: (1) An empirical Green's function approach fitted to observations of transient tracers (Khatiwala et al., 2009), (2) a model-based Green's function approach fitted to anthropogenic CO_2 reconstructions (MikaloffFletcher et al., 2006), (3) data-driven relationships between surface pCO_2 and temperature and salinity (Park et al., 2010), and (4) process-oriented global ocean biogeochemical models forced by observed meteorological fields (Assmann et al., 2010; Aumont and Bopp, 2006; Doney et al., 2009; LeQuere et al., 2010). All these different methods suggest that in the absence of recent climate change and climate variability, the ocean anthropogenic CO_2 sink should have increased by 0.20 ± 0.05 PgC yr^{-1} between the 1980s and the 1990s, and by 0.30 ± 0.06 PgC yr^{-1} between the 1990s and the 2000s, where the uncertainty represents ±1 Mean Absolute Deviation of the ensemble (Figure 6.14). The different rates of change are caused by the faster rate of increase of atmospheric CO_2 in the later decade. Climate change and variability has no noticeable effect on the difference between the 1980s and the 1990s (0.02 ± 0.02 PgC yr^{-1}), but it is estimated by models to have reduced the ocean CO_2 sink by 0.19 ± 0.10 PgC yr^{-1} between the 1990s and the 2000s (Table 6.4).

Table 6.4: Estimates of changes in ocean-to-atmosphere CO_2 flux compared to 1990–1999.

	19801989 GtC yr^{-1}	1990–1999 GtC yr^{-1}	2000–2009 GtC yr^{-1}
Anthropogenic			
(Assmann et al., 2010) (to 2007 only)	0.28	reference	–0.35
ETH model [b]	0.15	reference	–0.25
(Doney et al., 2009)	0.15	reference	–0.39
(LeQuere et al., 2010) - NCEP	0.16	reference	–0.32
(LeQuere et al., 2010) - ECMWF	–	reference	–0.39
(LeQuere et al., 2010) –JPL	–	reference	–0.32
(Khatiwala et al., 2009) a	0.24	reference	-0.20
(MikaloffFletcher et al., 2006)[c]	0.4	reference	–0.44
Average[a]	0.23 ± 0.12		–0.33 ± 0.06
Natural			
(Assmann et al. 2010) (to 2007 only)	0.07	reference	0.00
ETH model [b]	0.02	reference	0.27
(Thomas et al., 2008)	–0.02	reference	0.21
(LeQuere et al., 2010) -NCEP	0.02	reference	0.27
(LeQuere et al., 2010) -ECMWF	–	reference	0.14
(LeQuere et al., 2010) -JPL	–	reference	0.36
(Park et al., 2010)	–	reference	0.15
Average[a]	0.02 ± 0.02		0.19 ± 0.10

Notes:
(a) Average of all methods. The uncertainty represents ±1 Mean Absolute Deviation from the mean. The anthropogenic average includes results Le Quéré et al. (2010)-NCEP only because the other model versions do not differ sufficiently to be considered separately.
(b) Using the model of (Doney et al., 2009) with quadratic relationship with wind speed and different atmospheric forcing.
(c) As published by (Sarmiento et al., 2010).

[INSERT FIGURE 6.14 HERE]
Figure 6.14: Trends in the air-sea flux of CO_2 in response to (top) variability and trends in surface climate, (middle) increasing atmospheric CO_2, and (bottom) the sum of both effects from a range of methods (PgC yr^{-1}). All estimates are normalized to zero during 1950-1960 to highlight the trends. Estimates are updates from: (Doney, 2010), dark blue for standard version, green for ETH version; (Aumont and Bopp, 2006), magenta; (LeQuere et al., 2010), cyan; (Assmann et al., 2010), red; (Park et al., 2010), top black; (Khatiwala et al., 2009), middle black.

6.3.2.4.2 Regional air-sea fluxes

Because of the importance of the natural carbon cycle, the net air-sea fluxes of CO_2 show regions in the ocean where CO_2 is absorbed from the atmosphere, and regions where CO_2 is released to the atmosphere, even though overall the oceans absorb about 2 PgC every year. The Equatorial Pacific (14°N–14°S) is a major source for atmospheric CO_2, losing about 0.5 Pg C yr^{-1}. The temperate oceans, between 14° and 50° in the both hemispheres, are major sink zones. On a per unit area basis, the high latitude North Atlantic, including the Nordic Seas and portion of the Arctic, is the most intense CO_2 sink region due to the combination of high wind speeds and low pCO_2 caused by strong biological productivity and strong cooling. The CO_2 sink is not as intense in the Southern Ocean (<44°S) because of a cancellation of the summer uptake with the winter release of CO_2 caused by the upwelling of CO_2-enriched deepwater (Gruber et al., 2009).

6.3.2.4.3 Regional changes in carbon storage

Data-based estimates for the global ocean inventory of anthropogenic carbon (Khatiwala et al., 2009; Sabine et al., 2004; Waugh et al., 2006) extended to the end of year 2010 using the ocean uptake of anthropogenic carbon of Table 6.1 agree well among each other with values of 154 ± 20 PgC, 144 ± 14 PgC and 151 ± 40 PgC, respectively. The flux of anthropogenic carbon into the ocean is increasing faster in the high latitudes than in the tropics and subtropics where the uptake is relatively low (Khatiwala et al., 2009). Total changes in carbon storage can be observed from repeat measurements from hydrographic sections. A number of ocean cross sections have been run over the last decade and the observed changes, summarized in Table 6.5, suggest that some locations see rates of carbon accumulation that are higher and others that are lower than the global average estimated by (Khatiwala et al., 2009). No global synthesis of these observations exists at present. Model results suggest that there may be an effect of climate change and variability in the storage of total carbon in the ocean (Table 6.4), but it is small (~2 PgC over the past 50 years; Figure 6.14) in the historical context of the uptake of anthropogenic carbon. We adopt in this chapter an estimate of 154 ± 20 PgC of anthropogenic C accumulated into the world oceans for the 1750–2010 time period, based on (Sabine et al., 2004) up to 1994 as it is the estimate most closely based on observations, and the contemporary CO_2 sink estimates based on combined observations and model trends for 1994–2010 (Table 6.1).

Table 6.5: Regional rates of change in inorganic carbon storage

Section	Time	Storage rate (mol m^{-2} yr^{-1})	Data source
Global average	2008	0.53 ± 0.16	(Khatiwala et al., 2009)
Pacific Ocean			
Section along 30°S	1992–2003	1.0 ± 0.4	(Murata et al., 2007)
N of 50°S, 120°W–180°W	1974–1996	0.9 ± 0.3	(Peng et al., 2003)
154°W, 20°–50°S	1991–2006	0.56 ± 0.04	(Sabine et al., 2008)
140°E – 170°W, 45°S–65°S	1968–1991/1996	0.40 ± 0.20	(Matear and McNeil, 2003)
149° W, 4°S–10°N	1993– 2005	0.3 ± 0.1	(Murata et al. 2009)
149° W, 24°N–30°N	1993– 2005	0.6 ± 0.2	(Murata et al. 2009)
Northeast Pacific	1973–1991	1.3 ± 0.5	(Peng et al., 2003)
~160°E ~45°N	1997–2008	0.40 ± 0.08	(Wakita et al., 2010)
North of 20°N	1994–2004/2005	0.39 ± 0.15	(Sabine et al., 2008)
150°W, 20°S–20°N	1991/1992–2006	0.25 ± 0.09	(Sabine et al., 2008)
Indian Ocean			
20°S–10°S	1978–1995	0.1	(Peng et al., 1998)
10°S–5°N	1978–1995	0.65	(Peng et al., 1998)
Section along 20°S	1995–2003/2004	1.0 ± 0.1	(Murata et al., 2010)
Atlantic Ocean			
Section along 30°S	1992/1993–2003	0.6 ± 0.1	(Murata et al., 2010)
~30°W, 56°S–15°S	1989–2005	0.76	(Wanninkhof et al., 2010)
20°W, 64°N–15°N	1993–2003	0.57	(Wanninkhof et al., 2010)
~25°W, 15°N–15°S	1993–2003	0.2	(Wanninkhof et al., 2010)
40°N–65°N	1981–1997/1999	2.2 ± 0.7	(Friis et al., 2005)

20°N– 40°N	1981–2004	1.2 ± 0.3	(Tanhua et al., 2007)
Nordic Seas	1981–2002/2003	0.9 ± 0.2	(Olsen et al., 2006)
Sub-decadal variations			
Irminger Sea	1981–1991	0.55 ± 0.39	(Perez et al., 2008)
Irminger Sea	1991–1996	2.3 ± 0.6	(Perez et al., 2008)
Irminger Sea	1997–2006	0.75 ± 0.16	(Perez et al., 2008)

6.3.2.4.4 Interannual variability in air-sea fluxes

The variability in the global ocean CO_2 sink is small compared to the variability coming from the terrestrial biosphere. In general, the oceans take up a few tenth of PgC yr^{-1} more CO_2 during El Niño years (Park et al., 2010). This is because of the temporary suppression of the source of CO_2 to the atmosphere over the eastern Pacific, during El Nino episodes. Similar interannual variability of ≈0.3 PgC yr^{-1} has been reported for the North Atlantic (Watson et al., 2009). The detection of changes in surface ocean CO_2 over several years to decades and attributions of drivers is a challenge because of the large heterogeneity of the surface ocean and the large seasonal cycle (~60 ppm at high latitudes; (Takahashi et al., 2009)). In regions where there are sufficient observations (>2 decades), the anthropogenic CO_2 uptake (through air-sea exchange) is usually the main driver of the air-sea CO_2 flux changes. However, this is modulated by natural variability on interannual to decadal time scales (McKinley et al., 2011).

6.3.2.5 Land Sinks

6.3.2.5.1 Global land sink

The land sink of CO_2 cannot be measured directly because of the huge heterogeneity of terrestrial ecosystem fluxes and pools. However, independent constraints allow an assessment of the magnitude and variability of land sink at the global scale. Global budget analyses constrained by observations of atmospheric CO_2 concentrations, fossil fuel emissions and ocean observations and models arrive at an aggregated estimate of the net land sink processes as a residual necessary to satisfy mass conservation, giving an uptake of 1.4 ± 0.8, 2.4 ± 0.8 and 2.3 ± 0.9 PgC yr^{-1} for the 1980s, 1990s, and 2000s, respectively (Table 6.1). The larger sink of anthropogenic carbon in the early 1990s has been associated with the response of the terrestrial ecosystems to the eruption of Mount Pinatubo and its effect on temperature and light (Mercado et al., 2009).

Global biospheric models forced by the same observationally-constrained surface weather field and observed atmospheric CO_2 concentrations estimate a sink of 1.8 ± 0.7 for the 1980s, 2.3 ± 0.9 for the 1990s and 2.6 ± 1.4 for the 2000s (Table 6.6). None of these models include land use change effects nor forest demography changes. The net flux of anthropogenic C into the terrestrial biosphere (including land use change emissions plus the residual sinks) has intensified globally from a small sink of 0.1 ± 0.7 PgC yr^{-1} in the 1980s to a larger sink of 1.1 ± 0.6 and 1.4 ± 0.7 PgC yr^{-1} during the 1990s and 2000s, respectively (Table 6.1; (Sarmiento et al., 2010)). This is consistent with trends in the net flux over land estimate from inversion methods, which estimate an increasing air-to-land flux of 0.57 ± 0.1 PgC yr^{-1} per decade (Gurney and Eckels, 2011), and could be driven by a combination of decreased land use change emissions since 2000 (Table 6.1) and response of vegetation to climate change and variability (Figure 6.15).

Table 6.6: Estimates of land-to-atmosphere CO_2 flux by Global Vegetation Models.

Model name	N-limitation (yes/no)	1980–1989 GtC yr^{-1}	1990–1999 GtC yr^{-1}	2000–2009 GtC yr^{-1}
CLM4C[b, c]	?	1.53	1.62	1.46
CLM4CN[b, c]	Yes	1.13	1.16	1.23
HY[d]	No	2.83	3.59	4.47
LPJ[e]	No	1.19	1.89	2.14

LPJ_GUESS[f]	No	1.05	1.56	0.92
OCN[g]	Yes	1.52	1.84	2.23
ORC[h]	No	2.08	3.05	3.74
SDGVM[i]	?	1.69	2.01	2.22
TRI[j]	?	1.78	2.59	3.84
VEGAS[k]	No	0.65	0.90	0.76
VISIT[l]	No	4.45	5.06	5.96
Average[a]		1.80 ± 0.72	2.30 ± 0.93	2.63 ± 1.36

Notes:
(a) Average of all methods. The uncertainty represents ±1 Mean Absolute Deviation from the mean.
(b) (Oleson et al., 2010)
(c) (Lawrence et al., 2011)
(d) (Levy et al., 2004)
(e) (Sitch et al., 2003)
(f) Smith et al., 2001
(g) (Zaehle and Friend, 2010)
(h) (Krinner et al., 2005)
(i) (Woodward and Lomas, 2004)
(j) (Cox, 2001a);
(k) (Zeng, 2003)
(l) (Ito, 2008).
All these models run through considering rising CO2 concentration and climate change following the historical climate carbon cycle model intercomparison project (Trendy) protocol (http://www.globalcarbonproject.org/global/pdf/DynamicVegetationModels.pdf).

[INSERT FIGURE 6.15 HERE]
Figure 6.15: Time series for the land CO_2 sink showing the residual of the budget (emissions from fossil fuel and land use change, minus the atmospheric growth and the ocean sink; gray shading) and results from global biospheric models (see Table 6.6 for references). The gray shading shows one Mean Absolute Deviation from the mean.

6.3.2.5.2 Regional air-land fluxes

Atmospheric CO_2 inversions, terrestrial models and forest inventories consistently show that the largest net terrestrial CO_2 sink is located in the Northern ex-tropics (Gurney and Eckels, 2011; Jacobson et al., 2007; Pan et al., 2011; Sitch et al., 2008) (Figure 6.16). The tropics remain highly unconstrained with atmospheric CO_2 stations, and inversion approaches show flux estimates ranging from neutral to a net source of at least 0.5–1.0 PgC (Gurney and Eckels, 2011; Jacobson et al., 2007). (Stephens et al., 2007) selected from ensemble of inversion models, those that were consistent with independent aircraft cross-validation data, and inferred a Tropical net land CO_2 source of 1.5 ± 0.6 PgC yr^{-1} during the period 1992–1996, and a northern hemisphere net land CO_2 sink of equivalent magnitude.

[INSERT FIGURE 6.16 HERE]
Figure 6.16: Decadal average CO_2 fluxes for 22 regions of the globe for the 1990s (blue) and 2000s (cyan). The mean values are calculated from monthly-mean fluxes from 17 inverse models of the TRANSCOM project for the period of 1990–2008,and standard deviations shown as error bars are for model-to-model differences within each decade. The minimum and maximum ranges of averages for the decade of 2000s are shown as the shaded envelope.

A number of regions have compared and reconciled regional flux estimates from multiple approaches and so providing an important test for the degree of confidence on their net carbon balance and contribution to global fluxes. This approach has yielded regional sink estimates including a 0.5 PgC yr^{-1} sink for North America (SOCCR: 2007), 0.3 PgC yr^{-1} sink for Europe (Schulze, 2009), 0.2 PgC yr^{-1} sink for China (Piao et al., 2009b), and 0.4 ± 0.4 PgC yr^{-1} sink for the Arctic (McGuire et al., 2009). A broader analysis of regional contributions estimated a 1.7 PgC yr^{-1} sink in the Northern Hemisphere above 20°N with consistent estimates from terrestrial models and inventories (uncertainty: ±0.3 PgC yr^{-1}) and atmospheric CO_2 inversions (uncertainty: ±0.7 PgC yr^{-1}) (Ciais et al., 2010). In these studies, accounting for other GHGs, in addition to CO_2, leads to decreased strength of regional sinks and, in some instances, to the complete

cancellation; Europe's 0.3 PgC yr^{-1} net CO_2 sink is largely cancelled out by CH_4 and N_2O emissions from agriculture and livestock (Schulze et al., 2009).

An assessment of the contribution of forest to regional land sinks based on forest biomass inventory data, with coarse estimates of soil carbon balance, and the bookkeeping model of (Houghton, 2003) for deforestation emissions, estimated a biome distribution of the 2000–2007 sink of 0.5 PgC yr^{-1} to boreal forests, 0.8 PgC yr^{-1} to temperate forests, and a net zero flux (sinks minus deforestation emissions) to tropical forests (Pan et al., 2011).

6.3.2.5.3 Interannual variability of land fluxes

Variability of the global land sink of anthropogenic carbon can be inferred from the residual term of the global budget, which shows that land flux variability accounts for most of the interannual variability of the atmospheric CO_2 growth rate (Figures 6.8 and 6.14). CO_2 regional anomalies suggest that the tropical land dominates the global CO_2 variability with positive anomalies with El Nino years (Baker et al., 2006; Bousquet et al., 2000; Rodenbeck et al., 2003), which is consistent with an inversion of atmospheric ^{13}C and CO_2 measurements (Rayner et al., 2008). A combined ENSO-Volcanic index time series explains 75% of the observed variability (Raupach et al., 2008). Positive phase of ENSO (El Niño) is associated with enhanced land CO_2 source, and negative phase (La Niña) is associated with enhanced land CO_2 sink (Jones and Cox, 2001; Peylin et al., 2005). Observations from eddy covariance networks suggest that interannual carbon flux variability in the tropics and temperate regions is dominated by precipitation, while boreal ecosystem fluxes are more sensitive to temperature and shortwave radiation variation (Jung et al., 2011).

6.3.2.5.4 Land-ocean fluxes

Estimates of the delivery of carbon from land to the oceans through riverine transport are ~0.2 for Dissolved Organic Carbon (DOC), 0.3 for Dissolved Inorganic Carbon (DIC), and 0.1-0.4 Pg yr^{-1} for Particulate Organic Carbon (POC) (Mayorga et al., 2010; Seitzinger et al., 2005; Syvitski et al., 2005). Regional DIC lateral fluxes are elevated by agricultural practices (Hamilton et al., 2007; Oh and Raymond, 2006; Perrin et al., 2008) and coupled with climate change can lead to large increases in regional scale DIC export in watersheds with a large agricultural footprint (Raymond et al., 2008). Furthermore, urban/suburbanization also elevate DIC fluxes (Baker et al., 2008; Barnes and Raymond, 2009) which collectively suggests that anthropogenic activities could contribute a significant portion of the annual global DIC flux to the ocean, but a partition between natural and anthropogenic is not yet possible.

Land clearing and management have led to an acceleration of POC transport, much of which is trapped in alluvial and colluvial deposition zones, lakes, reservoirs, and wetlands (Smith et al., 2001; Stallard, 1998; Syvitski et al., 2005). One study has argued that due to its long residence time in these new depositional environments this process leads to a sink of ~0.1 PgC yr^{-1} (Van Oost et al., 2007). Due to the central role of wetlands on DOC export (Seitzinger et al., 2005) the loss of global wetlands is probably the largest anthropogenic driver of global DOC fluxes to date, although a global estimate of this alteration is not available.

6.3.2.6 Airborne Fraction

The fraction of the total emissions of CO_2 (fossil fuel + LUC) that remain in the atmosphere - the 'airborne fraction' (AF) - is an important diagnostic of the efficiency and variability of the CO_2 sinks at absorbing excess CO_2 from anthropogenic emissions. Several factors can influence the AF. First and most importantly, the sinks respond to the rate of change of the emissions. The AF should be constant if emissions grow exponentially with a constant e-folding time (Bacastow and Keeling, 1979; Gloor et al., 2010). However, other secondary factors can influence the AF, such as the response of carbon reservoirs to elevated CO_2, nutrient availability, land management, warming, changes in physical climate and changes in terrestrial and marine ecosystems (ie, non linear carbon-climate feed backs). Climate and CO_2 effects were suggested to be important drivers of AF changes in future projections (Friedlingstein et al., 2006), increasing the AF by 0.07 (median of 11 models; range of 0.01–0.22; (Canadell et al., 2007)) in 2100 under the A2 high emissions scenario.

Up to AR4 no significant trend in AF had been identified in the recent past. Until recently, the uncertainty in LUC emissions was too large to provide a meaningful measure of the trend in AF, and a definition of the AF

using fossil fuel emissions only was used, including Figure 7.4 in AR4. Improved forest area loss statistics (FAO, 2010) and satellite surveys (Hansen et al., 2010; Regalado, 2010) have contributed to reducing the uncertainty in tropical LUC estimates (Section 6.3.5.2). A positive trend in AF of ~0.3% yr^{-1} was found by all recent studies using total CO_2 emissions over the ~1960-2010 time period, but there is disagreement on the significance and cause of this trend (Canadell et al., 2007; Gloor et al., 2010; Knorr, 2009; Raupach et al., 2008). The significance of the AF positive trend is influenced by the specific consideration of uncertainty and by the method used to filter out known variability associated with El Niño and volcanic activity. It was above 90% significant (90% chances that the trend is not accidental) in (Raupach et al., 2008) and related papers, but not in the other two independent studies. The cause of the trend is difficult to establish in the context where there is considerable uncertainty as to its significance. Although the preeminent role of changes in emissions growth rates in determining the AF trend is not disputed, (Gloor et al., 2010) and (LeQuere et al., 2009) cannot account for a positive trend with the observed changes in emissions alone. (LeQuere et al., 2009) can explain a positive trend using a multi-model ensemble of seven global models (4 land and 3 ocean models) only when climate change and variability are taken into account, suggesting that the AF trend was caused by the response of the carbon sinks to climate. (Gloor et al., 2010) argue that the observed positive trend in AF is driven by four extreme events only and that the fact that the trend is positive is accidental. It is too early to conclude on the significance and cause of the AF trend given the lack of agreement in the published literature.

6.3.2.7 Processes Driving CO_2 Fluxes

6.3.2.7.1 Ocean processes

Three type of processes are thought to have an important effect on the fluxes of CO_2 between the atmosphere and the ocean on century time scales: 1) the dissolution of CO_2 at the ocean surface and its chemical equilibrium with other forms of carbon in the ocean (mainly carbonate and bicarbonate), 2) the transport of carbon between the surface and the intermediate and deep ocean, and 3) the cycling of carbon through marine ecosystem processes.

The surface dissolution and equilibration of carbon with the atmosphere is well understood and quantified. It varies with the surface ocean conditions, in particular with temperature and alkalinity (the ability of the water to neutralize acids). The capacity of the oceans to take up additional CO_2 decreases at warmer temperature and at elevated CO_2. These effects are well established and have been included in all previous IPCC Assessments.

The transport of carbon between the surface and the intermediate and deep ocean regulates the rate at which the oceans take up CO_2. The time scales of mixing between the surface and intermediate ocean (500–1000 m) are typically 10–50 years and 100s of years for mixing with the deeper ocean. Because these time scales are relatively long, the rate of increase of CO_2 in the atmosphere largely determines the rate of uptake of CO_2 in the oceans, so that the ocean can absorb a larger fraction of the CO_2 emitted to the atmosphere when the emissions occur more slowly. If ocean circulation changes, the uptake of carbon by the oceans would change, both because the uptake of anthropogenic carbon would change but also because the natural cycle of carbon would be modified. A more vigorous circulation generally results in more uptake of anthropogenic carbon, compensated by an outgassing of natural carbon.

Marine plants and other organisms take up carbon in the surface ocean, which eventually form aggregates of organic matter that sink and are remineralized in the intermediate and deep ocean, thus increasing the carbon content of the deep ocean. The uptake of carbon by marine ecosystems is thought to be limited primarily by nutrient supply, in particular nitrogen and iron. Although changes in ocean circulation and global biogeochemical cycles have the potential to alter the carbon fluxes through changes in marine ecosystems, and studies of marine ecosystems suggest changes in biomass or composition in recent decades (Beaugrand, 2009), modeling studies show only small biological variability that has not significantly impacted the response of the ocean carbon cycle over the recent period (Bennington et al., 2009) and there is no evidence that changes in ecosystems have had a large impact on the ocean CO_2 sink in recent decades, except through a possible increase in iron fertilisation over the ocean from dust deposition, which could have enhanced the ocean cumulative CO_2 uptake by 8 PgC (over a total of 154 ± 20 during 1750–2010) (Mahowald et al., 2010).

The recent increase in North Atlantic surface water pCO_2 values since about 1990 at rates faster than atmospheric CO_2 (causing a sink decrease) appear to be related to sea surface warming (Corbiere et al., 2007) and/or changes in ocean circulation (Schuster and Watson, 2007; Schuster et al., 2009). The recent changes could be in part linked to North Atlantic Oscillation (NAO) shift in the mid-nineties and/or Atlantic Multidecadal Variability (AMV) positive state (McKinley et al., 2011; Thomas et al., 2007; Ullman et al., 2009). In addition, rapid increases of pCO_2 observed in winter 2003–2008 (observed pCO_2 increases between 5 to 7 µatm yr^{-1}) have been attributed to an increase of deep convection (import of rich-CO_2 subsurface and deep waters) that dominates the effect of recent cooling on pCO_2 (Metzl et al., 2010).

A weakening of the Southern Ocean CO_2 sink has been identified from atmospheric and ocean CO_2 observations (LeQuere et al., 2007; Metzl, 2009; Takahashi et al., 2009). Model studies suggest that the Southern Ocean weakening occurs in response to an increase in Southern Ocean winds driving increase upwards transport of carbon-rich deep waters (Lenton and Matear, 2007; LeQuere et al., 2010; Lovenduski et al., 2007; Verdy et al., 2007), with changes only partly compensated by increasing eddy fluxes outside the Southern Ocean and by primary production and export changes (Lenton et al., 2009). The increase in winds has been attributed to the depletion of stratospheric ozone (Thompson and Solomon, 2002), and is projected to recover sometime this century. There is less evidence available to attribute the observed changes in other regions to changes in underlying processes or climate change and variability.

Model studies suggest that the response of the ocean to recent climate change since 1960 and variability decrease the rate at which CO_2 is absorbed by the oceans ((Sarmiento et al., 2010); Section 6.4). This result was repeated by four ocean models, using climate forcing fields from NCEP, NCEP2 and ECMWF reanalysis data and from JPL wind product based on satellite data (Figure 6.14). The weakening of the sink was attributed in one model to increases in winds in the Southern Ocean and in the equatorial Pacific, with a ~20% contribution from warming and a 30% amplification of the response to climate change and variability due to surface ocean warming (LeQuere et al., 2010). No formal attribution to anthropogenic climate change has been made outside the Southern Ocean.

6.3.2.7.2 Land processes

Three type of processes are thought to have an important effect on the fluxes of CO2 between the atmosphere and the land: 1) processes driven by changes in atmospheric composition (eg, CO_2 and Nitrogen deposition inducing a "fertilization effect" on ecosystem productivity), 2) processes driven by changes in the physical climate (e.g., Net Primary Productivity and respiration, disturbance response to changes in temperature, radiation or precipitation), and 3) processes driven by changes in land use (eg, deforestation, afforestation) and land management (agricultural practice, forestry).

An understanding of the relative contribution of processes to the global net land sink is still limited, in part because processes are highly interactive and often regionally explicit. A combination of experimental data, observations and modeling suggest that the sink processes involved in the contemporary land C sink include CO_2 fertilization effect on photosynthesis (including increased water use efficiency under rising CO_2), N fertilization (Bonan and Levis, 2010; Gerber et al., 2010; McCarthy et al., 2010; Piao et al., 2009a; Thornton et al., 2007; Zaehle et al., 2010b), forest regrowth and afforestation (Houghton, 2010; Pacala et al., 2001), and increase radiation in the tropics (Gloor et al., 2009; Nemani et al., 2003). Dominant anthropogenic sources are emissions from deforestation (Houghton, 2010).

The role of the CO_2 fertilization effect on NPP remains highly unconstrained despite its dominant role in the net carbon exchange as estimated by terrestrial models (Sitch et al., 2008). Although some experiments where ecosystems are exposed to elevated CO_2 most often show continuous stimulation of NPP to rising CO_2 (McCarthy et al., 2010) other experiments show a decreasing effect of the CO_2 fertilization over time. These latter experiments suggest that nutrient limitation is the possible cause of the decline, particularly in N-limited boreal and temperate forests (Canadell et al., 2007; Johnson, 2006; Körner, 2006; Norby et al., 2010). A recent meta-analysis of data also suggests that soil respiration may decrease with added nitrogen (Janssens et al., 2010).

Phosphorus (P) limitation of land carbon uptake have received much less attention (Vitousek et al., 2010). Ecosystems with well-weathered soils in tropics and subtropics are therefore more P-limited than freshly

deglaciated regions in temperate and high latitude regions as demonstrated in a global terrestrial C, N, and P modeling study (Wang et al., 2010a).

Finally, trophospheric ozone (O_3) is known to diminish carbon sequestration, with one case of a 2.6–6.8% reduction of the NPP of the U.S. during 1980–1990 (Felzer et al., 2004). Trophospheric ozone results from photochemical reaction between hydrocarbons and nitrogen oxides both from various pollution sources, and causes cellular damage inside leaves which reduces stomatal conductance and photosynthetic rates.

Process attribution of regional sinks has been more successful than global attribution given the wider availability of observations to combine and use in modeling approaches. Legacies of past forest clearing and decreased harvest removal are key process to explain the US and European carbon sinks but in both cases changes in forest extent and demographics fall short in fully explaining the observed C sink; other processes such as CO_2 and N fertilization need to be invoked (Bellassen et al., 2010; Pan et al., 2009; Schulze et al., 2010; Williams et al., 2011) with a tight coupling among them (Churkina et al., 2010). Other parts of the temperate world such as East Asia, flux attribution is also calling for the same set of processes but higher uncertainty exist (Piao et al., 2010). Increased incident solar radiation due to decrease cloud cover over the last two decades in the tropics is suggested to be an important processes for the C sink in this region (Nemani et al., 2003), as well as the CO_2 fertilization effect largely invoke in the absence of other possible processes (Lewis et al., 2009; Pan et al., 2011). Other processes such as export from a region through river transport, wood products, and net exports of food and wood can be significant components of the regional C balance (Pacala et al., 2001).

Disturbances such as fires, insect damage, and drought are significant forces in driving inter-annual variability of regional C sinks (Ciais et al., 2005; Lewis et al., 2011). It is not well understood to which degree disturbance losses of CO_2 are compensated by regrowth (e.g., savannas fires) or constitute net losses (e.g., peat fire, (Page et al., 2002); deforestation fires, (van der Werf et al., 2010).

As climate change proceeds over the next decades, disturbances are expected become more important in driving long-term trend dynamics of regional C sinks, as it has already being observed in managed Canadian forests due to increased fire frequency and insect damage (Kurz et al., 2008b).

More extensive climate change effects in driving the net carbon balance are in rising importance as suggested by coupled carbon-climate models (Friedlingstein et al., 2006), and longer term processes with potentially large carbon consequences including i) permafrost thawing (Koven et al., 2011; Schaefer et al., 2011; Schuur et al., 2009) and ii) the savanization of the drier parts of the tropics (Cox et al., 2000; Lapola et al., 2009).

Warming (and probably the CO_2 fertilization effect) had been estimated from trends in satellite greenness observations to be responsible for a 6% NPP increase (3.4 PgC over 18 years) during the 1980s and 1990s primarily to due relaxation of climatic constraints to plant growth, particularly in high latitudes (Nemani et al., 2003). Although more recently Zhao and Running (2010) reported a reduction of 0.1% of NPP during the period 2000–2009, a controversy has risen as the trend was a product of the NPP model used (Medlyn, 2011; Samanta et al., 2011; Zhao and Running, 2011).

6.3.3 Global CH_4 Budget

AR5 is the first assessment providing a complete CH_4 budget and not only the reporting of a series of published estimates as in TAR and AR4. An ensemble of atmospheric CH_4 inversion models (top-down), and of process-based models and inventories (bottom-up) is used to derive the main emission sources and their regional contributions for the past decades (Table 6.7, Budget). In the following, bottom-up approaches are used to estimate decadal budgets per process emitting methane. Top-down inversions provide an atmospheric-based constraint for the total methane source. Estimations of CH_4 sinks in tropospheric-OH, soils and stratosphere are also reported for the past decades.

6.3.3.1 Atmosphere

Since preindustrial times, the concentration of CH_4 increased by a factor 2.5 (from 730 ppb to 1794 ppb in 2010) as observed by the network of more than 100 surface sites (Dlugokencky et al., 2011), aircraft profiles in the planetary boundary layer, and to its establishment from analyses of trapped air bubbles on firn air and ice cores (see Chapter 5 and Section 6.2). Figure 6.11. The growth is largely in response to increasing anthropogenic emissions and the inter-hemisphere concentration gradient with higher concentration in the north is consistent with human emissions. Currently, the vertically averaged CH_4 concentration field can be determined by remote sensing from the surface using FTIR instruments and from space by three satellite instruments: SCIAMACHY since 2003, IASI and GOSAT more recently. As an example, SCIAMACHY (Frankenberg et al., 2008) clearly shows the gradient between the two hemispheres as well as increased concentrations over South East Asia, explained by emissions from agriculture, waste, and energy production (Figure 6.1).

The growth rate of CH_4 has declined since 1984 and quasi-stabilized concentrations are observed during the years 1999–2006 associated with very low growth rates (Figure 6.17). The reasons for this decline are still debated but different lines of evidence include: reduced emissions from the gas industry and other fossil fuel related activities in the countries of the former Soviet union (Dlugokencky et al., 2003), reduced global fossil fuel related emissions estimated using ethane as a proxy for fossil fuel methane emissions (Aydin et al., 2011b), compensation between increasing anthropogenic emissions and decreasing wetland emissions (Bousquet et al., 2006), reduced emissions from rice paddies (Kai et al., 2011), or change in OH concentrations (Rigby et al., 2008).

[INSERT TABLE 6.7 HERE]

Table 6.7: Global CH_4 budget for the past three decades. T.-D. stands for top-down inversions and B.-U. for Bottom up approaches. Full references are given at the end of the chapter. Ranges represent minimum and maximum values from the cited references. The sum of sources and sinks from B-U approaches does not automatically balance the atmospheric changes.

Since 2007 the growth of CH_4 is increasing again with additional emissions of 21 Tg and 18 Tg inverted respectively for 2007 and 2008 (Bousquet et al., 2011) as compared to the 1999–2006 period. The increase was found dominated by wetlands (Bousquet et al., 2011) and with some role of high latitudes in 2007 (Bousquet et al., 2011; Dlugokencky et al., 2009) as seen in the Hovmöller diagram of the growth rate vs latitude (Figure 6.17) (Dlugokencky et al., 2009). Increasing CH_4 concentrations are in line with the EDGAR4 emission inventory, which shows increasing anthropogenic emissions in the period 2000–2005, related to increased energy production in growing Asian economies (EDGAR4). However, it remains difficult to reconcile a scenario of compensating tendencies in the emissions from fossil fuel production and natural wetlands with the observed global trends in CH_4 and ^{13}C-CH_4 (Kai et al., 2011; Monteil et al., 2011).

[INSERT FIGURE 6.17 HERE}

Figure 6.17: Upper panel: Globally averaged growth rate of atmospheric CH4 in ppm yr–1 determined from the GLOBALVIEW data product, representative for the marine boundary layer (Masarie and Tans, 1995). Orange dots indicate annual values augmented by a smooth line to guide the eye. Lower panel: Atmospheric growth rate of CH4 as a function of latitude determined from the GLOBALVIEW data product.

6.3.3.2 Emissions and Spatial Attribution

Regional CH_4 budgets are composed by various methane sources around the globe, which are biogenic, thermogenic, or pyrogenic in origin (Neef et al., 2010), and they can be the direct result of either human activities or natural processes (Table 6.7). Biogenic sources are due to degradation of organic matter in anaerobic conditions (natural wetlands, ruminants, waste, landfills, rice paddies, fresh waters, termites). Thermogenic sources come from the transformation of organic matter into fossil fuels on geological timescales (natural gas, coal, oil). Pyrogenic sources are due to incomplete combustion of organic matter (biomass and biofuel burning). Some sources can eventually combine a biogenic and a thermogenic origin (e.g., natural geological sources such as oceanic seeps, mud volcanoes, or hydrates). Each of these three processes is characterized by a range of different fractionations regarding the use of $^{13}CH_4$ molecules: –55–70‰ for biogenic, –25–45% for thermogenic, and –13–25‰ for pyrogenic. Measurements in $^{13}CH_4$ can help partitioning the different methane sources (Bousquet et al., 2006; Monteil et al., 2011; Neef et al., 2010) if process discriminations are reasonably known.

During the decade of the 2000s, natural sources of methane represent 244–368 $TgCH_4\ yr^{-1}$ (Table 6.7). The single most dominant CH_4 source of the global flux and inter-annual variability is CH_4 emissions from wetlands from the tropics and high latitudes (174–280 $TgCH_4\ yr^{-1}$). The term "wetlands" covers a variety of areas emitting methane: wet soils, swamps, peatlands, fresh waters from lakes and rivers. They are highly sensitive to natural and human-induced climate change and variability, as seen in the recent 2007–2008 positive anomalies in precipitation and temperature. The relatively dry conditions that prevailed in some regions of the northern hemisphere continents during the late 1990s and early 2000s may have decreased wetland emissions at this period (Bousquet et al., 2006). Although improving rapidly, the calculation of methane emissions from natural wetlands by process-based models still shows significant discrepancies in magnitude and variability reflecting the difficulty to represent and quantify the variety of underlying processes (WETCHIMP intercomparison).

Since AR4, natural geological sources have received more attention and have been re-evaluated and synthesized by (Etiope et al., 2008). Emissions from terrestrial (13–29 $TgCH_4$) and marine (1–10 $TgCH_4$) seepages, mud volcanoes (6–9 $TgCH_4$), hydrates (5–10 $TgCH_4\ yr^{-1}$), and geothermal and volcanic areas (3–6 $TgCH_4$) may represent between 42 and 64 $TgCH_4\ yr^{-1}$. This large contribution from natural, geological, and partly fossil, CH_4 is consistent with a recent $^{13}CH_4$ analysis re-evaluating that natural and anthropogenic fossil contributions to the global methane budget to be around 30% (Lassey et al., 2007) and not around 20% as previously thought.

Of the natural sources of CH_4, emissions from thawing permafrost and methane hydrates, particularly in the Arctic, are potentially important in the next century because they could increase dramatically due to the rapid climate warming of the Arctic and the large C pools stored there (Tarnocai et al., 2009). Super saturation of dissolved CH_4 at the bottom and surface waters in the East Siberian Arctic Shelf demonstrate some CH_4 activity of the region, with a net flux sea-air flux of 7.9 $TgC\text{-}CH_4$ which is similar in magnitude of the flux for the entire oceans (Shakhova et al., 2010). The ebullition from decomposing thaw lake sediments in north Siberia with estimated flux of ~4 Tg $CH_4\ yr^{-1}$ is another demonstration of the activity of the region with its future potential (van Huissteden et al., 2011; Walter et al., 2006). Over the past decades, however, there exist no evidence for significant emission of CH_4 from permafrost and hydrates has been detected (Dlugokencky et al., 2009).

Pyrogenic sources of CH_4 has small contribution in the global flux (17–24 $TgCH_4\ yr^{-1}$) but plays a role in inter-annual variability particularly from the burning of tropical and boreal forests in response to regional droughts and deforestation. Tropical fire activity during the 1997–1998 ENSO, dominated by the burning of forests and peatland in Indonesia and Malaysia, released 12 $TgCH_4$ (Langenfelds et al., 2002; van der Werf et al., 2004), with other fire emissions occurrence observed during the dry spell over the northern mid-latitudes in 2002–2003, in particular with high fires over Eastern Siberia in 2003 (Simmonds et al., 2005) and possibly Russia in 2010. Biofuel burning is estimated to be a source of 10 $TgCH_4$ per year (Yevich and Logan, 2003).

(Keppler et al., 2006) reported that plants under aerobic conditions were able to emit CH_4 emissions, and so adding a large emission source that had not been previously considered in the global CH_4 budget. Later studies do not support plant emissions as a wide spread mechanism as suggested by Keppler et al. (Dueck et al., 2007; Nisbet et al., 2009; Wang et al., 2008). Methane emissions have been detected from dry organic material exposed to UV radiation, but the emission rates are about an order of magnitude lower (Vigano et al., 2008). Alternative mechanisms have been suggested involving adsorption and desorption, and not new production (Kirschbaum and Walcroft, 2008; Nisbet et al., 2009), degradation of organic matter under strong UV light (Dueck et al., 2007; Nisbet et al., 2009). Nisbet et al. (2009) concluded that emissions of methane by plants under aerobic conditions are not a large source of the global methane production.

Anthropogenic CH_4 sources range between 235 and 338 $TgCH_4\ yr^{-1}$ during the 2000s (Table 6.7) and include rice-paddies agriculture, ruminant animals, sewage and waste, landfills, and fossil fuel extraction, storage, transformation, transportation and use (coal mining, gas, oil and industry); they are now dominant over natural sources for top-down inversions but of the same for bottom-up models and inventories (Table 6.7). Rice paddies emit between 28 and 44 $TgCH_4\ yr^{-1}$, continuously flooded paddies having much higher emissions per square meter than drought-prone or rain-fed paddies. 90% of emissions come from Monsoon Asia, and more than 50% from China and India alone (Yan et al., 2009). Ruminant livestock, such as cattle,

sheep, goats, and deer produce methane by food fermentation in their anoxic rumens with a total estimated between 73 and 94 $TgCH_4\,yr^{-1}$. Major regional contributions to this flux come from India, China, Brazil, and the US (EPA, 2006). India, with the world's largest livestock population (485 Millions), emitted 12 $TgCH_4$ in 2003, including emission from enteric fermentation (11 Tg) and manure management (1 Tg) (Chhabra et al., 2009). Methanogenesis in livestock manure and wasted waters produce between 14 and 25 $TgCH_4\,y^{-1}$ due to anoxic conditions and a high availability of acetate, CO_2 and H_2. The same conditions generally apply to landfills that are responsible for emissions of 34 to 49 $TgCH_4\,yr^{-1}$. Loss of natural gas (~90% methane) is the largest contributor to fossil fuel related emissions (52–69 $TgCH_4\,yr^{-1}$). Fugitive emissions are high in the Russian Federation, as they relate to older energy infrastructure, and in the USA (EPA 2006). Coal mining contributes between 18 and 35 $TgCH_4\,yr^{-1}$. Residual emissions are due to oil industry.

Global methane emissions, as estimated from the sum of bottom-up models and inventories, are still very uncertain (479–706 $TgCH_4\,yr^{-1}$) for the years 2000s. However, top-down inversions provide a more narrowed range (518–550 $TgCH_4\,yr^{-1}$), based on the assimilation of atmospheric observations of methane, and can help closing the methane budget, although they do not provided as detailed budget per emitting process as bottom-up approaches (Table 6.7).

6.3.3.3 Sinks

The main sink of atmospheric methane is its oxidation by OH radicals which takes place mostly in the troposphere and stratosphere (Table 6.7). OH removes about 90% of atmospheric CH_4 determining a lifetime of about 9 years (7–11 years) for an atmospheric burden of 4800 $TgCH_4$ (4700–4900 $TgCH_4$) (ACCMIP intercomparison). Oxidation in dry soils take about 22–28 $TgCH_4\,yr^{-1}$. A small sink is suspected, but still debated, in the marine boundary layer due to a reaction with Chlorine (Allan et al., 2007).

There have been a number of published estimates of global OH concentrations and variations over the past decade (Bousquet et al., 2005; Dentener et al., 2003; Montzka et al., 2011; Prinn et al., 2001; Prinn et al., 2005; Rigby et al., 2008). The very short lifetime of OH makes it difficult to estimate global OH concentrations from the aggregation of sparse direct measurements. Either chemistry transport models (CTMs) or proxy methods have to be used to get a global mean value and time variations. CTMs produce small variations of OH radicals, typically of 1–3% due to a high buffering of this radical by the atmospheric photochemical reactions. Atmospheric inversions using methyl-chloroform as a proxy (MCF) find much larger variations for the 1980s and the 1990s (5–10%), likely because of a too large sensitivity to uncertainties on methyl-chloroform emissions (Montzka et al., 2011). For the 2000s, the reduction of MCF in the atmosphere, due to the Montreal protocol, allows a consistent estimate of OH variations between atmospheric inversions (within 5%) and CTMs (within 3%). However, the very low atmospheric values reached by MCF (a few ppt in 2010) impose to find another OH proxy in the next years. The mean global OH value from CTMs, mostly determining the global source of CH_4 compatible with the atmospheric changes, is still very uncertain (473–594 $TgCH_4\,yr^{-1}$) for the 2000s. Finally, changes in OH concentrations are found to play a significant (Rigby et al., 2008) to only small role (Bousquet et al., 2011) in this increase of atmospheric methane since 2007.

6.3.4 Global N_2O Budget

The Fourth Assessment Report of IPCC (AR4) estimated total N_2O emissions in the 1990s (Table 6.8). Since then, a number of studies have been published that give reason to update some of the N_2O emission estimates.

First and most importantly, the IPCC Guidelines have been revised in 2006 (IPCC, 2006). In particular the emission factors for estimating agricultural emissions have been updated (De Klein et al., 2007). Applying these 2006 emission factors to global agricultural statistics, results in direct emissions from agriculture (from fertilized soils and animal production) that are higher than in AR4, but indirect emissions (mainly from leaching and runoff) that are considerably lower (Table 6.8).

[INSER TABLE 6.8 HERE]

Table 6.8: Section 1 gives the Global N budget ($TgN\,yr^{-1}$): a) creation of reactive N, b) emissions of NO_x, NH_3 in 2000s to atmosphere, c) deposition of N to land and oceans and d) discharge of total N to coastal ocean. Section 2 gives the N_2O budget for the year 2005, and for the 1990s compared to AR4. Unit: Tg N_2O-N yr^{-1}.

Second, it has been recently recognized that the open oceans are an anthropogenic source of N_2O (Duce et al., 2008). Atmospheric deposition of anthropogenic N (nitrogen oxides and ammonia) may increase N_2O emissions from the open ocean. This anthropogenic source was not considered in AR4, but is included now in Table 6.8.

Third, a first estimate was published of global N_2O uptake at the Earth's surface (Syakila and Kroeze, 2011; Syakila et al., 2010), based on reviews of measurements of N_2O uptake in soils and sediments (Chapuis-Lardy et al., 2007; Kroeze et al., 2007). The uncertainty in this estimate is large. On the global scale, surface uptake may seem negligible. At the local scale, however, it may not be irrelevant. It is therefore included in Table 6.8.

6.3.4.1 Atmosphere

The concentration of N_2O has increased by 20% (from 270 ppb to 324 ppb in [years needed] since the onset of the Industrial Revolution (Figure 6.11), (MacFarling-Meure et al., 2006)).

Figure 6.18 shows concentration and annual growth rate of atmospheric N_2O estimated from direct measurements (NOAA/ESRL program). On decadal time scales the concentration of N_2O keeps rising steadily at a rate of 0.73 ± 0.03 ppb yr^{-1}. Interannual variations of the N_2O growth rate are clearly discernible, although the sparseness of the station network and lower quality of the instrumentation make the early record prior to 1986 less robust. The origin of the interannual variability is poorly understood. It has been shown to be correlated to changes in northern hemisphere soils water content (Ishijima et al., 2009), however, since only a few long term stations are used to estimate the global growth rate, atmospheric transport processes and in particular variations in stratosphere-troposphere exchange also contribute to the observed interannual variability (Nevison et al., 2007).

[INSERT FIGURE 6.18 HERE]

Figure 6.18: Globally averaged growth rate of N_2O in ppm yr^{-1} determined from the observations of the NOAA/ESRL halocarbons program. Brown dots indicate annual values augmented by a smoothed line to guide the eye.

6.3.4.2 Sources and Sinks

Most N_2O is produced during biological (bacterial) processes such as nitrification and denitrification in soils and sediments. In general, more N_2O is formed when more reactive nitrogen is available. The production of N_2O shows a large spatial and temporal variation. Experimental data are mostly available for terrestrial systems in temperate zones. As a result emission estimates for tropical regions and for aquatic systems are relatively uncertain.

Table 6.8 does not include formation of atmospheric nitrous oxide from the abiotic decomposition of ammonium nitrate in the presence of light, appropriate relative humidity and a surface. This abiotic production has been recently proposed as a potentially important source of N_2O (Rubasinghege et al., 2011). A global estimate of the source strength, however, does not yet exist.

Table 6.8 indicates that the global N_2O emissions in the mid 1990s are now estimated at 18.5 Tg N yr^{-1}. This is 3% higher than the estimate in AR4 (17.7 Tg N yr^{-1} in AR4). Anthropogenic emissions have steadily increased since over the last two decades and in 2006 were 15% higher than the value in the early 1990's. Overall, anthropogenic emissions are now a factor of 8 greater than the level in 1900. These trends are consistent with observed increases in atmospheric N_2O (Syakila et al., 2010).

6.3.4.3 Feedbacks from N_2O and Climate

Early studies have suggested a considerable positive feedback between N_2O and climate (Khalil and Rasmussen, 1989) supported by observed glacial-interglacial swings in atmospheric N_2O (Fluckiger et al., 1999). Climate changes influence marine and terrestrial sources, but their individual contribution and even the sign of their response to climate variations are difficult to estimate, and there appears to be no consensus about the sources responsible for the long-term (glacial-interglacial) N_2O concentration changes. Simulations of a terrestrial biosphere model suggests a moderate increase of global N_2O emissions with recent climatic

changes (Zaehle and Dalmonech, 2011). However, most of the change in atmospheric N_2O is attributed to to anthropogenic reactive nitrogen (Nr) and industrial emissions (Davidson, 2009; Holland et al., 2005; Zaehle and Dalmonech, 2011). Significant uncertainty remains in the N2O-climate feedback from land ecosystems, as it is very sensitive to the changes in the seasonal and frequency distribution of precipitation, and also because agricultural emissions themselves may also be sensitive to climate.

Methods to monitor ecosystem exchanges of N_2O have greatly improved in recent years, but technological challenges remain and the network remains very sparse (Sutton et al., 2007). Climate change will directly affect nitrification and denitrification processes, and thus N2O production, due to its effect on temperature and soil moisture regimes (Butterbach-Bahl and Dannenmann, 2011). N_2O emissions may also be influenced indirectly by the effects of CO_2 fertilisation or N deposition induced changes in soil moisture or nitrogen availability due to plant-soil interactions (Barnard et al., 2005; Singh et al., 2010). The few warming experiments of ecosystems reporting changes in N_2O emissions show varying responses, likely due to co-occuring changes in soil moisture or water-table (Chantarel et al., 2011; Lohila et al., 2010; Menyailo and Hungate, 2006). The response of N_2O emissions to elevated CO2 can be either an enhancement (Ineson et al., 1998; vanGroenigen et al., 2011) or reduction (Billings et al., 2002; Mosier et al., 2002), resulting from the varying response of soil N availability to CO_2 enhancement (Reich et al., 2006). In ecosystems where N is not limiting, the N_2O response to temperature and atmospheric CO2 increases will likely be positive (Butterbach-Bahl and Dannenmann, 2011).

Regional to global scale model application suggest a strong effect of climate variability on interannual variability of land N_2O emissions (Tian et al., 2010; Zaehle and Dalmonech, 2011). Only few projections of the effects of terrestrial N_2O emissions to future climate changes and elevated CO_2 conditions exist, and there is little confidence in the overall response, (Kesik et al., 2006) found that for European forest ecosystems that climate change reduced N_2O emissions on average, associated with decreased soil moisture and warmer temperatures, despite increases of up to 20% in central Europe, while other modelling studies have found no significant effect (Abdalla et al., 2010).

6.3.4.4 Global N Sources

The anthropogenic sources of newly created reactive N to the global system are dominated by food production—N fertilizer and cultivation induced biological N fixation account total 170 TgN yr^{-1}, out of an anthropogenic total of 219 TgN yr^{-1}. Other important sources, creation of NO_x by combustion of fossil fuels and creation of NH_3 as an industrial feedstock (e.g., nylon production), are of the same magnitude (24 TgN yr^{-1}) but have very different fates. The former is directly emitted into the atmosphere with rapid distribution to other environmental systems, while the latter is becomes part of an industrial stream and little is known about its ultimate fate. There is a net transfer of reactive N from the continental atmosphere to the marine atmosphere, resulting in N deposition to the oceans that is greater than riverine discharge.

6.3.5 New Observations and Evaluation of Carbon Cycle Models

6.3.5.1 New Observations

Since AR4, there are a number of new observations which provide addition knowledge and datasets to validate and further constrain global carbon cycle models.

[INSERT FIGURE 6.19 HERE]

Figure 6.19: New observations since AR4: a) Climatological mean annual sea–air CO_2 flux (gC m^{-2} yr^{-1}) for the reference year 2000 (Takahashi et al., 2009); b) Column inventory of anthropogenic carbon in the ocean in 2008 (Khatiwala et al., 2009); c) Distribution of forest aboveground biomass (circa 2000) (Saatchi et al., 2011); d) Soil organic carbon content in the northern circumpolar permafrost region (Tarnocai et al., 2009); e) Median annual GPP (gC m^{-2} yr^{-1}) (Beer et al., 2010); f) Forest fluxes and its regional attribution, PgC yr^{-1} (Pan et al. 2011); g) Column averaged CH_4 concentration retrieved by the SCIAMACHY instrument on board of the ENVISAT satellite; 7-year average 2003-2009 (Schneising et al., 2009); g) mean annual carbon emissions from biomass burning and wildfires (gC m^{-2} yr^{-1}), averaged 1997–2010 (updated from van der Werf et al., 2010).

6.3.5.1.1 Surface ocean pCO_2

Repeated observations have provided new information on the rate of change of ocean CO_2 with respect to the atmosphere (Schuster et al., 2009; Takahashi et al., 2009), with 2 million additional observations since the AR4 (Figure 6.19a).

6.3.5.1.2 History of anthropogenic carbon in the ocean

A reconstruction of the spatially resolved and time-dependent history of anthropogenic carbon in the ocean estimated a total inventory of 151 ± 40 Pg C and an uptake rate of 2.3 ± 0.6 Pg for 2008, updated from (Khatiwala et al., 2009) (Figure 6.19b).

6.3.5.1.3 Biomass of tropical forests

Using a combination of data from 4,079 in situ inventory plots and satellite light detection and ranging (Lidar) samples of forest structure, (Saatchi et al., 2011) mapped the spatial distribution of total forest biomass over tropical regions. Tropical total forest biomass is about 247 PgC, which is close to another independent estimation of 264–274 PgC based on forest inventory data and long-term ecosystem carbon studies (Pan et al., 2011). (Figure 6.19c)

6.3.5.1.4 Carbon pools in the northern circumpolar permafrost region

A new estimate of the carbon stores in the permafrost region shows that the size of the pool is 1672 PgC which includes pool size estimates from less conventional pools such a carbon in deltaic and deep yedoma deposits (Tarnocai et al., 2009) (Figure 6.19d).

6.3.5.1.5 Gross primary production

Using eddy covariance and satellite observation, a recent data-oriented estimation shows that global GPP is about 123 ± 8 PgC yr^{-1}, and tropical vegetation accounts for 60% of the global GPP (Beer et al., 2010). Note that most eddy covariance towers are located in northern temperate regions, and remote sensing techniques are only partially effective in tropical regions. However, the current accepted size of GPP flux has been recently challenged (Welp et al., 2011) (Figure 6.19e). See Box 6.3 for more detail.

6.3.5.1.6 Forests carbon fluxes

A combination of forest inventories, remote sensing and modeling enabled to estimate the net global forest sink at 1.1 ± 0.8 PgC yr^{-1} during 1990–2007 with its regional contributions. The global flux was made up of 2.4 ± 0.4 PgC yr^{-1} sink in established forests, 2.9 ± 0.5 PgC yr^{-1} source from deforestation in the tropics, and 1.6 ± 0.5 PgC yr^{-1} sink in regrowing tropical forests (Pan et al., 2011). (Figure 6.19f).

6.3.5.1.7 Satellite column CH_4

Column averaged CH_4 concentration retrieved by the SCIAMACHY instrument on board of the ENVISAT satellite; averaged over the year 2005 (Schneising et al., 2009). (Figure 6.19g).

[START BOX 6.3 HERE]

Box 6.3: Trends in Satellite Based Data on Global Terrestrial Photosynthetic Capacity from 1982 to 2010

The large difference in reflected amounts of near-infrared (~ 800 to 1100 nanometers, nm) and red (~ 600 to 700 nm) components of solar radiation (~ 250 to 2500 nm) is unique to green vegetation, and when appropriately normalized, as in the case of the Normalized Difference Vegetation Index (NDVI), this difference is a radiometric proxy of vegetation photosynthetic capacity. Typical NDVI values range between –0.2 and 0.1 for snow, inland water bodies, deserts, and exposed soils, and increase from about 0.1 to over 0.9 for increasing amounts of vegetation.

The Global Inventory Monitoring Modeling Studies (GIMMS) group at National Aeronautics and Space Administration (NASA) Goddard Space Flight Center (GSFC; PI: Compton J. Tucker) recently produced a third generation NDVI data set (NDVI3g) with raw data from the Advanced Very High Resolution Radiometers (AVHRR) onboard a series of National Oceanic and Atmospheric Administration (NOAA) satellites numbered 7, 9, 11, 14, 16, 17 and 18). The NDVI3g data set has a spatial resolution of 8km by 8km

square pixels. The maximum NDVI value over a 15-day period is used to represent each 15-day interval because atmospheric corruption of measured radiances decreases the magnitude of NDVI. This compositing scheme results in two maximum-value NDVI composites per month. The NDVI3g record spans the period July 1981 to December 2010. A method was developed to define the start and end dates of the growing season and the number of growing seasons per year for each pixel (Figure 1A-rbm).

Statistically significant (10% level) trends in GSI NDVI for the 1980s (Figure 1B-rbm), 1980s plus 1990s (Figure 1C-rbm) and 1980s plus 1990s and 2000s (Fig. 1D-rbm) show a tendency for more greening than browning of global vegetation (Table 3-rbm). For example, during the first 19 years of the NDVI data record (1982 to 2000), about 23% of the global vegetation showed a statistically significant increase in GSI NDVI, about 3% showed a decline and 69% showed no change (the remaining 5% had invalid NDVI data to evaluate trends). When the same trends are evaluated for the entire 29 years of the data record (1982 to 2010), the percentage of greening vegetated areas increases by 9% and browning also increases by 7%. Although these changes, due to adding 10 years of data from 2000s, are comparable, the percentage of global vegetation exhibiting greening is three times larger than the browning vegetation (31% vs. 10%). Together these results suggests a greening planet either due to continuing relaxation of climatic constraints to plant growth and/or reflects other processes such as CO_2 fertilization effects modulated by interannual variability in climatic factors governing plant growth.

[END BOX 6.3 HERE]

6.3.5.2 Model Evaluation of Global and Regional Carbon Balance

Ocean models have reproduced to a first order the air-sea fluxes of CO_2 derived from observations (Takahashi et al., 2009) for at least ten years, including their general patterns and amplitude (Sarmiento et al., 2000), the anthropogenic uptake of CO_2 (Orr et al., 2001), and the regional distribution of air-sea fluxes (Gruber et al., 2009). The model spread is largest in the Southern Ocean (Matsumoto et al., 2004), where intense mixing occurs and model skills is relatively low. Tracer observations (Schmittner et al., 2009) and water mass analysis (Iudicone et al., 2011) have been used to reduce the uncertainty associated with ocean mixing and improve carbon fluxes in models.

6.3.5.2.1 Sensitivity to climate and CO_2

*Sensitivity of carbon cycle to CO_2.*The sensitivity of ocean models to the level and rate of change of CO_2 in the atmosphere can be evaluated from several studies that have isolated the uptake of anthropogenic CO_2 from changes in the natural carbon cycle using combinations of observations. Over the 1750–2010 time period, the oceans took up 154 ± 20 PgC for an increase in atmospheric CO_2 of 112 ppm, which gives an average uptake per unit of atmospheric CO_2 increase (or "Beta-ocean" factor) of 1.4 ± 0.2 PgC ppm^{-1}. Over the past three decades only, estimates of the Beta-ocean are similar at 1.3 ± 0.3 PgC ppm^{-1}. The estimate of (Khatiwala et al., 2009) also provides time-varying information for Beta-ocean for the annual ocean CO_2 uptake, and show a peak in Beta of 1.7 in the early 1950s decreasing to 1.4 around 2005. Models that have estimated the anthropogenic CO_2 uptake for 1800–1990 give a median Beta factor of 1.7 (1.4–1.9) (Orr et al. 2001), also with a peak around the early 1950s. Thus both models and observations support a decreasing Beta factor in recent decades. The analysis of (Khatiwala et al., 2009) further suggests that the decreasing Beta factor is mostly a response to the time varying atmospheric CO_2 rather than to the effect of non-linear chemistry associated with elevated atmospheric CO_2.

Sensitivity of carbon cycle to climate. It is more difficult to evaluate the sensitivity of ocean models to temperature and other changes in climate which drive ocean circulation changes, and thereby ocean carbon cycle changes. The relationship between air-sea CO_2 flux and temperature is strongly dependent on the oceanic region and on the time-scale. In general, the ocean takes up more CO_2 during El Niño events when the world temperature is warm (see Section 6.3.6.4), and more CO_2 during glacial periods when the world temperature was cold (see Section 6.2.2.1.1). These time scales are not fully relevant to climate dynamics this century. Changes in atmospheric CO_2 by less than 25 ppm during Dansgaard-Oeschger events were thought to be caused by the ocean (Schmittner and Galbraith, 2008) on a millennial time scale. Although these events are relevant, they were associated with a re-organisation of the surface temperature rather than global mean temperature change. The three ocean carbon cycle models used in (LeQuere et al., 2009) give a

decrease ocean CO_2 uptake of 0–43 PgC during 1959–2008 in response to climate change and variability. This corresponds to a sensitivity of the cumulative CO_2 uptake to global temperature (gamma-ocean) of 0–72 PgC/°C over the past 50 years, a similar range as the –14 to –67 Pg C/°C simulated in carbon-climate models for year 2100 (Friedlingstein et al., 2006).

6.3.5.2.2 Processes missing in models

The most important process missing in ocean carbon cycle models is the representation of small-scale physical mixing, which has an important influence on the vertical transport of water, heat and carbon. In particular, physical mixing in the Southern Ocean is thought to have caused most of the 80–100 ppm changes in atmospheric CO_2 during glaciations (Sigman et al., 2010), a signal which is not entirely reproduced by models (Section 6.2) and suggests that the sensitivity of ocean models could be underestimated by an amount equivalent to up to ~20 ppm/°C over millennial time scales.

Ecosystem processes in ocean models are also limited to the lower trophic levels, with crude parameterizations for bacterial and other loss processes and their temperature-dependence. Nevertheless models reproduce to a first extent the patterns and seasonal amplitude of surface ocean pCO_2 and the uptake of anthropogenic carbon, suggesting that up to now changes in ecosystem processes have not had a dominant effect on ocean CO_2. Nevertheless, projected changes in temperature, ocean acidification, and top-down control by fisheries are all considered potentially important, though not yet quantified.

6.3.5.3 Model Evaluation of Global and Regional Terrestrial Carbon Balance

Evaluation of model outputs is done against ground and/or satellite observations including i) measured carbon fluxes and storage at particular sites around the world (Jung et al., 2007; Schwalm et al., 2011; Stockli et al., 2008; Tan et al., 2010), ii) observed spatio-temporal change in LAI (Lucht et al., 2002; Piao et al., 2006), and iii) interannual and seasonal change in atmospheric CO_2 (Cadule et al., 2010; Randerson et al., 2009).

Figure 6.15 compares global terrestrial net ecosystem exchange, NEE, simulated by different global carbon cycle models without accounting land use change, with the residual land sink estimated as the sum of fossil fuel emission, cement emission and land use change emissions minus the atmospheric and ocean CO_2 sinks from 1980 to 2009 (Friedlingstein and Prentice, 2010; LeQuere et al., 2009). The observed magnitude of residual land sink and its trend is reproduced by the multi-model mean, despite of the large discrepancies among individual models. Poor availability of in situ measurements, particularly in the tropics, limits the progress towards reducing uncertainty.

At the regional scale, modeling terrestrial carbon dynamics are better constrained because higher availability of data. Current inventory approach shows that forest carbon budget over Europe is about $–89 \pm 19$ gC m^{-2} yr^{-1}, which is comparable with the model estimation with afforestation (–63 gC m^{-2} yr^{-1}) (Luyssaert et al., 2010). The model estimated vegetation productivity, however, is substantially larger than inventory estimation by 43%. (Schwalm et al., 2010) evaluated 22 terrestrial carbon cycle models' ability to simulate seasonal cycle of CO_2 exchange from 44 eddy covariance flux towers in North America, and found that the difference between observations and simulations was about 10 times of observational uncertainty. In China, although the magnitude of carbon sink produced by five carbon cycle models (–0.22 to –0.13 PgC yr^{-1}) was close to the inventory-satellite estimation ($–0.177 \pm 73$ PgC yr^{-1}) (Piao et al., 2009a), the interannual variation in carbon balance simulated by different models is weakly correlated (Piao et al., 2011). After calibration of model parameters with observations, however, the interannual variance in the carbon cycle are mostly consistent among models and observations over East Asia (Ichii et al., 2010).

6.3.5.3.1 Evaluation of sensitivity of terrestrial carbon cycle to climate and CO_2

Sensitivity of carbon cycle to CO_2. The sensitivity of carbon cycle to rising atmospheric CO_2 concentration is one of the key metrics used to evaluate terrestrial (and ocean) carbon cycle models. Results from Free Air CO_2 experiments (FACE) on diverse ecosystems generally show sustained increase in net primary productivity (NPP) under elevated atmospheric CO_2 (Luo et al., 2005; McCarthy et al., 2010; Norby et al., 2005). Some studies, however, failed to show a fertilization effect, and co-located experiments of nitrogen addition inferred that nitrogen limitation suppressed growth in these regions (Norby et al., 2010). Long-term tree ring studies suggest a more complex picture on the universality of the CO_2 fertilization effect (Gedalof

and Berg, 2010; Peñuelas et al., 2011), albeit these studies have their own limitations in separating other interactive factors such as temperature and the availability of water and nutrients.

Sensitivity of carbon cycle to climate change. Current rising temperature exerts direct controls on the terrestrial C exchange with the atmosphere since both photosynthesis and respiration are sensitive to changes in temperature. A meta-analysis of field warming experiments suggested an average of 19% increases in aboveground plant productivity (Rustad et al., 2001), along with an increase or no change in NEP under experimental warming (Luo, 2007; Marchand et al., 2004). These results were mostly limited to temperate and boreal regions.

Estimation from the observed residual land sink shows that global terrestrial net carbon uptake in response to 1°C increase of global mean annual temperature could decrease by about 4 PgC yr^{-1} $°C^{-1}$ (Figure 6.15). Multi-model comparison shows a large uncertainty in model estimated interannual temperature sensitivity of global NEE which ranges between 0.5 PgC yr^{-1} $°C^{-1}$ and 6.2 PgC yr^{-1} $°C^{-1}$, although the average of the model estimated sensitivity (3.5 PgC yr^{-1} $°C^{-1}$)is close to the estimation derived by residual land sink. The long-term temperature sensitivity of carbon storage was estimated as about 3.6~45.6 PgC $°C^{-1}$ (or 1.7~21.4 ppmv CO_2 $°C^{-1}$) using ice-core data of the Little Ice Age from 1050 to 1800 when human impacts on atmosphere CO_2 was assumed to be negligible (Frank et al., 2010).

Previous model studies suggested that carbon release in response to future drying is one of the dominant contributors to the positive carbon cycle-climate feedback found in previous coupled models (Cox, 2001b; Friedlingstein et al., 2006; Sitch et al., 2008). Direct observations of the precipitation sensitivity of terrestrial carbon cycle, however, are very limited. Both the observed residual land sink and all global carbon cycle models show a positive response of global NEP to precipitation increase, although a large difference exists among different estimations (Figure 6.20). In comparison to the estimation based on residual land sink (-0.01 PgC yr^{-1} mm^{-1}), most models (eight of nine models) overestimate the interannual precipitation sensitivity of global terrestrial net carbon uptake.

[INSERT FIGURE 6.20 HERE]

Figure 6.20: Interannual sensitivity of model estimated global Net Ecosystem Production (NEP) and residual global carbon sink to change in atmospheric CO_2 and climate during 1980–2009. The global residual land sink was estimated by the difference between the sum of fossil fuel emission and land use change emission and the sum of atmospheric growth rate and modeled ocean sink (Friedlingstein and Prentice, 2010; LeQuere et al., 2009). The sensitivities to temperature, precipitation and atmospheric CO_2 are estimated by a multiple linear regression approach with three variables (mean annual temperature, annual precipitation, and atmospheric CO_2 concentration). Negative value indicates increase in carbon sink.

6.3.5.3.2 Processes missing in models

Currently most carbon cycle models mainly consider the effects of climate change and atmospheric CO_2 fertilization, but still miss some other key processes governing the carbon cycle dynamics. First, carbon cycle models usually simulate biomass and soil carbon contents directly, but most of them do not represent stand growth processes (Bellassen et al., 2010). For example, eddy covariance observations show that the strength of net carbon uptake of forest ecosystem is mostly regulated by forest age (Amiro et al., 2010). Second, processes relevant to feedbacks from organic soils are limited, including those in permafrost regions and tropical peatlands which hold large carbon stores and are vulnerable to warming and land use change (Hooijer et al., 2010; Koven et al., 2011; Page et al., 2010; Tarnocai et al., 2009). Third, despite several studies highlighted the important role of N cycle in regulating carbon cycle (Magnani et al., 2007), N dynamics has only coupled in a few carbon cycle models. Fourth, the effects of ozone pollution were also not taken into account for most of current carbon cycle models. It was found that increase in the tropospheric ozone level would reduce vegetation growth, and thus further decrease NEP (Sitch et al., 2007). Finally, human managements including fertilization and irrigation may also substantially influence C cycle at regional scales (Gervois et al., 2008), but it was not considered in most of current model studies.

6.4 Future Projections of Carbon and other Biogeochemical Cycles

6.4.1 Introduction

Here we assess our ability to project changes in the evolution of CO_2, CH_4 and N_2O concentration, and hence the role of biogeochemical cycles in future climate and socio-economic emission scenarios.

IPCC AR4 reported how climate change can affect the natural carbon cycle in a way which could feedback onto climate itself. (Cox et al., 2000) presented simulations showing a large response of the carbon cycle to climate change which amplified global warming and also led to a significant dieback of the Amazon forest. A subsequent comparison of 11 climate-carbon cycle models (Coupled Climate-Carbon Cycle Model Intercomparison Project; C4MIP, (Friedlingstein et al., 2006) showed that all 11 models simulated a positive feedback (climate change reduced natural carbon uptake and accelerated CO_2 increases). However, substantial quantitative uncertainty in future CO2 and temperature projections remains both across coupled carbon-climate models (Friedlingstein et al., 2006) and within models (Booth et al., submitted) and is of comparable magnitude to uncertainty caused by physical climate processes (Denman et al., 2007; Gregory et al., 2009; Huntingford et al., 2009).

Very few such models include representation of nutrient cycles which are an important component of the terrestrial carbon cycle affecting both its ability to take up anthropogenic carbon and its response to future climate changes (Section 6.4.6). Recent studies (Sokolov et al., 2008; Thornton et al., 2009; Zaehle et al., 2010a) have found that representation of nitrogen in terrestrial carbon cycle models substantially alters the response of future CO_2 projections and can even change the sign of the climate-carbon feedback (Figure 6.21). The effects of nitrogen to limit the natural uptake of carbon by terrestrial ecosystems, and also to reduce the potential sensitivity of land carbon sink to future climate change highlight the need to see the future response of the carbon cycle as two competing effects and not just a climate-carbon feedback (Arneth et al., 2010; Gregory et al., 2009).

Coupled climate-carbon cycle models provide a predictive link between fossil fuel CO_2 emissions and future CO_2 concentrations and are an important component of the CMIP5 experiment design (http://cmip-pcmdi.llnl.gov/cmip5/index.html) (Hibbard et al., 2007). The main conceptual advance of CMIP5 models analysed in this chapter, compared to the C4MIP first generation coupled carbon-climate models in AR4, is their treatment of land use change fluxes, as a perturbation of the carbon cycle driven by local land cover change, instead of an external prescribed emission. Simplified models calibrated against complex coupled carbon-climate models have been used to extrapolate findings to new or longer scenarios (House et al., 2008; Meehl et al., 2007; Plattner et al., 2008). As the complexity of Earth System Models continues to increase it is important to reflect any new findings in such policy relevant assessments.

Biogeochemical cycles and feedbacks other than the carbon cycle play an important role in the future of the climate system, although the carbon cycle represents the strongest of these. Natural CH4 emissions from wetland and fires are sensitive to climate change (Section 6.4.7). Changes in the nitrogen cycle, in addition to interactions with CO_2 sources and sinks, affect emissions of N_2O both on land and from the ocean (Section 6.4.6). A recent review highlighted the complexity of terrestrial biogeochemical feedbacks (Arneth et al., 2010). A similar degree of complexity exists in the ocean and in interactions between land, atmosphere and ocean cycles (Figure 6.21). Many of these processes are not yet represented in coupled climate-biogeochemistry models and so their magnitudes have to be estimated in offline or simpler models which makes their quantitative assessment difficult. It is likely there will be non-linear interactions between many of these processes, but these are not yet quantified. Therefore any assessment of the future feedbacks between climate and biogeochemical cycles still contains large uncertainty.

[INSERT FIGURE 6.21 HERE]

Figure 6.21: A summary of the magnitude of biogeochemical feedbacks. (Gregory et al., 2009) proposed a framework for expressing non-climate feedbacks in common units (W m^{-2} K^{-1}) with physical feedbacks, and (Arneth et al., 2010) extended this beyond carbon cycle feedbacks to other terrestrial feedbacks. The figure shows the results compiled by (Arneth et al., 2010), with ocean carbon feedbacks from C4MIP also added. Some further biogeochemical feedbacks from the HadGEM2-ES Earth System model (Collins et al., 2011a) are also shown. Black dots represent single estimates, and coloured bars denote the simple mean of the dots with no weighting or assessment being made to likelihood of any single estimate. Confidence in the magnitude of these estimates is low for feedbacks with only one, or few, dots. The role of nitrogen limitation on carbon uptake is also shown – this is not a separate feedback, but rather a modulation to the climate-carbon and concentration-carbon feedbacks. This list is not exhaustive. These feedback metrics are also likely to be state or scenario dependent and so cannot always be compared like-for-like (see Section 6.4.2.2). Results have been compiled from (a) (Arneth et al., 2010), (b) (Friedlingstein et al., 2006), (c) HadGEM2-ES (Collins et al., 2011a) simulations.

6.4.2 Carbon Cycle Feedbacks from the Idealised CMIP5 1% yr^{-1} Model Simulations

6.4.2.1 Global Analysis

The C4MIP study (Friedlingstein et al., 2006) derived a method to characterize global carbon cycle interactions with climate. This comprises metrics that measure how the climate responds to CO_2, α (K ppm^{-1}), how the land and ocean carbon cycle respond to CO_2, β (GtC ppm^{-1}, split between land and ocean) and how the land and ocean carbon cycle respond to climate change, usually characterised by temperature, γ (GtC K^{-1}, split between land and ocean). (Friedlingstein et al., 2006) also defined how to combine these metrics into a single climate-carbon cycle gain factor, g but (Gregory et al., 2009) discuss that the carbon cycle response is better viewed as two strong and opposing feedbacks, both uncertain. The climate-carbon response determines changes in carbon storage due to changes in climate and the concentration-carbon response determines changes in storage due to elevated CO_2. Unlike physical feedbacks relative to a well known black-body response, the concentration-carbon response is very uncertain, (see Section 6.3) and there is no suitable observation against which to evaluate accurately the climate-carbon cycle gain factor for the next century. The β and γ metrics have been evaluated for the C4MIP and CMIP5 models (Figure 6.22).

[INSERT FIGURE 6.22 HERE]

Figure 6.22: Comparison of carbon cycle feedback metrics between the C4MIP ensemble of 7 GCMs and 4 EMICs (Friedlingstein et al., 2006) and CMIP5 models (HadGEM2-ES, IPSL, CanESM, MPI-ESM). Black dots represent a single model simulation and coloured bars show the mean ±1 standard deviation of the multi-model results. The comparison with C4MIP is for context, but these metrics are known to be variable across different scenarios and rates of change (see Section 6.4.2.2). Some of the CMIP5 models are derived from models that contributed to C4MIP and some are new to this analysis. Table 6.9 lists the main attributes of each CMIP5 model used in this analysis. The SRES A2 scenario is closer in rate of change to a 0.5% yr^{-1} scenario and as such it should be expected that the CMIP5 gamma terms are comparable, but the beta terms are likely to be around 20% smaller for CMIP5 than for C4MIP. This high dependence on scenario (Section 6.4.2.2) reduces confidence in any quantitative statements of how CMIP5 carbon cycle feedbacks differ from C4MIP.

[INSERT TABLE 6.9 HERE]

Table 6.9: CMIP5 model descriptions in terms of carbon cycle attributes and processes.

The role of the idealised experiments is to study model processes and understand how the feedbacks work and what causes the differences between models. Whilst γ (especially on land) has been identified as the largest contributor to model spread in the gain factor, g, β (land) is the largest contributor to model spread in future CO_2 concentration and α the largest contributor to spread in future temperature (Figure 6.23). Whilst land and ocean contribute equally to the total response, model *spread* in the land response is greater than for ocean, but no single process or region dominates the total uncertainty with the most important process depending on the quantity of interest.

[INSERT FIGURE 6.23 HERE]

Figure 6.23: Impact of model spread in the C4MIP metrics (α, β, γ). Scatter plots show the success of the linear alpha/beta/gamma framework to estimate 2100 CO_2 and temperature change from the C4MIP models, and right panels show the relative spread that comes from each term – model spread in β_L is the dominant cause of spread in 2100 CO_2, and α for spread in 2100 ΔT.

Other feedback analysis techniques exist. (Boer and Arora, 2010) analyse the carbon cycle response to climate and CO_2 at a grid-point level and present maps of these factors in a method analogous to that used for physical radiative feedback analyses and Yoshikawa et al (2008) also present geographical analysis of the feedback metrics. (Goodwin and Lenton, 2009) show that feedbacks can be expressed as an equivalent emission. Feedback factors can also be expressed in terms of sensitivity of fluxes (GtC yr^{-1} per ppm or per K) or sensitivity of changes in carbon storage (GtC per K or per ppm). In an exactly linear framework these metrics would be equivalent, but given non-linearities in the system, these approaches yield different quantitative results. Hence any feedback framework should be seen as a technique for assessing relative sensitivities of models and understanding their differences, rather than as an absolute measure of an invariant system property.

6.4.2.2 Scenario Dependence of Feedbacks

The C4MIP metrics can vary markedly for different scenarios and as such cannot be used to compare model simulations with different time periods, nor intercompare model simulations with different scenarios. (Gregory et al., 2009) demonstrate how sensitive the feedback metrics are to the rate of change of CO_2 in the forcing scenario. Combined land and ocean uptake due to CO_2 increase was found to vary under different rates of increase of CO_2 (0.5% yr^{-1}, 1% yr^{-1} and 2% yr^{-1}) for 2 models; β decreased by around 20% from 0.5% yr^{-1} to 1% yr^{-1} and from 1% yr^{-1} to 2% yr^{-1}. Faster rates of CO_2 increase lead to reduced beta values as the carbon uptake (especially in the ocean) lags further behind the forcing. γ is much less sensitive to the scenario, especially between 0.5 % yr^{-1} and 1% yr^{-1}, as both global temperature and carbon uptake lag the forcing.

6.4.2.3 Regional Feedback Analysis

The linear feedback analysis of (Friedlingstein et al., 2006) has been applied at the regional scale to future (2010–2100) oceanic CO_2 uptake by (Roy et al., 2011). Figure 6.24 shows this analysis extended to land and ocean points for the CMIP5 models.

[INSERT FIGURE 6.24 HERE]

Figure 6.24: The spatial distributions of land and ocean β and γs for 3 CMIP5 models using the 1% idealised simulations. For land and ocean, β and γ are defined from changes in terrestrial carbon storage and changes in air-sea accumulated fluxes respectively, from the beginning to the end of the 1% idealised simulation relative to global (not local) CO_2 and temperature change.

6.4.2.3.1 Ocean

Over the ocean, β_O values are almost always positive with the exception of some limited areas as the Peruvian-Chilean upwelling region. The spatial distributions of β are broadly consistent between the models and with (Roy et al., 2011) analysis, with the largest βs in the high-latitudes of both the northern and southern hemispheres. On average, the regions with the highest βs are the North Atlantic and the Southern Ocean. The magnitude and distribution of βs in the ocean closely resemble the distribution of historical anthropogenic CO_2 flux from inversion studies and forward modelling studies (Gruber et al., 2009), with the dominant anthropogenic CO_2 uptake regions in the subpolar Southern Ocean.

The spatial distributions of γ are also broadly consistent between the models and with (Roy et al., 2011) analysis, with slightly positive γs in the Arctic, the Antarctic and in the equatorial pacific (meaning that climate change increases CO_2 uptake in these regions) and negative γs elsewhere. The North Atlantic and the mid-latitude Southern Ocean have the largest negative γs. The magnitude and distribution of γs show reduced CO_2 uptake in response to climate change in the subpolar Southern Ocean and the tropical regions, due to decreased CO_2 solubility, and reduced CO_2 uptake in the mid-latitudes, due to decreased CO_2 solubility and increased vertical stratification. Increased uptake in the Arctic and the polar Southern Ocean are partly associated with a reduction in the fractional sea-ice coverage (Roy et al., 2011). Changes in circulation or sea-ice extent due to climate change may influence the response of ocean uptake to increased CO_2.

6.4.2.3.2 Land

Over land, β_L values vary regionally but are always positive. Largest values occur over tropical land, in humid rather than arid regions, and are associated with enhanced carbon uptake in forested areas. In the zonal totals there is a secondary peak over northern hemisphere temperate and boreal zones partly due to a greater land area there but also coincident with large areas of forest. Areas with greater existing biomass appear to experience greater increases in carbon uptake.

Global γ_L values are negative for all of these models (none of which have a coupled nitrogen cycle), but γ_L can be seen to vary in sign regionally with negative values over most of the world, but positive values north of 50–60°N. This threshold appears quite robust across models. This, along with an area of positive γ_L over the Himalayan region demonstrates that cold regions see an increase in vegetation productivity and carbon uptake under warming which exceeds any increase in heterotrophic respiration of soil organic material. (Jones and Falloon, 2009) showed that changes in soil organic matter were the most important driver of the

climate-carbon cycle feedback across C4MIP models, but these changes are not necessarily driven by soil processes.(Matthews et al., 2005) have previously shown that vegetation productivity is a larger cause of model spread than modelled soil carbon decomposition processes.

6.4.3 Implications of the Future Projections for the Carbon Cycle

The CMIP5 simulations include 4 future scenarios referred to as "Representative Concentration Pathways" or RCPs (Moss et al., 2010): RCP2.6, RCP4.5, RCP6.0, RCP8.5. These future scenarios include CO_2 concentration and emissions, and have been generated by four integrated assessment models (IAMs) and are labelled according to the approximate global radiative forcing level at 2100. See chapter 1 for more details on the RCP scenarios.

6.4.3.1 Consistency of IAMs and ESMs

It is important to understand any differences between the ESMs running the RCPs and the IAMs which created them. (van Vuuren et al., 2011) have shown that the basic climate and carbon cycle response of IAMs is generally consistent with the spread of climate and carbon cycle response from ESMs. Some of the IAMs which created the RCPs are more complex than others and some use common climate and carbon cycle components. For the RCPs 3 of the 4 IAMs (GCAM, RCP4.5; AIM, RCP6.0; MESSAGE, RCP8.5) use a version of the MAGICC simple climate and carbon cycle model that has been commonly used in IPCC reports. Hence for the physical and biogeochemical components of the RCP scenarios 4.5, 6.0 and 8.5, the underlying IAMs are closely related. Only IMAGE which created RCP2.6 differs markedly, using a newer version of MAGICC climate and more sophisticated carbon cycle components for land and ocean carbon cycle (see Table 6.10).

Table 6.10: Description of carbon cycle parameterizations in integrated assessment models.

IAM Model Name	Scenario	Climate	Land carbon	Resolution	Vegetation Dynamics	Ocean Carbon
IMAGE	3PD	MAGICC6	Detailed description	0.5 x 0.5 degree	Biome model	Bern model
GCAM	4.5	MAGICC5.3	GCAM submodel	Regional/land use type	N	MAGICC
AIM	6	MAGICC4	MAGICC	Regional	N	MAGICC
MESSAGE	8.5	MAGICC4.1[a]	Explicit for forests (DIMA), otherwise via MAGICC	Regional	N	MAGICC

Notes:
(a) Some parameters have been adjusted.

6.4.3.1.1 Land-use

ESMs and IAMs use a large diversity of approaches for representing land-use changes (Table 6.11), including different land-use classifications, parameter settings, allocation rules, and geographical scales. To meet the challenge of tracking gridded land-use effects in ESMs, a "harmonized" set of annual gridded land-use change scenarios (1500–2100) was developed for CMIP5 (Hurtt et al., 2011) connecting spatially gridded historical reconstructions of land use with future projections in a format required by ESMs. Land-use transitions describe the annual changes in each land use type, such as harvesting trees and establishing or abandoning agricultural land.

Table 6.11: Processes of land-use incorporated in IAMs and ESMs.

Model	Deforestation	Wood Harvest	Explicit Age Classes	Crop Management	Explicit Biofuels
IAMS					
IMAGE	Y	Y	N	Y	Y
GCAM	Y	Y	N	Y	Y
AIM	Y	Y	N	Y	Y

MESSAGE	Y	Y	N	Y	Y
ESMs					
HadGEM2-ES	Y	N	N	N	N
IPSL					
CESM1 (NCAR/DOE)	Y	Y	N	N	N
GFDL	Y	Y	Y	Y (harvest)	N
MPI	Y	Y	N	N	N

Not all the ESMs use the full range of information available from the land-use change scenarios such as wood harvest projections, sub-grid scale shifting cultivation or representation of primary and secondary forests. This has implications for their ability to simulate carbon fluxes associated with land use change because sensitivity studies indicated that shifting cultivation, wood harvesting, and simulation start date all strongly affect secondary land area and age, and estimated carbon fluxes (Hurtt et al., 2011). For most metrics, the choice of RCP had a smaller impact than the inclusion of wood harvest, shifting cultivation and choice of start date.

Land-use in the future will be a significant driver of forest land cover change and terrestrial carbon storage. Land use trajectories in the RCPs show very distinct trends and cover a wide-range of projections, that appear to be driven more by the assumptions of the individual modelling teams than by the radiative forcing levels (Figure 6.25). (Wise et al., 2009) and (Thomson et al., 2010) use the GCAM model to highlight large sensitivity of future land-use requirements to modelling assumptions such as increases in crop yield technology. The area of cropland and grasslands increases in RCP8.5, mostly driven by an increasing global population. But cropland area also increases in the RCP2.6, despite a smaller population increase, as a result of bio-energy production. RCP6 shows an increasing use of cropland but a decline in pasture land. RCP4.5 shows a clear turning point in global land use based on the assumption that carbon in natural vegetation will be valued as part of global climate policy.

Within the IAMs land use is translated into carbon emissions as shown in Figure 6.25(c). The degree of process detail strongly depends on the model and hence differs between the RCP scenarios. IAMs typically model the demand and supply of land use related commodities (food crops, feed, animal products and timber) at the level of world regions. The CO_2 emissions from land use (change) are then estimated from the calculated land use patterns. Depending on the IAM, this may be done at an aggregated, regional, level – or using a detailed representation of vegetation and carbon flows at the grid level. The CO_2 emissions from land use change in the RCPs tend to decline over time due to a slow down (or even reversal) of agricultural land expansion. As most scenarios expect the population growth to stabilise (or even decline), agricultural production levels are expected to stabilize as well.

Among the ESMs which represent land use and land cover change processes explicitly, differing levels of mechanistic detail and assumptions about how the standardized land use change datasets are related to ESM vegetation types and state variables lead to differences in estimated land use flux components. There is not presently explicit reconciliation of the carbon cycle models intrinsic to IAMs, the harmonization model (GLM, (Hurtt et al., 2011)), and ESMs, and so the land use fluxes prescribed for the RCP scenarios differ from fluxes estimated by the subset of ESMs which represent land use processes explicitly. Table 6.12 shows the net influence of land use change in the IAMs and ESMs, and also provides a breakdown of the net land use flux into several component fluxes. Not all models are capable of estimating all component fluxes. The most process-rich ESMs are suitable to capture the diversity of land use processes represented by the historical record and the four RCPs (e.g., Lawrence et al., submitted), but quantitative differences suggest that inconsistencies between carbon cycle models in IAMs and ESMs are still significant.

Table 6.12: Comparison of IAM and ESM cumulative fluxes from land use and land cover change.

Model	Net LULCC flux[a]	LU conversion flux	Wood harvest flux	Product pool decomposition	Disturbance recovery flux[b]
Historical (1850–2005)					
GLM			101.5		

ESMs					
CESM1 (coupled)		63.0	64.0	55.6	
CESM1 (offline)	134.1	51.1	105.5	95.7	–12.6[c]
RCP2.6 (2006–2100)					
IMAGE/ GLM			164.6		
ESMs					
CESM1		44.8	135.9	130.0	
RCP4.5 (2006–2100)					
GCAM/ GLM			179.6		
ESMs					
CESM1		10.1	144.4	138.1	
RCP6.0 (2006–2100)					
AIM/ GLM			182.7		
ESMs					
CESM1		32.6	156.8	147.9	
RCP8.5 (2006–2100)					
MESSAGE/ GLM			248.2		
ESMs					
CESM1		33.9	241.3	222.6	

[INSERT FIGURE 6.25 HERE]

Figure 6.25: Land-use trends and emissions. Global changes in croplands and grassland from the historical record and the RCP scenarios (top panels), and associated land-use emissions of CO_2 (middle panels). Data are plotted as changes in time (left-hand side) and against the global radiative forcing for each RCP (right-hand side). There is no logical relationship (nor is there intended to be) between the land use calculated by IAMs for the RCPs and the radiative forcing level of each RCP. Bottom row shows fossil fuel emissions plotted against radiative forcing for comparison.

6.4.3.2 Projections of Future Carbon Cycle Response Under the RCP Scenarios

ESM simulations can be "emissions-driven" (i) or "concentration-driven" (ii) as in the RCP prescribed CO2 concentration scenarios (Hibbard et al., 2007). In each case the ESM simulates the land and ocean exchange of CO_2 with the atmosphere in response to atmospheric CO_2 concentration and simulated climate:

	d [CO_2]/ dt	=	Emissions	-	(land + ocean uptake)
(i)	interactive		prescribed		simulated
(ii)	prescribed		diagnosed *		simulated

* the diagnosed emissions are hereafter called 'compatible emissions'

In the case of prescribed CO_2 emissions (as in the C4MIP study) the models simulate "freely" the evolution of atmospheric CO_2 concentration. In the case of a prescribed CO_2 concentration pathway, as in RCP experiments done in CMIP5, the models can be used to diagnose the compatible emissions required to follow it. The driving CO_2 scenario and simulated changes in land and ocean carbon storage are shown in Figure 6.26. The associated changes in airborne fraction (AF) and land and ocean uptake fraction are summarised in Figure 6.27. The dominant driver of changes in AF is the emissions scenario and not carbon cycle feedbacks. AF systematically increases under increasing CO_2 rise in RCP8.5, decreases under the stabilised or peak-and-decline scenarios (RCP2.6 and RCP4.5) and remains of similar magnitude in the intermediate RCP6.0 scenario.

[INSERT FIGURE 6.26 HERE]

Figure 6.26: CO_2 concentration pathway in the 4 RCP scenarios (top), and the cumulative changes in land and ocean (bottom left, bottom right) carbon storage (GtC) simulated by ESMs (HadGEM2-ES, CanESM1, IPSL, MIROC – see Table 6.9) for ocean uptake the spread between models is smaller than between scenarios, but for land carbon storage the spread between models is greater than between scenarios.

[INSERT FIGURE 6.27 HERE]

Figure 6.27: changes in airborne, land and ocean fraction of fossil fuel carbon emissions. The figure shows 3 axes whose sum is always unity – airborne fraction (AF) increases vertically, land fraction (LF) from top to bottom right, and ocean fraction (OF) from right to left. The fractions are defined as the changes in storage in each component (atmosphere, land, ocean) divided by the compatible fossil fuel emissions derived from each simulation. Open circles show model simulations for the 1990s, and the solid circle shows the observed estimate based on Table 6.10. The coloured lines and symbols denote the change in uptake fractions under the different RCP scenarios for each model, calculated using the cumulative change in carbon from 2005–2100. Due to the difficulty estimating fossil and land-use emissions from the ESMs this figure uses a fossil fuel definition of airborne fraction, rather than the preferred definition of fossil+land use emissions discussed in Section 6.3.

6.4.3.2.1 Compatible fossil-fuel emissions

Compatible fossil fuel emissions from the four RCP scenarios are shown in Figure 6.28 and summarised in Table 6.13. There is significant spread between ESMs, but no systematic inconsistency between the ESMs and the 'original' emissions themselves estimated by IAMs to be compatible with each RCP scenario. The IMAGE IAM predicts that global negative emissions are required to achieve the RCP2.6 decline in radiative forcing from 3 W m^{-2} to 2.6 W m^{-2} by 2100. There is disagreement between the complex ESMs over the necessity for global emissions to become negative to achieve this with 2 models simulating negative compatible emissions and 2 models simulating positive emissions throughout the 21st century. The RCP2.6 scenario achieves this negative emission rate through use of large-scale bio-energy with carbon-capture and storage (BECCS). This would be classed as geoengineering under the definition used in this IPCC report, and is discussed further in Section 6.5. (Rogelj et al., 2011) also demonstrate the importance of BECCS to achieve a 2°C climate target, but any such negative emissions should be offset against existing forest carbon sinks which may be displaced (Hudiburg et al., 2011). It is important to note that the ESMs themselves make no assumptions about how the compatible emissions could or would be achieved, merely the global total that is required to follow the CO_2 concentration pathway.

Table 6.13: The range of compatible fossil fuel emissions (GtC) simulated by the CMIP5 models for the historical period and the 4 RCP scenarios, expressed as cumulative fossil fuel emission from 2005 to 2100. Historical estimates of fossil fuel are as recommended by CMIP5 (Andres et al., 2011).

	Hist / RCP scenario	ESM		
		min	Mean	max
1860–2005	313.1	268.5	335.6	386.4
RCP2.6	334.4	203.2	312.5	427.6
RCP4.5	767.3	622.7	768.6	961.2
RCP6.0	1144.7	957.2	1060.1	1163.0
RCP8.5	1753.8	1373.3	1606.1	1825.1

[INSERT FIGURE 6.28 HERE]

Figure 6.28: Compatible fossil fuel emissions simulated by the CMIP5 models for the 4 RCP scenarios. Top: timeseries of instantaneous emission rate. Thick lines represent the historical estimates and emissions calculated by the integrated assessment models (IAM) used to define the RCP scenarios, thin lines show results from CMIP5 ESMs. Bottom: cumulative emissions for the historical period (1860–2005) and 21st century (defined in CMIP5 as 2005–2100) for historical estimates and RCP scenarios (bars) and ESMs (symbols). In the CMIP5 model results, total carbon in the land-atmosphere-ocean system can be tracked and changes in this total must equal fossil fuel emissions to the system (see also Table 6.13). Other sources and sinks of CO_2 such as from volcanism, sedimentation or rock weathering, which are very small on centennial timescales are not considered here. Hence the compatible emissions are given by cumulative-Emissions = $\Delta C_A + \Delta C_L + \Delta C_O$ remission rate = d/dt $[C_A + C_L + C_O]$, where C_A, C_L, C_O are carbon stored in atmosphere, land and ocean respectively.

Several studies (Jones et al., 2006; Matthews, 2006; Miyama and Kawamiya, 2009; Plattner et al., 2008) have shown that carbon cycle feedbacks affect the compatible anthropogenic emissions to follow a given scenario of CO_2 concentration. ESM simulations for RCP4.5 without a climate feedback on carbon uptake allow analysis to quantify the direct effects of climate and carbon feedbacks on compatible emissions (Figure 6.29). In the 2 models used here, cumulative emissions from 2005–2100 are reduced by between 11% and 21% due to the climate-carbon cycle feedback. Such uncoupled simulations have not been performed for the other scenarios, but previous work has shown that compatible emissions are reduced by a greater degree under higher CO_2 scenarios which exhibit a greater degree of climate change (Jones et al., 2006).

[INSERT FIGURE 6.29 HERE]

Figure 6.29: Diagnosed compatible fossil fuel emissions (top panel) in the presence (red) and absence (blue) of the climate impact on the carbon cycle for the RCP4.5 scenario, and the difference between them (bottom panel). This shows the impact of climate change on the compatible emissions to achieve the RCP4.5 CO_2 concentration pathway. HadGEM2-ES and CanESM results shown here project reductions from 977 and 891 GtC respectively to 865 and 707 GtC.

6.4.3.2.2 ESM simulations of land use fluxes

Simulated land-use emissions cannot be deduced by this method as they leave no net effect on the total carbon in the system. It remains a technical challenge to diagnose land-use carbon emissions consistently across the CMIP5 models. (Arora and Boer, 2010) diagnosed land-use emissions using different techniques and discuss the difficulty of comparing ESM results with historical reconstructions as Houghton (2008) which is a commonly used dataset for input emissions to ESM simulations.

Representation of land-use processes in ESMs is an advance since C4MIP, but the range of processes included differs greatly between models making comparison with historical trends and RCP scenarios difficult (Section 6.4.3.1). Quantifying the emissions from those included is not straightforward due to their far-reaching influence on land carbon, atmospheric CO2 and climate. When a land-use change is imposed, the simulation deviates from the course it would otherwise have taken as the land biosphere evolves differently. The net effect of a time-varying LU scenario on the carbon balance can be understood by comparison with a second simulation without LU changes (Arora and Boer, 2010).

In the CMIP5 concentration-driven simulations, the prescribed CO_2 concentration implicitly includes contributions from both fossil and land-use sources (Figure 6.30). However, if ESMs are unable to match exactly the impact on the carbon cycle due to LU change, this affects diagnosis of compatible fossil fuel emissions. Thus, diagnosed compatible emissions represent fossil emissions combined with the error between the simulated and actual LU emissions. Inability of ESMs to quantify accurately LU emissions introduces the greatest uncertainty in compatible emissions when the driving CO_2 scenario has a significant LU component. This is primarily the case during the earlier part of the historical period and in the RCP2.6 scenario where fossil fuel emissions reduce to very low (and even negative) values. (Rose et al., 2011) show that land-based mitigation can contribute an equivalent of 100–340 GtC reduction in fossil fuel emissions. Better representation of these processes in ESMs remains an important challenge.

[INSERT FIGURE 6.30 HERE]

Figure 6.30: Interactions between the atmosphere, land and ocean carbon stores as simulated in ESMs. Solid arrows represent the atmosphere-to-land (F_{AL}) and atmosphere-to-ocean (F_{AO}) fluxes simulated by the ESMs. Dashed lines represent land/ocean to atmosphere fluxes (F_{LA}, F_{OA}) diagnosed in concentration-driven simulations and interactive in emission-driven simulations. The dotted arrows represent the prescribed CO_2 pathway (ΔC_A) applied in concentration-driven simulations and a scenario of land-use which may be imposed on the land carbon cycle (see Section 6.4.3.1). Associated changes in C_L caused by this land-use change may not match those implicit in the prescribed ΔC_A.

6.4.3.3 Uncertainty

A range of feedback strengths and future CO_2 concentrations arise within the C4MIP models (Friedlingstein et al., 2006). Comparing the relative contribution of carbon-cycle processes with other contributions such as climate sensitivity uncertainty is not straight forward. (Huntingford et al., 2009) used a simple model to characterise the relative role of carbon cycle and climate sensitivity uncertainties in contributing to the range of future temperature changes, concluding that the range of carbon cycle processes represent about 40% of the physical feedbacks. Section 6.4.2 also showed that the climate response to CO_2 dominates the model spread in future temperature (Figure 6.23) but carbon cycle processes (especially land carbon response to

CO_2) dominate spread in future CO_2 concentration. Perturbed parameter ensembles (Booth et al., submitted) systematically explore land carbon cycle parameter uncertainty and illustrate that a wide range of carbon cycle responses are consistent with the same underlying model structures and plausible parameter ranges. Figure 6.31 shows the comparable range of future climate change (A1B SRES) arises from parametric uncertainty in land carbon cycle and atmospheric feedbacks. The same ensemble shows that the range of atmospheric CO_2 in the land carbon cycle ensemble is wider than the range of business as usual concentrations when carbon cycle uncertainties are neglected.

[INSERT FIGURE 6.31 HERE]

Figure 6.31: Uncertainty in global mean temperature from HadCM3 results exploring atmospheric physics and terrestrial carbon cycle parameter perturbations (Booth et al., submitted; Murphy et al., 2004). Relative uncertainties in the Perturbed Carbon Cycle (PCC, green plume) and Perturbed Atmospheric Processes (PAP, blue) on global mean anomalies of temperature (plotted with respect to the 1980–1999 period). The green/blue hatching illustrates where these two ensembles overlap. The standard simulations from the two ensembles, HadCM3 (black solid) and HadCM3C (black dashed) are also shown. Four bars are shown on the right illustrating the 2100 temperature anomalies associated with the CMIP3/AR4 ensemble (black) the PAP ensemble (blue) the land carbon cycle (PCC) and the weighted land carbon ensemble wPCC (both green). The range (thin line), 10th–90th (medium line) and 25th–75th (thick line) and 50th percentiles (central bar) are all shown.

6.4.4 Future Ocean Acidification

As CO_2 increases in the atmosphere, more also dissolves in the ocean, reducing surface ocean pH and carbonate ion concentrations. The associated chemistry is not debated by the scientific community, and expected changes are in line with what is measured at ocean time-series stations (see Chapter 3). Multi-model projections discussed in AR4 demonstrate large decreases in pH and carbonate ion concentration [CO_3^{2-}] during the 21st century throughout the world oceans (Orr et al., 2005). The largest changes in surface [CO_3^{2-}] occur in the warmer low and mid-latitudes, which are naturally rich in this ion; however, it is the colder high-latitude oceans that first become undersaturated with respect to aragonite D (i.e., for $\Omega_A < 1$, where $\Omega_A = [Ca^{+2}][CO_3^{2-}]/Ksp$, where Ksp is the solubility product for the metastable form of $CaCO_3$ known as aragonite). This undersaturation in surface waters is reached within decades in the Southern Ocean as highlighted in AR4, but occurs sooner and is more intense in the Arctic (Steinacher et al., 2009). Ten percent of Arctic surface waters become undersaturated when atmospheric CO_2 reaches 428 ppm (by 2025 under all IPCC SRES scenarios). That proportion increases to 50% when atmospheric CO_2 reaches 534 ppm. By 2100 under the A2 scenario, much of the Arctic surface becomes undersaturated with respect to calcite (Feely et al., 2009). Surface waters would then be corrosive to all $CaCO_3$ minerals.

Future reductions in surface ocean pH and $CaCO_3$ saturation states are controlled mostly by the direct geochemical effect of increasing atmospheric CO_2. Other effects due to future climate change counteract less than 10% of the CO_2-induced reductions in $CaCO_3$ saturation (Cao et al., 2007; McNeil and Matear, 2006; Orr et al., 2005). Warming dominates other effects from climate-change by reducing CO_2 solubility and thus enhancing [CO_3^{2-}]. The exception is the Arctic Ocean where reductions in pH and $CaCO_3$ saturation states (for both aragonite and calcite, the stable form) are projected to be exacerbated by effects from increased freshwater input due to enhanced sea-ice melt, more precipitation, and greater air-sea CO_2 fluxes due to less sea-ice cover (Steinacher et al., 2009). The projected effect of freshening is consistent with current observations of lower saturation states and lower pH values near river mouths and in areas under substantial fresh-water influence (Salisbury et al., 2008) (Yamamoto-Kawai et al., 2009).

Surface $CaCO_3$ saturation also varies seasonally, particularly in the high latitudes, where observed saturation is higher in summer and lower in winter (Feely et al., 1988; Sweeney, 2004; Merico et al., 2006; Findlay et al., 2008). Future projections indicate that undersaturated conditions will first be reached in winter (Orr et al., 2005). In the Southern Ocean, it is projected that wintertime undersaturation with respect to aragonite will begin when atmospheric CO_2 reaches 450 ppm, which is about 100 ppm sooner (~30 years under the IS92a scenario) than for the annual mean (McNeil and Matear, 2008).

Penetration of anthropogenic CO_2 into the ocean reduces subsurface pH and saturation states. Although projected changes are generally largest at the surface, i the greatest pH changes in the subtropics occur between 200–300 m where subsurface changes in anthropogenic CO_2 are similar to surface changes but the carbonate buffering capacity is lower (Orr, 2011). This more intense projected subsurface pH reduction is

consistent with the observed subsurface changes in pH in the subtropical North Pacific (Dore et al. 2009,) (Byrne et al., 2010; Ishii et al., 2011). As subsurface saturation states decline, the horizon separating undersaturated waters below from supersaturated waters above is projected to move upward (shoal). By 2100 under the IS92a scenario, the median model projection from the Ocean Carbon-Cycle Model Intercomparison Project (OCMIP) is that this interface (aragonite saturation horizon) will shoal from 180 m up to the surface in the subarctic Pacific, from 1040 m up to the surface in the Southern Ocean, and from 2820 m to 110 m in the North Atlantic (Orr, 2011; Orr et al., 2005). Under the A2 scenario, the volume of ocean with supersaturated waters is projected to decline from 42% in the preindustrial era to 25% in 2100 (Steinacher et al., 2009). Yet even if atmospheric CO_2 is held at 450 ppm, most of the deep ocean volume is projected to become undersaturated with respect to both aragonite and calcite after several centuries (Caldeira and Wickett, 2005). Nonetheless, the most recent projections under AR5 mitigation scenarios illustrate that limiting atmospheric CO_2 will greatly influence the level of ocean acidification that will be experienced (Joos et al., 2011).

[INSERT FIGURE 6.32 HERE]

Figure 6.32: Changes in surface pH (upper panels) and surface carbonate ion concentrations (lower panels), as a function of time (left) or atmospheric CO_2 (right), simulated by 6 ESMs (IPSL-CM4-LOOP, UVIC2.8, NCAR CSM1.4, NCAR-CCSM3, BCCR-BCM, MPI-M) over the historical period and over 2000–2100 following the SRES-A2 scenarios. Three regions (discussed in the text) are shown : the Arctic Ocean (north of 70°N, dark blue), the Tropical Oceans (20°S–20°N, red) and the Southern Ocean (south of 60°S, light blue). [PLACEHOLDER FOR SECOND ORDER DRAFT: Results from the CMIP5 models].

6.4.5 Future Ocean Oxygen Depletion

It is likely that global warming will lead to declines in dissolved O_2 in the ocean interior through warming-induced reduction in O_2 solubility and increased stratification (see Box 6.4). This would have implications for nutrient and carbon cycling, ocean productivity and marine habitat (Keeling et al. 2010).

[START BOX 6.4 HERE]

Box 6.4: IPCC AR5 Ocean Deoxygenation

A general decrease in the oxygen concentration of the ocean has been observed across much of the coastal and open ocean over the latter decades of the 20th Century (Gilbert et al., 2010; Helm et al., 2011); (Keeling et al., 2010). Changes in oceanic oxygen (ΔO_2^{tot}) can be related to climate forcing, both directly through the reduced solubility of oxygen in warm waters (ΔO_2^{sol}), and indirectly through changes in ocean mixing and ventilation processes (ΔO_2^{vent}) and changes in biological activity (ΔO_2^{bio}). These processes are highlighted in Figure 1 and combine simply as follows:

$$\Delta O_2^{tot} = \Delta O_2^{sol} + \Delta O_2^{vent} + \Delta O_2^{bio} \quad (6.3.1)$$

The processes that influence ocean oxygen also affect the ocean carbon cycle, albeit in different proportions. Thus climate signatures of ocean deoxygenation provide important insight into the functioning of the oceans and its capacity to take up CO_2. Models consistently estimate that changes in ocean ventilation explain most of the observed "deoxygenation" of the ocean, causing oxygen decreases about four times those expected from ocean warming alone, and exceeding any oxygen increases that may be caused by decreases in biological productivity at low latitudes. However, although the observed deoxygenation is consistent with a signal expected from climate change, formal attribution has not been made and the observed signal could be caused by natural variability in the climate system. Ocean deoxygenation leads to increases the oceanic emissions of N_2O, and has impacts on marine ecosystems.

[INSERT BOX 6.4, FIGURE 1 HERE]

Box 6.4, Figure 1: *The ocean O_2 cycle*. The oceanic reservoir of oxygen communicates with the atmosphere via air-sea gas exchange (F_{O2}). In the ocean interior a change in dissolved O_2 concentration over time can be driven by changes in: (1) surface ocean O_2 solubility ΔO_2^{sol}, (2) the ventilation age of a water parcel advected into the subsurface (ΔO_2^{vent}) (3) biological utilisation of oxygen in remineralization of Dissolved Organic Carbon (DOC; ΔO_2^{bio}).

[END BOX 6.4 HERE]

These future changes in dissolved O_2 have been investigated using EMICs (Plattner et al., 2001; Schmittner et al., 2008); (Oschlies et al., 2008; Shaffer et al., 2009) and ESMs (Bopp et al., 2002; Frolicher et al., 2009; Matear and Hirst, 2003; Matear et al., 2000; Sarmiento et al., 1998). There is broad consensus that the global oceanic oxygen inventory will decline significantly under future scenarios. Simulated declines in mean dissolved O_2 concentration for the global ocean range from 6 to 12 μmol kg^{-1} for year 2100 (Table 6.14), with a projection of 3–4 μmol kg^{-1} in one model with low climate sensitivity (Frolicher et al., 2009). The global decline in oxygen concentration is mainly caused by enhanced surface ocean stratification leading to reductions in convective mixing and deep water formation with a contribution of 18–50% from ocean warming-induced reduction in solubility, in part compensated by a small increase in O_2 concentration from projected reductions in biological export production (Bopp et al., 2001; Steinacher et al., 2010) or changes in ventilation age of the tropical thermocline (Gnanadesikan et al., 2007). The largest regional decreases in oxygen concentration (~20–100 μmol μmol kg^{-1}) are projected for the intermediate (200–400 m) to deep waters of the North Atlantic and Southern Ocean for 2100 (Plattner et al., 2002; (Frolicher et al., 2009; Matear and Hirst, 2003; Matear et al., 2000) (Figure 6.33).

Table 6.14 Model configuration and predictions for marine O_2 depletion by 2100 (adapted from Keeling et al., 2010)

Study	Model	Forcing	Mean [O_2] Decrease (μmol kg^{-1})[a,b]	Solubility Contribution (%)	Net Sea-Air O_2 Flux at 2100 (mol m^{-2} y^{-1})[b]
(Sarmiento et al., 1998)	GFDL		7[c]		
(Matear et al., 2000)	CSIRO	IS92a		18	0.40
(Plattner et al., 2002)	Bern 2D	SRES A1	12	35	
(Bopp et al., 2002)	OPAICE-LMD5	SRES A2[d]	4	25	0.35
(Matear and Hirst, 2003)	CSIRO	IS92a	9	26	
(Schmittner et al., 2008)	UVic	SRES A2	9		
(Oschlies et al., 2008; Shaffer et al., 2009)	UVic	SRES A2	9[e]		
	UVic-variable C:N	SRES A2	12[e]		
(Frolicher et al., 2009)	NCAR CSM1.4-CCCM	SRES A2	4	50	0.23 ± 0.1
		SRES B1	3		
(Shaffer et al., 2009)	DCESS	SRES A2	10[e]		

Notes:
(a) Assuming a total ocean mass of 1.48 x 1021 kg–1
(b) Relative to pre-industrial baseline
(c) Model simulation ends at 2065
(d) Radiative forcing of non-CO2 GHGs omitted
(e) For simulations with reduced ocean exchange, assuming modern average ocean O2 concentration of 178μmol kg–1 (Sarmiento and Gruber, 2006).

There is not such a broad consensus on the evolution of the extent of hypoxic (<60 μmol kg^{-1}) and suboxic (<5 μmol kg^{-1}) waters. Most models show even some increase in oxygen in most O_2-poor waters and thus a slight decrease in the extent of suboxic waters under the SRES-A2 scenario (Figure 6.33). This rise in oxygen in most suboxic waters has been shown to be caused in one model study by an increased supply of oxygen due to lateral diffusion (Gnanadesikan et al., 2011).

A number of biogeochemical feedbacks, not yet included in most EMICs or ESMs, could also impact upon future trends in ocean deoxygenation. For example, model experiments which include a pCO_2-sensitive C:N drawdown in primary production, as established by mesocosm experiments (Riebesell et al., 2007), project future increases of up to 50% in the volume of the suboxic waters by 2100 (Oschlies et al., 2008; Tagliabue

et al., 2011) (Figure 6.33). In addition, future marine hypoxia could be amplified by changes in the Particulate Organic Carbon - $CaCO_3$ export ratio in response to rising pCO_2 (Hofmann and Schellnhuber, 2009). Reduction in biogenic calcification due to ocean acidification would weaken the strength of $CaCO_3$ 'mineral ballasting' feedback which would lead organic material to be remineralised at a shallower depth exacerbating the future expansion of shallow hypoxic waters.

These estimates do not take into account processes that are specific to the coastal ocean and may amplify deoxygenation. Recent observations for the period 1976–2000 have shown that dissolved O_2 concentrations have declined at a faster rate in the coastal ocean (–0.28 μmol kg^{-1} y^{-1}) than the open ocean (–0.02 μmol kg^{-1} y^{-1}) (Gilbert et al., 2010). Hypoxia in the shallow coastal ocean is largely eutrophication-driven and is controlled by the anthropogenic flux of nutrients (N and P) and organic matter from rivers. If continued industrialisation and intensification of agriculture yield larger nutrient loads in the future, eutrophication should intensify (Rabalais et al., 2010), and further increase the coastal ocean deoxygenation.

On longer time scales, ocean de-oxygenation is projected to keep increasing after 2100, with models simulating a tripling in the volume of suboxic waters by 2500 (Schmittner et al., 2008). Ocean deoxygenation and further expansion of suboxic waters could persist on millennial timescales, with average dissolved O_2 concentrations projected to reach minima of up to 56 μmol kg^{-1} below pre-industrial levels in experiments with high CO_2 emissions and high climate sensitivity (Shaffer et al., 2009).

The potential expansion of hypoxic water over large parts of the future is also likely to impact the marine cycling of important nutrients, particularly nitrogen. In particular, the marine flux of N_2O depends critically upon the volume of low-O_2 waters since nitrification and denitrification, which provide the main pathways for N_2O production, are inhibited by oxic conditions (Nevison et al., 2003). The intensification of low oxygen waters will likely lead to significant increases in global N_2O emissions (e.g., Codispoti, 2010; Naqvi et al., 2009). A tripling in the volume of suboxic waters would lead to a quadrupling in global water column denitrification and a doubling in marine N_2O flux by the year 4000 (Schmittner et al., 2008). Changes in denitrification and nitrogen fixation in a deoxygenated ocean are also likely to impact upon the marine inventory of fixed nitrogen, however the sign and magnitude of this feedback is uncertain (e.g., Codispoti et al., 2001; Deutsch et al., 2007; Lam and Kuypers, 2010).

[INSERT FIGURE 6.33 HERE]

Figure 6.33: a) Model-mean (IPSL-CM4-LOOP, UVIC2.8, NCAR CSM1.4, NCAR-CCSM3, BCCR-BCM) changes in O2 concentrations (microM) at 400 m for the 2090–2100 minus 1990–2000 (SRES-A2 scenario). To indicate consistency in the sign of change, regions are stippled where at least 4 out of the 5 models agree on the sign of the mean change. b) Model range and model-mean evolution of global air-sea flux of O2 in Tmol yr–1. Negative values indicate net outgassing of O2 to the atmosphere. c) Relative change in the evolution of suboxic waters (O2 <5 micromol/L), simulated by the above mentioned 5 models (red) and by (Tagliabue et al., 2011) (grey). [PLACEHOLDER FOR SECOND ORDER DRAFT: results from the CMIP5 models].

6.4.6 Future Trends in the Nitrogen Cycle and Impact on Carbon Fluxes

6.4.6.1 Projections for Formation of Reactive N by Human Activity

Human activity now introduces more reactive N into the biosphere than natural processes due to food production, industrial activity and fossil fuel combustion (Box 6.1, Figure 1). A simple conceptual model of the future global use of nitrogen fertilizer is based on the current use and the expected developments of drivers that influence this use (Erisman et al., 2008). In this system, five driving parameters (population growth, biofuels use, food equity, increased N-use efficiency and diet optimization) are used to project future N demands (Figure 6.34). As this century unfolds, the parameters are expected to change from just a slight increase to roughly doubling with respect to the year 2005 situation. Despite the uncertainties and the non-inclusion of many important drivers, all scenarios point towards an increase in future production of reactive nitrogen. [PLACEHOLDER FOR SECOND ORDER DRAT: projections will be updated using the RCPs and including energy-NO_x).

The actual amounts of N released to the environment in the future will depend on the demand for food (and its type), and the demand for energy (and its type).

[INSERT FIGURE 6.34 HERE]

Figure 6.34: Global nitrogen fertilizer consumption scenarios (left) and the impact of individual drivers on 2100 consumption (right). This resulting consumption is always the sum (denoted at the end points of the respective arrows) of elements increasing as well as decreasing nitrogen consumption. Other relevant estimates (FAO, 2000; Tilman et al., 2001; Tubiello and Fischer, 2007) are presented for comparison (Erisman et al., 2008). The A1, B1, A2 and B2 scenarios draw from the assumptions of the IPCC Special Report Emission Scenarios (SRES) emission scenario storylines (Nakicenovic and Swart, 2000). Figure adapted from Erisman et al. (2008).

With the continuing increases in the formation of reactive nitrogen from anthropogenic activities will come increased injection into environmental reservoirs, especially the atmosphere, groundwater and the coastal oceans.

The main driver of future global N deposition is the emission trajectory. For the atmosphere, in some RCP scenarios, deposition of $NO_y + NH_x$ is projected to remain relatively constant globally although there is a balance between increases in NH_x deposition and decreases in NO_y deposition. On a regional basis, there are decreases in North America and Northern Europe, and generally increases in Asia. The regional impacts (spatial patterns) for deposition are more complex and sensitive to, apart from its sources, climate change and corresponding changes in precipitation, temperature and atmospheric circulation. Large uncertainties remain in understanding of removal mechanisms, which also depend on climatic changes lead to major uncertainties in deposition fluxes, particularly in regions removed from anthropogenic emissions (Dentener et al. 2006). The large internal variability associated with precipitation projections confounds extraction of an anthropogenic-forced climate signal in deposition projections (Hedegaard et al., 2008; Langner et al., 2005).

The area of natural vegetation exposed to critical loads of nitrogen deposition in excess of 1000 mg N m^2 yr^{-1} is projected to increase under future emissions scenarios for 2050. Under all RCP scenarios but RCP4.5, nitrogen deposition is expected to increase in many regions, following projected increases in NH_3 emissions but overall decreases in anthropogenic NO_x emissions (Lamarque et al., 2011). By 2050, emission-driven change could more than double atmospheric nitrogen deposition to some world biodiversity hotspots (under a IS92a scenario), with half of these hotspots subjected to nitrogen deposition rates over at least 10% of their total area above 15 kg N ha^{-1} yr^{-1}, exceeding critical loads set for sensitive European ecosystems (Bleeker et al., 2011; Phoenix et al., 2006).

Deposition of SO_x is also projected to decrease (Figure 6.35). Estimates for sulfur deposition in 2050, based on scenarios prior to RCPs, strongly depend on regional projections for SO_2 emissions, with all scenarios projecting decreases in North America and Europe, but potential for large growth (or reductions) in regions such as South America, Africa, South and East Asia (Dentener et al., 2006; Tagaris et al., 2008) (Figure 6.37). Under the RCP scenarios, SO_x deposition ultimately decreases strongly throughout the globe by 2100 (Lamarque et al., 2011) but in some regions, SO_2 emission increases will very likely lead to higher sulfate deposition in the near-term under some of the RCPs.

With increasing introduction of Nr into terrestrial systems will come increased flux from rivers into coastal systems. As illustrated by the Global NEWS 2 model, in 2000, discharge of dissolved inorganic nitrogen (DIN) to marine coastal waters was >1,000 kg N km^{-2} watershed for most systems downstream of either high population or extensive agricultural activity (Figure 6.38a) (Mayorga et al., 2010; Seitzinger et al., 2010). The change in DIN discharge under the Global Orchestration (GO) scenario of the Millennium Ecosystem Assessment (MEA) (the scenario with the most extreme pressures) can be estimated by examining the change between the base year 2000, and the projection year, in this case 2030 (Figure 6.38b). Manure is the most important contributor as a result of assumed high per capita meat consumption, although there are considerable regional differences/variations (Seitzinger et al., 2010). At the other extreme is the projected change in the riverine flux between 2000 and 2030 for the Adapting Mosaic scenario, the most ambitious in terms of nutrient managements of the MEA scenarios. These two scenarios provide a range of what DIN riverine fluxes might look like by the year 2030.

[INSERT FIGURE 6.35 HERE]

Figure 6.35: Deposition of SO_x (left panel) and reactive N ($NO_y + NH_x$; right panel) from 1850 to 2000 and projections of deposition to 2050 under the 4 RCP emission scenarios (Van Vuuren et al., 2011; (Lamarque et al., 2011). Also

shown are the 2030 scenarios using the SRES B1/A2 energy scenario with assumed current legislation and maximum technically feasible reduction air pollutant controls (Dentener et al., 2006).

[INSERT FIGURE 6.36 HERE]
Figure 6.36: Spatial variability of N deposition in 2000 with projections for 2050, using the 2.6 and 8.5 RCP scenarios (to indicate the range), kg N ha^{-1} yr^{-1} (Lamarque et al., 2010).

[INSERT FIGURE 6.37 HERE]
Figure 6.37: Spatial variability of S deposition in 2000 with projections for 2050, using the 2.6 and 8.5 RCP scenarios (to indicate the range), kg N ha^{-1} yr^{-1} (Lamarque et al., 2010).

[INSERT FIGURE 6.38 HERE]
Figure 6.38: a) Dissolved inorganic nitrogen river discharge to coastal zone (mouth of rivers) in 2000, based up on Global NEWS 2 model, b) change in DIN discharge from 2000 to 2030, based upon Global Orchestration and the Adaptive Mosaic scenarios, Millennium Ecosystem Assessment, (Mayorga et al., 2010; Seitzinger et al., 2010). Units are kg N per km^2 watershed per year, as an average for each watershed.

In addition to these future changes the atmospheric and riverine fluxes of short-lived N species, there are also projected to be increases in N_2O emissions. This is illustrated with by the comparison of emissions from 1850 to those in 2000 and 2050, using the IMAGE model (Figure 6.39). (Note, the MEA scenarios will be more closely tied to the RCP scenarios), A comprehensive spatially explicit inventory of N budgets in livestock and crop production systems (Bouwman et al., 2011) show that between 1900 and 1950 global soil N surplus almost doubled to 36 Tg yr^{-1} and between 1950 and 2000 to 138 Tg yr^{-1} of N. The scenario portrays a world with a further increasing global crop (+82% for 2000–2050) and livestock production (+115%); despite rapidly increasing N recovery in crop (+35%) and livestock (+35%) production, global nutrient surpluses continue to increase (N +23%). Associated agricultural emission of nitrous oxide **(**soil emission from agricultural fields**)** increased from 2.5 Tg in 1900 to 7.0 Tg of N_2O-N per year in 2000, with a continued increase to 9.3 Tg per year, reflecting the above developments.

[INSERT FIGURE 6.39 HERE]
Figure 6.39: N_2O emissions in 1900, 2000 and projected to 2050 (Bouwman et al., 2011).

6.4.6.2 Impact of Future N on Carbon Uptake and Storage

Anthropogenic Nr addition and natural N-cycle responses to global changes will have an important impact on the global carbon cycle. As a principal nutrient for plant growth, nitrogen can both limit future carbon uptake and stimulate it depending on changes in nitrogen availability. A range of global models have been developed since AR4 that integrate nitrogen dynamics into the simulation of land carbon cycling (Churkina et al., 2009; Esser et al., 2011; Gerber et al., 2010; Jain et al., 2009; Sokolov et al., 2008; Thornton et al., 2007; Zaehle and Friend, 2010). Only three of these models have so far been used to estimate the consequences for future interactions with the climate system up to 2100 (Sokolov et al., 2008; Thornton et al., 2009; Zaehle and Friend, 2010); Figure 6.40a,b).

These models show a strong effect of N availability on the response of plant growth and land carbon sequestration to elevated atmospheric CO_2, consistent with the observational evidence (Finzi et al., 2006; Norby et al., 2010; Palmroth et al., 2006). At the global scale, estimates of nutrient limitation range between 50–70% of the global carbon sequestration projected by the corresponding carbon-cycle only model resulting in a decreased β_L (Figure 6.21, and Figure 6.40). (Thornton et al., 2007) have shown for their model that this reduction is not a result of the globally lower vegetation productivity simulated by C–N cycle models, but a consequence of the nitrogen dynamics acting on long-term carbon cycling. N limitation on 21st century C sequestration is generally strongest in the boreal zone and decreases towards the temperate and tropical latitudes, but its magnitude and geographical distribution varies strongly between the models.

In response to climate warming, increased decomposition of soil organic matter increases N mineralisation, which can enhance N uptake and growth of vegetation. Generally higher C:N ratio in woody vegetation causes increased N uptake and hence ecosystem carbon storage (Melillo et al., 2011). Each of the three global land C-N models show a reduction of C loss under climate change, although with differing spatial patterns. In two models, (Sokolov et al., 2008; Thornton et al., 2009), this effect is strong enough to turn the

carbon-climate interaction into a small negative feedback (positive γ_L; Figures 6.21, 6.40), whereas in the other the carbon-climate interaction remains positive (negative γ_L; Figures 6.21, 6.40). (Sokolov et al., 2008) note, however, that the land biosphere eventually becomes a net C source despite nitrogen feedbacks.

These analyses are affected by the projected future trajectories of anthropogenic Nr deposition. The effects of N availability interacts synergistically with the N constraints on CO_2 fertilisation and climate (Churkina et al., 2009; Zaehle et al., 2010a). Estimates of the total net C storage on land due to Nr deposition between 1860 and 2100 range between 27 and 66 Pg C (Thornton et al., 2009; Zaehle et al., 2010a), based on diverging assumptions about the future evolution of N deposition.

The different magnitude and spatial distribution of N limitation across the models is caused by uncertainty about key mechanisms controlling C-N couplings (Zaehle and Dalmonech, 2011). Alternative mechanisms to represent N limitation, loss and stoichiometry, have important consequences for determining the N requirement associated with an increase in land carbon stocks (Sokolov et al., 2008). (Zaehle et al., 2010b) demonstrated the use of ecosystem manipulation experiments to constrain model responses, however, the observational data to evaluate, carbon-nitrogen coupling in these models remains vague. (Wang and Houlton, 2009) have suggested a model that projects globally significant changes in biological N fixation might occur under altered climate and atmospheric CO_2 concentrations. (Esser et al., 2011) also find that interactions between CO_2 fertilisation and N fixation are potentially important for estimating the future net land C sequestration.

The effect on land C storage due to climate-induced N release from soils is of comparable magnitude to the C storage associated with increased anthropogenic Nr. Models disagree, however, which of the two factors is more important, with both effects dependent on the choice of scenario. Crucially, the effect of N limitation on vegetation growth and ecosystem carbon storage under elevated CO_2 is the strongest effect of the natural and disturbed N cycle on terrestrial C dynamics (Bonan and Levis, 2010; Zaehle et al., 2010a).

In consequence, the projected atmospheric CO_2 concentrations (and thus degree of climate change) in 2100 are higher in –CN model projections than those projected by traditional carbon-cycle-only climate models.

[INSERT FIGURE 6.40 HERE]

Figure 6.40: a) Projection of land C storage due to changes in atmospheric CO_2, climate, N deposition and the combination of these factors (taken from the SRES A2 scenarion using LMDz-CM4) simulated by one CN model without (blue) and with (red) nitrogen dynamics (O-CN; (Zaehle et al., 2010a)). b) Difference in projected year 2100 land C storage from a) due to nitrogen dynamics. c) Development of b_l over the 21st century simulated by O-CN, compared to estimates from the carbon-cycle and carbon-nitrogen cycle simulations using CLM-CN (Thornton et al., 2007; Thornton et al., 2009), IGSM-CN (Sokolov et al., 2008), and the carbon-cycle only C4 MIP ensemble (Friedlingstein et al., 2006). d) the same for g_l, where the dashed lines red is accounting for the synergistic interactions between all factors in the O-CN model.

6.4.7 Future Changes in CH_4 Emissions

Wetlands exist most commonly in the tropics and high latitudes and are natural sources of methane due to anaerobic decomposition (methanogenesis) of organic matter in water-logged soils. Future changes in wetland extent or methane production and oxidation may change emissions. Permafrost especially can contribute to CH4 emissions in multiple ways: (1) poor drainage due to impermeable permafrost may cause surface wetlands and lakes; (2) thawing of permafrost may cause ground subsidence (thermokarst) and the inundation of surface soils; (3) thawing of permafrost may result in the decomposition of deep carbon and its release as CO_2 or CH_4 to the atmosphere. Methane hydrate deposits, both in permafrost soils and in subsea sediments, may become unstable and escape to the atmosphere, though the quantities stored in hydrates are not well known Methane is also emitted to the atmosphere by fires. Figure 6.41 shows the relative timescale and magnitude of future CH_4 emissions.

[INSERT FIGURE 6.41 HERE]

Figure 6.41: Summary diagram of the relative sizes and time scales associate with changing methane emissions (after O'Connor et al. (2010). Present day anthropogenic emissions are shown for reference, as is the effect on CH_4 from biogenic volatile organic compounds (BVOCs). BVOCs affect the atmospheric lifetime of CH_4 as they react with [OH], but are not directly emissions of CH_4. Atmospheric chemistry is not discussed further in this chapter.

6.4.7.1 *Future Wetland and Permafrost CH_4 Emissions*

Future changes in methane emissions due to climate change can be separated into changes in wetland extent and changes of methane emissions per unit area.

Wetland extent is determined by soil moisture which depends on precipitation, evapotranspiration, drainage and runoff which may all change in future. Increasing temperature can lead to higher rates of evapotranspiration, reducing soil moisture and therefore reduced wetland extent. Regional projections of precipitation changes are especially uncertain (see Chapter 12).

Permafrost thaw may lead to increased drainage and a net reduction in wetlands, a process that has already begun to be seen in lakes in the discontinuous permafrost zone (Smith et al., 2005), or alternatively to lake growth in continuous permafrost areas underlain by ice-rich material subject to thermokarst (Plug and West, 2009). There is high agreement between models that permafrost extent is expected to reduce during the 21st century, with particularly rapid warming at high latitudes. However, estimates vary widely as to the pace of degradation. (Lawrence and Slater, 2005), using the NCAR CCSM3, predict widespread loss (60–90%) of permafrost within the upper 3m of soils during the 21st century. (Burn and Nelson, 2006) argue that this is an overestimate, as it does not include many of the known stabilizing effects for permafrost; however, subsequent improvements to this model to include some of these mechanisms still show large permafrost losses (Lawrence et al., 2008). The LPJ-WHyMe model projected permafrost area loss of 30% (SRES B1) and 47% (SRES A2) by 2100 (Wania, 2007). (Marchenko et al., 2008) calculate that by 2100, 57% of Alaska will lose permafrost within the top 2m. For the RCP scenarios, the loss of permafrost area projected by the UVic ESCM in the 21st century ranged from 23% for RCP2.6 to 42.7% for RCP8.5 (Avis et al., 2011).

Simulated methane emissions from a bog in western Siberia approximately doubled when temperature (+3–5°C) and precipitation (+10–15%) were increased at the same time (Bohn et al., 2007). However, in the same study, an increase in only temperature led to such a big decrease in methane emissions that methane oxidation became larger than the emissions and the simulated site became a CH4 sink. Field-based experiments in Alaska showed a less strong response to water table manipulations and warming experiments: warming and flooding increased methane fluxes on average by 79%, while lowering the water table reduced the flux by up to 36% (Turetsky et al., 2008). Methane oxidation in soils has been projected to increase by 23% from 24.8 $TgCH_4\,yr^{-1}$ to 30.4 $TgCH_4\,yr^{-1}$ (Curry, 2009).

Thawing of deeper unsaturated Yedoma deposits was postulated to produce significant CH_4 emissions (Khvorostyanov et al., 2008), however more recent estimates with Yedoma carbon lability constrained by incubation observations (Dutta et al., 2006) argue for smaller emissions at 2100 (Koven et al., 2011). Other significant sources of uncertainty are the fraction of thawed carbon that becomes available as a substrate for methanogenesis; the impact of vegetation shifts on soil gas transport and substrate supply.

Typically, ESMs that simulate wetland CH_4 emissions neglect permafrost effects on hydrology, but can still show some complex dynamics, with wetland extent increasing in some areas due to increased precipitation, and decreasing in others due to increased ET and drainage, and earlier snowmelt (Koven et al., 2011; Ringeval et al., 2011). The UVic ESCM has projected loss of wetland area north of 45°N in the 21st century from 6.6% for RCP2.6 to 19.8% for RCP8.5 (Avis et al., 2011). Projected changes in future wetland methane emissions range from +20% to a doubling (Anisimov, 2007; Eliseev et al., 2008; Gedney et al., 2004; Wania, 2007; Zhuang et al., 2007; Zhuang et al., 2006). CO_2 fertilization may lead to increases in CH_4 emissions (vanGroenigen et al., 2011), (Ringeval et al., 2011) but CO_2 fertilization and temperature may both enhance plant growth in the Arctic (AMAP, 2009; Zhuang et al., 2007) and permafrost thawing can also lead to higher carbon accumulation rates (Turetsky et al., 2007).

The effect of climate change on the two largest natural sources of global methane emissions, tropical wetlands (Section 6.3; Bergamaschi et al., 2007; Chen and Prinn, 2006) and wet mineral soils (Spahni et al., 2011), has received little attention. Tropical wetlands are likely to experience multiple disturbances (Hamilton, 2010; Mitsch et al., 2010). Wet mineral soils, defined as mineral soils that are not inundated but whose soil moisture can intermittently reach a level that facilitates methane emissions, have been estimated as a source of 63.2 $TgCH_4\,yr^{-1}$ compared to 80.4 $TgCH_4\,yr^{-1}$ allocated to inundated wetlands (Spahni et al.,

2011). Regional changes in soil moisture will affect heterotrophic respiration in mineral soils (Falloon et al., 2011) and could also lead to a change in methane emissions from wet soils, but the sign of such a change is uncertain.

6.4.7.2 CH_4 Hydrate Emissions and Climate

Gas hydrates are ice-like cage-structures that confine low molecular-weight gasses, primarily methane. Substantial quantities of methane are believed to be stored within submarine hydrate deposits of continental margins; studies suggest between 500 and 3000 Pg of methane carbon (Archer et al., 2009a; Milkov, 2004). There is concern that warming of overlying waters may melt these deposits, releasing methane into the ocean and atmosphere systems.

Considering a potential warming of bottom-waters by 1, 3 and 5 K during the next 100 years, (Reagan and Moridis, 2007), hereafter RM07, found that hydrates residing in a typical deep ocean setting (4°C and 1000 m depth) would be stable during this timeframe. Within a typical shallow low-latitude setting (6°C and 560 m) sea-floor methane fluxes did not exceed calculated ranges of methane oxidation and consumption within the sediments. But in a typical cold-shallow Arctic setting (0.4°C and 320 m) these scenarios resulted in methane fluxes that exceeded rates of benthic sediment depletion. Observations of gas venting along the Svalbard margin seafloor (Westbrook et al., 2009) are consistent with modelling (Reagan and Moridis, 2009), indicating that observed regional warming of 1°C during the last 30 years is driving hydrate disassociation. (Elliott et al., 2011), incorporating the Arctic methane fluxes of RM07 into an ocean biogeochemistry model, demonstrated significant impacts on marine hypoxia and acidity, although atmospheric CH_4 release is small. These findings are supported by the modeling study of (Biastoch et al., 2011). Using output from RM07 and the multi-model response to AR4 1% yr^{-1} CO_2 increase, (Lamarque, 2008) predicted a global sea-floor flux of between 560–2140 $TgCH_4$ yr^{-1}, mostly in the high-latitudes.

(Archer, 2007) suggests that chronic methane release could lead to climate impacts over the next century of potentially similar magnitude to other methane sources such as terrestrial biosphere sources. Considering longer-term impacts, (Archer et al., 2009a) estimated that between 35 and 940 PgC – up to half their predicted inventory - could be released over several thousand years following a sustained 3 K seafloor warming.

These studies do not consider subsea-permafrost hosted hydrates; recent observations suggest these could be regionally significant sources of methane (Shakhova et al., 2010). It is still uncertain how much of this methane release is driven by the inundation of terrestrial permafrost by warm waters since the last deglaciation (i.e., natural cycle) or by anthropogenic forcing.

6.4.7.3 Fire CH_4 Emissions and Climate

Fire is a significant source of CH_4, both from natural but mainly anthropogenic fires (see Table 6.7). Projected increases in future fire activity (Section 6.8.1) imply that CH_4 from fires will also increase, but there are no quantitative projections published on future fire CH_4 sources. Interactions with other processes, such as thawing of permafrost may also cause fire occurrence and CH_4 emissions to increase (Turetsky et al., 2011).

6.4.8 How Future Trends in other Biogeochemical Cycles will Affect the Carbon Cycle

6.4.8.1 Changes in Fire Under Climate Change / Scenarios of Anthropogenic Fire Changes

Fire is a disturbance process that affects the net landscape carbon balance. Regional studies for boreal regions suggest an increase in future fire activity (e.g., Amiro et al., 2009; Balshi et al., 2009; Flannigan et al., 2009a; Spracklen et al., 2009; Tymstra et al., 2007; Westerling et al., 2011; Wotton et al., 2010), which has the potential to turn the Canadian forest from a carbon sink into a carbon source (Kurz et al., 2008b). Research on future fire activity has so far mainly focused on boreal North America. Predicted changes show strong spatial variations of opposite sign due to regional variations in the climate – fire relationship and anthropogenic interference (Flannigan et al., 2009b; Kloster et al., 2011; Krawchuk et al., 2009; Pechony and Shindell, 2010; Scholze et al., 2006). The response in fire activity to climate change will depend on the

prevalent fire regime which can be limited by fuel availability or fuel moisture. Wetter conditions can reduce fire activity, but increased biomass availability can promote fires (Scholze et al., 2006).

Kloster et al. (2011) show fire carbon emissions in 2075–2099 that exceed present day emissions by 17–62% depending on scenario. The amount of carbon released from fires depends critically on the burn severity. Increasing burned area and more late season burning in the future will enhance ground-layer combustion and carbon emissions, which will become even more dramatic if climate change will continue to affect thawing of permafrost (Turetsky et al., 2011; Section 6.4.7).

Future fire activity will also depend on anthropogenic factors. Land use change, resulting in landscape fragmentation, reduced biomass and a less flammable landscape, might explain the observed decreasing trend in fire activity following 1870 (Kloster et al., 2010; Marlon et al., 2008; Pechony and Shindell, 2010). Fire management efforts to protect life and property will try to adapt to changes in fire activity, but might reach their limits with projected increases (Flannigan et al., 2009a). For the Amazon it is estimated that at present 58% of the area is too humid to allow deforestation fires. Climate change might reduce this area to 37% by 2050 (LePage et al., 2010). Golding and Betts (2008) highlight that future forest vulnerability to fire may depend non-linearly on combined pressure from climate change and deforestation.

Fire modelling in the CMIP5 ESMs does not sufficiently represent the complex fire-climate relationship and possible anthropogenic interferences for a quantitative assessment of projections of future fire carbon emissions.

6.4.8.2 Impacts of Tropospheric Ozone on the Land Carbon Cycle

Plants are known to suffer damage due to exposure to high levels of ozone (O_3) (Ashmore 2005) and are likely to respond to water limitation by reducing stomatal aperture, restricting leaf uptake of both CO_2 and O_3. (Anav et al., 2011) found reductions in Gross Primary Production of 22% due to interactions between plant O_3 uptake, water stress and reductions in plant production. (Tian et al., 2011) reported that O3 effects were responsible for a 7% reduction in the net carbon sink over China from 1961–2005. Using a 2030 current legislation scenario, Van Dingenen et al. (2009) estimated future reductions in global crop yields of 2–6% and 1–2% for wheat and rice, respectively. (Felzer et al., 2005) presented global simulations of plant O_3 damage on the carbon cycle and showed a reduction in net carbon exchange by 2100 from 4–140 PgC. (Sitch et al., 2007) found a significant suppression of the global land carbon sink due to O_3 damage to vegetation by up to 260 PgC by 2100 based on SRES A2 emission scenarios. Radiative forcing from the resulting increased CO_2 concentration could exceed that of the direct radiative effect of tropospheric O_3 increases.

6.4.8.3 Iron-Deposition to Ocean

Desert dust carries iron, which is an essential micronutrient for marine biogeochemistry and thus can modulate ocean carbon storage. Future projections of desert dust deposition over the ocean are still largely uncertain, even about the sign of changes (Mahowald et al., 2009; Tegen et al., 2004). (Tagliabue et al., 2008) present results showing relatively little impact of varying aeolian Fe input on cumulative ocean CO_2 fluxes and atmospheric pCO_2 over 2000–2100, but (Mahowald et al., 2011) show projected changes in ocean productivity as large as the changes in productivity due to CO_2 increases and climate change.

6.4.8.4 Impacts of Changes in Radiation Quality on the Land Carbon Cycle

Mercado et al. (2009) estimated that variations in diffuse fraction, associated largely with the 'global dimming' period (Stanhill and Cohen, 2001), enhanced the land carbon sink by approximately 25% between 1960 and 1999. This more than offsets the negative effect of reduced surface radiation on the land carbon sink. However Mercado et al. (2009) also showed local site optima in the relationship between photosynthesis and diffuse light conditions; under heavily polluted or dark cloudy skies, plant productivity will decline as the diffuse effect is insufficient to offset decreased surface irradiance (UNEP, 2011). Under a future scenario involving rapid reductions in sulphate and black carbon aerosols, the 'diffuse-radiation' fertilization declines to near zero by 2100. This implies steeper GHG emission cuts are required to stabilize climate if anthropogenic aerosols decline as expected.

6.4.9 The Longer Term Carbon Cycle and Stabilisation

Terrestrial ecosystems may respond abrupty to climate change (Cox et al., 2004; Lenton et al., 2008), in part because biophysical feedbacks exist between the land surface and climate especially pronounced in high-latitude regions and North Africa (Claussen et al., 1999; Foley et al., 1994). In Amazonia increased (decreased) forest cover leads to increased (decreased) precipitation, and vice-versa (Betts et al., 2004; Brovkin et al., 2009). Jones et al. (2009b) highlighted that terrestrial ecosystems may exhibit significant inertia and hence be subject to committed changes after stabilisation of climate in much the same way as sea level or ice sheet melting will continue to change for decades or centuries after GHG stabilization (Hare and Meinshausen, 2006; Plattner et al., 2008; Wigley, 1995). Ecosystems are already beginning to be observed to lag behind shifts in climate regimes (Bertrand et al., 2011) and this may be expected also in ocean ecosystems (Burrows et al., 2011).

Long term changes in vegetation structure and carbon storage potentially show larger changes than during the 21st century as the long timescale response of tree growth means that by 2100 only a part of the eventual committed change is realised (Jones et al., 2010b; Jones et al., 2009b). CMIP5 simulations to extend the RCP scenarios to 2300 allow analysis of this longer term response of the carbon cycle (Figure 6.42). Northward expansion of boreal forest may be considered likely because warming of high latitudes is common to most climate models (Chapter 12) and will enable forest ecosystems to extend north into present tundra regions (Kurz et al., 2008a; MacDonald et al., 2008). Both ESMs considered here simulate increases in both tree cover and terrestrial carbon storage north of 60°N. Changes in temperate forests and the southern boundary of the boreal forest are especially uncertain both across vegetation models and climate scenarios (Figure 6.42) with models showing either an increase or decrease in tree cover depending on scenario. Increases in fire or pest activity may drive loss of forest in these regions (Kurz et al., 2008a) but are poorly represented or not accounted at all in these models. Large scale loss of tropical forest has been found to be uncertain (Scholze et al., 2006) and depends strongly on the predicted future changes in precipitation (Good et al., 2011), although both models here simulate reduced tree cover and carbon storage for the RCP8.5 scenario. Earth System models also poorly simulate resilience of ecosystems to climate changes and usually do not account for possible existence of alternative ecosystem states such as tropical forest or savannah (Hirota et al., 2011).

[INSERT FIGURE 6.42 HERE]

Figure 6.42: Time evolution of tree cover (left) and terrestrial carbon storage (right) for three latitude bands; boreal (60–90°N), temperate (30–60°N) and tropics (30°S–30°N) for the RCP extensions to 2300. Models shown are HadGEM2-ES and the MPI-Hamburg ESM which both simulate vegetation dynamics. Note the RCP6.0 extension was not a CMIP5 required simulation. Anthropogenic land-use in these extension scenarios is kept constant at 2100 levels, so these results show the response of natural ecosystems to the climate change.

Long-term commitments to ecosystems also carry long-term commitments to changes in terrestrial carbon storage (Jones et al., 2010b) and permafrost (O'Connor et al., 2010) (Section 6.4.7). The short and long term response of terrestrial carbon storage may vary in sign over different time horizons (Jones et al., 2010b; Smith and Shugart, 1993). Rapid response of tropical ecosystems may lead to early loss of carbon which is later recovered due to a larger, but slower, uptake in enhanced high latitude forests. The compatible emissions required to maintain the RCP scenarios (Section 6.4.3) beyond 2100 will depend on long-term committed changes in ecosystems.

6.5 Effects of Carbon Dioxide Removal Methods and Solar Radiation Management on the Carbon Cycle

6.5.1 Introduction

To reverse the accumulation of CO_2 in the atmosphere since the preindustrial period (Section 6.2) and the projected increases in the future (Section 6.4), several methods have been proposed to accelerate the removal of atmospheric CO_2 and enhance its storage in the land, ocean and geological reservoirs. These methods have been categorized as “Carbon Dioxide Removal (CDR)” methods under a broad class of “climate intervention” proposals. Most of the currently proposed CDR methods are summarized in Table 6.15 and some are illustrated schematically in Figure 6.43. Since a subset of these CDR methods operate on large

spatial scales and have the potential to remove significant amounts of CO_2 from the atmosphere, they could result in large scale modification to the global climate and carbon cycle, and hence they are also known as "Geoengineering" proposals (Keith, 2001).

Table 6.15: Some of the proposed CDR methods

CC Process	CDR Methods	Means of Removal	Storage Location	Storage Form
Enhanced biological production over land	Afforestation/reforestation Improved forest management Sequestration in buildings Biomass burial[a] No till agriculture Biochar Conservation agriculture Fertilization of land plants Creation of wetlands Biomass Energy with Carbon Capture and Storage (BECCS)[b]	Biological	Land [a]Land/ocean floor [b]Ocean/geological formations	Organic [b]Inorganic
Enhanced biological production over oceans	Ocean fertilization Algae farming and burial[c] Blue carbon (mangrove, kelp farming)[c] Modifying ocean up-welling	Biological	Oceans	Inorganic [c]Organic
Accelerated weathering	Enhanced weathering over land[d] Enhanced weathering over oceans[e]	Chemical	[d]Soils and oceans [e]Oceans	Inorganic
Enhanced solubility pump	Modifying ocean downwelling	Chemical	Oceans	Inorganic
Others	Direct-air capture with CCS	Chemical	Oceans/geological formations	Inorganic

[INSERT FIGURE 6.43 HERE]

Figure 6.43: Illustration of some Carbon Dioxide Removal approaches: (a) CO_2 capture by and storage in land ecosystems, (b) combustion of biomass at an electric power plant with carbon capture and storage of CO_2 either underground or in the ocean, (c) industrialized capture of CO_2 in the atmosphere with storage either underground or in the ocean, (d) extraction of alkalinity from mined silicate rocks which are then combined with atmospheric CO_2 to produce solid carbonate minerals, (e) increasing the weathering rate of silicate rocks (some dissolved carbonate minerals are transported to the ocean), (f) alkalinity from solid minerals is added to the ocean which causes CO_2 to ingas from the atmosphere, (g) nutrients are added to the ocean, transporting carbon downward, some of which is replaced by CO_2 from the atmosphere.

By definition, Carbon Dioxide Removal methods *remove* atmospheric CO_2 and store it in land, ocean or geological reservoirs. Large scale industrial methods that *reduce CO_2 emissions* before emitting CO_2 into the atmosphere such as Carbon Capture and Storage (CCS) are not classified under CDR methods. Similarly, biofuel energy production and Reducing Emissions from Deforestation and Degradation (REDD) are not CDR methods since they provide alternatives to fossil fuels and reduce emissions to the atmosphere, respectively, and do not involve removal of CO_2 that is already in the atmosphere. Further, it may be noted that IPCC defines "mitigation" in the context of climate change as "implementing policies to reduce greenhouse gas emissions and enhance sinks." Thus, according to the IPCC definition of mitigation, most CDR methods could also be considered as climate change mitigation.

In general, CDR methods are believed to be relatively less risky in terms of unintended side effects than solar radiation management (SRM) schemes to moderate climate change because they counter the root cause by reducing atmospheric carbon dioxide concentrations rather than the effects of climate change. CDR schemes also reduce direct consequences of high CO_2 levels including surface ocean acidification whereas SRM only changes the planetary energy balance. However, the effects of CDR methods are in general slow

on account of long time scales required by carbon cycle processes (transport of CO_2 to deep ocean and weathering of silicate and carbonate rocks) to remove CO_2 from the atmosphere. Therefore, CDR methods do not present an option for rapid mitigation of climate change. However, if implemented on large scales and for long enough time, these schemes could potentially make a contribution in reducing atmospheric CO_2.

6.5.1.1 Why CDR Methods?

In December 2009 at Copenhagen, governments agreed to limit climate change to 2°C above preindustrial. Modeling studies suggest a cumulative emission of 1000–1300 PgC for CO_2-induced warming to peak at 2°C (Allen et al., 2009; Meinshausen et al., 2009). Since 550 PgC of carbon has been already emitted since preindustrial times, an additional of only 500 PgC can be emitted if climate change is to be stabilized at 2°C above preindustrial levels. The corresponding atmospheric CO_2 concentration is estimated 450 ppm. At the current rate of emissions of about 9 PgC per year (LeQuere et al., 2009), this implies temperature change will reach the 2°C target in another 50–70 years. However, emissions rates are increasing in the recent past (LeQuere et al., 2009). Modeling studies indicate that emissions should decline starting 2020 in order to stabilize CO_2 at 450 ppm and CO_2 emissions should be negative if stabilization is required below 400 ppm (Mathews, 2010).

It is now widely recognized that the atmospheric lifetime of anthropogenic CO_2 is extremely long. While more than half of emitted CO_2 is absorbed by natural carbon sinks on land and in the surface ocean, additional permanent removal requires transfer of carbon to the deep ocean, which occurs slowly over many centuries. More than two thirds of the peak atmospheric CO_2 will likely remain in the atmosphere after several centuries and on the order of one third of the peak atmospheric CO_2 may still be present after 10000 years (Eby et al., 2009). As a consequence, long-term stabilization at 550 ppm CO_2 requires cuts in emissions of 81 to 90% by 2300, and more beyond as a portion of the CO_2 emitted persists for centuries to millennia, and reductions of other greenhouse gases cannot compensate for the long-term effects of emitting CO_2 (House et al., 2008). Complete removal of anthropogenic CO_2 requires absorption by geologic processes such as continental weathering which operates over timescales of hundreds of thousands of years (Archer et al., 2009b).

Further, anthropogenic climate change and its impacts will persist for millennia even if CO_2 emissions are stopped; temperatures will remain elevated, relative preindustrial conditions, for many thousands of years (Lowe et al., 2009; Mathews, 2010). Therefore, it may not be possible to reverse climate change on time scales relevant to decadal to centennial timescales without employing strategies to accelerate or supplement the slow natural removal of anthropogenic CO_2. CDR methods may be one of the available strategies to permanently reverse accumulation of CO_2 in the atmosphere that has already manifested.

6.5.1.2 CDR Scientific Issues

To have a discernable climate effect, CDR schemes should be able to remove several PgC per year from the atmosphere over several decades in this century. Important scientific considerations for evaluating carbon dioxide removal methods include the storage capacity, permanence of the storage and potential adverse side effects (Report, 2009).

Geological reservoirs can store a few thousand PgC since their capacity is estimated at several thousand PgC (House et al., 2006; Metz et al., 2005; Orr, 2009). Oceans may also be able to store a few thousand PgC of anthropogenic carbon. However, terrestrial biosphere may be able to store only a few hundred PgC since the cumulative land use flux in the last 200 years is about ~150 PgC (Houghton, 2008). Therefore, this value may represent the maximum potential land carbon storage. However it is unrealistic to suggest that this potential can be realized given competing demands for land for agricultural production, infrastructure development, biofuels and other sectors (see Section 6.3).

Permanent and non-permanent CO_2 sequestration may have very different climate implications (Kirschbaum, 2003). Permanent sequestration has the potential to decrease cumulative carbon emissions over time, and consequently to decrease total climate warming. By contrast, non-permanent sequestration would not decrease cumulative emissions to the atmosphere. Emissions would be delayed only for an amount of time that depends on the lifetime of stored carbon (Mathews, 2010; Shaffer, 2010). As a consequence, attainment

of elevated levels of atmospheric CO_2 and climate warming would only be delayed, and may not be decreased in the long term (Figure 6.44). Nevertheless, temporary sinks may have value (Dornburg and Marland, 2008) because temporary sinks do decrease the cumulative impact of higher temperature and temporary sinks buy time, i.e., they reduce climate changes in the short time while creating or preserving options for the long term.

[INSERT FIGURE 6.44 HERE]

Figure 6.44: Effect of permanent and non-permanent CO_2 sequestration. Permanent sequestration of emitted CO_2 has the potential to decrease cumulative emissions and the resulting climate warming (blue line, compared to black). If the same carbon were sequestered in a non-permanent reservoir, and returned to the atmosphere over several centuries, climate change would be delayed only, and the eventual magnitude of climate change would be equivalent to the no-sequestration case (green line, compared to black). Figure modified from Figure 5 of Mathews (2010).

Carbon stored in the terrestrial biosphere or the ocean makes the sequestered carbon more susceptible to re-release, although some forms of storage may prove long lasting (e.g., creation of wetlands). In contrast, geological stores are less subject to future human actions and ecological processes. Carbon stored in the ocean in conjunction with alkaline minerals also appears to be effectively permanent on centennial timescales (Caldeira and Rau, 2000; Caldeira et al., 2005; Kheshgi, 1995). Furthermore, any storage in terrestrial biosphere or ocean also makes the sequestered carbon more vulnerable to re-release if these stores are affected by feedbacks between climate and carbon cycle processes. Hence we should consider any sink permanence issues in the light of climate change, not under present-day conditions.

In addition to permanence, another important scientific consideration for CDR methods is the so called "rebound effect". When carbon is stored in one reservoir, the concentration gradient between the atmosphere and carbon reservoirs is reduced and thereby the subsequent inherent rate of removal of CO_2 from the atmosphere by natural reservoirs is reduced or could be reversed. Simple models have shown that when carbon is removed from the atmosphere and stored permanently, the reduction in the atmospheric carbon is less than 50% of the sequestered carbon (Kirschbaum, 2003) because any CO_2 removal will be subject to exactly the same airborne fraction as an emission (removal is simply a negative emission). Ultimately, returning to pre-industrial CO_2 levels would require permanently sequestering an amount of carbon equal to total anthropogenic CO_2 emissions that have been released before the time of CDR (Cao and Caldeira, 2010b; Lenton and Vaughan, 2009; Mathews, 2010). Therefore, to maintain atmospheric CO_2 at low levels, not only does anthropogenic CO_2 in the atmosphere need to be removed, but anthropogenic CO_2 stored in the ocean and land needs to be removed as well when it outgases to the atmosphere (Figure 6.45)

[INSERT FIGURE 6.45 HERE]

Figure 6.45: Effects of an instantaneous cessation of CO_2 emissions (amber line), one-time removal of excess atmospheric CO_2 (blue line) and removal of excess atmospheric CO_2 followed by continued removal of CO_2 that degasses from the atmosphere and ocean (green line). To a first approximation, a cessation of emissions prevents further warming but does not lead to significant cooling on the century time scale. A one-time removal of excess atmospheric CO_2 eliminates approximately half of the warming experienced at the time of the removal. To cool the planet back to pre-industrial levels requires the removal of all previously emitted CO_2, an amount equivalent to approximately twice the amount of excess CO_2 in the atmosphere. Figure adapted from (Cao and Caldeira, 2010b).

6.5.2 Carbon Cycle Processes Involved in CDR Methods

CDR methods rely primarily on natural carbon cycle processes to accelerate the removal of atmospheric CO_2: enhanced biological production by photosynthesis on (1) land and (2) oceans, (3) accelerated chemical weathering reactions over (3) land and oceans and (4) enhanced solubility pump in the oceans. The exception is direct air capture which relies on artificial chemical methods to remove CO_2 directly from air. Once captured, CO_2 is stored over land, oceans or geological formations. Carbon storage over land in organic form but storage in oceans and geological formations is in inorganic forms.

6.5.2.1 Enhanced Biological Production over Land

The key process in biomass-based CDR methods on land (Table 6.15) is photosynthesis by plants which produces biomass with carbon content of about 120 PgC each year (Figure 6.1). The common strategy of many of this class of CDR methods is to increase the production of biomass each year and/or store a portion

of the biomass in forests, soils or elsewhere (e.g., afforestation/reforestation, biochar, biomass burial, sequestration in buildings) or use it for energy production and sequester the emitted CO_2 (BECCS). Carbon is stored in organic form except in the case of BECCS where the stored material is in inorganic form.

There is relatively little peer-reviewed literature for many of the land biomass-based CDR methods such as biochar and biomass burial. Estimates of the global potential for enhanced biomass production over land and for specific methods are uncertain because the achievable sequestration by any specific method is severely constrained by competing land needs (e.g., agriculture, biofuels, urbanization, and conservation) and sociocultural considerations. A first approximation to the physical potential of afforestation/reforestation is the cumulative historical deforestation flux from forest conversion to cropland and pasturelands which is estimated between 150 and 200 PgC (Canadell and Raupach, 2008; DeFries et al., 1999; Houghton, 2008).

The capacity for enhancing the soil carbon sink on agricultural and degraded lands is estimated as 50–60% of the historic loss of 42–78 PgC (Lal, 2004a). The ability to sequester carbon in soil saturates as the soil carbon storage potential is realized. Recent estimates suggest a cumulative potential of 30–60 PgC over 25–50 years (Lal, 2004b). Permanence of soil carbon sequestration as a CDR option can be lost with a change in soil and agricultural management. The maximum sustainable technical potential of biochar is estimated at 130 PgC over a century (Woolf et al., 2010). The residence time of carbon converted to biochar in soils, and the effect on soil productivity of adding large loadings of char is uncertain and further research is required (Report, 2009).

6.5.2.2 Enhanced Biological Production over Oceans

Ocean fertilization, algae farming and enhanced storage in coastal plants are CDR methods that rely primarily on enhanced biomass production in the oceans. The peer-reviewed literature on ocean-fertilization is sufficiently extensive to make a well-informed assessment. The carbon cycle process in ocean-fertilization is photosynthesis by microscopic plants (phytoplankton). A fraction of organic carbon produced by plankton is transported to deep oceans. The inorganic carbon in the surface layers of ocean that is removed by phytoplankton is subsequently replaced by atmospheric CO_2. This process of transporting carbon from surface layers to deep-ocean by biological production in the oceans is known as the "biological pump". It is limited by the supply of nutrients available that allow plankton growth in the surface layer. The basic idea behind ocean fertilization is to add nutrients that are otherwise limiting (e.g., iron, nitrogen and phosphate) to the surface layer of the oceans to stimulate photosynthesis and thereby draw down atmospheric CO_2. The net result could be an increase in the downward flux of carbon out of the ocean's near surface layers (Martin, 1990). Since downward flux of organic carbon is oxidized in the ocean column below the surface ocean, the sequestrated carbon stored primarily in inorganic form (Dissolved Inorganic Form or DIC) in deep ocean in CDR methods that rely on ocean biological production. In other cases like algae and kelp farming and burial, the carbon would be also stored in organic form.

Ocean-fertilization has been tested in more than a dozen limited release experiments in the last 15 years (Boyd et al., 2007) on small spatial scales (~10 km^2 scale). These experiments have demonstrated only limited transient effects as increased iron led to the predicted phytoplankton bloom, but the effect is moderated either by other limiting elements, respiration or by grazing by zooplankton. The effectiveness of ocean fertilization depends both on the amount of carbon fixed in the ocean's surface layers and on the ultimate fate of this carbon. Most of the carbon that is produced through photosynthesis in the surface layers is oxidized (respired, remineralized) in these same layers, and only a small fraction is ultimately transported into the deep sea (Lampitt et al., 2008). Increases in carbon export were measured in the 2002 SOFeX experiment in the Southern Ocean, however the amount of increased export was small relative to both natural phytoplankton blooms occurring in that area, and to the scale of anthropogenic carbon dioxide emissions (Buesseler et al., 2004).

Global or regional model studies have assessed the potential carbon sink that could be generated by iron fertilization (Aumont and Bopp, 2006; Jin et al., 2008; Zeebe and Archer, 2005). Maximum potential have been estimated from 15 ppm (Zeebe and Archer, 2005) to 33 ppm (Aumont and Bopp, 2006) for a high-range baseline scenario of 700–800 ppm in 2100. In idealized studies on ocean fertilization in global or only Southern Oceans (Cao and Caldeira, 2010a; Joos et al., 1991; Peng and Broecker, 1991; Watson et al., 1994),

the maximum potential atmospheric CO_2 reduction is estimated at about 10 % (less than100 ppmv) of anthropogenic CO_2 for perfect conditions.

Biological production in the surface water could be also enhanced if the supply of nutrients to surface layers is increased by upwelling (Karl and Letelier, 2008; Lovelock and Rapley, 2007). The amount of carbon sequestered by enhancing the upwelling will depend critically on location and may well be negative (Yool et al., 2009). Artificial upwelling, under most optimistic assumptions, has been estimated to sequester atmospheric CO_2 at a rate of about 0.9 PgC yr^{-1} (Oschlies et al., 2010b).

6.5.2.3 Accelerated Weathering

There is net removal of carbon dioxide from the atmosphere and transfer to the oceans over thousands to tens of thousands of years by processes involving the weathering or dissolution of silicate and carbonate minerals (Archer et al., 2009) as typified by:

$$CaCO_3 + H_2O + CO_2 \rightarrow Ca^{2+} + 2HCO_3^- \quad (6.1)$$

$$CaSiO_3 + 2CO_2 + H_2O \rightarrow Ca^{2+} + 2HCO_3^- + SiO_2 \quad (6.2)$$

These weathering reactions typically take place at a rate that is very slow relative to the rate at which fossil fuel is being burned. Natural chemical weathering reactions consume less than 0.1 PgC yr^{-1} of carbon dioxide from the atmosphere – approximately 1% of the rate of current anthropogenic emissions (LeQuere et al., 2009). Therefore, it would take tens of thousands of years for natural processes to remove CO_2 that we may emit in this century. It has been suggested that this removal rate could be accelerated by intentional efforts to increase the rate of some or all of these weathering reactions. As can be seen from reactions (6.1) and (6.2), storage would be in the form of inorganic carbon (mostly bicarbonate) in these CDR methods.

The goal of accelerated weathering approaches is to accelerate either reaction (6.1) or (6.2) and increase the storage of carbon dioxide in dissolved form in the ocean (mostly as bicarbonate, HCO_3^-). It has been proposed that large amounts of silicate minerals such as olivine could be mined, crushed, transported to, and distributed on agricultural land, with the intent that some of the atmospheric CO_2 will be stored as a component of carbonate minerals and some bicarbonate ions would be transported to the oceans (Schuiling and Krijgsman, 2006). Alternatively, the weathering reaction rate can be enhanced by exposing minerals such as basalt or olivine to elevated CO_2 levels (Kelemen and Matter, 2008). In these land based weathering, some carbon would be stored in soils and the remaining would be carried to the oceans by runoff.

In ocean based weathering proposals, carbonate rocks could be ground and reacted with concentrated CO_2 captured at power plants to produce bicarbonate solution which would be released to the oceans (Rau, 2008; Rau and Caldeira, 1999). Alternatively, carbonate minerals could be directly released into the oceans (Harvey, 2008; Kheshgi, 1995). It has also been proposed that strong bases, derived from silicate rocks, could be dissolved in oceans (House et al., 2007), which would cause the oceans to absorb additional CO_2. Carbonate minerals such as limestone could be heated to produce lime ($Ca(OH)_2$); this lime could be added to the oceans to increase ocean's alkalinity and thereby promote ocean uptake of atmospheric CO_2 (Kheshgi, 1995).

6.5.2.4 Enhanced Solubility Pump

It has been proposed that invigorating the overturning circulation of the oceans could cause increased transport of DIC from surface ocean in high latitudes to deep ocean (Zhou and Flynn, 2005) since most of the CO_2 in the deep sea is transported there by the overturning circulation (the 'solubility pump') and not by biological pump (Sarmiento and Gruber, 2006). Ocean carbonate chemistry is the carbon cycle process that removes atmospheric CO_2 in this method. Since surface waters are already saturated in CO_2, the proposal is to increase the volume of downwelling waters. In this process, carbon would be stored in the deep ocean in inorganic form (DIC). Realistic enhancement of downwelling by1 million m^3 s^{-1} is estimated to increase ocean uptake of carbon by only ~0.01–0.02 PgC yr^{-1} (Zhou and Flynn, 2005).

6.5.2.5 Other CDR Methods

6.5.2.5.1 Direct air capture

Air capture refers to the chemical process by which pure CO_2 stream is produced by capturing CO_2 from the ambient air. The captured CO_2 would be transported and used for commercial purposes or sequestered in inorganic form in geological reservoirs or deep-ocean. At least three methods have been proposed to capture CO_2 from the atmosphere: adsorption on solids (Gray et al., 2008; Lackner, 2009, 2010); absorption into highly alkaline solutions (Mahmoudkhani and Keith, 2009; Stolaroff et al., 2008). The main scientific factor that provides a barrier to air capture of CO_2 is thermodynamic barrier due to the lower concentration of CO_2 in air (CO_2 content of the air is only about 0.04%) and hence there is large uncertainty on the effectiveness of this method.

6.5.2.6 Impacts of CDR Methods on Carbon Cycle and Climate

One impact that is common to all CDR methods is related to the thermal inertia of the climate system. Many aspects of the earth system may continue to respond for decades or centuries to the original increases in CO_2 even after CDR is applied. Therefore, decreases in surface temperature would lag CDR-induced decreases in atmospheric CO_2 concentrations. This could potentially lead to hysteresis behaviour in many climate variables with respect to atmospheric CO_2. Second, hysteresis can happen with respect on temperature if some variables have large fast climate response because of changes in atmospheric CO_2 (Bala et al., 2009). For instance, modeling studies (Cao et al., 2011; Wu et al., 2010) shown that there will be a temporary acceleration of the global hydrological cycle and global-mean precipitation would increase temporarily in response to a reduction in atmospheric CO_2 concentrations (Figure 6.46). Another effect that is common to all CDR methods is that implementation of CDR methods could lead to reduced plant productivity when compared to the elevated level expected with high CO_2 concentration.

[INSERT FIGURE 6.46 HERE]

Figure 6.46: HadCM3L results from a simulation with 2% annual change in atmospheric CO_2: (a) global and annual mean changes in precipitation as a function of atmospheric CO_2; (b) global and annual mean changes in precipitation as a function of global and annual mean changes in surface temperature. Red dots represent the first 70-year simulation phase with 2% annual CO_2 increase (ramp_up) and time moves forward from the lower left to the upper right. Blue dots represent the subsequent 70-year period with 2% annual CO_2 decrease (ramp_down) and time moves forward from the upper right to the lower left. Black dots represent the following 150-years with the constant control CO_2 concentration and time moves forward from the upper right to the lower left. The simulation states when atmospheric CO_2 reaches $1 \times CO_2$ and $4 \times CO_2$ concentrations are marked with yellow circles. Due to the ocean thermal inertia one atmospheric CO_2 state corresponds to two different states of temperature and precipitation, and due to the precipitation sensitivity to atmospheric CO_2 content changes (Bala et al., 2009), one temperature state corresponds to two different precipitation states. Figure adopted from Cao et al. (2011).

6.5.2.6.1 Enhanced biological production over land

CDR methods that enhance biomass in forests carries the risk that carbon stores may return to the atmosphere by disturbances such as fire and insect outbreaks, exacerbated by climate extremes and climate change, or by future forest clearing. When considering activities such as afforestation/reforestation, it is important to account for all climatic effects of forests because reforestation/reforestation will change the surface characteristics like albedo, evapotranspiration and surface roughness (Bonan, 2008). Many modelling studies have shown that afforestation in the seasonally snow covered boreal and temperate regions could decrease the land surface albedo and have a net warming effect, and tropical afforestation in low latitudes could have a net cooling effect due to enhanced latent heat flux from evapotranspiration (Bala et al., 2007; Bathiany et al., 2010; Betts, 2000; Bonan et al., 1992; Montenegro et al., 2009). Changes in evapotranspiration have the potential to alter humidity and cloudiness and hence surface temperature, particularly in tropical regions (Bala et al., 2007). Because of these biophysical effects as well as the biogeochemical effect of carbon sequestration in vegetation, the location of biomass production methods need to considered when evaluating the net effects (Bala et al., 2007). For instance, in a recent study, warming reductions per unit afforested area are estimated as three times higher in the tropics than in the boreal and northern temperate regions, suggesting that afforestation in the tropics are effective forest management strategies from a climate perspective (Arora and Montenegro, 2011).

6.5.2.6.2 Enhanced biological production over oceans

In the case of ocean fertilization, the utilization of macronutrients such as nitrogen and phosphate in the fertilized region can lead to a decrease in production "downstream" from the fertilized region (Gnanadesikan and Marinov, 2008; Gnanadesikan et al., 2003; Watson et al., 2008). This effect can occur, for example, if nutrients such as nitrogen and phosphate are depleted in the fertilized region. A sustained global-ocean iron fertilization could also acidify the deep ocean by storing more DIC there while not significantly reducing the surface ocean acidification problem (Cao and Caldeira, 2010a). Other environmental risks associated with ocean fertilization include expanded regions with low oxygen concentration (Oschlies et al., 2010a), increased production of N_2O and CH_4 (Jin and Gruber, 2003; Oschlies et al., 2010a), and possible disruptions to marine ecosystems (Denman, 2008).

In the case of enhanced biological production through increased ocean upwelling, there could be disturbance to regional carbon balance, since the upwelling must be balanced by downwelling at another location. Along will growth-supporting nutrients, enhanced concentrations of DIC are also brought to surface waters which could degas to the atmosphere and partially offset carbon sequestration through enhanced biological production. Further, whenever artificial upwelling is stopped, surface temperatures and atmospheric CO_2 concentrations could rise rapidly for decades to centuries to levels even somewhat higher than experienced in a world that never engaged in artificial upwelling. This is because carbon removed from atmosphere and stored in soils due to cooling of land caused by upwelling can be suddenly released when artificial upwelling is stopped (Oschlies et al., 2010b).

6.5.2.6.3 Accelerated weathering

The pH and carbonate mineral saturation of soils and ocean surface waters would be raised locally. In the marine environment, the elevated pH and increased alkalinity could have potential application to counteract effects of ocean acidification.

6.5.2.6.4 Enhanced solubility pump

Artificially increased ocean downwelling (or upwelling) must be compensated by increased upwelling (or downwelling) at another location which may affect the regional carbon balance.

6.5.3 Summary

CDR methods propose to accelerate the removal of atmospheric CO_2 through either natural carbon cycle processes or by artificial means and store the removed CO_2 in land, ocean and geological reservoirs. Storage capacity, permanence of the storage system and the potential side effects are important considerations for CDR methods. While quantifying the amount of sequestered CO_2, the rebound effect in which removal of carbon from the atmosphere increases its release from its reservoirs, thereby diminishing the effectiveness of CDR methods should be also considered. CDR methods can be broadly classified into 4 types according to the natural carbon cycle process involved in the removal of atmospheric CO_2: enhanced biomass production over land, enhanced biomass production over oceans, accelerated weathering and enhanced solubility pump. Other CDR methods such as direct air capture and absorbing cement depend on synthetic chemical reactions to accelerate the atmospheric CO_2 removal. The CO_2 that is removed from the atmosphere is proposed to be stored in carbon reservoirs in land biosphere, deep ocean or geological reservoirs. Carbon would be stored in organic form in land biosphere and in inorganic form in deep ocean and geological reservoirs.

The characteristics of CDR methods are listed in Table 6.15 and Table 6.16 lists features of some specific CDR methods for which peer-reviewed literature exists. There are potential climate and carbon cycle side effects from both CDR and SRM methods. Some examples of the side effects are: 1) Removal of atmospheric CO_2 would lead to acceleration in global water cycle. 2) Large scale biological production over land will have climate consequences by altering the surface characteristics such as albedo and evapotranspiration. Because of this, quantification of the net impact of these methods has large uncertainty. 3) Enhanced biological production over oceans could potentially lead to expanded regions with low oxygen concentration, increased production of N_2O and CH_4, possible disruptions to marine ecosystems and disturbance to regional carbon cycle. 4) Enhanced solubility pump could potentially disturb the regional carbon balance.

Table 6.16: Characteristics of some CDR methods which have peer-reviewed literature. It should be noted that a variety of economic, environmental, and other constraints could also limit deployment.

Carbon Dioxide Removal method	Means of removing CO_2 from atmosphere	Carbon storage /form	Time scale of carbon storage	Physical potential of CO_2 removed in a century*	Reference
Afforestation and reforestation	Biological	Land /Organic	Decades to centuries	80–140 PgC[a], 48 PgC[b]	[a](Canadell and Raupach, 2008; [b]Sitch et al., 2005)
Biomass energy with carbon capture and storage	Biological	Geological or ocean /Inorganic	Effectively permanent for geologic, centuries for ocean	100 PgC	[≠]See the footnote
Biochar	Biological	Land /Organic	Decades to centuries	130 PgC	(Woolf et al., 2010)
Ocean fertilization	Biological	Ocean /Inorganic	Centuries to millennia	30–66 PgC[a] 200PgC[b]	[a](Aumont and Bopp, 2006; Zeebe and Archer, 2005; Cao and Caldeira, 2010)
Accelerated weathering over land	Geo-chemical	Ocean (and some soils) /Inorganic	Centuries to millennia for carbonates, permanent for silicate weathering	No obvious limit	(Kelemen and Matter, 2008; Schuiling and Krijgsman, 2006)
Ocean-based weathering	Geo-chemical	Ocean /Inorganic	Centuries to millennia for carbonates, permanent for silicate weathering	No obvious limit	(Rau, 2008; Kheshgi, 1995)
Direct air capture	Chemical	Geological or ocean /Inorganic	Effectively permanent for geologic, centuries for ocean	No obvious limit	(Keith et al., 2006; Shaffer, 2010)
Modification of upwelling/ down welling	Biological/ chemical	Ocean /Inorganic	Centuries to millennia	[a]90 PgC [b]1–2 PgC	[a](Oschlies et al., 2010a; [b]Lenton and Vaughan, 2009; Zhou and Flynn, 2005)

Notes:
*Physical potential does not account for economic or environmental constraints of CDR methods, for example the value of the physical constraint for afforestation and reforestation does not consider the conflicts with land needed for agricultural production
[≠] If 2.5 tC per year per hectare can be harvested on a sustainable basis (Kraxner et al., 2003) on 3% (~400 million hectares, about one fourth of global agricultural land area) of global land (13.4 billion hectares) for BECS, approximately 1 PgC per year could be removed or about 100 PgC in this century.

6.5.4 Impacts of Solar Radiation Management on Carbon Cycle

The other class of climate intervention, SRM techniques could also have impacts on the carbon cycle. SRM methods aim to counter the long wave radiative effect of greenhouse forcing by reducing the amount of incoming solar radiation to the earth surface. Balancing reduced outgoing radiation by reduced incoming radiation may be able to counter global mean temperature changes but will lead to a less intense global hydrological cycle (Bala et al., 2008) and may not completely cancel regional changes in temperature or precipitation (Govindasamy et al., 2003; Irvine et al., 2010; Ricke et al., 2010) and hence have effects on the regional carbon cycle budgets.

Earth System Models (ESMs) have been used to assess the degree to which SRM techniques successfully counter climate change and to quantify any possible residual impacts on the carbon cycle and ecosystems. (Jones et al., 2009a) and (Jones et al., 2010a) analyse the impacts on the climate and carbon cycle of SRM through injection of SO_2 into the stratosphere (Crutzen, 2006) and sea-salt injection into the marine boundary layer (Latham et al., 2008). In both SRM schemes global temperatures are much reduced compared to the no-geoengineering control case, but regional climate changes persist including persistent warming at high latitudes and regional changes in precipitation. The effect of these local changes on the carbon cycle varies

regionally and is likely to vary between models. There is potential for some SRM schemes to negatively affect the efficiency of existing sinks of anthropogenic carbon by altering the winds in the Southern Ocean, although the magnitude or duration of this affect is uncertain (Vaughan and Lenton, 2011).

Whilst SRM techniques may counter the radiative effects of CO_2 they do not remove any direct effects of CO_2 on natural ecosystems. In the ocean, acidification caused by elevated CO_2 (Section 6.4.5) which may be detrimental to marine ecosystems, is not prevented by SRM. On land, elevated CO_2 stimulates uptake by terrestrial vegetation and hence enhances vegetation and soil carbon stocks (Govindasamy et al., 2002). However, due to the strong coupling between climate and the carbon cycle, SRM could indirectly affect the carbon cycle. For instance, modelling studies have shown that SRM methods could indirectly affect ocean chemistry (Matthews et al. 2009): SRM significantly re-distributes carbon emissions among atmosphere, land and ocean reservoirs with enhanced carbon stocks over land simulated for an SRM case. This redistribution could slow pH decreases in the ocean somewhat relative to a non-SRM case, but does not affect the level of aragonite (a type of carbonate) saturation due to opposing responses of pH and aragonite saturation to temperature changes. Without enhanced accumulation in the land biosphere, this modelling study finds that SRM has little effect on pH, and could lead to accelerated declines in aragonite saturation.

There is much evidence that SRM schemes will not precisely counteract all of the regional climate effects of elevated CO_2 and cannot counteract the direct effects of CO_2 on ecosystems. Over land, elevated atmospheric CO_2 but cooler temperatures in an SRM-case could lead to enhanced NPP but a reduction in terrestrial respiration. The net result could be a significant reduction in atmospheric CO_2 and increased carbon accumulation in the terrestrial biosphere, especially soils (Vaughan and Lenton, 2011). The stomatal response of plants to elevated CO_2 has also been shown to affect land temperatures, evapotransipration and hence runoff (Betts et al. 2007; Cao et al. 2010; Gedney et al. 2006; Piao et al. 2007). SRM will not prevent this CO_2-physiological effect on both climate and carbon cycle. More research is needed to understand the multiple implications of SRM methods.

The SRM method of artificial injection of aerosols into the stratosphere (Report, 2009) is likely to increase the amount of diffuse solar insolation at the surface at the expense of direct light (Crutzen, 2006). Recent theoretical and observational studies have demonstrated that photosynthesis is more efficient under diffuse light conditions (Gu et al., 2003; Niyogi et al., 2004; Oliveira et al., 2007). A recent modelling study estimates that variations in diffuse fraction, associated largely with the 'global dimming' period (Liepert and Tegen, 2002; Liepert, 2002; Stanhill and Cohen, 2001) enhanced the terrestrial carbon uptake by approximately one quarter between 1960 and 1999(Mercado et al., 2009). Therefore, SRM schemes that increase the diffuse fraction of sunlight (e.g., stratospheric aerosol injection) has the potential to enhance the terrestrial carbon sink. However, reduction in Photosynthetically Active Radiation (PAR) due to SRM methods could cause a drop in land uptake of carbon. Sufficient information is lacking to ascertain whether the net effect of such SRM schemes would be to enhance the carbon sink due to enhanced diffuse light, or to reduce it due to a reduction in overall PAR.

[START FAQ 6.1 HERE]

FAQ 6.1: What Happens to Carbon Dioxide After it is Emitted into the Atmosphere?

The ocean and the land biosphere take up a fraction of the excess CO_2 emitted into the atmosphere and the carbon is subsequently redistributed among the different reservoirs of the global carbon cycle on a multitude of time scales. Depending on the amount of CO_2 released, 20–40% will remain in the atmosphere for up to 2000 years when a new balance is established between the atmosphere, the land biosphere and the ocean. A further reduction by geological processes will take time scales from tens to hundred thousand years and more. Enhanced atmospheric CO_2 and associated climate impacts of present emissions will thus persist for a very long time into the future.

Carbon dioxide is an inert gas, which is mixed throughout the entire troposphere rapidly within less than a year. In contrast to chemical compounds in the atmosphere (e.g., CH_4) that are removed and destroyed by sink processes, carbon is not lost, but simply redistributed among the different reservoirs of the global carbon

cycle. A simplified diagram of the global carbon cycle is shown in FAQ 6.1, Figure 1. The open arrows indicate typical times for carbon atoms to be transferred through the different reservoirs.

[INSERT FAQ 6.1, FIGURE 1 HERE]

FAQ6.1, Figure 1: Simplified schematic of the global carbon cycle including its major reservoirs and turnover time scales.

At the ocean surface CO_2 molecules are constantly exchanged between the air and the sea by molecular diffusion. In the sea water, the invading CO_2 becomes carbonic acid, which reacts chemically very fast with the large pool of dissolved inorganic carbon in the ocean consisting of bi-carbonate and carbonate ions. Currents and mixing processes transport the carbon between the surface layer and the interior of the ocean. The marine biota also redistributes carbon: marine organisms grow organic tissue and calcareous shells in surface waters, which after death sink to depth where it is transformed back to inorganic forms by microbes. A small fraction reaches the sea floor and forms sediments.

On land the vegetation absorbs CO_2 by photosynthesis and converts it into organic matter. A fraction of this carbon is immediately returned to the atmosphere as CO_2 by plant respiration. The remainder leads to growth of the vegetation. Dead plant material forms soils, which are eventually decomposed by microbes and respired back into the atmosphere as CO_2.

In a steady, equilibrium state, the exchange fluxes of the global carbon cycle are balanced, i.e., carbon inflows match the outflows of each carbon pool. A net emission of carbon dioxide into the atmosphere, however, induces a disequilibrium. Firstly, the global CO_2 concentration rises. This rise modifies the exchange processes of CO_2 with the carbon pools in direct contact with the atmosphere, i.e., surface ocean and land vegetation, and subsequently within and among carbon reservoirs on land, in the ocean and eventually the earth crust. Thus, the excess carbon is redistributed within the entire global carbon cycle until the carbon exchange fluxes between the different carbon pools have reached a new balanced state. The time it takes to reach this balance depends on the transfer times of carbon through the different reservoirs.

What determines the ocean CO_2 uptake?

Over the ocean the increased atmospheric concentration directly increases the air-to-sea flux of CO_2 molecules. In the surface ocean, the carbonate chemistry quickly adjusts to the CO_2 invasion. As a consequence areas with a shallow surface ocean become balanced with the atmosphere rapidly within 1-2 years. Further ocean uptake is controlled by mixing with deeper waters on time scales of decades to many centuries. On still longer time scales acidification of the invading CO_2 leads to dissolution of carbonate sediments, which still further enhances ocean uptake.

What controls land CO_2 uptake?

An increase in atmospheric CO_2 stimulates photosynthesis and thus carbon uptake, however, however, additional factors such as water and nutrient availability are important as well. Furthermore, the relatively short transfer times of carbon through most terrestrial carbon reservoirs imply only a modest and relatively temporary uptake capacity for excess carbon compared to the ocean.

How fast is the equilibration within the global carbon cycle taking place?

Equilibration takes place over a multitude of time scales: firstly among the “fast” carbon reservoirs (atmosphere, ocean, land vegetation and soils) over time scales up to a few thousand years. Subsequently, on longer time scales the very slow geological processes become important: dissolution of carbonate sediments and sediment burial into the earth crust. FAQ 6.1, Figure 2 shows as an example the decay of the atmospheric CO_2 concentration as a fraction of the initial pulse input computed with a global carbon cycle - climate model. Because of the ocean chemistry, the size of the initial input is important: higher emissions imply a larger fraction of CO_2 remaining in the atmosphere.

[INSERT FAQ 6.1, FIGURE 2 HERE]

FAQ 6.1, Figure 2: Decrease of an atmospheric CO_2 pulse emission of 1000 PgC emitted at time 0 showing the different time scales of the equilibration with the different reservoirs in the global carbon cycle. Displayed is the percentage of the initial perturbation taken up by atmosphere, land and ocean (after Archer et al., 2009; the graph shows the simulation results from the CLIMBER-2 model). Note the different time scales in the three sections of the graph.

How do changes in climate affect the redistribution of carbon in the global carbon cycle?

All carbon cycle exchange processes depend directly or indirectly on the prevailing climate, e.g., temperature and/or the availability of water. The climate change impact of a CO_2 emission will therefore modify the exchange fluxes between the carbon reservoirs, the relevant adjustment times and the final equilibrium. E.g., warmer seawater has a lower CO_2 solubility and shifted chemical carbon reactions lead to a lower ocean uptake of excess atmospheric CO_2. Likewise on land higher temperatures foster longer vegetation periods in temperate and higher latitudes, but also faster respiration of soil carbon. The net effect depends on additional factors, such as type of vegetation, availability of water and nutrients. Overall, model calculations indicate that a warmer climate leads to less carbon uptake by the ocean and land implying enhanced atmospheric CO_2 concentration when climate effects are taken into account.

How much CO_2 will remain in the atmosphere forever?

Depending on the amount of CO_2 released 20–40% will remain in the atmosphere for up to 2000 years when the carbon flows between atmosphere, land vegetation, soils and ocean have reached a new balance. A further reduction by carbonate sediment dissolution and reactions with igneous rocks (a.o. silicate weathering, sediment burial) will take geological time scales from tens to hundred thousand years and more. Enhanced atmospheric CO_2 and associated climate impacts of present emissions will thus persist for a very long time into the future.

[END FAQ 6.1 HERE]

[START FAQ 6.2 HERE]

FAQ 6.2: Could Rapid Release of Methane and Carbon Dioxide from Thawing Permafrost or Ocean Warming Substantially Increase Warming?

Permafrost are permanently frozen soils occurring primarily in high latitudes of the Arctic. Permafrost soils, including the sub-sea permafrost on the shallow shelves of the Arctic Ocean, contain organic carbon; at least twice the amount of what is currently in the atmosphere as carbon dioxide. Release of a sizable fraction of this carbon as methane and carbon dioxide would lead to warmer atmospheric temperatures, causing yet more methane and carbon dioxide to be released. It would thus create a positive feedback loop that amplifies global warming.

[INSERT FAQ 6.2, FIGURE 1 HERE]

FAQ 6.2, Figure 1: Simplified graph of major carbon pools and flows in the Arctic domain, including permafrost on land, continental shelves and ocean (Adapted from McGuire et al., 2009 and Tarnocai et al., 2008).

What are the mechanisms and timescales involved in this process?

Permafrost organic carbon

Most of the carbon in permafrost on land and also on ocean shelves is stored in organic forms, which needs to be mineralized by microorganisms in order to become volatile either as carbon dioxide under aerobic conditions or as methane under anaerobic conditions.

On land, permafrost is overlain by an “active layer” at the surface, which thaws during summer and forms part of the tundra ecosystem. Increasing temperatures lead to a longer seasonal time period when the active layer is above freezing temperatures, and it will also increase its thickness. This makes more organic carbon accessible for microbial decomposition, but the extended vegetation periods will also promote enhanced CO_2 uptake by photosynthesis of the arctic vegetation. Hence the net carbon balance of these regions is a delicate balance between enhanced uptake and enhanced release of carbon. Additionally, the hydrological conditions

during the summer thaw phase are important: In shallow lakes or inundated topographic depressions anaerobic conditions will prevail and decomposition of thawed permafrost organic soil carbon will result in methane emissions. Which of these different processes will dominate on a global scale under climate warming is not very well known. However, the timescales involved to liberate significant permafrost soil carbon are relatively large because heat diffusion and melting permafrost takes time, in fact present Arctic permafrost can be seen as a relict of the last glaciation, which is still slowly eroding.

Under aerobic conditions, remineralisation of organic soil carbon involves the release of heat (similar to a compost), which, during summer, may foster further permafrost melting. Depending on the amount of carbon and ice content of the permafrost and the hydrological regime, this mechanism could trigger under warming relatively fast local permafrost degradation.

Existing modeling studies of global warming induced feedback on permafrost dynamics indicate a modest positive feedback, which operates on timescales of 100 years, and is similar in magnitude to other biogeochemical feedbacks.

Methane hydrates

A second frozen form of carbon in permafrost but occurring also on ocean shelves, shelf slopes and deeper ocean bottom sediments are methane hydrates. These consist of methane and water molecule clusters, which are stable in a specific window of low temperatures and high pressures. Most of these hydrates on land and ocean originate from marine or terrestrial biogenic carbon, decomposed under anaerobic conditions and trapped in an aquatic environment under suitable temperature-pressure conditions. Warming of permafrost soils, ocean waters and sediments or changes in pressure, e.g., by sea level changes, could destabilize these hydrates and release the methane to the ocean and the atmosphere. The pool of these hydrates is very large, alone in the Arctic the amount of methane stored as hydrates may be more than 10 times the present amount of methane in the global atmosphere.

How vulnerable are these methane hydrate pools under global warming?

On land, liberating the hydrates is a slow process, similar to the melting of the permafrost soils operating on centennial scales. In the ocean, deeper regions and bottom sediments will take centuries to millennia to become warmed to destabilize the hydrates. Furthermore, methane released in deeper waters has to reach the surface and atmosphere in order to become climatically active. Most of the methane from deeper waters is expected to be consumed by microorganisms before reaching the surface. Only the methane from hydrates from shallow shelves, such as in the Arctic ocean north of Eastern Siberia, may indeed reach the atmosphere and have a climate impact.

Is there any observational evidence for enhanced methane emissions caused by the recent anthropogenic warming from permafrost or vulnerable ocean regions?

Several studies recently have documented locally significant methane emissions in the Arctic; over the arctic Siberian shelf and from Siberian lakes. There is no evidence available, however, whether these sources have been enhanced due to recent regional warming. Hence it may be possible, that these methane seepages may have been present since the last deglaciation. In magnitude, these documented Arctic/permafrost methane sources are very small in the global methane budget. This is also confirmed by atmospheric methane concentration observations from in-situ stations and satellite measurements, which do not exhibit substantially enhanced values over the Arctic domain.

It is expected that methane and carbon dioxide emissions will increase under Arctic warming and that they provide a positive climate feedback. However on timescales of centuries this feedback will be moderate and similar in magnitude to other climate-terrestrial ecosystem feedbacks. On time scales of millennia and longer, however, carbon dioxide and methane releases from permafrost and shelves/shelf slopes are much more important because of the large carbon and methane hydrate pools at stake.

[END FAQ 6.2 HERE]

References

Abdalla, M., M. Jones, J. Yeluripati, P. Smith, J. Burke, and M. Williams, 2010: Testing DayCent and DNDC model simulations of N2O fluxes and assessing the impacts of climate change on the gas flux and biomass production from a humid pasture. *Atmospheric Environment*, **44**, 2961-2970.

Achard, F., H. D. Eva, P. Mayaux, H.-J. Stibig, and A. Belward, 2004: Improved estimates of net carbon emissions from land cover change in the tropics for the 1990s. *Global Biogeochemical Cycles*, **18**, doi:10.1029/2003GB002142.

Achard, F., H. Eva, H. Stibig, P. Mayaux, J. Gallego, T. Richards, and J. Malingreau, 2002: Determination of deforestation rates of the world's humid tropical forests. *Science*, **297**, 999-1002.

Adkins, J. F., K. McIntyre, and D. P. Schrag, 2002: The salinity, temperature and δ18O of the glacial deep ocean. *Science*, **298**, 1769-1773.

Ahn, J., and E. J. Brook, 2008: Atmospheric CO2 and climate on millennial time scales during the last glacial period. *Science*, **322**, 83-85.

Ahn, J., et al., submitted: Atmospheric CO2 over the last 1000 years: A high resolution record from the West Antarctic Ice Sheet (WAIS) Divide ice core. *Global Biogeochemical Cycles*.

Allan, W., H. Struthers, and D. C. Lowe, 2007: Methane carbon isotope effects caused by atomic chlorine in the marine boundary layer: Global model results compared with Southern Hemisphere measurements. *Journal of Geophysical Research-Atmospheres*, **112**.

Allen, M. R., D. J. Frame, C. Huntingford, C. D. Jones, J. A. Lowe, M. Meinshausen, and N. Meinshausen, 2009: Warming caused by cumulative carbon emissions towards the trillionth tonne. *Nature*, **458**, 1163-1166.

AMAP, 2009: Update on selected climate issues of concern, 15pp pp.

Amiro, B., A. Cantin, M. Flannigan, and W. de Groot, 2009: Future emissions from Canadian boreal forest fires. *Canadian Journal of Forest Research-Revue Canadienne De Recherche Forestiere*, **39**, 383-395.

Amiro, B., et al., 2010: Ecosystem carbon dioxide fluxes after disturbance in forests of North America. *Journal of Geophysical Research-Biogeosciences*, **115**, -.

Anav, A., L. Menut, D. Khvorostyanov, and N. Viovy, 2011: Impact of tropospheric ozone on the Euro-Mediterranean vegetation. *Global Change Biology*, **17**, 2342-2359.

Anderson, R. F., M. Q. Fleisher, Y. Lao, and G. Winckler, 2008: Modern CaCO3 preservation in equatorial Pacific sediments in the context of late-Pleistocene glacial cycles. *Marine Chemistry*, **111**, 30-46.

Andres, R., J. Gregg, L. Losey, G. Marland, and T. Boden, 2011: Monthly, global emissions of carbon dioxide from fossil fuel consumption. *Tellus Series B-Chemical and Physical Meteorology*, **63**, 309-327.

Anisimov, O., 2007: Potential feedback of thawing permafrost to the global climate system through methane emission. *Environmental Research Letters*, **2**, -.

Archer, D., 2007: Methane hydrate stability and anthropogenic climate change. *Biogeosciences*, **4**, 521-544.

Archer, D., and E. Maierreimer, 1994: Effect of deep-sea sedimentary calcite preservation on atmospheric CO2 concentration. *Nature*, **367**, 260-263.

Archer, D., and V. Brovkin, 2008: The millennial atmospheric lifetime of anthropogenic CO2. *Climatic Change*, **90**, 283-297.

Archer, D., B. Buffett, and V. Brovkin, 2009a: Ocean methane hydrates as a slow tipping point in the global carbon cycle. *Proceedings of the National Academy of Sciences*, **106**, 20596-20601.

Archer, D., A. Winguth, D. Lea, and N. Mahowald, 2000: What caused the glacial/interglacial atmospheric pCO(2) cycles? *Reviews of Geophysics*, **38**, 159-189.

Archer, D., et al., 2009b: Atmospheric Lifetime of Fossil Fuel Carbon Dioxide. *Annual Review of Earth and Planetary Sciences*, **37**, 117-134.

Arneth, A., et al., 2010: Terrestrial biogeochemical feedbacks in the climate system. *Nature Geoscience*, **3**, 525-532.

Arora, V., et al., 2011: Carbon emission limits required to satisfy future representative concentration pathways of greenhouse gases. *Geophysical Research Letters*, **38**, -.

Arora, V. K., and G. J. Boer, 2010: Uncertainties in the 20th century carbon budget associated with land use change. *Global Change Biology*, **16**, 3327-3348.

Arora, V. K., and A. Montenegro, 2011: Small temperature benefits provided by realistic afforestation efforts. *Nature Geoscience*, **4(8)**, 514-518.

Assmann, K. M., M. Bentsen, J. Segschneider, and C. Heinze, 2010: An isopycnic ocean carbon cycle model. *Geoscientific Model Development*, **3**, 143-167.

Aumont, O., and L. Bopp, 2006: Globalizing results from ocean in situ iron fertilization studies. *Global Biogeochemical Cycles*, **20**.

Avis, C., A. Weaver, and K. Meissner, 2011: Reduction in areal extent of high-latitude wetlands in response to permafrost thaw. *Nature Geoscience*, **4**, 444-448.

Aydin, M., K. R. Verhulst, and e. al., 2011a: Recent decreases in fossil-fuel emissions of ethane and methane derived from firn air. *Nature*, **476**, 198-201.

Aydin, M., et al., 2011b: Recent decreases in fossil-fuel emissions of ethane and methane derived from firn air. *Nature*, **476**, 198-201.

Ayres, R. U., W. H. Schlesinger, and R. H. Socolow, 1994: Human impacts on the carbon and nitrogen cycles. *Industrial Ecology and Global Change*, R. H. Socolow, Andrews, C., Berkhout, R, and V. Thomas (eds.), Ed., 121-155.

Bacastow, R. B., and C. D. Keeling, 1979: Models to predict future atmospheric CO2 concentrations. *Workshop on the Global Effects of Carbon Dioxide from Fossil Fuels,*, United States Department of Energy, 72-90.

Baker, A., S. Cumberland, and N. Hudson, 2008: Dissolved and total organic and inorganic carbon in some British rivers. *Area*, **40**, 117-127.

Baker, D. F., et al., 2006: TransCom 3 inversion intercomparison: Impact of transport model errors on the interannual variability of regional CO2 fluxes, 1988–2003. *Global Biogeochemical Cycles*, **20**.

Bala, G., P. B. Duffy, and K. E. Taylor, 2008: Impact of geoengineering schemes on the global hydrological cycle. *P Natl Acad Sci USA*, **105**, 7664-7669.

Bala, G., K. Caldeira, and R. Nemani, 2009: Fast versus slow response in climate change: implications for the global hydrological cycle. *Climate Dynamics*, **DOI 10.1007/s00382-009-0583-y**.

Bala, G., K. Caldeira, M. Wickett, T. J. Phillips, D. B. Lobell, C. Delire, and A. Mirin, 2007: Combined climate and carbon-cycle effects of large-scale deforestation. *P Natl Acad Sci USA*, **104**, 6550-6555.

Balshi, M., A. McGuire, P. Duffy, M. Flannigan, D. Kicklighter, and J. Melillo, 2009: Vulnerability of carbon storage in North American boreal forests to wildfires during the 21st century. *Global Change Biology*, **15**, 1491-1510.

Barnard, R., P. W. Leadley, and B. A. Hungate, 2005: Global change, nitrification, and denitrification: A review. *Global Biogeochemical Cycles*, **19**.

Barnes, R. T., and P. A. Raymond, 2009: The contribution of agricultural and urban activities to inorganic carbon fluxes within temperate watersheds. *Chemical Geology*, **266**, 318-327.

Bathiany, S., M. Claussen, V. Brovkin, T. Raddatz, and V. Gayler, 2010: Combined biogeophysical and biogeochemical effects of large-scale forest cover changes in the MPI earth system model. *Biogeosciences*, **7**, 1383-1399.

Batjes, N., 1996: Total carbon and nitrogen in the soils of the world. *European Journal of Soil Science*, **47**, 151-163.

Beaulieu, J. J., et al., 2011: Nitrous oxide emission from denitrification in stream and river networks. *P Natl Acad Sci USA*, **108**, 214-219.

Beer, C., et al., 2010: Terrestrial Gross Carbon Dioxide Uptake: Global Distribution and Covariation with Climate. *Science*, **329**, 834-838.

Bellassen, V., G. Le Maire, J. F. Dhote, P. Ciais, and N. Viovy, 2010: Modelling forest management within a global vegetation model. Part 1: Model structure and general behaviour. *Ecological Modeling*, **221**, 2458-2474.

Bennington, V., G. A. McKinley, S. Dutkiewicz, and D. Ulman, 2009: What does chlorophyll variability tell us about export and air-sea CO2 flux variability in the North Atlantic? *Global Biogeochemical Cycles*, **23**, -.

Bergamaschi, P., et al., 2007: Satellite chartography of atmospheric methane from SCIAMACHYon board ENVISAT: 2. Evaluation based on inverse model simulations. *Journal of Geophysical Research-Atmospheres*, **112**, -.

Berger, W. H., 1982: Increase of carbon-dioxide in the atmosphere during deglaciation - the coral-reef hypothesis. *Naturwissenschaften*, **69**, 87-88.

Berner, R. A., 1992: Weathering, plants, and the long-term carbon-cycle. *Geochimica Et Cosmochimica Acta*, **56**, 3225-3231.

Bertrand, R., et al., 2011: Changes in plant community composition lag behind climate warming in lowland forests. *Nature*, doi:10.1038/nature10548.

Betts, R., P. Cox, M. Collins, P. Harris, C. Huntingford, and C. Jones, 2004: The role of ecosystem-atmosphere interactions in simulated Amazonian precipitation decrease and forest dieback under global climate warming. *Theoretical and Applied Climatology*, DOI 10.1007/s00704-004-0050-y. 157-175.

Betts, R. A., 2000: Offset of the potential carbon sink from boreal forestation by decreases in surface albedo. *Nature*, **408**, 187-190.

Biastoch, A., et al., 2011: Rising Arctic Ocean temperatures cause gas hydrate destabilization and ocean acidification. *Geophysical Research Letters*, **38**, -.

Billings, S. A., S. M. Schaeffer, and R. D. Evans, 2002: Trace N gas losses and N mineralization in Mojave desert soils exposed to elevated CO2. *Soil Biology & Biochemistry*, **34**, 1777-1784.

Bird, M. I., J. Lloyd, and G. D. Farquhar, 1996: Terrestrial carbon storage from the last glacial maximum to the present. *Chemosphere*, **33**, 1675-1685.

Bleeker, A., K. Hicks, F. Dentener, and J. Galloway, 2011: N deposition as a threat to the World's protected areas under the Convention on Biological Diversity. *Environmental pollution*, **159**, 2280-2288.

Blunier, T., J. Chappellaz, J. Schwander, B. Stauffer, and D. Raynaud, 1995: Variations in atmospheric methane concentration during the Holocene epoch. *Nature*, **374**, 46-49.

Bock, M., J. Schmitt, L. Moller, R. Spahni, T. Blunier, and H. Fischer, 2010: Hydrogen Isotopes Preclude Marine Hydrate CH4 Emissions at the Onset of Dansgaard-Oeschger Events. *Science*, **328**, 1686-1689.

Boden, T., G. Marland, and R. Andres. Global CO2 Emissions from Fossil-Fuel Burning,Cement Manufacture, and Gas Flaring: 1751-2008. [Available online at http://cdiac.ornl.gov/trends/emis/meth_reg.html.]

Boer, G., and V. Arora, 2010: Geographic Aspects of Temperature and Concentration Feedbacks in the Carbon Budget. *Journal of Climate*, **23**, 775-784.

Bohn, T., D. Lettenmaier, K. Sathulur, L. Bowling, E. Podest, K. McDonald, and T. Friborg, 2007: Methane emissions from western Siberian wetlands: heterogeneity and sensitivity to climate change. *Environmental Research Letters*, **2**, -.

Bonan, G. B., 2008: *Ecological Climatology.* Cambridge University.

Bonan, G. B., and S. Levis, 2010: Quantifying carbon-nitrogen feedbacks in the Community Land Model (CLM4). *Geophysical Research Letters*, **37**, -.

Bonan, G. B., D. Pollard, and S. L. Thompson, 1992: Effects of Boreal Forest Vegetation on Global Climate. *Nature*, **359**, 716-718.

Booth, B. B., et al., submitted: High sensitivity of future global warming to land carbon cycle processes. *Environmental Research Letters*.

Bopp, L., K. E. Kohfeld, C. Le Quere, and O. Aumont, 2003: Dust impact on marine biota and atmospheric CO2 during glacial periods. *Paleoceanography*, **18**.

Bopp, L., C. Le Quere, M. Heimann, A. C. Manning, and P. Monfray, 2002: Climate-induced oceanic oxygen fluxes: Implications for the contemporary carbon budget. *Global Biogeochem. Cycles*, **16**, 1022.

Bopp, L., et al., 2001: Potential impact of climate change on marine export production. *Global Biogeochem. Cycles*, **15**, 81-99.

Bousquet, P., D. A. Hauglustaine, P. Peylin, C. Carouge, and P. Ciais, 2005: Two decades of OH variability as inferred by an inversion of atmospheric transport and chemistry of methyl chloroform. *Atmospheric Chemistry and Physics*, **5**, 2635-2656.

Bousquet, P., P. Peylin, P. Ciais, C. Le Quere, P. Friedlingstein, and P. Tans, 2000: Regional changes in carbon dioxide fluxes of land and oceans since 1980. *Science*. 1342-1346.

Bousquet, P., et al., 2006: Contribution of anthropogenic and natural sources to atmospheric methane variability. *Nature*, **443**, 439-443.

Bousquet, P., et al., 2011: Source attribution of the changes in atmospheric methane for 2006–2008. *Atmos. Chem. Phys.*, **11**, 3689-3700.

Bouttes, N., D. Paillard, D. M. Roche, V. Brovkin, and L. Bopp, 2011: Last Glacial Maximum CO2 and d13C successfully reconciled. *Geophysical Research Letters*, **38**.

Bouwman, A. F., et al., 2011: Exploring global changes in nitrogen and phosphorus cycles in agriculture induced by livestock production over the 1900–2050 period. *P Natl Acad Sci USA*, 10.1073/pnas.1012878108.

Boyd, P. W., et al., 2007: Mesoscale iron enrichment experiments 1993-2005: Synthesis and future directions. *Science*, **315**, 612-617.

Bozbiyik, A., M. Steinacher, F. Joos, T. F. Stocker, and L. Menviel, 2011: Fingerprints of changes in the terrestrial carbon cycle in response to large reorganizations in ocean circulation. *Climate of the Past*, **7**, 319-338.

Broecker, W. S., and T. H. Peng, 1986: Carbon cycle - 1985 glacial to interglacial changes in the operation of the global carbon cycle. *Radiocarbon*, **28**, 309-327.

Broecker, W. S., E. Clark, D. C. McCorkle, T. H. Peng, I. Hajdas, and G. Bonani, 1999: Evidence for a reduction in the carbonate ion content of the deep sea during the course of the Holocene. *Paleoceanography*, **14**, 744-752.

Brovkin, V., A. Ganopolski, D. Archer, and S. Rahmstorf, 2007: Lowering of glacial atmospheric CO2 in response to changes in oceanic circulation and marine biogeochemistry. *Paleoceanography*, **22**.

Brovkin, V., J. H. Kim, M. Hofmann, and R. Schneider, 2008: A lowering effect of reconstructed Holocene changes in sea surface temperatures on the atmospheric CO2 concentration. *Global Biogeochemical Cycles*, **22**.

Brovkin, V., T. Raddatz, C. H. Reick, M. Claussen, and V. Gayler, 2009: Global biogeophysical interactions between forest and climate. *Geophysical Research Letters*, **36**.

Brovkin, V., S. Sitch, W. von Bloh, M. Claussen, E. Bauer, and W. Cramer, 2004: Role of land cover changes for atmospheric CO2 increase and climate change during the last 150 years. *Global Change Biology*, **10**, 1253-1266.

Brovkin, V., J. Bendtsen, M. Claussen, A. Ganopolski, C. Kubatzki, V. Petoukhov, and A. Andreev, 2002: Carbon cycle, vegetation, and climate dynamics in the Holocene: Experiments with the CLIMBER-2 model. *Global Biogeochemical Cycles*, **16**.

Buesseler, K. O., J. E. Andrews, S. M. Pike, and M. A. Charette, 2004: The effects of iron fertilization on carbon sequestration in the Southern Ocean. *Science*, **304(5669)**, 414-417.

Burn, C., and F. Nelson, 2006: Comment on "A projection of severe near-surface permafrost degradation during the 21st century" by David M. Lawrence and Andrew G. Slater. *Geophysical Research Letters*, **33**, -.

Burrows, M. T., et al., 2011: The Pace of Shifting Climate in Marine and Terrestrial Ecosystems. *Science*, **334**, 652-655.

Butterbach-Bahl, K., and M. Dannenmann, 2011: Denitrification and associated soil N2O emissions due to agricultural activities in a changing climate. *Current Opinion in Environmental Sustainability*, **3**, 389-395.

Byrne, R., S. Mecking, R. Feely, and X. Liu, 2010: Direct observations of basin-wide acidification of the North Pacific Ocean. *Geophysical Research Letters*, **37**, -.

Cadule, P., et al., 2010: Benchmarking coupled climate-carbon models against long-term atmospheric CO2 measurements. *Global Biogeochemical Cycles*, **24**, -.

Caldeira, K., and G. H. Rau, 2000: Accelerating carbonate dissolution to sequester carbon dioxide in the ocean: Geochemical implications. *Geophysical Research Letters*, **27(2)**, 225-228.

Caldeira, K., and M. E. Wickett, 2005: Ocean model predictions of chemistry changes from carbon dioxide emissions to the atmosphere and ocean. *J Geophys Res-Oceans*, **110**.
Caldeira, K., et al., 2005: Ocean storage. In: IPCC Special Report on Carbon Dioxide Capture and Storage. Prepared by Working Group III of the Intergovernmental Panel on Climate Change [Metz, B., O. Davidson, H. C. de Coninck, M. Loos, and L. A. Meyer (eds.)]. Cambridge University Press, 442pp.
Canadell, J. G., and M. R. Raupach, 2008: Managing forests for climate change mitigation. *Science*, **320**, 1456-1457.
Canadell, J. G., et al., 2007: Contributions to accelerating atmospheric CO2 growth from economic activity, carbon intensity, and efficiency of natural sinks. *P Natl Acad Sci USA*, **104**, 18866-18870.
Cao, L., and K. Caldeira, 2010a: Can ocean iron fertilization mitigate ocean acidification? *Climatic Change*, **99**, 303-311.
——, 2010b: Atmospheric carbon dioxide removal: long-term consequences and commitment. *Environmental Research Letters*, **5**.
Cao, L., K. Caldeira, and A. K. Jain, 2007: Effects of carbon dioxide and climate change on ocean acidification and carbonate mineral saturation. *Geophysical Research Letters*, **34**.
Cao, L., G. Bala, and K. Caldeira, 2011: Why is there a short-term increase in global precipitation in response to diminished CO(2) forcing? *Geophysical Research Letters*, **38**.
Carcaillet, C., et al., 2002: Holocene biomass burning and global dynamics of the carbon cycle. *Chemosphere*, **49**, 845-863.
Chantarel, A. M., J. M. G. Bloor, N. Deltroy, and J.-F. Soussana, 2011: Effects of climate change drivers on nitrous oxide fluxes in an upland temperate grassland. *Ecosystems*, **14**, 223-233.
Chapuis-Lardy, L., N. Wrage, A. Metay, J. L. Chotte, and M. Bernoux, 2007: Soils, a sink for N2O? A review. *Global Change Biology*, **13**, 1-17.
Chen, Y., and R. Prinn, 2006: Estimation of atmospheric methane emissions between 1996 and 2001 using a three-dimensional global chemical transport model. *Journal of Geophysical Research-Atmospheres*, **111**, -.
Chhabra, A., K. R. Manjunath, S. Panigrahy, and J. S. Parihar, 2009: Spatial pattern of methane emissions from Indian livestock. *Current Science*, **96**, 683-689.
Churkina, G., V. Brovkin, W. von Bloh, K. Trusilova, M. Jung, and F. Dentener, 2009: Synergy of rising nitrogen depositions and atmospheric CO2 on land carbon uptake moderately offsets global warming. *Global Biogeochemical Cycles*, **23**.
Churkina, G., et al., 2010: Interactions between nitrogen deposition, land cover conversion, and climate change determine the contemporary carbon balance of Europe. *Biogeosciences*, DOI 10.5194/bg-7-2749-2010. 2749-2764.
Ciais, P., P. Rayner, F. Chevallier, P. Bousquet, M. Logan, P. Peylin, and M. Ramonet, 2010: Atmospheric inversions for estimating CO2 fluxes: methods and perspectives. *Climatic Change*, **103**, 69-92.
Ciais, P., et al., 2005: Europe-wide reduction in primary productivity caused by the heat and drought in 2003. *Nature*, DOI 10.1038/nature03972. 529-533.
Claussen, M., C. Kubatzki, V. Brovkin, A. Ganopolski, P. Hoelzmann, and H. J. Pachur, 1999: Simulation of an abrupt change in Saharan vegetation in the mid-Holocene. *Geophysical Research Letters*, **26**, 2037-2040.
Codispoti, L. A., 2010: Interesting Times for Marine N2O. *Science*, **327**, 1339-1340.
Codispoti, L. A., A. H. Devol, S. W. A. Naqvi, H. W. Paerl, and T. Yoshinari, 2001: The oceanic fixed nitrogen and nitrous oxide budgets: Moving targets as we enter the anthropocene? *Scientia Marina*, **65**, 85-105.
Collins, W. J., et al., 2011a: Development and evaluation of an Earth-system model - HadGEM2. *Geosci. Model Dev. Discuss.*, **4**, 997-1062.
Collins, W. J., et al., 2011b: Development and evaluation of an Earth-system model - HadGEM2. *Geosci. Model Dev. Discuss.*, **4**, 997-1062.
Conrad, R., 1996: Soil microorganisms as controllers of atmospheric trace gases (H2, CO, CH4, OCS, N2O, and NO). *Microbiological Reviews*, **60**, 609-640.
Conway, T., and P. Tans. Global CO2. [Available online at http://www.esrl.noaa.gov/gmd/ccgg/trends/global.html.]
Conway, T. J., P. P. Tans, L. S. Waterman, and K. W. Thoning, 1994: Evidence for interannual variability of the carbon cycle from the national oceanic and atmospheric administration climate monitoring and diagnostics laboratory global air sampling network. *Journal of Geophysical Research - Atmospheres*, **99**, 22831-22855.
Corbiere, A., N. Metzl, G. Reverdin, C. Brunet, and A. Takahashi, 2007: Interannual and decadal variability of the oceanic carbon sink in the North Atlantic subpolar gyre. *Tellus Series B-Chemical and Physical Meteorology*, **59**, 168-178.
Cox, P., and C. Jones, 2008: Climate change - Illuminating the modern dance of climate and CO2. *Science*, DOI 10.1126/science.1158907. 1642-1644.
Cox, P. M., 2001a: Description of the TRIFFID dynamic global vegetation model. *Technical Note 24 HadleyCentre, Met Office*.
Cox, P. M., 2001b: Description of the TRIFFID dynamic global vegetation model. Technical Note 24 HadleyCentre, Met Office.
Cox, P. M., R. A. Betts, C. D. Jones, S. A. Spall, and I. J. Totterdell, 2000: Acceleration of global warming due to carbon-cycle feedbacks in a coupled climate model. *Nature*, **408**, 184-187.

Cox, P. M., R. A. Betts, M. Collins, P. P. Harris, C. Huntingford, and C. D. Jones, 2004: Amazonian forest dieback under climate-carbon cycle projections for the 21st century. *Theoretical and Applied Climatology*, **78**, 137-156.
Crutzen, P. J., 2006: Albedo enhancement by stratospheric sulfur injections: A contribution to resolve a policy dilemma? *Climatic Change*, **77**, 211-219.
Curry, C., 2009: The consumption of atmospheric methane by soil in a simulated future climate. *Biogeosciences*, **6**, 2355-2367.
Davidson, E. A., 2009: The contribution of manure and fertilizer nitrogen to atmospheric nitrous oxide since 1860. *Nature Geoscience*, **2**, 659-662.
De Klein, C., et al., 2007: N_2O Emissions from Managed Soils, and CO_2 Emissions from Lime and Urea Application. *2006 IPCC Guidelines for National Greenhouse Gas Inventories*, 1-54.
DeFries, R., and C. Rosenzweig, 2010: Toward a whole-landscape approach for sustainable land use in the tropics. *Proceedings of the National Academy of Sciences*, **107**, 19627-19632.
DeFries, R., R. A. Houghton, M. Hansen, C. Field, D. L. Skole, and J. Townshend, 2002: Carbon emissions from tropical deforestation and regrowth based on satellite observations for the 1980s and 90s. *Proceedings of the National Academy of Sciences*, **99**, 14256-14261.
DeFries, R. S., C. B. Field, I. Fung, G. J. Collatz, and L. Bounoua, 1999: Combining satellite data and biogeochemical models to estimate global effects of human-induced land cover change on carbon emissions and primary productivity. *Global Biogeochemical Cycles*, **13**, 803-815.
Delmas, R. J., J. M. Ascencio, and M. Legrand, 1980: Polar ice evidence that atmospheric CO2 20,000-yr BP was 50-percent of present. *Nature*, **284**, 155-157.
Denman, K. L., 2008: Climate change, ocean processes and ocean iron fertilization. *Marine Ecology Processes Series*, **364**, 219-225.
Denman, K. L., et al., 2007: Couplings Between Changes in the Climate System and Biogeochemistry.
Dentener, F., W. Peters, M. Krol, M. van Weele, P. Bergamaschi, and J. Lelieveld, 2003: Interannual variability and trend of CH4 lifetime as a measure for OH changes in the 1979-1993 time period. *Journal of Geophysical Research-Atmospheres*, **108**.
Dentener, F., et al., 2006: The global atmospheric environment for the next generation. *Environ. Sci. Technol.*, **40**, 3586-3594.
Deutsch, C., J. L. Sarmiento, D. M. Sigman, N. Gruber, and J. P. Dunne, 2007: Spatial coupling of nitrogen inputs and losses in the ocean. *Nature*, **445**, 163-167.
Dlugokencky, E. J., P. M. Lang, and K. A. Masarie, 2010: Atmospheric Methane dry air mole fractions from teh NOAA ESRL carbon cycle cooperative global air sampling network, 1983-2009. NOAA/ESRL.
Dlugokencky, E. J., E. G. Nisbet, R. Fisher, and D. Lowry, 2011: Global atmospheric methane: budget, changes and dangers. *Philosophical Transactions of the Royal Society a-Mathematical Physical and Engineering Sciences*, **369**, 2058-2072.
Dlugokencky, E. J., S. Houweling, L. Bruhwiler, K. A. Masarie, P. M. Lang, J. B. Miller, and P. P. Tans, 2003: Atmospheric methane levels off: Temporary pause or a new steady-state? *Geophysical Research Letters*, **30**.
Dlugokencky, E. J., et al., 2009: Observational constraints on recent increases in the atmospheric CH4 burden. *Geophys. Res. Lett.*, **36**, L18803.
Doney, S. C., 2010: The Growing Human Footprint on Coastal and Open-Ocean Biogeochemistry. *Science*, **328**, 1512-1516.
Doney, S. C., et al., 2009: Mechanisms governing interannual variability in upper-ocean inorganic carbon system and air-sea CO2 fluxes: physical climate and atmospheric dust. *Deep-Sea Res.*, **II**, 640-655.
Dornburg, V., and G. Marland, 2008: Temporary storage of carbon in the biosphere does have value for climate change mitigation: a response to the paper by Miko Kirschbaum. *Mitigation and Adaptation Strategies for Global Change*, **13**, 211-217.
Duce, R. A., et al., 2008: Impacts of atmospheric anthropogenic nitrogen on the open ocean. *Science*, **320**, 893-897.
Dueck, T. A., et al., 2007: No evidence for substantial aerobic methane emission by terrestrial plants: a (13)C-labelling approach. *New Phytologist*, **175**, 29-35.
Dutta, K., E. Schuur, J. Neff, and S. Zimov, 2006: Potential carbon release from permafrost soils of Northeastern Siberia. *Global Change Biology*, **12**, 2336-2351.
Eby, M., K. Zickfeld, A. Montenegro, D. Archer, K. J. Meissner, and A. J. Weaver, 2009: Lifetime of Anthropogenic Climate Change: Millennial Time Scales of Potential CO2 and Surface Temperature Perturbations. *Journal of Climate*, **22**, 2501-2511.
Eliseev, A., I. Mokhov, M. Arzhanov, P. Demchenko, and S. Denisov, 2008: Interaction of the methane cycle and processes in wetland ecosystems in a climate model of intermediate complexity. *Izvestiya Atmospheric and Oceanic Physics*, **44**, 139-152.
Elliott, S., M. Maltrud, M. Reagan, G. Moridis, and P. Cameron-Smith, 2011: Marine methane cycle simulations for the period of early global warming (vol 116, G01010, 2011). *Journal of Geophysical Research-Biogeosciences*, **116**, -.
Elsig, J., et al., 2009: Stable isotope constraints on Holocene carbon cycle changes from an Antarctic ice core. *Nature*, **461**, 507-510.

EPA, 2006: Global anthropogenic non-CO2 greenhouse gas emissions. US EPA report EPA-430-R-06-003. http://nepis.epa.gov/EPA/html/DLwait.htm?url=/Adobe/PDF/2000ZL5G.PDF.
Erisman, J. W., M. S. Sutton, J. N. Galloway, Z. Klimont, and W. Winiwarter, 2008: A century of ammonia synthesis. *Nature Geosciences*, **1**, 1-4.
Erisman, J. W., J. Galloway, S. Seitzinger, A. Bleeker, and K. Butterbach-Bahl, 2011: Reactive nitrogen in the environment and its effect on climate change. *Current Opinion in Environmental Sustainability*, **3**, 281-290.
Esser, G., J. Kattge, and A. Sakalli, 2011: Feedback of carbon and nitrogen cycles enhances carbon sequestration in the terrestrial biosphere. *Global Change Biology*, **17**, 819-842.
Etheridge, D. M., L. P. Steele, R. L. Langenfelds, R. J. Francey, J.-M. Barnola, and M. V. I., 1996: Natural and anthropogenic changes in atmospheric CO2 over the last 1000 years from air in Antarctic ice and firn. *Journal of Geophysical Research*, **101**, 4115-4128.
Etiope, G., K. R. Lassey, R. W. Klusman, and E. Boschi, 2008: Reappraisal of the fossil methane budget and related emission from geologic sources. *Geophysical Research Letters 35: L09307.*, **35**, L09307.
Falloon, P., C. Jones, M. Ades, and K. Paul, 2011: Direct soil moisture controls of future global soil carbon changes: An important source of uncertainty. *Global Biogeochemical Cycles*, **25**, -.
Fan, S., T. Blaine, and J. Sarmiento, 1999: Terrestrial carbon sink in the Northern Hemisphere estimated from the atmospheric CO2 difference between Manna Loa and the South Pole since 1959. *Tellus B*, **51**, 863-870.
FAO, 2000: Fertilizer Requirements in 2015 and 2030.
——, 2010: Global Forest Resources Assessment 2010. *FAO Forestry Paper 163*. 340 pp.
Feely, R. A., S. C. Doney, and S. R. Cooley, 2009: Ocean Acidification: Present Conditions and Future Changes in a High-CO2 World. *Oceanography*, **22**, 36-47.
Feely, R. A., T. Takahashi, R. Wanninkhof, M. J. McPhaden, C. E. Cosca, S. C. Sutherland, and M. E. Carr, 2006: Decadal variability of the air-sea CO2 fluxes in the equatorial Pacific Ocean. *J Geophys Res-Oceans*, **111**, -.
Felzer, B., D. Kicklighter, J. Melillo, C. Wang, Q. Zhuang, and R. Prinn, 2004: Effects of ozone on net primary production and carbon sequestration in the conterminous United States using a biogeochemistry model. *Tellus Series B-Chemical and Physical Meteorology*, **56**, 230-248.
Felzer, B., et al., 2005: Future effects of ozone on carbon sequestration and climate change policy using a global biogeochemical model. *Climatic Change*, **73**, 345-373.
Ferretti, D. F., et al., 2005: Unexpected changes to the global methane budget over the past 2000 years. *Science*, **309**, 1714-1717.
Finzi, A., et al., 2006: Progressive nitrogen limitation of ecosystem processes under elevated CO2 in a warm-temperate forest. *Ecology*, **87**, 15-25.
Fischer, H., et al., 2008: Changing boreal methane sources and constant biomass burning during the last termination. *Nature*, **452**, 864-867.
Flannigan, M., B. Stocks, M. Turetsky, and M. Wotton, 2009a: Impacts of climate change on fire activity and fire management in the circumboreal forest. *Global Change Biology*, **15**, 549-560.
Flannigan, M., M. Krawchuk, W. de Groot, B. Wotton, and L. Gowman, 2009b: Implications of changing climate for global wildland fire. *International Journal of Wildland Fire*, **18**, 483-507.
Fluckiger, J., A. Dallenbach, T. Blunier, B. Stauffer, T. F. Stocker, D. Raynaud, and J. M. Barnola, 1999: Variations in atmospheric N2O concentration during abrupt climatic changes. *Science*, **285**, 227-230.
Fluckiger, J., et al., 2002: High-resolution Holocene N2O ice core record and its relationship with CH4 and CO2. *Global Biogeochemical Cycles*, **16**.
Fluckiger, J., et al., 2004: N2O and CH4 variations during the last glacial epoch: Insight into global processes. *Global Biogeochemical Cycles*, **18**.
Foley, J. A., J. E. Kutzbach, M. T. Coe, and S. Levis, 1994: Feedbacks between climate and boreal forests during the Holocene epoch. *Nature*, **371**, 52-54.
Foley, J. A., C. Monfreda, N. Ramankutty, and D. Zaks, 2007: Our share of the planetary pie. *Proceedings of the National Academy of Sciences*, **104**, 12585.
Frank, D. C., J. Esper, C. C. Raible, U. Buntgen, V. Trouet, B. Stocker, and F. Joos, 2010: Ensemble reconstruction constraints on the global carbon cycle sensitivity to climate. *Nature*, **463**, 527-U143.
Frankenberg, C., et al., 2008: Tropical methane emissions: A revised view from SCIAMACHY onboard ENVISAT. *Geophysical Research Letters*, **35**, L15811.
Friedli, H., H. Lotscher, H. Oeschger, U. Siegenthaler, and B. Stauffer, 1986: Ice core record of the C-13/C-12 ratio of atmospheric CO2 in the past 2 centuries. *Nature*, **324**, 237-238.
Friedlingstein, P., and I. Prentice, 2010: Carbon-climate feedbacks: a review of model and observation based estimates. *Current Opinion in Environmental Sustainability*, DOI 10.1016/j.cosust.2010.06.002. 251-257.
Friedlingstein, P., et al., 2010: Update on CO2 emissions. *Nature Geoscience*, **3**, 811-812.
Friedlingstein, P., et al., 2006: Climate-carbon cycle feedback analysis: Results from the (CMIP)-M-4 model intercomparison. *Journal of Climate*, **19**, 3337-3353.
Friis, K., A. Kortzinger, J. Patsch, and D. W. R. Wallace, 2005: On the temporal increase of anthropogenic CO2 in the subpolar North Atlantic. *Deep-Sea Research Part I-Oceanographic Research Papers*, **52**, 681-698.

Frolicher, T. L., F. Joos, G. K. Plattner, M. Steinacher, and S. C. Doney, 2009: Natural variability and anthropogenic trends in oceanic oxygen in a coupled carbon cycle–climate model ensemble. *Global Biogeochem. Cycles*, **23**, GB1003.

Fuller, D. Q., J. van Etten, K. Manning, C. Castillo, E. Kingwell-Banham, and A. Weisskopf, et al., 2011: The contribution of rice agriculture and livestock pastoralism to prehistoric methane levels: an archaeological assessment. *The Holocene*.

Gaillard, M. J., et al., 2010: Holocene land-cover reconstructions for studies on land cover-climate feedbacks. *Climate of the Past*, **6**, 483-499.

Galloway, J., et al., 2004: Nitrogen cycles: past, present, and future. *Biogeochemistry*, **70**, 153-226.

Galloway, J. N., W. H. Schlesinger, H. Levy II, A. Michaels, and J. L. Schnoor, 1995: Nitrogen fixation: Anthropogenic enhancement – environmental response. *Global Biogeochem. Sci.*, **9**, 235-252.

Galloway, J. N., et al., 2008: Transformation of the nitrogen cycle: recent trends, questions and potential solutions. *Science*, **320**, 889-889.

Gedalof, Z., and A. A. Berg, 2010: Tree ring evidence for limited direct CO2 fertilization of forests over the 20th century. *Global Biogeochemical Cycles*, **24**, -.

Gedney, N., P. Cox, and C. Huntingford, 2004: Climate feedback from wetland methane emissions. *Geophysical Research Letters*, ARTN L20503, DOI 10.1029/2004GL020919. -.

Gent, P., et al., 2011: The Community Climate System Model Version 4. *Journal of Climate*, **24**, 4973-4991.

Gerber, S., L. O. Hedin, M. Oppenheimer, S. W. Pacala, and E. Shevliakova, 2010: Nitrogen cycling and feedbacks in a global dynamic land model. *Global Biogeochemical Cycles*, **24**.

Gerber, S., F. Joos, P. Brugger, T. F. Stocker, M. E. Mann, S. Sitch, and M. Scholze, 2003: Constraining temperature variations over the last millennium by comparing simulated and observed atmospheric CO2. *Climate Dynamics*, **20**, 281-299.

Gervois, S., P. Ciais, N. de Noblet-Ducoudre, N. Brisson, N. Vuichard, and N. Viovy, 2008: Carbon and water balance of European croplands throughout the 20th century. *Global Biogeochemical Cycles*, **22**, -.

Gilbert, D., N. N. Rabalais, R. J. Diaz, and J. Zhang, 2010: Evidence for greater oxygen decline rates in the coastal ocean than in the open ocean. *Biogeosciences*, **7**, 2283-2296.

Gloor, M., J. L. Sarmiento, and N. Gruber, 2010: What can be learned about carbon cycle climate feedbacks from the CO2 airborne fraction? *Atmospheric Chemistry and Physics*, **10**, 7739-7751.

Gloor, M., et al., 2009: Does the disturbance hypothesis explain the biomass increase in basin-wide Amazon forest plot data? *Global Change Biology*, **15**, 2418-2430.

Gnanadesikan, A., and I. Marinov, 2008: Export is not enough: nutrient cycling and carbon sequestration. *Marine Ecology-Progress Series*, **364**, 289-294.

Gnanadesikan, A., J. L. Sarmiento, and R. D. Slater, 2003: Effects of patchy ocean fertilization on atmospheric carbon dioxide and biological production. *Global Biogeochemical Cycles*, **17**.

Gnanadesikan, A., J. L. Russell, and F. Zeng, 2007: How does ocean ventilation change under global warming? *Ocean Science*, **3**, 43-53.

Gnanadesikan, A., J. P. Dunne, and J. John, 2011: Will open-ocean oxygen stress intensify under climate change? *Biogeosciences Discussions*, **8**, 7007-7032.

Goldewijk, K. K., A. Beusen, G. van Drecht, and M. de Vos, 2011: The HYDE 3.1 spatially explicit database of human-induced global land-use change over the past 12,000 years. *Global Ecology and Biogeography*, **20**, 73-86.

Golding, N., and R. Betts, 2008: Fire risk in Amazonia due to climate change in the HadCM3 climate model: Potential interactions with deforestation. *Global Biogeochemical Cycles*, ARTN GB4007, DOI 10.1029/2007GB003166. -.

Goldstein, B., F. Joos, and T. F. Stocker, 2003: A modeling study of oceanic nitrous oxide during the Younger Dryas cold period. *Geophysical Research Letters*, **30**, 1092.

Good, P., C. Jones, J. Lowe, R. Betts, B. Booth, and C. Huntingford, 2011: Quantifying Environmental Drivers of Future Tropical Forest Extent. *Journal of Climate*, **24**, 1337-1349.

Goodwin, P., and T. Lenton, 2009: Quantifying the feedback between ocean heating and CO2 solubility as an equivalent carbon emission. *Geophysical Research Letters*, **36**, -.

Govindasamy, B., K. Caldeira, and P. B. Duffy, 2003: Geoengineering Earth's radiation balance to mitigate climate change from a quadrupling of CO2. *Global and Planetary Change*, **37**, 157-168.

Govindasamy, B., S. Thompson, P. B. Duffy, K. Caldeira, and C. Delire, 2002: Impact of geoengineering schemes on the terrestrial biosphere. *Geophysical Research Letters*, **29**, 2061, doi:2010.1029/2002GL015911.

Gray, M. L., K. J. Champagne, D. Fauth, J. P. Baltrus, and H. Pennline, 2008: Performance of immobilized tertiary amine solid sorbents for the capture of carbon dioxide. *International Journal of Greenhouse Gas Control*, **2**, 3-8.

Gregg, J. S., R. J. Andres, and G. Marland, 2008: China: Emissions pattern of the world leader in CO2 emissions from fossil fuel consumption and cement production. *Geophysical Research Letters*, **35**, -.

Gregory, J., C. Jones, P. Cadule, and P. Friedlingstein, 2009: Quantifying Carbon Cycle Feedbacks. *Journal of Climate*, DOI 10.1175/2009JCLI2949.1. 5232-5250.

Gruber, N., et al., 2009: Oceanic sources, sinks, and transport of atmospheric CO2. *Global Biogeochemical Cycles*, **23**, -.

Gu, L. H., D. D. Baldocchi, S. C. Wofsy, J. W. Munger, J. J. Michalsky, S. P. Urbanski, and T. A. Boden, 2003: Response of a deciduous forest to the Mount Pinatubo eruption: Enhanced photosynthesis. *Science*, **299**, 2035-2038.

Gurney, K. R., and W. J. Eckels, 2011: Regional trends in terrestrial carbon exchange and their seasonal signatures. *Tellus Series B-Chemical and Physical Meteorology*, **63**, 328-339.

Hamilton, S., 2010: Biogeochemical implications of climate change for tropical rivers and floodplains. *Hydrobiologia*, **657**, 19-35.

Hamilton, S. K., A. L. Kurzman, C. Arango, L. Jin, and G. P. Robertson, 2007: Evidence for carbon sequestration by agricultural liming. *Global Biogeochemical Cycles*, **21**.

Hansen, M., S. Stehman, and P. V. Potapov, 2010: Quantification of global gross forest cover loss. *Proceedings of the National Academy of Sciences*, **107**, 8650-8655.

Hansen, M., S. Stehman, P. V. Potapov, B. Arunarwati, F. Stolle, and K. Pittman, 2009: Quantifying changes in the rates of forest clearing in Indonesia for 1990 to 2005 using remotely sensed data sets. *Environmental Research Letters*, **4**, 034001-034012.

Hare, B., and M. Meinshausen, 2006: How much warming are we committed to and how much can be avoided? *Climatic Change*, **75**, 111-149.

Harrison, K. G., 2000: Role of increased marine silica input on paleo-pCO(2) levels. *Paleoceanography*, **15**, 292-298.

Harvey, L. D. D., 2008: Mitigating the atmospheric CO2 increase and ocean acidification by adding limestone powder to upwelling regions. *J Geophys Res-Oceans*, **113**.

Hedegaard, G., J. Brandt, J. Christensen, L. Frohn, C. Geels, K. Hansen, and M. Stendel, 2008: Impacts of climate change on air pollution levels in the Northern Hemisphere with special focus on Europe and the Arctic. *Atmospheric Chemistry and Physics*, **8**, 3337-3367.

Helm, K. P., N. L. Bindoff, and J. A. Church, 2011: Observed decreases in oxygen content of the global ocean. *Geophysical Research Letters (in press)*, 10.1029/2011GL049513.

Herridge, D. F., M. B. Peoples, and R. M. Boddey, 2008: Global inputs of biological nitrogen fixation in agricultural systems. *Plant Soil*, **311**, 1-18.

Hibbard, K. A., G. A. Meehl, P. M. Cox, and P. Friedlingstein, 2007: A strategy for climate change stabilization experiments. *EOS, Transactions American Geophysical Union*, **88**.

Hirota, M., M. Holmgren, E. H. Van Nes, and M. Scheffer, 2011: Global Resilience of Tropical Forest and Savanna to Critical Transitions. *Science*, **334**, 232-235.

Hofmann, M., and H.-J. Schellnhuber, 2009: Oceanic acidification affects marine carbon pump and triggers extended marine oxygen holes. *Proceedings of the National Academy of Sciences*, **106**, 3017-3022.

Holland, E., J. Lee-Taylor, C. D. Nevison, and J. Sulzman, 2005: Global N cycle: Fluxes and N_2O mixing ratios originating from human activity. Oak Ridge National Laboratory Distributed Active Archive Center.

Honisch, B., N. G. Hemming, D. Archer, M. Siddall, and J. F. McManus, 2009: Atmospheric Carbon Dioxide Concentration Across the Mid-Pleistocene Transition. *Science*, **324**, 1551-1554.

Hooijer, A., S. Page, J. Canadell, M. Silvius, J. Kwadijk, H. Wosten, and J. Jauhiainen, 2010: Current and future CO2 emissions from drained peatlands in Southeast Asia. *Biogeosciences*, **7**, 1505-1514.

Houghton, J. T., 2008: Carbon flux to the atmosphere from land-use changes:1850–2005.

Houghton, R. A., 2003: Revised estimates of the annual net flux of carbon to the atmosphere from changes in land use and land management 1850-2000. *Tellus B*, **55**, 378-390.

Houghton, R. A., 2005: Aboveground forest biomass and the global carbon balance. *Global Change Biology*, **11**, 945-958.

——, 2010: How well do we know the flux of CO2 from land-use change? *Tellus Series B-Chemical and Physical Meteorology*, **62**, 337-351.

House, J. I., et al., 2008: What do recent advances in quantifying climate and carbon cycle uncertainties mean for climate policy? *Environmental Research Letters*, **3**.

House, K. Z., D. P. Schrag, C. F. Harvey, and K. S. Lackner, 2006: Permanent carbon dioxide storage in deep-sea sediments. *P Natl Acad Sci USA*, **103**, 14255.

House, K. Z., C. H. House, D. P. Schrag, and M. J. Aziz, 2007: Electrochemical acceleration of chemical weathering as an energetically feasible approach to mitigating anthropogenic climate change. *Environ. Sci. Technol.*, **41**, 8464-8470.

Huber, C., et al., 2006: Isotope calibrated Greenland temperature record over Marine Isotope Stage 3 and its relation to CH4. *Earth and Planetary Science Letters*, **243**, 504-519.

Hudiburg, T. W., B. E. Law, C. Wirth, and S. Luyssaert, 2011: Regional carbon dioxide implications of forest bioenergy production. *Nature Climate Change*, **1**, 419-423.

Huntingford, C., J. Lowe, B. Booth, C. Jones, G. Harris, L. Gohar, and P. Meir, 2009: Contributions of carbon cycle uncertainty to future climate projection spread. *Tellus Series B-Chemical and Physical Meteorology*, DOI 10.1111/j.1600-0889.2009.00414.x. 355-360.

Hurtt, G. C., et al., 2011: Harmonization of land-use scenarios for the period 1500-2100: 600 years of global gridded annual land-use transitions, wood harvest, and resulting secondary lands. *Climatic Change*, **DOI 10.1007/s10584-011-0153-2**.

Huybers, P., and C. Langmuir, 2009: Feedback between deglaciation, volcanism, and atmospheric CO2. *Earth and Planetary Science Letters*, **286**, 479-491.
Ichii, K., et al., 2010: Multi-model analysis of terrestrial carbon cycles in Japan: limitations and implications of model calibration using eddy flux. *Biogeosciences*, **7**, 2061-2080.
Indermuhle, A., et al., 1999: Holocene carbon-cycle dynamics based on CO2 trapped in ice at Taylor Dome, Antarctica. *Nature*, **398**, 121-126.
Ineson, P., P. A. Coward, and U. A. Hartwig, 1998: Soil gas fluxes of N2O, CH4 and CO2 beneath Lolium perenne under elevated CO2: The Swiss free air carbon dioxide enrichment experiment. *Plant and Soil*, **198**, 89-95.
Irvine, P. J., A. Ridgwell, and D. J. Lunt, 2010: Assessing the regional disparities in geoengineering impacts. *Geophysical Research Letters*, **37**.
Ishii, M., N. Kosugi, D. Sasano, S. Saito, T. Midorikawa, and H. Inoue, 2011: Ocean acidification off the south coast of Japan: A result from time series observations of CO2 parameters from 1994 to 2008. *J Geophys Res-Oceans*, **116**, -.
Ishijima, K., T. Nakazawa, and S. Aoki, 2009: Variations of atmospheric nitrous oxide concentration in the northern and western Pacific. *Tellus B*, **61**, 408-415.
Ito, A., 2008: The regional carbon budget of East Asia simulated with a terrestrial ecosystem model and validated using AsiaFlux data. *Agricultural And Forest Meteorology*, **148**, 738-747.
Iudicone, D., et al., 2011: Water masses as a unifying framework for understanding the Southern Ocean Carbon Cycle. *Biogeosciences*, **8**, 1031-1052.
Jaccard, S. L., and E. D. Galbraith, accepted: Large climate-driven changes of oceanic oxygen concentrations during the last deglaciation. *Nature Geosciences*.
Jaccard, S. L., G. H. Haug, D. M. Sigman, T. F. Pedersen, H. R. Thierstein, and U. Röhl, 2005: Glacial/Interglacial changes in subarctic North Pacific stratification. *Science*, **308**, 1003-1006.
Jacobson, A. R., S. E. Mikaloff Fletcher, N. Gruber, J. L. Sarmiento, and M. Gloor, 2007: A joint atmosphere-ocean inversion for surface fluxes of carbon dioxide: 2. Regional results. *Global Biogeochemical Cycles*, **21**.
Jain, A., X. Yang, H. Kheshgi, A. McGuire, W. Post, and D. Kicklighter, 2009: Nitrogen attenuation of terrestrial carbon cycle response to global environmental factors. *Global Biogeochemical Cycles*, **23**, -.
Janssens, I. A., et al., 2010: Reduction of forest soil respiration in response to nitrogen deposition. *Nature Geoscience*, **3**, 315-322.
Jin, X., and N. Gruber, 2003: Offsetting the radiative benefit of ocean iron fertilization by enhancing N2O emissions. *Geophysical Research Letters*, **30**.
Jin, X., N. Gruber, H. Frenzel, S. C. Doney, and J. C. McWilliams, 2008: The impact on atmospheric CO2 of iron fertilization induced changes in the ocean's biological pump. *Biogeosciences*, **5**, 385-406.
Johnson, D. W., 2006: Progressive N limitation in forests: Review and implications for long-term responses to elevated CO2. *Ecology*, **87**, 64-75.
Jones, A., J. Haywood, and O. Boucher, 2009a: Climate impacts of geoengineering marine stratocumulus clouds. *Journal of Geophysical Research-Atmospheres*, **114**, D10106, doi:10110.11029/12008JD011450.
Jones, A., J. Haywood, O. Boucher, B. Kravitz, and A. Robock, 2010a: Geoengineering by stratospheric SO2 injection: results from the Met Office HadGEM(2) climate model and comparison with the Goddard Institute for Space Studies ModelE. *Atmospheric Chemistry and Physics*, **10**, 5999-6006.
Jones, C., and P. Cox, 2001: Modeling the volcanic signal in the atmospheric CO2 record. *Global Biogeochemical Cycles*. 453-465.
Jones, C., S. Liddicoat, and J. Lowe, 2010b: Role of terrestrial ecosystems in determining CO2 stabilization and recovery behaviour. *Tellus Series B-Chemical and Physical Meteorology*, DOI 10.1111/j.1600-0889.2010.00490.x. 682-699.
Jones, C., J. Lowe, S. Liddicoat, and R. Betts, 2009b: Committed terrestrial ecosystem changes due to climate change. *Nature Geoscience*, DOI 10.1038/ngeo555. 484-487.
Jones, C., et al., 2011: The HadGEM2-ES implementation of CMIP5 centennial simulations. *Geoscientific Model Development*, **4**, 543-570.
Jones, C. D., and P. Falloon, 2009: Sources of uncertainty in global modelling of future soil organic carbon storage. *UNCERTAINTIES IN ENVIRONMENTAL MODELLING AND CONSEQUENCES FOR POLICY MAKING*, P. Bavaye, J. Mysiak, and M. Laba, Eds., Springer, 283-315.
Jones, C. D., P. M. Cox, and C. Huntingford, 2006: Impact of climate carbon cycle feedbacks on emission scenarios to achieve stabilization. *Avoiding Dangerous Climate Change*, W. C. H. J. Schellnhuber, N. Nakicenovic, T. Wigley and G. Yohe, Ed., Cambridge University Press.
Joos, F., J. L. Sarmiento, and U. Siegenthaler, 1991: Estimates of the Effect of Southern-Ocean Iron Fertilization on Atmospheric Co2 Concentrations. *Nature*, **349**, 772-775.
Joos, F., T. L. Frölicher, M. Steinacher, and G.-K. s. s. Plattner, 2011: Impact of climate change mitigation on ocean acidification projections. *Ocean Acidification*, J.-P. G. a. L. Hansson, Ed., Oxford University Press.
Joos, F., S. Gerber, I. C. Prentice, B. L. Otto-Bliesner, and P. J. Valdes, 2004: Transient simulations of Holocene atmospheric carbon dioxide and terrestrial carbon since the Last Glacial Maximum. *Global Biogeochemical Cycles*, **18**.

Jung, M., et al., 2007: Assessing the ability of three land ecosystem models to simulate gross carbon uptake of forests from boreal to Mediterranean climate in Europe. *Biogeosciences*, **4**, 647-656.
Jung, M., et al., 2011: Global patterns of land-atmosphere fluxes of carbon dioxide, latent heat, and sensible heat derived from eddy covariance, satellite, and meteorological observations. *Journal of Geophysical Research-Biogeosciences*, **116**.
Jungclaus, J. H., et al., 2010: Climate and carbon-cycle variability over the last millennium. *Climate of the Past*, **6**, 723-737.
Kai, F. M., S. C. Tyler, J. T. Randerson, and D. R. Blake, 2011: Reduced methane growth rate explained by decreased Northern Hemisphere microbial sources. *Nature*, **476**, 194-197.
Kaplan, J. O., G. Folberth, and D. A. Hauglustaine, 2006: Role of methane and biogenic volatile organic compound sources in late glacial and Holocene fluctuations of atmospheric methane concentrations. *Global Biogeochemical Cycles*, **20**.
Kaplan, J. O., I. C. Prentice, W. Knorr, and P. J. Valdes, 2002: Modeling the dynamics of terrestrial carbon storage since the Last Glacial Maximum. *Geophysical Research Letters*, **29**.
Kaplan, J. O., K. M. Krumhardt, E. C. Ellis, W. Ruddiman, and K. Klein Goldewijk, 2011: Holocene carbon emissions as a result of anthropogenic land cover change. *The Holocene*, 10.1177/0959683610386983.
Karl, D. M., and R. M. Letelier, 2008: Nitrogen fixation-enhanced carbon sequestration in low nitrate, low chlorophyll seascapes. *Marine Ecology Progress Series*, **364**, 257-268.
Keeling, C. D., S. C. Piper, and M. Heimann, 1989a: A three dimensional model of atmospheric CO2 transport based on observed winds: 4. Mean annual gradients and interannual variations. *Aspects of Climate Variability in the Pacific and the Western Americas*, D. H. Peterson, Ed., AGU, 305-363.
Keeling, C. D., R. B. Bacastow, A. E. Bainbridge, C. A. Ekdahl, P. R. Guenther, L. S. Waterman, and J. F. S. Chin, 1976: Atmospheric carbon-dioxide variations at Mauna-Loa observatory, Hawaii. *Tellus*, **28**, 538-551.
Keeling, C. D., S. C. Piper, R. B. Bacastow, M. Wahlen, T. P. Whorf, M. Heimann, and H. A. Meijer, 2005: Atmospheric CO_2 and $^{13}CO_2$ exchange with the terrestrial biosphere and oceans from 1978 to 2000: observations and carbon cycle implications. *A History of Atmospheric CO_2 and Its Effects on Plants, Animals, and Ecosystems*, J. R. Ehleringer, T. E. Cerling, and M. D. Dearing, Eds., Springer, 83-113.
Keeling, C. D., et al., 1989b: A three-dimensional model of atmospheric CO2 transport based on observed winds: 1. Analysis of observational data. *AGU Geophysical Monograph*, **55**, 165-236.
Keeling, R. F., and S. R. Shertz, 1992: Seasonal and interannual variations in atmospheric oxygen and implications for the global carbon cycle. *Nature*, **358**, 723-727.
Keeling, R. F., S. C. Piper, and M. Heimann, 1996: Global and hemispheric CO2 sinks deduced from changes in atmospheric O2 concentration. *Nature*, **381**, 218-221.
Keith, D. W., 2001: Geoengineering. *Nature*, **409**, 420-420.
Keith, D. W., M. Ha-Duong, and J. K. Stolaroff, 2006: Climate strategy with CO2 capture from the air. *Climatic Change*, **74**, 17-45.
Kelemen, P. B., and J. Matter, 2008: In situ carbonation of peridotite for CO2 storage. *P Natl Acad Sci USA*, **105**, 17295-17300.
Keppler, F., J. T. G. Hamilton, M. Brass, and T. Rockmann, 2006: Methane emissions from terrestrial plants under aerobic conditions. *Nature*, **439**, 187-191.
Kesik, M., et al., 2006: Future scenarios of N(2)O and NO emissions from European forest soils. *Journal of Geophysical Research-Biogeosciences*, **111**.
Khalil, M. A. K., and R. A. Rasmussen, 1989: Climate-induced feed backs for the global cycles of methane and nitrous oxide. *Tellus B*, **41B**, 554-559.
Khatiwala, S., F. Primeau, and T. Hall, 2009: Reconstruction of the history of anthropogenic CO2 concentrations in the ocean. *Nature*, **462**, 346-349.
Kheshgi, H. S., 1995: Sequestering atmospheric carbon-dioxide by incresing ocean alkalinity. *Energy*, **20**, 915-922.
Khvorostyanov, D., P. Ciais, G. Krinner, and S. Zimov, 2008: Vulnerability of east Siberia's frozen carbon stores to future warming. *Geophysical Research Letters*, **35**, -.
Kim, J. H., et al., 2004: North Pacific and North Atlantic sea-surface temperature variability during the holocene. *Quaternary Science Reviews*, **23**, 2141-2154.
Kirschbaum, M. U. F., 2003: Can trees buy time? An assessment of the role of vegetation sinks as part of the global carbon cycle. *Climatic Change*, **58**, 47-71.
Kirschbaum, M. U. F., and A. Walcroft, 2008: No detectable aerobic methane efflux from plant material, nor from adsorption/desorption processes. *Biogeosciences*, **5**, 1551-1558.
Kleinen, T., V. Brovkin, and R. Getzieh, 2011: A dynamic model of wetland extent and peat accumulation: results for the Holocene. *Biogeosciences Discussions*, **8**, 4805–4839.
Kleinen, T., V. Brovkin, W. von Bloh, D. Archer, and G. Munhoven, 2010: Holocene carbon cycle dynamics. *Geophysical Research Letters*, **37**.
Kloster, S., N. M. Mahowald, J. T. Randerson, and P. L. Lawrence, 2011: The impacts of climate, land use, and demography on fires during the 21st century simulated by CLM-CN. *Biogeosciences Discussion*, **8**, 9709-9746.
Kloster, S., et al., 2010: Fire dynamics during the 20th century simulated by the Community Land Model. *Biogeosciences*, **7**, 1877-1902.

Knorr, W., 2009: Is the airborne fraction of anthropogenic emissions increasing? *Geophysical Research Letters*, **36**, L21710, doi:21710.21029/22009GL040613.
Kohfeld, K. E., and A. Ridgwell, 2009: Glacial-interglacial variability in atmospheric CO2. *Surface Ocean - Lower Atmospheres Processes*, C. L. Q. r. a. E. S. Saltzman, Ed., 350 pp.
Konijnendijk, T. Y. M., S. L. Weber, E. Tuenter, and M. van Weele, 2011: Methane variations on orbital timescales: a transient modeling experiment. *Climate of the Past*, **7**, 635-648.
Körner, C., 2006: Plant CO2 responses: an issue of definition, time and resource supply. *New Phytologist*, **172**, 393-411.
Koven, C. D., et al., 2011: Permafrost carbon-climate feedbacks accelerate global warming. *Proceedings of the National Academy of Sciences, August 18, 2011*, 10.1073/pnas.1103910108.
Krawchuk, M., M. Moritz, M. Parisien, J. Van Dorn, and K. Hayhoe, 2009: Global Pyrogeography: the Current and Future Distribution of Wildfire. *Plos One*, **4**, -.
Kraxner, F., S. Nilsson, and M. Obersteiner, 2003: Negative emissions from BioEnergy use, carbon capture and sequestration (BECS) - the case of biomass production by sustainable forest management from semi-natural temperate forests. *Biomass Bioenerg.*, **24**, 285-296.
Krinner, G., et al., 2005: A dynamic global vegetation model for studies of the coupled atmosphere-biosphere system. *Global Biogeochemical Cycles*, ARTN GB1015, DOI 10.1029/2003GB002199. -.
Kroeze, C., L. Bouwman, and C. P. Slomp, 2007: Sinks for N_2O at the Earth's surface. *Greenhouse Gas Sinks*, *M. H. Raey D.S., J. Grace and K.A. Smith*, Ed., *CAB International*, 227-243.
Kroeze, C., E. Dumont, and S. Seitzinger, 2010: Future trends in emissions of N_2O from rivers and estuaries. *Journal of Integrative Environmental Sciences*, **7**, 71 - 78.
Kurahashi-Nakamura, T., A. Abe-Ouchi, Y. Yamanaka, and K. Misumi, 2007: Compound effects of Antarctic sea ice on atmospheric pCO(2) change during glacial-interglacial cycle. *Geophysical Research Letters*, **34**.
Kurz, W. A., G. Stinson, and G. Rampley, 2008a: Could increased boreal forest ecosystem productivity offset carbon losses from increased disturbances? *Philosophical Transactions of the Royal Society B-Biological Sciences*, **363**, 2261-2269.
Kurz, W. A., G. Stinson, G. J. Rampley, C. C. Dymond, and E. T. Neilson, 2008b: Risk of natural disturbances makes future contribution of Canada's forests to the global carbon cycle highly uncertain. *Proceedings of the National Academy of Sciences*, **105**, 1551-1555.
Lackner, K. S., 2009: Capture of carbon dioxide from ambient air. *European Physical Journal-Special Topics*, **176**, 93-106.
——, 2010: Washing CARBON OUT OF THE AIR. *Scientific American*, **302**, 66-71.
Lal, R., 2004a: Soil carbon sequestration impacts on global climate change and food security. *Science*, **304**, 1623-1627.
——, 2004b: Soil carbon sequestration to mitigate climate change. *Geoderma*, **123**, 1-22.
Lam, P., and M. M. M. Kuypers, 2010: Microbial Nitrogen Cycling Processes in Oxygen Minimum Zones. *Annual Review of Marine Science*, **3**, 317-345.
Lamarque, J.-F., et al., 2010: Historical (1850-2000) gridded anthropogenic and biomass burning emissions of reactive gases and aerosols: methodology and application. *Atmos. Chem. Phys.*, **10**, 7017-7039.
Lamarque, J., 2008: Estimating the potential for methane clathrate instability in the 1%-CO2 IPCC AR-4 simulations. *Geophysical Research Letters*, **35**, -.
Lamarque, J. F., et al., 2011: Global and regional evolution of short-lived radiatively-active gases and aerosols in the Representative Concentration Pathways. *Climatic Change*.
Lampitt, R. S., et al., 2008: Ocean fertilization: a potential means of geoengineering? *Philosophical Transaction of the RoyalSociety A*, **1882**, 3919-3945.
Langenfelds, R. L., R. J. Francey, B. C. Pak, L. P. Steele, J. Lloyd, C. M. Trudinger, and C. E. Allison, 2002: Interannual growth rate variations of atmospheric CO_2 and its $d^{13}C$, H_2, CH_4, and CO between 1992 and 1999 linked to biomass burning. *Global Biogeochemical Cycles*, **16**, 1048, doi:1010.1029/2001GB001466.
Langner, J., R. Bergstrom, and V. Foltescu, 2005: Impact of climate change on surface ozone and deposition of sulphur and nitrogen in Europe. *Atmospheric Environment*, **39**, 1129-1141.
Lapola, D. M., M. D. Oyama, and C. A. Nobre, 2009: Exploring the range of climate biome projections for tropical South America: The role of CO2 fertilization and seasonality. *Global Biogeochemical Cycles*, **23**.
Lassey, K. R., D. C. Lowe, and A. M. Smith, 2007: The atmospheric cycling of radiomethane and the "fossil fraction" of the methane source. *Atmos Chem Phys*, **7**, 2141-2149.
Latham, J., et al., 2008: Global temperature stabilization via controlled albedo enhancement of low-level maritime clouds. *Philosophical Transactions of the Royal Society a-Mathematical Physical and Engineering Sciences*, **366**, 3969-3987.
Lawrence, D., and A. Slater, 2005: A projection of severe near-surface permafrost degradation during the 21st century. *Geophysical Research Letters*, **32**, -.
Lawrence, D., A. Slater, V. Romanovsky, and D. Nicolsky, 2008: Sensitivity of a model projection of near-surface permafrost degradation to soil column depth and representation of soil organic matter. *Journal of Geophysical Research-Earth Surface*, **113**, -.
Lawrence, D., et al., 2011: Parameterization Improvements and Functional and Structural Advances in Version 4 of the Community Land Model. *Journal of Advances in Modeling Earth Systems*, **3**, 27 pp.

Lawrence, P. J., et al., submitted: Simulating the biogeochemical and biogeophysical impacts of transient land cover change and wood harvest in the Community Climate System Model (CCSM4) from 1850 to 2100.
Lemmen, C., 2009: World distribution of land cover changes during Pre- and Protohistoric Times and estimation of induced carbon releases. *Geomorphologie-Relief Processus Environnement*. 303-312.
Lenton, A., and R. J. Matear, 2007: Role of the Southern Annular Mode (SAM) in Southern Ocean CO2 uptake. *Global Biogeochemical Cycles*, **21**, -.
Lenton, A., F. Codron, L. Bopp, N. Metzl, P. Cadule, A. Tagliabue, and J. Le Sommer, 2009: Stratospheric ozone depletion reduces ocean carbon uptake and enhances ocean acidification. *Geophysical Research Letters*, **36**, -.
Lenton, T. M., and C. Britton, 2006: Enhanced carbonate and silicate weathering accelerates recovery from fossil fuel CO2 perturbations. *Global Biogeochemical Cycles*, **20**.
Lenton, T. M., and N. E. Vaughan, 2009: The radiative forcing potential of different climate geoengineering options. *Atmospheric Chemistry and Physics*, **9**, 5539-5561.
Lenton, T. M., H. Held, E. Kriegler, J. W. Hall, W. Lucht, S. Rahmstorf, and H. J. Schellnhuber, 2008: Tipping elements in the Earth's climate system. *P Natl Acad Sci USA*, **105**, 1786-1793.
LePage, Y., G. R. van der Werf, D. C. Morton, and J. M. C. Pereira, 2010: Modeling fire-driven deforestation potential in Amazonia under current and projected climate conditions. *Journal of Geophysical Research-Biogeosciences*, **115**, -.
LeQuere, C., T. Takahashi, E. T. Buitenhuis, C. Rodenbeck, and S. C. Sutherland, 2010: Impact of climate change and variability on the global oceanic sink of CO2. *Global Biogeochemical Cycles*, **24**, -.
LeQuere, C., et al., 2007: Saturation of the Southern Ocean CO2 sink due to recent climate change. *Science*, **316**, 1735-1738.
LeQuere, C., et al., 2009: Trends in the sources and sinks of carbon dioxide. *Nature Geoscience*, **2**, 831-836.
Levin, I., et al., 2010: Observations and modelling of the global distribution and long-term trend of atmospheric 14CO 2. *Tellus B*, **62**, 26-46.
Levy, P. E., M. G. R. Cannell, and A. D. Friend, 2004: Modelling the impact of future changes in climate, CO2 concentration and land use on natural ecosystems and the terrestrial carbon sink. *Global Environmental Change*, **14**, 21-30.
Lewis, S. L., P. M. Brando, O. L. Phillips, G. M. F. v. d. Heijden, and D. Nepstad, 2011: The 2010 Amazon Drought. *Science*, **331**, 554.
Lewis, S. L., et al., 2009: Increasing carbon storage in intact African tropical forests. *Nature*, **457**, 1003-1006.
Liepert, B., and I. Tegen, 2002: Multidecadal solar radiation trends in the United States and Germany and direct tropospheric aerosol forcing. *Journal of Geophysical Research-Atmospheres*, **107**.
Liepert, B. G., 2002: Observed reductions of surface solar radiation at sites in the United States and worldwide from 1961 to 1990. *Geophysical Research Letters*, **29**.
Lohila, A., M. Aurela, J. Hatakka, M. Pihlatie, K. Minkkinen, T. Penttila, and T. Laurila, 2010: Responses of N2O fluxes to temperature, water table and N deposition in a northern boreal fen. *European Journal of Soil Science*, **61**, 651-661.
Loulergue, L., et al., 2008: Orbital and millennial-scale features of atmospheric CH4 over the past 800,000 years. *Nature*, **453**, 383-386.
Lovelock, J. E., and C. G. Rapley, 2007: Ocean pipes could help the Earth to cure itself. *Nature*, **449**, 403-403.
Lovenduski, N. S., N. Gruber, S. C. Doney, and I. D. Lima, 2007: Enhanced CO2 outgassing in the Southern Ocean from a positive phase of the Southern Annular Mode. *Global Biogeochemical Cycles*, **21**, -.
Lowe, J. A., C. Huntingford, S. C. B. Raper, C. D. Jones, S. K. Liddicoat, and L. K. Gohar, 2009: How difficult is it to recover from dangerous levels of global warming? *Environmental Research Letters*, **4**.
Lucht, W., et al., 2002: Climatic control of the high-latitude vegetation greening trend and Pinatubo effect. *Science*. 1687-1689.
Luo, Y., D. Hui, and D. Zhang, 2005: Elevated CO2 stimulates net accumulations of carbon and nitrogen in land ecosystems: a meta-analysis. *Ecological Society of America*.
Luo, Y. Q., 2007: Terrestrial carbon-cycle feedback to climate warming. *Annu Rev Ecol Evol S*, **38**, 683-712.
Luthi, D., et al., 2008: High-resolution carbon dioxide concentration record 650,000-800,000 years before present. *Nature*, **453**, 379-382.
Luyssaert, S., et al., 2010: The European carbon balance. Part 3: forests. *Global Change Biology*, **16**, 1429-1450.
MacDonald, G. M., K. V. Kremenetski, and D. W. Beilman, 2008: Climate change and the northern Russian treeline zone. *Philosophical Transactions of the Royal Society B-Biological Sciences*, **363**, 2285-2299.
MacFarling-Meure, C., et al., 2006: Law Dome CO(2), CH(4) and N(2)O ice core records extended to 2000 years BP. *Geophysical Research Letters*, **33**.
Magnani, F., et al., 2007: The human footprint in the carbon cycle of temperate and boreal forests. *Nature*, **447**, 848-850.
Mahmoudkhani, M., and D. W. Keith, 2009: Low-energy sodium hydroxide recovery for CO2 capture from atmospheric air-Thermodynamic analysis. *International Journal of Greenhouse Gas Control*, **3**, 376-384.
Mahowald, N., et al., 1999: Dust sources and deposition during the last glacial maximum and current climate: A comparison of model results with paleodata from ice cores and marine sediments. *Journal of Geophysical Research-Atmospheres*, **104**, 15895-15916.

Mahowald, N., et al., 2009: Atmospheric Iron Deposition: Global Distribution, Variability, and Human Perturbations. *Annual Review of Marine Science*, **1**, 245-278.
Mahowald, N. M., D. R. Muhs, S. Levis, P. J. Rasch, M. Yoshioka, C. S. Zender, and C. Luo, 2006: Change in atmospheric mineral aerosols in response to climate: Last glacial period, preindustrial, modern, and doubled carbon dioxide climates. *Journal of Geophysical Research-Atmospheres*, **111**.
Mahowald, N. M., et al., 2011: Desert dust and anthropogenic aerosol interactions in the Community Climate System Model coupled-carbon-climate model. *Biogeosciences*, **8**, 387-414.
Mahowald, N. M., et al., 2010: Observed 20th century desert dust variability: impact on climate and biogeochemistry. *Atmospheric Chemistry and Physics*, **10**, 10875-10893.
Maier-Reimer, E., I. Kriest, J. Segschneider, and P. Wetzel, 2005: The HAMburg Ocean Carbon Cycle model HAMOCC 5.1 – Technical description, Release 1.1. Max-Planck Institute for Meteorology.
Manning, A. C., and R. F. Keeling, 2006: Global oceanic and land biotic carbon sinks from the Scripps atmospheric oxygen flask sampling network. *Tellus Series B-Chemical and Physical Meteorology*, **58**, 95-116.
Marchand, F. L., I. Nijs, H. J. de Boeck, F. Kockelbergh, S. Mertens, and L. Beyens, 2004: Increased turnover but little change in the carbon balance of High-Arctic tundra exposed to whole growing season warming. *Arct Antarct Alp Res*, **36**, 298-307.
Marchenko, S. S., V. Romanovsky, and G. S. Tipenko, 2008: Numerical modeling of spatial permafrost dynamics in Alaska. *Ninth International Conference on Permafrost.*
Marland, G., and R. M. Rotty, 1984: Carbon-dioxide emissions from fossil-fuels - A procedure for estimation and results for 1950 - 1982. *Tellus Series B-Chemical and Physical Meteorology*, **36**, 232-261.
Marlon, J. R., et al., 2008: Climate and human influences on global biomass burning over the past two millennia. *Nature Geoscience*, **1**, 697-702.
Martin, J. H., 1990: Glacial-interglacial CO2 change: the iron hypothesis. *Paleoceanography*, **5**, 1-13.
Masarie, K. A., and P. P. Tans, 1995: Extension and integration of atmospheric carbon-dioxide data into a globally consistent measurement record. *Journal of Geophysical Research-Atmospheres*, **100**, 11593-11610.
Matear, R. J., and A. C. Hirst, 2003: Long-term changes in dissolved oxygen concentrations in the ocean caused by protracted global warming. *Global Biogeochem. Cycles*, **17**, 1125.
Matear, R. J., and B. I. McNeil, 2003: Decadal accumulation of anthropogenic CO2 in the Southern Ocean: A comparison of CFC-age derived estimates to multiple-linear regression estimates. *Global Biogeochemical Cycles*, **17**.
Matear, R. J., A. C. Hirst, and B. I. McNeil, 2000: Changes in dissolved oxygen in the Southern Ocean with climate change. *Geochem. Geophys. Geosyst.*, **1**.
Mathews, D., 2010: Can carbon cycle geoengineering be a useful complement to ambitious climate mitigation? *Carbon Management*, **1**, 135-144.
Matsumoto, K., 2007: Biology-mediated temperature control on atmospheric pCO(2) and ocean biogeochemistry. *Geophysical Research Letters*, **34**.
Matsumoto, K., J. L. Sarmiento, and M. A. Brzezinski, 2002: Silicic acid leakage from the Southern Ocean: A possible explanation for glacial atmospheric pCO(2). *Global Biogeochemical Cycles*, **16**.
Matsumoto, K., et al., 2004: Evaluation of ocean carbon cycle models with data-based metrics. *Geophysical Research Letters*, **31**.
Matthews, H., M. Eby, A. Weaver, and B. Hawkins, 2005: Primary productivity control of simulated carbon cycle-climate feedbacks. *Geophysical Research Letters*, **32**, -.
Matthews, H. D., 2006: Emissions targets for CO2 stabilization as modified by carbon cycle feedbacks. *Tellus*, **58B**, 591-602.
Mayorga, E., et al., 2010: Global Nutrient Export from WaterSheds 2 (NEWS 2): Model development and implementation. *Environmental Modelling & Software*, **25**, 837-853.
McCarthy, M., M. Best, and R. Betts, 2010: Climate change in cities due to global warming and urban effects. *Geophysical Research Letters*, ARTN L09705, DOI 10.1029/2010GL042845. -.
McGuire, A. D., et al., 2009: Sensitivity of the carbon cycle in the Arctic to climate change. *Ecological Monographs*, **79**, 523-555.
McKinley, G., A. Fay, T. Takahashi, and N. Metzl, 2011: Convergence of atmospheric and North Atlantic carbon dioxide trends on multidecadal timescales. *Nature Geoscience*, **4**, 606-610.
McNeil, B., and R. Matear, 2006: Projected climate change impact on oceanic acidification. *Carbon balance and management*, 10.1186/1750-0680-1-2.
McNeil, B. I., and R. J. Matear, 2008: Southern Ocean acidification: A tipping point at 450-ppm atmospheric CO2. *P Natl Acad Sci USA*, **105**, 18860-18864.
McWethy, D. B., C. Whitlock, J. M. Wilmshurst, M. S. McGlone, and X. Li, 2009: Rapid deforestation of South Islands, New Zealands, by early Polynesian fires. *Holocene*, **19**, 883-897.
Medlyn, B. E., 2011: Comment on "Drought-induced reductions in global terrestrial net primary production from 2000 through 2009". *Science*, **333**, 1093-d.
Meehl, G. A., et al., 2007: Chapter 10: Global Climate Projections, 996 pp.
Meinshausen, M., et al., 2009: Greenhouse-gas emission targets for limiting global warming to 2 degrees C. *Nature*, **458**, 1158-U1196.

Melillo, J., et al., 2011: Soil warming, carbon-nitrogen interactions, and forest carbon budgets. *P Natl Acad Sci USA*, **108**, 9508-9512.
Menviel, L., and F. Joos, submitted: Toward explaining the Holocene carbon dioxide and carbon isotope records: Results from transient ocean carbon cycle-climate simulations. *Paleoceanography*.
Menviel, L., A. Timmermann, A. Mouchet, and O. Timm, 2008: Meridional reorganizations of marine and terrestrial productivity during Heinrich events. *Paleoceanography*, **23**.
Menyailo, O. V., and B. A. Hungate, 2006: Tree species and moisture effects on soil sources of N2O: Quantifying contributions from nitrification and denitrification with O-18 isotopes. *Journal of Geophysical Research-Biogeosciences*, **111**.
Mercado, L. M., N. Bellouin, S. Sitch, O. Boucher, C. Huntingford, M. Wild, and P. M. Cox, 2009: Impact of changes in diffuse radiation on the global land carbon sink. *Nature*, **458**, 1014-U1087.
Metz, B., O. Davidson, H. C. De Coninck, M. Loss, and L. A. E. Meyer, 2005: IPCC Special Report on Carbon Dioxide Capture and Storage, 442 pp., Cambridge University Press, Cambridge, UK.
Metzl, N., 2009: Decadal increase of oceanic carbon dioxide in Southern Indian Ocean surface waters (1991-2007). *Deep-Sea Res Pt Ii*, **56**, 607-619.
Metzl, N., et al., 2010: Recent acceleration of the sea surface fCO(2) growth rate in the North Atlantic subpolar gyre (1993-2008) revealed by winter observations. *Global Biogeochemical Cycles*, **24**, -.
MikaloffFletcher, S. E., et al., 2006: Inverse estimates of anthropogenic CO2 uptake, transport, and storage by the ocean. *Global Biogeochemical Cycles*, **20**.
Milkov, A., 2004: Global estimates of hydrate-bound gas in marine sediments: how much is really out there? *Earth-Science Reviews*, **66**, 183-197.
Mischler, J. A., et al., 2009: Carbon and hydrogen isotopic composition of methane over the last 1000 years. *Global Biogeochemical Cycles*, **23**.
Mitchell, L. E., E. J. Brook, T. Sowers, J. R. McConnell, and K. Taylor, 2011: Multidecadal variability of atmospheric methane, 1000-1800 CE. *Journal of Geophysical Research-Biogeosciences*, **116**.
Mitsch, W., A. Nahlik, P. Wolski, B. Bernal, L. Zhang, and L. Ramberg, 2010: Tropical wetlands: seasonal hydrologic pulsing, carbon sequestration, and methane emissions. *Wetlands Ecology and Management*, **18**, 573-586.
Miyama, T., and M. Kawamiya, 2009: Estimating allowable carbon emission for CO2 concentration stabilization using a GCM-based Earth system model. *Geophysical Research Letters*, **36**, -.
Monnin, E., et al., 2001: Atmospheric CO2 concentrations over the last glacial termination. *Science*, **291**, 112-114.
Monnin, E., et al., 2004: Evidence for substantial accumulation rate variability in Antarctica during the Holocene, through synchronization of CO2 in the Taylor Dome, Dome C and DML ice cores. *Earth and Planetary Science Letters*, **224**, 45-54.
Monteil, G., S. Houweling, E. J. Dlugockenky, G. Maenhout, B. H. Vaughn, J. W. C. White, and T. Rockmann, 2011: Interpreting methane variations in the past two decades using measurements of CH(4) mixing ratio and isotopic composition. *Atmospheric Chemistry and Physics*, **11**, 9141-9153.
Montenegro, A., V. Brovkin, M. Eby, D. Archer, and A. J. Weaver, 2007: Long term fate of anthropogenic carbon. *Geophysical Research Letters*, **34**.
Montenegro, A., M. Eby, Q. Z. Mu, M. Mulligan, A. J. Weaver, E. C. Wiebe, and M. S. Zhao, 2009: The net carbon drawdown of small scale afforestation from satellite observations. *Global and Planetary Change*, **69**, 195-204.
Montzka, S. A., M. Krol, E. Dlugokencky, B. Hall, P. Joeckel, and J. Lelieveld, 2011: Small Interannual Variability of Global Atmospheric Hydroxyl. *Science*, **331**, 67-69.
Mosier, A., C. Kroeze, C. Nevison, O. Oenema, S. Seitzinger, and O. van Cleemput, 1998: Closing the global N2O budget: nitrous oxide emissions through the agricultural nitrogen cycle - OECD/IPCC/IEA phase II development of IPCC guidelines for national greenhouse gas inventory methodology. *Nutrient Cycling in Agroecosystems*, **52**, 225-248.
Mosier, A. R., J. A. Morgan, J. Y. King, D. LeCain, and D. G. Milchunas, 2002: Soil-atmosphere exchange of CH4, CO2, NOx, and N2O in the Colorado shortgrass steppe under elevated CO2. *Plant and Soil*, **240**, 201-211.
Moss, R., et al., 2010: The next generation of scenarios for climate change research and assessment. *Nature*, **463**, 747-756.
Murata, A., Y. Kumamoto, S. Watanabe, and M. Fukasawa, 2007: Decadal increases of anthropogenic CO2 in the South Pacific subtropical ocean along 32 degrees S. *J Geophys Res-Oceans*, **112**.
Murata, A., Y. Kumamoto, K. Sasaki, S. Watanabe, and M. Fukasawa, 2010: Decadal increases in anthropogenic CO2 along 20 degrees S in the South Indian Ocean. *J Geophys Res-Oceans*, **115**.
Murphy, J., D. Sexton, D. Barnett, G. Jones, M. Webb, and D. Stainforth, 2004: Quantification of modelling uncertainties in a large ensemble of climate change simulations. *Nature*, **430**, 768-772.
Nakicenovic, N., and R. Swart, Eds., 2000: *Special Report on Emissions Scenarios*. Cambridge University Press, 570 pp pp.
Naqvi, S. W. A., H. W. Bange, L. Farias, P. M. S. Monteiro, M. I. Scranton, and J. Zhang, 2009: Coastal hypoxia/anoxia as a source of CH4 and N2O. *Biogeosciences Discuss.*, **6**, 9455-9523.
Neef, L., M. van Weele, and P. van Velthoven, 2010: Optimal estimation of the present-day global methane budget. *Global Biogeochemical Cycles*, **24**.

Neftel, A., H. Oeschger, J. Schwander, B. Stauffer, and R. Zumbrunn, 1982: Ice core sample measurements give atmospheric CO2 content during the past 40,000 yr. *Nature*, **295**, 220-223.
Nemani, R. R., et al., 2003: Climate-driven increases in global terrestrial net primary production from 1982 to 1999. *Science*, **300**, 1560-1563.
Nepstad, D., et al., 2009: The end of deforestation in the Brazilian Amazon. *Science*, **326**, 1350-1351.
Nevison, C., J. H. Butler, and J. W. Elkins, 2003: Global distribution of N2O and the ΔN2O-AOU yield in the subsurface ocean. *Global Biogeochem. Cycles*, **17**, 1119.
Nevison, C. D., N. M. Mahowald, R. F. Weiss, and R. G. Prinn, 2007: Interannual and seasonal variability in atmospheric N2O. *Global Biogeochemical Cycles*, **21**, GB3017.
Nevle, R. J., and D. K. Bird, 2008: Effects of syn-pandemic fire reduction and reforestation in the tropical Americas on atmospheric CO2 during European conquest. *Palaeogeography Palaeoclimatology Palaeoecology*, **264**, 25-38.
Nevle, R. J., D. K. Bird, W. F. Ruddiman, and R. A. and Dull, 2011: Neotropical human landscape interactions, fire, and atmospheric CO_2 during European conquest. *The Holocene*.
Nisbet, R. E. R., et al., 2009: Emission of methane from plants. *Proceedings of the Royal Society B-Biological Sciences*, **276**, 1347-1354.
Niyogi, D., et al., 2004: Direct observations of the effects of aerosol loading on net ecosystem CO2 exchanges over different landscapes. *Geophysical Research Letters*, **31**.
Norby, R. J., J. M. Warren, C. M. Iversen, B. E. Medlyn, and R. E. McMurtrie, 2010: CO2 enhancement of forest productivity constrained by limited nitrogen availability. *P Natl Acad Sci USA*, **107**, 19368-19373.
Norby, R. J., et al., 2005: Forest response to elevated CO2 is conserved across a broad range of productivity. *P Natl Acad Sci USA*, **102**, 18052-18056.
O'Connor, F. M., et al., 2010: Possible role of wetlands, permafrost, and methane hydrates in the methane cycle under future climate change: A review. *Reviews of Geophysics*, ARTN RG4005, DOI 10.1029/2010RG000326. -.
Oh, N.-H., and P. A. Raymond, 2006: Contribution of agricultural liming to riverine bicarbonate export and CO2 sequestration in the Ohio River basin. *Global Biogeochemical Cycles*, **20**.
Oleson, K. W., et al., 2010: Technical description of version 4.0 of the Community Land Model (CLM).
Oliveira, P. H. F., et al., 2007: The effects of biomass burning aerosols and clouds on the CO2 flux in Amazonia. *Tellus Series B-Chemical and Physical Meteorology*, **59**, 338-349.
Olivier, J., J. Aardenne, F. Dentener, L. Ganzeveld, and J. Peters, 2005: Recent trends in global greenhouse emissions: regional trends 1970-2000 and spatial distribution of key sources in 2000. *Environmental Science*, **2**, 81-99.
Olofsson, J., and T. Hickler, 2008: Effects of human land-use on the global carbon cycle during the last 6,000 years. *Vegetation History and Archaeobotany*, **17**, 605-615.
Olsen, A., et al., 2006: Magnitude and origin of the anthropogenic CO2 increase and C-13 Suess effect in the Nordic seas since 1981. *Global Biogeochemical Cycles*, **20**.
Orr, F. M., 2009: Onshore Geologic Storage of CO_2. *Science*, **325**, 1656-1658.
Orr, J., et al., 2001: Estimates of anthropogenic carbon uptake from four three-dimensional global ocean models. *Global Biogeochemical Cycles*, **15**, 43-60.
Orr, J. C., 2011: Future changes in ocean carbonate chemistry. *Ocean Acidification*, J.-P. G. a. L. Hansson, Ed., Oxford University Press.
Orr, J. C., V. J. Fabry, O. Aumont, and *i.* s. e. al., 2005: Anthropogenic ocean acidification over the twenty-first century and its impact on calcifying organisms. *Nature*, **437**, 681-686.
Oschlies, A., K. G. Schulz, U. Riebesell, and A. Schmittner, 2008: Simulated 21st century's increase in oceanic suboxia by CO2-enhanced biotic carbon export. *Global Biogeochem. Cycles*, **22**, GB4008.
Oschlies, A., K. W., W. Rickels, and K. Rehdanz, 2010a: Side effects and accounting aspects of hypothetical large-scale Southern Ocean iron fertilization. *Biogeosciences*, **7**, 4017-4035.
Oschlies, A., M. Pahlow, A. Yool, and R. J. Matear, 2010b: Climate engineering by artificial ocean upwelling: Channelling the sorcerer's apprentice. *Geophysical Research Letters*, **37**.
Otto, D., D. Rasse, J. Kaplan, P. Warnant, and L. Francois, 2002: Biospheric carbon stocks reconstructed at the Last Glacial Maximum: comparison between general circulation models using prescribed and computed sea surface temperatures. *Global and Planetary Change*, **33**, 117-138.
Pacala, S. W., et al., 2001: Consistent land- and atmosphere-based US carbon sink estimates. *Science*, **292**, 2316-2320.
Page, S. E., J. O. Rieley, and C. J. Banks, 2010: Global and regional importance of the tropical peatland carbon pool. *Global Change Biology*, **17**, 798-818.
Page, S. E., F. Siegert, J. O. Rieley, H.-D. V. Boehm, A. Jayak, and S. Limin, 2002: The amount of carbon released from peat and forest fires in Indonesia during 1997. *Nature*, **420**, 61-65.
Palmroth, S., et al., 2006: Aboveground sink strength in forests controls the allocation of carbon below ground and its [CO2]-induced enhancement. *PNAS*, **103**, 19362-19367.
Pan, Y. D., R. Birdsey, J. Hom, and K. McCullough, 2009: Separating effects of changes in atmospheric composition, climate and land-use on carbon sequestration of US Mid-Atlantic temperate forests. *Forest Ecology and Management*, **259**, 151-164.
Pan, Y. D., et al., 2011: A Large and Persistent Carbon Sink in the World's Forests. *Science*, **333**, 988-993.

Parekh, P., F. Joos, and S. A. Müller, 2008: A modeling assessment of the interplay between aeolian iron fluxes and iron-binding ligands in controlling carbon dioxide fluctuations during Antarctic warm events. *Paleoceanography*, **23**.
Parekh, P., S. Dutkiewicz, M. J. Follows, and T. Ito, 2006: Atmospheric carbon dioxide in a less dusty world. *Geophysical Research Letters*, **33**.
Park, G.-H., et al., 2010: Variability of global net air-sea CO2 fluxes over the last three decades using empirical relationships. *Tellus B*, **62**, 352-368.
Pechony, O., and D. Shindell, 2010: Driving forces of global wildfires over the past millennium and the forthcoming century. *P Natl Acad Sci USA*, **107**, 19167-19170.
Peng, T. H., and W. S. Broecker, 1991: Dynamic Limitations on the Antarctic Iron Fertilization Strategy. *Nature*, **349**, 227-229.
Peng, T. H., R. Wanninkhof, and R. A. Feely, 2003: Increase of anthropogenic CO2 in the Pacific Ocean over the last two decades. *Deep-Sea Res Pt Ii*, **50**, 3065-3082.
Peng, T. H., R. Wanninkhof, J. L. Bullister, R. A. Feely, and T. Takahashi, 1998: Quantification of decadal anthropogenic CO2 uptake in the ocean based on dissolved inorganic carbon measurements. *Nature*, **396**, 560-563.
Peñuelas, J., J. G. Canadell, and R. Ogaya, 2011: Increased water-use-efficiency during the 20th century did not translate into enhanced tree growth. *Global Ecology and Biogeography*, **20**, 597-608.
Perez, F. F., M. Vazquez-Rodriguez, E. Louarn, X. A. Padin, H. Mercier, and A. F. Rios, 2008: Temporal variability of the anthropogenic CO2 storage in the Irminger Sea. *Biogeosciences*, **5**, 1669-1679.
Perrin, A.-S., A. Probst, and J.-L. Probst, 2008: Impact of nitrogenous fertilizers on carbonate dissolution in small agricultural catchments: Implications for weathering CO2 uptake at regional and global scales. *Geochimica et Cosmochimica Acta*, **72**, 3105-3123.
Peters, G. P., J. C. Minx, C. L. Weber, and O. Edenhofer, 2011: Growth in emission transfers via international trade from 1990 to 2008. *PNAS*.
Petit, J. R., et al., 1999: Climate and atmospheric history of the past 420,000 years from the Vostok ice core, Antarctica. *Nature*, **399**, 429-436.
Petrenko, V. V., et al., 2009: (CH4)-C-14 Measurements in Greenland Ice: Investigating Last Glacial Termination CH4 Sources. *Science*, **324**, 506-508.
Peylin, P., et al., 2005: Multiple constraints on regional CO2 flux variations over land and oceans. *Global Biogeochemical Cycles*, ARTN GB1011, DOI 10.1029/2003GB002214. -.
Phoenix, G., et al., 2006: Atmospheric nitrogen deposition in world biodiversity hotspots: the need for a greater global perspective in assessing N deposition impacts. *Global Change Biology*, **12**, 470-476.
Piao, S., P. Friedlingstein, P. Ciais, L. Zhou, and A. Chen, 2006: Effect of climate and CO2 changes on the greening of the Northern Hemisphere over the past two decades. *Geophysical Research Letters*, ARTN L23402, DOI 10.1029/2006GL028205. -.
Piao, S., et al., 2010: Forest annual carbon cost: a global-scale analysis of autotrophic respiration. *Ecology*. 652-661.
Piao, S., et al., 2011: Contribution of climate change and rising CO_2 to terrestrial carbon balance in East Asia: A multi-model analysis. *Global and Planetary Change*, **75**, 133-142.
Piao, S. L., P. Ciais, P. Friedlingstein, N. de Noblet-Ducoudre, P. Cadule, N. Viovy, and T. Wang, 2009a: Spatiotemporal patterns of terrestrial carbon cycle during the 20th century. *Global Biogeochemical Cycles*, **23**, -.
Piao, S. L., J. Y. Fang, P. Ciais, P. Peylin, Y. Huang, S. Sitch, and T. Wang, 2009b: The carbon balance of terrestrial ecosystems in China. *Nature*, **458**, 1009-U1082.
Piao, S. L., et al., 2008: Net carbon dioxide losses of northern ecosystems in response to autumn warming. *Nature*, **451**, 49-U43.
Plattner, G.-K., F. Joos, and T. Stocker, 2002: Revision of the global carbon budget due to changing air-sea oxygen fluxes. *Global Biogeochemical Cycles*, **16**, 1096.
Plattner, G.-K., F. Joos, T. F. Stocker, and O. Marchal, 2001: Feedback mechanisms and sensitivities of ocean carbon uptake under global warming. *Tellus B*, **53/5**, 564-592.
Plattner, G.-K., et al., 2008: Long-term climate commitments projected with climate-carbon cycle models. *Journal of Climate*, DOI 10.1175/2007JCLI1905.1. 2721-2751.
Plug, L., and J. West, 2009: Thaw lake expansion in a two-dimensional coupled model of heat transfer, thaw subsidence, and mass movement. *Journal of Geophysical Research-Earth Surface*, **114**, -.
Pongratz, J., C. H. Reick, T. Raddatz, and M. Claussen, 2009: Effects of anthropogenic land cover change on the carbon cycle of the last millennium. *Global Biogeochemical Cycles*, **23**.
Pongratz, J., K. Caldeira, C. H. Reick, and M. Claussen, 2011: Coupled climateâ€“carbon simulations indicate minor global effects of wars and epidemics on atmospheric CO2 between AD 800 and 1850. *The Holocene*, 10.1177/0959683610386981.
Power, M. J., et al., 2008: Changes in fire regimes since the Last Glacial Maximum: an assessment based on a global synthesis and analysis of charcoal data. *Climate Dynamics*, **30**, 887-907.
Prentice, I. C., and S. P. Harrison, 2009: Ecosystem effects of CO_2 concentration: evidence from past climates. *Climate of the Past*, **5**, 297-307.

Prentice, I. C., et al., 2001: The Carbon Cycle and Atmospheric Carbon Dioxide. *Climate Change 2001: The Scientific Basis*, J. T. Houghton, et al., Eds., Cambridge University Press.
Prinn, R. G., et al., 2001: Evidence for substantial variations of atmospheric hydroxyl radicals in the past two decades. *Science*, **292**, 1882-1888.
Prinn, R. G., et al., 2005: Evidence for variability of atmospheric hydroxyl radicals over the past quarter century. *Geophysical Research Letters*, **32**.
Prinn, R. G., et al., 2000: A history of chemically and radiatively important gases in air deduced from ALE/GAGE/AGAGE. *Journal of Geophysical Research-Atmospheres*, **105**, 17751-17792.
Rabalais, N. N., R. J. Diaz, L. A. Levin, R. E. Turner, D. Gilbert, and J. Zhang, 2010: Dynamics and distribution of natural and human-caused hypoxia. *Biogeosciences*, **7**, 585-619.
Raddatz, T., et al., 2007: Will the tropical land biosphere dominate the climate-carbon cycle feedback during the twenty-first century? *Climate Dynamics*, **29**, 565-574.
Rafelski, L. E., S. C. Piper, and R. F. Keeling, 2009: Climate effects on atmospheric carbon dioxide over the last century. *Tellus B*, **61**, 718-731.
Ramankutty, N., and J. A. Foley, 1999: Estimating historical changes in global land cover: Croplands from 1700 to 1992. *Global Biogeochemical Cycles*, **13**, 997-1027.
Ramankutty, N., C. Delire, and P. Snyder, 2006: Feedbacks between agriculture and climate: An illustration of the potential unintended consequences of human land use activities. *Global and Planetary Change*, **54**, 79-93.
Randerson, J. T., et al., 2009: Systematic assessment of terrestrial biogeochemistry in coupled climate-carbon models. *Global Change Biology*, **15**, 2462-2484.
Rau, G. H., 2008: Electrochemical Splitting of Calcium Carbonate to Increase Solution Alkalinity: Implications for Mitigation of Carbon Dioxide and Ocean Acidity. *Environ. Sci. Technol.*, **42**, 8935-8940.
Rau, G. H., and K. Caldeira, 1999: Enhanced carbonate dissolution: a means of sequestering waste CO2 as ocean bicarbonate. *Energy Conversion and Management*, **40**, 1803-1813.
Raupach, M. R., J. G. Canadell, and C. Le Quere, 2008: Anthropogenic and biophysical contributions to increasing atmospheric CO2 growth rate and airborne fraction. *Biogeosciences*, **5**, 1601-1613.
Raupach, M. R., G. Marland, P. Ciais, C. Le Quere, J. G. Canadell, G. Klepper, and C. B. Field, 2007: Global and regional drivers of accelerating CO2 emissions. *P Natl Acad Sci USA*, **104**, 10288-10293.
Raymond, P. A., and J. J. Cole, 2003: Increase in the export of alkalinity from North America's largest river. *Science*, **301**, 88-91.
Raymond, P. A., N.-H. Oh, R. E. Turner, and W. Broussard, 2008: Anthropogenically enhanced fluxes of water and carbon from the Mississippi River. *Nature*, **451**, 449-452.
Rayner, P. J., R. M. Law, C. E. Allison, R. J. Francey, C. M. Trudinger, and C. Pickett-Heaps, 2008: Interannual variability of the global carbon cycle (1992–2005) inferred by inversion of atmospheric CO2andδ13CO2measurements. *Global Biogeochemical Cycles*, **22**.
Reagan, M., and G. Moridis, 2007: Oceanic gas hydrate instability and dissociation under climate change scenarios. *Geophysical Research Letters*, **34**, -.
——, 2009: Large-scale simulation of methane hydrate dissociation along the West Spitsbergen Margin. *Geophysical Research Letters*, **36**, -.
Regalado, A., 2010: BIODIVERSITY Brazil Says Rate of Deforestation in Amazon Continues to Plunge. *Science*, **329**, 1270-1271.
Reich, P. B., et al., 2006: Nitrogen limitation constrains sustainability of ecosystem response to CO2. *Nature*, **440**, 922-925.
Report, R. S., 2009: Geoengineering the climate; Science, governance and uncertainty.
Ricke, K. L., G. Morgan, and M. R. Allen, 2010: Regional climate response to solar-radiation management. *Nature Geoscience*, **3**, 537-541.
Ridgwell, A., and R. E. Zeebe, 2005: The role of the global carbonate cycle in the regulation and evolution of the Earth system. *Earth and Planetary Science Letters*, **234**, 299-315.
Ridgwell, A., and J. C. Hargreaves, 2007: Regulation of atmospheric CO2 by deep-sea sediments in an Earth system model. *Global Biogeochemical Cycles*, **21**.
Ridgwell, A. J., 2001: Glacial-interglacial perturbations in the global carbon cycle, University of East Anglia, Norwich, UK., 134 pp.
Ridgwell, A. J., A. J. Watson, M. A. Maslin, and J. O. Kaplan, 2003: Implications of coral reef buildup for the controls on atmospheric CO2 since the Last Glacial Maximum. *Paleoceanography*, **18**, doi:10.1029/2003PA000893.
Riebesell, U., K. G. Schulz, R. G. J. Bellerby, M. Botros, P. Fritsche, M. Meyerhofer, and C. Neill, 2007: Enhanced biological carbon consumption in a high CO_2 ocean. *Nature*, **450**, 545-548.
Rigby, M., et al., 2008: Renewed growth of atmospheric methane. *Geophysical Research Letters*, **35**.
Ringeval, B., P. Friedlingstein, C. Koven, P. Ciais, N. de Noblet-Ducoudre, B. Decharme, and P. Cadule, 2011: Climate-CH4 feedback from wetlands and its interaction with the climate-CO2 feedback. *Biogeosciences*, **8**, 2137-2157.
Rodenbeck, C., S. Houweling, and M. H. Gloor, M., 2003: CO2 flux history 1982–2001 inferred from atmospheric data using a global inversion of atmospheric transport. *Atmos Chem Phys Discuss*, **3**, 2575-2659.

Rogelj, J., et al., 2011: Emission pathways consistent with a 2oC global temperature limit. *Nature Climate Change*, **1**, 413-418.
Rose, S. K., et al., 2011: Land-based mitigation in climate stabilisation. *Energy Economics*, doi:10.1016/j.eneco.2011.06.004.
Roth, R., and F. Joos, submitted: A possible role for volcanic carbon emissions in regulating glacial-interglacial CO2 variations? *Earth and Planetary Science Letters*.
Rothlisberger, R., M. Bigler, E. W. Wolff, F. Joos, E. Monnin, and M. A. Hutterli, 2004: Ice core evidence for the extent of past atmospheric CO2 change due to iron fertilisation. *Geophysical Research Letters*, **31**.
Rotty, R. M., 1983: Distribution of and changes in industrial carbon-cycle production. *Journal of Geophysical Research - Ocean and Atmosphere*, **88**, 1301-1308.
Roy, T., et al., 2011: Regional Impacts of Climate Change and Atmospheric CO2 on Future Ocean Carbon Uptake: A Multimodel Linear Feedback Analysis. *Journal of Climate*, **24**, 2300-2318.
Rubasinghege, G., S. N. Spak, C. O. Stanier, G. R. Carmichael, and V. H. Grassian, 2011: Abiotic Mechanism for the Formation of Atmospheric Nitrous Oxide from Ammonium Nitrate. *Environ. Sci. Technol.*, **45**, 2691-2697.
Ruddiman, W. F., 2003: The anthropogenic greenhouse era began thousands of years ago. *Climatic Change*, **61**, 261-293.
——, 2007: The early anthropogenic hypothesis: Challenges and responses. *Reviews of Geophysics*, **45**.
Rustad, L. E., et al., 2001: A meta-analysis of the response of soil respiration, net nitrogen mineralization, and aboveground plant growth to experimental ecosystem warming. *Oecologia*, **126**, 543-562.
Saatchi, S. S., et al., 2011: Benchmark map of forest carbon stocks in tropical regions across three continents. *Proceedings of the National Academy of Sciences*, **108**, 9899-9904.
Sabine, C. L., R. A. Feely, F. J. Millero, A. G. Dickson, C. Langdon, S. Mecking, and D. Greeley, 2008: Decadal changes in Pacific carbon. *J Geophys Res-Oceans*, **113**.
Sabine, C. L., et al., 2004: The oceanic sink for anthropogenic CO2. *Science*. 367-371.
Samanta, A., M. H. Costa, E. L. Nunes, S. A. Viera, L. Xu, and R. B. Myneni, 2011: Comment on "Drought-induced reductions in global terrestrial net primary production from 2000 through 2009". *Science*, **333**, 1093-c.
Sarmiento, J. L., and N. Gruber, 2006: *Ocean Biogeochemical Dynamics.* Princeton University.
Sarmiento, J. L., T. M. C. Hughes, R. J. Stouffer, and S. Manabe, 1998: Simulated response of the ocean carbon cycle to anthropogenic climate warming. *Nature*, **393**, 245-249.
Sarmiento, J. L., P. Monfray, E. Maier-Reimer, O. Aumont, R. Murnane, and J. Orr, 2000: Air-sea CO2 Fluxes and carbon transport: a comparison of three ocean general circulation models. *Global Biogeochemical Cycles*, **14**, 1267-1281.
Sarmiento, J. L., et al., 2010: Trends and regional distributions of land and ocean carbon sinks. *Biogeosciences*, **7**, 2351-2367.
Schaefer, K., T. Zhang, L. Bruhwiler, and A. P. Barrett, 2011: Amount and timing of permafrost carbon release in response to climate warming. *Tellus B*, **63**, 165-180.
Scheffer, M., V. Brovkin, and P. M. Cox, 2006: Positive feedback between global warming and atmospheric CO2 concentration inferred from past climate change. *Geophysical Research Letters*, **33**.
Schilt, A., M. Baumgartner, T. Blunier, J. Schwander, R. Spahni, H. Fischer, and T. F. Stocker, 2010a: Glacial-interglacial and millennial-scale variations in the atmospheric nitrous oxide concentration during the last 800,000 years. *Quaternary Science Reviews*, **29**, 182-192.
Schilt, A., et al., 2010b: Atmospheric nitrous oxide during the last 140,000 years. *Earth and Planetary Science Letters*, **300**, 33-43.
Schmittner, A., and E. D. Galbraith, 2008: Glacial greenhouse-gas fluctuations controlled by ocean circulation changes. *Nature*, **456**, 373-376.
Schmittner, A., A. Oschlies, H. D. Matthews, and E. D. Galbraith, 2008: Future changes in climate, ocean circulation, ecosystems, and biogeochemical cycling simulated for a business-as-usual CO_2 emission scenario until year 4000 AD. *Global Biogeochemical Cycles*, **22**.
Schmittner, A., N. M. Urban, K. Keller, and D. Matthews, 2009: Using tracer observations to reduce the uncertainty of ocean diapycnal mixing and climate-carbon cycle projections. *Global Biogeochemical Cycles*, **23**.
Schneising, O., M. Buchwitz, J. P. Burrows, H. Bovensmann, P. Bergamaschi, and W. Peters, 2009: Three years of greenhouse gas column-averaged dry air mole fractions retrieved from satellite - Part 2: Methane. *Atmos Chem Phys*, **9**, 443-465.
Scholze, M., W. Knorr, N. Arnell, and I. Prentice, 2006: A climate-change risk analysis for world ecosystems. *P Natl Acad Sci USA*, **103**, 13116-13120.
Schuiling, R. D., and P. Krijgsman, 2006: Enhanced weathering: An effective and cheap tool to sequester CO2. *Climatic Change*, **74**, 349-354.
Schulze, E. D., S. Luyssaert, P. Ciais, A. Freibauer, I. A. Janssens, and e. al., 2009: Importance of methane and nitrous oxide for Europe's terrestrial greenhouse-gas balance. *Nature Geoscience*, **2**, 842-850.
Schulze, E. D., et al., 2010: The European carbon balance. Part 4: integration of carbon and other trace-gas fluxes. *Global Change Biology*, **16**, 1451-1469.

Schurgers, G., U. Mikolajewicz, M. Groger, E. Maier-Reimer, M. Vizcaino, and A. Winguth, 2006: Dynamics of the terrestrial biosphere, climate and atmospheric CO2 concentration during interglacials: a comparison between Eemian and Holocene. *Climate of the Past*, **2**, 205-220.

Schuster, U., and A. J. Watson, 2007: A variable and decreasing sink for atmospheric CO2 in the North Atlantic. *J Geophys Res-Oceans*, **112**.

Schuster, U., et al., 2009: Trends in North Atlantic sea-surface fCO(2) from 1990 to 2006. *Deep-Sea Res Pt Ii*, **56**, 620-629.

Schuur, E. A. G., J. G. Vogel, K. G. Crummer, H. Lee, J. O. Sickman, and T. E. Osterkamp, 2009: The effect of permafrost thaw on old carbon release and net carbon exchange from tundra. *Nature*, **459**, 556-559.

Schwalm, C. R., C. A. Williams, K. Schaefer, I. Baker, G. J. Collatz, and C. Roedenbeck, 2011: Does terrestrial drought explain global CO(2) flux anomalies induced by El Nino? *Biogeosciences*, **8**, 2493-2506.

Schwalm, C. R., et al., 2010: A model-data intercomparison of CO_2 exchange across North America: Results from the North American Carbon Program site synthesis. *Journal of Geophysical Research*, **115**, G00H05.

Seitzinger, S. P., J. A. Harrison, E. Dumont, A. H. W. Beusen, and A. F. Bouwman, 2005: Sources and delivery of carbon, nitrogen, and phosphorus to the coastal zone: An overview of Global Nutrient Export from Watersheds (NEWS) models and their application. *Global Biogeochemical Cycles*, **19**.

Seitzinger, S. P., et al., 2010: Global river nutrient export: A scenario analysis of past and future trends. *Global Biogeochemical Cycles*, **24**, GB0A08.

Shackleton, N. J., 2000: The 100,000-year ice-age cycle identified and found to lag temperature, carbon dioxide, and orbital eccentricity. *Science*, **289(5486)**, 1897-1902.

Shaffer, G., 2010: Long-term effectiveness and consequences of carbon dioxide sequestration. *Nature Geoscience*, **3**, 464-467.

Shaffer, G., S. M. Olsen, and J. O. P. Pedersen, 2009: Long-term ocean oxygen depletion in response to carbon dioxide emission from fossil fuels. *Nature Geoscience*, **2**, 105-109.

Shakhova, N., I. Semiletov, A. Salyuk, V. Yusupov, D. Kosmach, and O. Gustafsson, 2010: Extensive Methane Venting to the Atmosphere from Sediments of the East Siberian Arctic Shelf. *Science*, **327**, 1246-1250.

Shevliakova, E., et al., 2009: Carbon cycling under 300 years of land use change: Importance of the secondary vegetation sink. *Global Biogeochemical Cycles*, **23**, -.

Siegenthaler, U., et al., 2005a: Supporting evidence from the EPICA Dronning Maud Land ice core for atmospheric CO2 changes during the past millennium. *Tellus Series B-Chemical and Physical Meteorology*, **57**, 51-57.

Siegenthaler, U., et al., 2005b: Stable carbon cycle-climate relationship during the late Pleistocene. *Science*, **310**, 1313-1317.

Sigman, D., M. Hain, and G. Haug, 2010: The polar ocean and glacial cycles in atmospheric CO2 concentration. *Nature*, **466**, 47-55.

Simmonds, P. G., A. J. Manning, R. G. Derwent, P. Ciais, M. Ramonet, V. Kazan, and D. Ryall, 2005: A burning question. Can recent growth rate anomalies in the greenhouse gases be attributed to large-scale biomass burning events? *Atmospheric Environment*, **39**, 2513-2517.

Singarayer, J. S., P. J. Valdes, P. Friedlingstein, S. Nelson, and D. J. Beerling, 2011: Late Holocene methane rise caused by orbitally controlled increase in tropical sources. *Nature*, **470**, 82-U91.

Singh, B. K., R. D. Bartgett, P. Smith, and D. S. Peay, 2010: Microorganisms and climate change: terrestrial feedbacks and mitigation options. *Nature Microbiology*, **8**, 779-790.

Sitch, S., P. M. Cox, W. J. Collins, and C. Huntingford, 2007: Indirect radiative forcing of climate change through ozone effects on the land-carbon sink. *Nature*, **448**, 791-U794.

Sitch, S., V. Brovkin, W. von Bloh, D. van Vuuren, B. Assessment, and A. Ganopolski, 2005: Impacts of future land cover changes on atmospheric CO2 and climate. *Global Biogeochemical Cycles*, **19**.

Sitch, S., et al., 2003: Evaluation of ecosystem dynamics, plant geography and terrestrial carbon cycling in the LPJ dynamic global vegetation model. *Global Change Biology*, **9**, 161-185.

Sitch, S., et al., 2008: Evaluation of the terrestrial carbon cycle, future plant geography and climate-carbon cycle feedbacks using five Dynamic Global Vegetation Models (DGVMs). *Global Change Biology*, **14**, 2015-2039.

Smith, L., Y. Sheng, G. MacDonald, and L. Hinzman, 2005: Disappearing Arctic lakes. *Science*, **308**, 1429-1429.

Smith, S. V., W. H. Renwick, R. W. Buddemeier, and C. J. Crossland, 2001: Budgets of soil erosion and deposition for sediments and sedimentary organic carbon across the conterminous United States. *Global Biogeochemical Cycles*, **15**, 697-707.

Smith, T. M., and H. H. Shugart, 1993: The transient-response of terrestrial carbon storage to a perturbed climate. *Nature*, **361**, 523-526.

Sokolov, A. P., D. W. Kicklighter, J. M. Melillo, B. S. Felzer, C. A. Schlosser, and T. W. Cronin, 2008: Consequences of considering carbon-nitrogen interactions on the feedbacks between climate and the terrestrial carbon cycle. *Journal of Climate*, **21**, 3776-3796.

Sowers, T., 2001: N2O record spanning the penultimate deglaciation from the Vostok ice core. *Journal of Geophysical Research-Atmospheres*, **106**, 31903-31914.

——, 2006: Late quaternary atmospheric CH4 isotope record suggests marine clathrates are stable. *Science*, **311**, 838-840.

Spahni, R., et al., 2011: Constraining global methane emissions and uptake by ecosystems. *Biogeosciences*, **8**, 1643-1665.
Spracklen, D., L. Mickley, J. Logan, R. Hudman, R. Yevich, M. Flannigan, and A. Westerling, 2009: Impacts of climate change from 2000 to 2050 on wildfire activity and carbonaceous aerosol concentrations in the western United States. *Journal of Geophysical Research-Atmospheres*, **114**, -.
Stallard, R. F., 1998: Terrestrial sedimentation and the carbon cycle: Coupling weathering and erosion to carbon burial. *Global Biogeochemical Cycles*, **12**, 231-257.
Stanhill, G., and S. Cohen, 2001: Global dimming: a review of the evidence for a widespread and significant reduction in global radiation with discussion of its probable causes and possible agricultural consequences. *Agricultural and Forest Meteorology*, **107**, 255-278.
Steinacher, M., F. Joos, T. L. Frolicher, G. K. Plattner, and S. C. Doney, 2009: Imminent ocean acidification in the Arctic projected with the NCAR global coupled carbon cycle-climate model. *Biogeosciences*, **6**, 515-533.
Steinacher, M., et al., 2010: Projected 21^st century decrease in marine productivity: a multi-model analysis. *Biogeosciences*, **7**, 979-1005.
Stephens, B. B., and R. F. Keeling, 2000: The influence of Antarctic sea ice on glacial-interglacial CO2 variations. *Nature*, **404**, 171-174.
Stephens, B. B., et al., 2007: Weak Northern and Strong Tropical Land Carbon Uptake from Vertical Profiles of Atmospheric CO2. *Science*, **316**, 1732-1735.
Stocker, B. D., K. Strassmann, and F. Joos, 2011: Sensitivity of Holocene atmospheric CO2 and the modern carbon budget to early human land use: analyses with a process-based model. *Biogeosciences*, **8**, 69-88.
Stockli, R., et al., 2008: Use of FLUXNET in the community land model development. *Journal of Geophysical Research-Biogeosciences*, **113**, -.
Stolaroff, J. K., D. W. Keith, and G. V. Lowry, 2008: Carbon dioxide capture from atmospheric air using sodium hydroxide spray. *Environ. Sci. Technol.*, **42**, 2728-2735.
Strassmann, K. M., F. Joos, and G. Fischer, 2008: Simulating effects of land use changes on carbon fluxes: past contributions to atmospheric CO2 increases and future commitments due to losses of terrestrial sink capacity. *Tellus Series B-Chemical and Physical Meteorology*, **60**, 583-603.
Stuiver, M., and P. D. Quay, 1981: Atmospheric C-14 changes resulting from fossil-fuel CO2 release and cosmic-ray flux variability. *Earth and Planetary Science Letters*, **53**, 349-362.
Sutton, M. A., et al., 2007: Challenges in quantifying biosphere-atmosphere exchange of nitrogen species. *Environmental Pollution*, **150**, 125-139.
Syakila, A., and C. Kroeze, 2011: The Global N_2O Budget Revisited. *Greenhouse Gas Measurement and Mitigation*, **1**, 17-26.
Syakila, A., C. Kroeze, and C. P. Slomp, 2010: Neglecting sinks for N_2O at the earth's surface: does it matter? *Journal of Integrative Environmental Sciences*, **7**, 79-87.
Syvitski, J. P. M., C. J. Vorosmarty, A. J. Kettner, and P. Green, 2005: Impact of humans on the flux of terrestrial sediment to the global coastal ocean. *Science*, **308**, 376-380.
Tagaris, E., K. Liao, K. Manomaiphiboon, J. Woo, S. He, P. Amar, and A. Russell, 2008: Impacts of future climate change and emissions reductions on nitrogen and sulfur deposition over the United States. *Geophysical Research Letters*, **35**, -.
Tagliabue, A., L. Bopp, and O. Aumont, 2008: Ocean biogeochemistry exhibits contrasting responses to a large scale reduction in dust deposition. *Biogeosciences*, **5**, 11-24.
Tagliabue, A., L. Bopp, and M. Gehlen, 2011: The response of marine carbon and nutrient cycles to ocean acidification: Large uncertainties related to phytoplankton physiological assumptions. *Global Biogeochemical Cycles*, **25**, -.
Takahashi, T., S. C. Sutherland, R. A. Feely, and R. Wanninkhof, 2006: Decadal change of the surface water pCO(2) in the North Pacific: A synthesis of 35 years of observations. *J Geophys Res-Oceans*, **111**, -.
Takahashi, T., et al., 2009: Climatological mean and decadal change in surface ocean pCO(2), and net sea-air CO2 flux over the global oceans. *Deep-Sea Res Pt Ii*, **56**, 554-577.
Tan, K., et al., 2010: Application of the ORCHIDEE global vegetation model to evaluate biomass and soil carbon stocks of Qinghai-Tibetan grasslands. *Global Biogeochemical Cycles*, **24**.
Tanhua, T., A. Kortzinger, K. Friis, D. W. Waugh, and D. W. R. Wallace, 2007: An estimate of anthropogenic CO2 inventory from decadal changes in oceanic carbon content. *P Natl Acad Sci USA*, **104**, 3037-3042.
Tans, P., T. Conway, and T. Nakazawa, 1989: Latitudinal distribution of the sources and sinks of atmospheric carbon-dioxide derived from surface observations and an atmospheric transport model. *Journal of Geophysical Research-Atmospheres*, **94**, 5151-5172.
Tarnocai, C., J. G. Canadell, E. A. G. Schuur, P. Kuhry, G. Mazhitova, and S. Zimov, 2009: Soil organic carbon pools in the northern circumpolar permafrost region. *Global Biogeochemical Cycles*, **23**.
Tegen, I., M. Werner, S. P. Harrison, and K. E. Kohfeld, 2004: Relative importance of climate and land use in determining present and future global soil dust emission. *Geophysical Research Letters*, **31**.
Thomas, H., et al., 2008: Changes in the North Atlantic Oscillation influence CO2 uptake in the North Atlantic over the past 2 decades. *Global Biogeochemical Cycles*, **22**, -.
Thomas, H., et al., 2007: Rapid decline of the CO2 buffering capacity in the North Sea and implications for the North Atlantic Ocean. *Global Biogeochemical Cycles*, **21**, -.

Thompson, D., and S. Solomon, 2002: Interpretation of recent Southern Hemisphere climate change. *Science*, **296**, 895-899.
Thomson, A. M., et al., 2010: Climate mitigation and the future of tropical landscapes. *PNAS*, **107**, 19633-19638.
Thornton, P. E., J. F. Lamarque, N. A. Rosenbloom, and N. M. Mahowald, 2007: Influence of carbon-nitrogen cycle coupling on land model response to CO2 fertilization and climate variability. *Global Biogeochemical Cycles*, **21**.
Thornton, P. E., et al., 2009: Carbon-nitrogen interactions regulate climate-carbon cycle feedbacks: results from an atmosphere-ocean general circulation model. *Biogeosciences*, **6**, 2099-2120.
Tian, H., X. Xu, M. Liu, W. Ren, C. Zhang, G. Chen, and C. Lu, 2010: Spatial and temporal patterns of CH4 and N2O fluxes in terrestrial ecosystems of North America during 1979-2008: application of a global biogeochemistry model. *Biogeosciences*, **7**, 2673-2694.
Tian, H., et al., 2011: China's terrestrial carbon balance: Contributions from multiple global change factors. *Global Biogeochemical Cycles*, **25**, -.
Tilman, D., et al., 2001: Forecasting Agriculturally Driven Global Environmental Change. *Science*, **292**, 281-284.
Toggweiler, J., J. L. Russell, and S. R. Carson, 2006: Midlatitude westerlies, atmospheric CO_2, and climate change during the ice ages. *Paleoceanography*, **21**.
Toggweiler, J. R., 1999: Variation of atmospheric CO2 by ventilation of the ocean's deepest water. *Paleoceanography*, **14**, 571-588.
Trudinger, C. M., I. G. Enting, P. J. Rayner, and R. J. Francey, 2002: Kalman filter analysis of ice core data - 2. Double deconvolution of CO2 and delta C-13 measurements. *Journal of Geophysical Research-Atmospheres*, **107**.
Tubiello, F., and G. Fischer, 2007: Reducing climate change impacts on agriculture: Global and regional effects of mitigation, 2000-2080. *Technol. Forecasting Soc. Change*, **74**, 1030-1056.
Turetsky, M., R. Wieder, D. Vitt, R. Evans, and K. Scott, 2007: The disappearance of relict permafrost in boreal north America: Effects on peatland carbon storage and fluxes. *Global Change Biology*, **13**, 1922-1934.
Turetsky, M., C. Treat, M. Waldrop, J. Waddington, J. Harden, and A. McGuire, 2008: Short-term response of methane fluxes and methanogen activity to water table and soil warming manipulations in an Alaskan peatland. *Journal of Geophysical Research-Biogeosciences*, **113**, -.
Turetsky, M., E. Kane, J. Harden, R. Ottmar, K. Manies, E. Hoy, and E. Kasischke, 2011: Recent acceleration of biomass burning and carbon losses in Alaskan forests and peatlands. *Nature Geoscience*, **4**, 27-31.
Tymstra, C., M. Flannigan, O. Armitage, and K. Logan, 2007: Impact of climate change on area burned in Alberta's boreal forest. *International Journal of Wildland Fire*, **16**, 153-160.
Tyrrell, T., J. G. Shepherd, and S. Castle, 2007: The long-term legacy of fossil fuels. *Tellus Series B-Chemical and Physical Meteorology*, **59**, 664-672.
Ullman, D. J., G. A. McKinley, V. Bennington, and S. Dutkiewicz, 2009: Trends in the North Atlantic carbon sink: 1992-2006. *Global Biogeochemical Cycles*, **23**, -.
UNEP, 2011: Integrated Assessment of Black Carbon and Tropospheric Ozone: Summary for Decision Makers. UNEP, WMO, 36 pp.
Valdes, P. J., D. J. Beerling, and C. E. Johnson, 2005: The ice age methane budget. *Geophysical Research Letters*, **32**.
van der Werf, G. R., et al., 2004: Continental-scale partitioning of fire emissions during the 1997 to 2001 El Nino/La Nina period. *Science*, **303**, 73-76.
van der Werf, G. R., et al., 2009: CO2 emissions from forest loss. *Nature Geoscience*, **2**.
van der Werf, G. R., et al., 2010: Global fire emissions and the contribution of deforestation, savanna, forest, agricultural, and peat fires (1997-2009). *Atmospheric Chemistry and Physics*, **10**, 11707-11735.
Van Dingenen, R., F. Dentener, F. Raes, M. Krol, L. Emberson, and J. Cofala, 2009: The global impact of ozone on agricultural crop yields under current and future air quality legislation. *Atmospheric Environment*, **43**, 604-618.
van Huissteden, J., C. Berrittella, F. J. W. Parmentier, Y. Mi, T. C. Maximov, and A. J. Dolman, 2011: Methane emissions from permafrost thaw lakes limited by lake drainage. *Nature Climate Change*, **1**, 119-123.
van Minnen, J. G., K. K. Goldewijk, E. Stehfest, B. Eickhout, G. van Drecht, and R. Leemans, 2009: The importance of three centuries of land-use change for the global and regional terrestrial carbon cycle. *Climatic Change*, **97**, 123-144.
Van Oost, K., et al., 2007: The impact of agricultural soil erosion on the global carbon cycle. *Science*, **318**, 626-629.
van Vuuren, D. P., L. F. Bouwman1, S. J. Smith, and F. Dentener, 2011: Global projections for anthropogenic reactive nitrogen emissions to the atmosphere: an assessment of scenarios in the scientific literature. *Current Opinions in Environmental Sustainability*, **3**, 359-369.
vanGroenigen, K. J., C. Osenberg, and B. Hungate, 2011: Increased soil emissions of potent greenhouse gases under increased atmospheric CO2. *Nature*, **475**, 214-216.
vanMinnen, J. G., K. K. Goldewijk, E. Stehfest, B. Eickhout, G. van Drecht, and R. Leemans, 2009: The importance of three centuries of land-use change for the global and regional terrestrial carbon cycle. *Climatic Change*, **97**, 123-144.
Verdy, A., S. Dutkiewicz, M. J. Follows, J. Marshall, and A. Czaja, 2007: Carbon dioxide and oxygen fluxes in the Southern Ocean: Mechanisms of interannual variability. *Global Biogeochemical Cycles*, **21**, -.
Vigano, I., H. van Weelden, R. Holzinger, F. Keppler, A. McLeod, and T. Rockmann, 2008: Effect of UV radiation and temperature on the emission of methane from plant biomass and structural components. *Biogeosciences*, **5**, 937-947.

Vitousek, P. M., S. Porder, B. Z. Houlton, and O. A. Chadwick, 2010: Terrestrial phosphorus limitation: mechanisms, implications, and nitrogen-phosphorus interactions. *Ecol. Appl.*, **20**, 5-15.
Waelbroeck, C., et al., 2009: Constraints on the magnitude and patterns of ocean cooling at the Last Glacial Maximum. *Nature Geoscience*, **2**, 127-132.
Wahlen, M., et al., 1989: C-14 in Methane Sources and in Atmospheric Methane - the Contribution From Fossil Carbon. *Science*, **245**, 286-290.
Wakita, M., S. Watanabe, A. Murata, N. Tsurushima, and M. Honda, 2010: Decadal change of dissolved inorganic carbon in the subarctic western North Pacific Ocean. *Tellus Series B-Chemical and Physical Meteorology*, **62**, 608-620.
Walker, J. C. G., and J. F. Kasting, 1992: Effects of fuel and forest conservation on future levels of atmospheric carbon dioxide. *Palaeogeography Palaeoclimatology Palaeoecology*, **97**, 151-189.
Walter, K. M., S. A. Zimov, J. P. Chanton, D. Verbyla, and F. S. Chapin, 2006: Methane bubbling from Siberian thaw lakes as a positive feedback to climate warming. *Nature*, **443**, 71-75.
Wang, Y., and B. Houlton, 2009: Nitrogen constraints on terrestrial carbon uptake: Implications for the global carbon-climate feedback. *Geophysical Research Letters*, **36**, -.
Wang, Y. P., R. M. Law, and B. Pak, 2010a: A global model of carbon, nitrogen and phosphorus cycles for the terrestrial biosphere. *Biogeosciences*, **7**, 2261-2282.
Wang, Z., J. Chappellaz, K. Park, and J. E. Mak, 2010b: Large Variations in Southern Hemisphere Biomass Burning During the Last 650 Years. *Science*, **330**, 1663-1666.
Wang, Z. P., X. G. Han, G. G. Wang, Y. Song, and J. Gulledge, 2008: Aerobic methane emission from plants in the Inner Mongolia steppe. *Environ. Sci. Technol.*, **42**, 62-68.
Wania, R., 2007: Modelling northern peatland land surface processes, vegetation dynamics and methane emissions, Bristol, UK.
Wanninkhof, R., S. C. Doney, J. L. Bullister, N. M. Levine, M. Warner, and N. Gruber, 2010: Detecting anthropogenic CO2 changes in the interior Atlantic Ocean between 1989 and 2005. *J Geophys Res-Oceans*, **115**.
Watanabe, S., et al., 2011: MIROC-ESM 2010: model description and basic results of CMIP5-20c3m experiments. *Geoscientific Model Development*, **4**, 845-872.
Watson, A., et al., 2009: Tracking the Variable North Atlantic Sink for Atmospheric CO2. *Science*, **326**, 1391-1393.
Watson, A. J., and A. C. N. Garabato, 2006: The role of southern Ocean mixing and upwelling in glacial-interglacial atmospheric CO_2 change. *Tellus, Ser. B*, **58**, 73-87.
Watson, A. J., D. C. E. Bakker, A. J. Ridgwell, P. W. Boyd, and C. S. Law, 2000: Effect of iron supply on Southern Ocean CO2 uptake and implications for glacial atmospheric CO2. *Nature*, **407**, 730-733.
Watson, A. J., P. W. Boyd, S. M. Turner, T. D. Jickells, and P. S. Liss, 2008: Designing the next generation of ocean iron fertilization experiments. *Marine Ecology-Progress Series*, **364**, 303-309.
Watson, A. J., et al., 1994: Minimal effect of iron fertilization on sea-surface carbon-dioxide concentartions. *Nature*, **371**, 143-145.
Waugh, D. W., T. M. Hall, B. I. McNeil, R. Key, and R. J. Matear, 2006: Anthropogenic CO2 in the oceans estimated using transit time distributions. *Tellus Series B-Chemical and Physical Meteorology*, **58**, 376-389.
Welp, L. R., et al., 2011: Interannual variability in the oxygen isotopes of atmospheric CO2 driven by El Nino. *Nature*, **477**, 579-582.
Westbrook, G., et al., 2009: Escape of methane gas from the seabed along the West Spitsbergen continental margin. *Geophysical Research Letters*, **36**, -.
Westerling, A., M. Turner, E. Smithwick, W. Romme, and M. Ryan, 2011: Continued warming could transform Greater Yellowstone fire regimes by mid-21st century. *P Natl Acad Sci USA*, **108**, 13165-13170.
Wigley, T. M. L., 1995: Global mean temperature and sea-level consequences of greenhouse-gas concentration stabilization. *Geophysical Research Letters*, **22**, 45-48.
Williams, C. A., G. J. Collatz, J. Masek, and S. N. Goward, 2011: Carbon consequences of forest disturbance and recovery across the conterminous United States. *Global Biogeochemical Cycles*, **in press**.
Wise, M., et al., 2009: Implications of Limiting CO2 Concentrations for Land Use and Energy. *Science*, **324**, 1183-1186.
Woodward, F. I., and M. R. Lomas, 2004: Simulating vegetation processes along the Kalahari transect. *Global Change Biology*, **10**, 383-392.
Woolf, D., J. E. Amonette, F. A. Street-Perrott, J. Lehmann, and S. Joseph, 2010: Sustainable biochar to mitigate global climate change. *Nature Communications*, **1**.
Wotton, B., C. Nock, and M. Flannigan, 2010: Forest fire occurrence and climate change in Canada. *International Journal of Wildland Fire*, **19**, 253-271.
Wu, P. L., R. Wood, J. Ridley, and J. Lowe, 2010: Temporary acceleration of the hydrological cycle in response to a CO_2 rampdown. *Geophysical Research Letters*, **37**.
Yamamoto-Kawai, M., F. A. McLaughlin, E. C. Carmack, S. Nishino, and K. Shimada, 2009: Aragonite Undersaturation in the Arctic Ocean: Effects of Ocean Acidification and Sea Ice Melt. *Science*, **326**, 1098-1100.
Yan, X., H. Akiyama, K. Yagi, and H. Akimoto, 2009: Global estimations of the inventory and mitigation potential of methane emissions from rice cultivation conducted using the 2006 Intergovernmental Panel on Climate Change Guidelines. *Global Biogeochemical Cycles*, **23**.

Yang, X., T. Richardson, and A. Jain, 2010: Contributions of secondary forest and nitrogen dynamics to terrestrial carbon uptake. *Biogeosciences*, **7**, 3041-3050.

Yevich, R., and J. A. Logan, 2003: An assessment of biofuel use and burning of agricultural waste in the developing world. *Global Biogeochemical Cycles*, **17**.

Yool, A., J. G. Shepherd, H. L. Bryden, and A. Oschlies, 2009: Low efficiency of nutrient translocation for enhancing oceanic uptake of carbon dioxide. *J Geophys Res-Oceans*, **114**.

Yu, J. M., W. S. Broecker, H. Elderfield, Z. D. Jin, J. McManus, and F. Zhang, 2010: Loss of Carbon from the Deep Sea Since the Last Glacial Maximum. *Science*, **330**, 1084-1087.

Yu, Z., 2011: Holocene carbon flux histories of the worldâ€™s peatlands: Global carbon-cycle implications. *The Holocene*, 10.1177/0959683610386982.

Zaehle, S., and A. Friend, 2010: Carbon and nitrogen cycle dynamics in the O-CN land surface model: 1. Model description, site-scale evaluation, and sensitivity to parameter estimates. *Global Biogeochemical Cycles*, **24**, -.

Zaehle, S., and D. Dalmonech, 2011: Carbon-nitrogen interactions on land at global scales: Current understanding in modelling climate biosphere feedbacks. *Current Opinions in Environmental Sustainability*, **3**, 311-320.

Zaehle, S., P. Friedlingstein, and A. D. Friend, 2010a: Terrestrial nitrogen feedbacks may accelerate future climate change. *Geophysical Research Letters*, **37**, -.

Zaehle, S., A. D. Friend, P. Friedlingstein, F. Dentener, P. Peylin, and M. Schulz, 2010b: Carbon and nitrogen cycle dynamics in the O-CN land surface model: 2. Role of the nitrogen cycle in the historical terrestrial carbon balance. *Global Biogeochemical Cycles*, **24**.

Zeebe, R. E., and D. Wolf-Gladrow, 2001: *CO2 in Seawater: Equilibrium, Kinetics, Isotopes.*

Zeebe, R. E., and D. Archer, 2005: Feasibility of ocean fertilization and its impact on future atmospheric CO2 levels. *Geophysical Research Letters*, **32**.

Zeng, N., 2003: Glacial-interglacial atmospheric CO2 change —The glacial burial hypothesis. *Advances In Atmospheric Sciences*, **20**, 677-693.

Zhao, M. S., and S. W. Running, 2011: Response to Comments on "Comment on "Drought-induced reductions in global terrestrial net primary production from 2000 through 2009"". *Science*, **333**, 1093-e.

Zhou, S., and P. C. Flynn, 2005: Geoengineering downwelling ocean currents: A cost assessment. *Climatic Change*, **71**, 203-220.

Zhuang, Q., et al., 2007: Net emissions of CH4 and CO2 in Alaska: Implications for the region's greenhouse gas budget. *Ecol. Appl.*, **17**, 203-212.

Zhuang, Q., et al., 2006: CO2 and CH4 exchanges between land ecosystems and the atmosphere in northern high latitudes over the 21st century. *Geophysical Research Letters*, **33**, -.

Tables

Table 6.7: Global CH4 budget for the past three decades. T.-D. stands for top-down inversions and B.-U. for Bottom-Up approaches. Full references are given at the end of the chapter. Ranges represent minimum and maximum values from the cited references. The sum of sources and sinks from B-U approaches does not automatically balance the atmospheric changes.

$TgCH_4\ yr^{-1}$	1980–1989 Top-Down	1980–1989 Bottom-Up	1980–1989 References	1990–1999 Top-Down	1990–1999 Bottom-Up	1990–1999 References	2000–2099 Top-Down	2000–2099 Bottom-Up	2000–2099 References
Natural Sources	**217 [201–231]**	**290 [237–346]**		**185 [168–202]**	**292 [239–349]**		**206 [202–209]**	**303 [244–368]**	
Natural Wetlands	**198**	**184**		**155**	**186**		**169**	**197**	
Natural Wetlands	198 [165–231]	184 [183–184]	T-D: Bou11, Hei97 B-U: Rin11, Hod11	155 [144–163]	186 [185–187]	T-D: Bou11, C&P06 B-U: Spa11, Rin11, Hod11	169 [159–184]	197 [174–280]	T-D: Bou11, Hou(P), Bru(P) B-U: Spa11, Rin11, Hod11
Others	**19**	**106**		**30**	**106**		**37**	**106**	
Freshwater (Lakes & Rivers)		38 [8–73]	B-U: Bas04, Bas11, Wal07		38 [8–73]	B-U: Bas04, Bas11, Wal07		38 [8–73]	B-U: Bas04, Bas11, Wal07
Wild Animals?									
Wildfires		2.5 [1–4]	B-U: EPA10, Lev00, vdW06, Hoe04, Ito04		2.5 [1–4]	B-U: EPA10, Lev00, vdW06, Hoe04, Ito04		2.5 [1–4]	B-U: EPA10, Lev00, vdW06, Hoe04, Ito04
Termites	19 [0–37]	11 [2–20]	T-D: Boul1, Hei97 B-U: EPA10, San96, Sug98, Sug00	30 [23–36]	11 [2–20]	T-D: Bou11, C&P06 B-U: EPA10, San96, Sug98, Sug00	37 [25–47]	11 [2–20]	T-D: Bou11, Hou(P) B-U: EPA10, San96, Sug98, Sug00
Geological (Incl. Oceans & Hydrates)		54 [43–65]	T-D: Bou11 B-U: E]08, Rhe09		54 [43–65]	T-D: Bou11, C&P06 B-U: E]08, Rhe09		54 [43–65]	T-D: Bou11, Hou(P) B-U: E]08, Rhe09
Anthropogenic Sources	**350 [337–361]**	**278 [–]**		**381 [334–428]**	**269 [226–313]**		**338 [334–344]**	**287 [235–338]**	
Agriculture & Waste	**202**	**173**		**241**	**168**		**209**	**181**	
Rice	202 [185–218]	43	T-D: Bou11, Hei97 B-U: Eur10	241 [178–301]	36 [27–44]	T-D: Bou11, C&P06 B-U: Eur10, Den04, Spa11, EPA11	209 [184–242]	36 [28–44]	T-D: Bou11, Hou(P), Bru(P) B-U: Eur10, Den04, Spa11, EPA11
Ruminants		85	T-D: Bou11, Hei97 B-U: Eur10		81 [71–91]	T-D: Bou11, C&P06 B-U: Eur10, Den04, EPA11		85 [73–94]	T-D: Bou11, Hou(P), Bru(P) B-U: Eur10, Den04, EPA11
Landfills & Waste		45	T-D: Bou11, Hei97 B-U: Eur10		51 [44–55]	T-D: Bou11, C&P06 B-U: Eur10, Den04, EPA11		60 [48–76]	T-D: Bou11, Hou(P), Bru(P) B-U: Eur10, Den04,

									EPA11
Biomass Burning	**45**	**17**		**45**	**25**		**29**	**18**	
Biomass Burning (Incl. Biofuels)	45 [43–45]	17	T-D: Bou11, Hei97 B-U:Sch07[a]	45 [43–46]	25 [21–28]	T-D: Bou11, C&P06 B-U: Sch07[a], vdW10	29 [14–47]	18 [16–20]	T-D: Bou11, Hou(P), Bru(P) B-U: vdW10, Wie11
Fossil Fuels	**103**	**88**		**95**	**76**		**100**	**88**	
Fossil Gas Industry & Use	103 [100–105]	57[b]	T-D: Bou11, Hei97 B-U: Eur10	95 [84–103]	52[b] [44–63]	T-D: Bou11, C&P06 B-U: Eur10, Den04, EPA11	100 [78–119]	59[b] [52–69]	T-D: Bou11, Hou(P), Bru(P) B-U: Eur10, Den04, EPA11
Fossil Oil Industry & Use									
Fossil Coal Industry & Use		31	T-D: Bou11, Hei97 B-U: Eur10		24 [19–23]	T-D: Bou11, C&P06 B-U: Eur10, Den04, EPA11		29 [18–35]	T-D: Bou11, Hou(P), Bru(P) B-U: Eur10, Den04, EPA11
Sinks	**535**	**481**		**547**	**514**		**541**	**555**	
OH Total	**510 [486–533]**	**456 [399–488]**	T-D: Bou11, Hei97 B-U: ACCMIP	**522 [489–554]**	**489 [473–509]**	T-D: Bou11, C&P06 B-U: ACCMIP	**516 [510–525]**	**529 [473–594]**	T-D: Bou11, Hou(P) B-U:ACCMIP
OH Troposphere	477	433 [382–461]	T-D: Bou11 B-U: ACCMIP	480	460 [453–472]	T-D: Bou11 B-U:ACCMIP	502	501 [454–559]	T-D: Bou11 B-U:ACCMIP
OH Stratosphere	11	23 [12–40]	T-D: Bou11 B-U: ACCMIP	11	29 [13–52]	T-D: Bou11 B-U:ACCMIP	14	28 [12–53]	T-D: Bou11 B-U:ACCMIP
Soils	25 [25–26]	25 [22–28]	T-D: Bou11, Hei97 B-U: Spa11, Cur07, Dut07	25	25 [22–28]	T-D: Bou11 B-U: Spa11, Cur07, Dut07	25	25 [22–28]	T-D: Bou11 B-U: Spa11, Cur07, Dut07
Chlorine									
Global									
Sum of Sources	**567 [538–592]**	**568 [515–624]**	T-D: Bou11, Hei97	**566 [536–596]**	**561 [465–662]**	T-D: Bou11, C&P06	**544 [518–550]**	**590 [479–706]**	T-D: Bou11, Hou(P), Bru(P)
Sum of Sinks	**535 [511–559]**	**481 [421–506]**		**547 [514–579]**	**514 [495–537]**		**541 [512–550]**	**555 [495–622]**	
Imbalance (Sources-Sinks)	**32 [27–33]**			**19 [17–22]**			**3 [0–6]**		
Atmospheric Growth Rate	**34**			**17**			**6**		

Notes:
To be determined: Uncertainties reporting (may use expert judgement if no formal uncertainty analysis available)
**** = 95% certain that the actual value is within 10% of the estimate reported
*** = 95% certain that the actual value is within 33% of the estimate reported
** = 95% certain that the actual value is within 66% of the estimate reported

* = 95% certain that the actual value is within 100% of the estimate reported
(a) Excluding biofuels
(b) Combined oil and gas

Table 6.8: Section 1 gives the Global N budget (TgN yr^{-1}): a) creation of reactive N, b) emissions of NO_x, NH_3 in 2000s to atmosphere, c) deposition of N to land and oceans and d) discharge of total N to coastal ocean. Section 2 gives the N_2O budget for the year 2005, and for the 1990s compared to AR4. Unit: Tg N_2O-N yr^{-1}.

SECTION 1

a. Conversion of N_2 to Nr	**2005**		**References**
Anthropogenic sources			
Fossil Fuel Combustion	24.5		Galloway et al., 2008
Haber-Bosch Process			
Fertilizer	100		Galloway et al., 2008
Industrial Feedstock	24		Galloway et al., 2008
BNF	70 (60–80)		Herridge et al. (2008)
Anthropogenic total	**219**		
Natural sources			
BNF, terrestrial	100 (90–120)		Galloway et al., 2004
BNF, marine	100 (60–200)		Duce et al., 2008
Lightning	4 (3–5)		AR4
Natural total	**204**		
Total Conversion of N_2 to reactive N	**423**		
b. Emissions to atmosphere			
	NO_x	**NH_3**	
Fossil Fuel Combustion & industrial processes	28.3	0.5	Dentener et al., 2006
Agriculture	3.7	30.4	Dentener et al., 2006
Biomass and biofuel burning	5.5	9.2	Dentener et al., 2006
Anthropogenic total	**37.5**	**40.1**	
Natural Sources			
Soils under natural vegetation	7.3 (5–8)	2.4 (1–10)	AR4
Oceans	-	8.2 (3.6)	AR4
Lightning	4 (3–5)	-	AR4
Natural total	**11.3**	**10.6**	AR4
Total Sources	**48.8**	**50.7**	
c. Deposition from the atmosphere			
	NO_y	**NH_x**	
Continents	27.1	36.1	Larmarque et al., 2010
Oceans	19.8	17.0	Larmarque et al., 2010
Total	46.9	53.1	
d. Discharge to coastal ocean			
Surface water N flux	45		Mayorga et al., 2010

SECTION 2

	AR5 (2006)	**AR5 (mid-1990s)**	**AR4 (1990s)**
Anthropogenic sources			
Fossil fuel combustion & industrial processes	0.7 (0.2–1.8)[a]	0.7 (0.2–1.8)[a]	0.7 (0.2–1.8)
Agriculture	4.1 (1.7–4.8) [b]	3.7 (1.7–4.8) [b]	2.8 (1.7–4.8)
Biomass and biofuel burning	0.7 (0.2–1.0)[a]	0.7 (0.2–1.0)[a]	0.7 (0.2–1.0)
Human excreta	0.3 (0.1–0.4)[a]	0.3 (0.1–0.4)[a]	0.2 (0.1–0.3)
Rivers, estuaries, coastal zones	0.6 (0.1–2.9)[c]	0.6 (0.1–2.9)[c]	1.7 (0.5–2.9)

Atmospheric deposition	0.4 (0.3–0.9)[d]	0.4 (0.3–0.9)[d]	0.6 (0.3–0.9)
Deep ocean	1.0 (0.5–1.5)[e]	0.9 (0.5–1.4)[e]	-
Surface sink	–0.01 (0–1)[f]	–0.01 (0-1)[f]	-
Anthropogenic total	**7.7**	**7.2**	**6.7**
Natural sources[a]			
Soils under natural vegetation	6.6 (3.3–9.0)	6.6 (3.3–9.0)	6.6 (3.3–9.0)
Oceans	3.8 (1.8–5.8)	3.8 (1.8–5.8)	3.8 (1.8–5.8)
Lightning	–	–	–
Atmospheric chemistry	0.6 (0.3–1.2)	0.6 (0.3–1.2)	0.6 (0.3–1.2)
Natural total	**11.0**	**11.0**	**11.0**
Total sources	**18.7 (8.9–28.2)**	**18.2 (8.5–28.1)**	**17.7 (8.5–27.7)**

Notes:
(a) As in AR4 (not based on 2006 IPCC Guidelines)
(b) Direct soil emissions and emissions from animal production; calculated following 2006 IPCC Guidelines (Syakila and Kroeze, 2011); Range from AR4.
(c) Following 2006 IPCC Guidelines (Kroeze et al., 2010; Syakila and Kroeze, 2011); Higher end of range from AR4; lower end of range from 1996 IPCC Guidelines (Mosier et al., 1998). Note that a recent studies indicates that IPCC may underestimate emissions from rivers (Beaulieu et al., 2011)
(d) Following 2006 IPCC Guidelines (Syakila and Kroeze, 2011)
(e) (Duce et al., 2008; Syakila and Kroeze, 2011); Range an estimated ±50%
(f) (Syakila et al., 2010)

Table 6.9: CMIP5 model descriptions in terms of carbon cycle attributes and processes.

ESM	Group	Atmos Resolution	Ocean Resolution	Land-Carbon						Ocean Carbon				Reference
				Model name	Dynamic vegetation cover?	#PFTs	Incl. LUC?	N-cycle	Fire	Model name	#plankton types	Micro-nutrients?	Ocean DMS concentration?	
CanESM2	CCCma	T63, L35	1.41° × 0.94°, L40	CTEM	N	9	Y	N	N	CMOC	1	N	N	(Arora et al., 2011)
CESM1	NCAR/DOE	FV 0.9 x 1.25	1 degree	CLM4	N	15	Y	Y	Y	BEC	4	Y	N	(Gent et al., 2011; Thornton et al., 2009)
HadGEM2-ES	MOHC	N96 (ca. 1.6°), L38	1 degree, L40	JULES	Y	5	Y	N	N	Diat-HadOCC	3	Y	Y	(Collins et al., 2011b; Jones et al., 2011)
IPSL-CM5A-LR	IPSL	3.75x1.9 , L39	Zonal 2°, Meridional 2°–0.5° L31	ORCHIDEE	N	13	Y	N	Y	PISCES	2	Y	N	(Dufresne et al., 2011)
MIROC-ESM	JAMSTEC	T42, L80	Zonal: 1.4 degree, Meridional: 0.5–1.7 degree, Vertical: L43+BBL1	SEIB-DGVM	Y	13	Y	N	N	NPZD (Oschlies 2001)	2 (Phyoto-plankton and Zoolo-plankton)	N	N	(Watanabe et al., 2011)
MPI-ESM	MPI	T63 (ca. 1.9°), L47	ca.1.5°, L47	JSBACH	Y	12 (8 natural)	Y	N	Y	HAMOCC	2	Y	N	(Raddatz et al., 2007; Brovkin et al., 2009; Maier-Reimer et al., 2005)

Chapter 6: Carbon and Biogeochemical Cycles

Coordinating Lead Authors: Philippe Ciais (France), Christopher Sabine (USA)

Lead Authors: Govindswamy Bala (India), Laurent Bopp (France), Victor Brovkin (Germany), Josep Canadell (Australia), Abha Chhabra (India), Ruth DeFries (USA), Jim Galloway (USA), Martin Heimann (Germany), Christopher Jones (UK), Corinne Le Quéré (UK), Ranga Myneni (USA), Shilong Piao (China), Peter Thornton (USA)

Contributing Authors: George Hurtt (US), Guido van der Werf (Netherlands), Nicolas Gruber (Switzerland), Taro Takahashi (USA), Samar Khatiwala (USA), Jan Willem Erisman (NL), Gregg Marland (USA), Ralph Keeling (USA), Stephen Piper (USA), Andy Ridgwell (UK), Jerome Chappellaz (France), Andreas Schmittner (USA), Jed Kaplan (Switzerland), Fortunat Joos (Switzerland), Johann Jungclaus (Germany), David Archer (USA), Peter Cox (UK), Pierre Friedlingstein (UK), Yiqi Luo (USA), Paul Hanson (USA), Richard Norby (USA), Edward Schuur (USA), Eugenie Euskirchen (USA), Cory Cleveland (USA), David McGuire (USA), Elena Shevliakova (USA), Soenke Zaehle (Germany), Detlef van Vuuren (Netherlands), Stephen Sitch (UK), Nicolas Metzl (France), Andrew Lenton (Australia), James Orr (France), Oliver Andrews (UK), Alberto Borges (Belgium), Gordon Bonan (USA), Damon Mathews (Canada), Kenneth Caldeira (USA), Carolien Kroeze (Netherlands), Julia Pongratz (USA), Ayako Abe-Ouchi (Japan), Rita Wania (Canada), Charlie Koven (USA), Ben Booth (UK), Long Cao (USA), Stephen Hunter (UK), Silvia Kloster (Germany), Spencer Liddicoat (UK), Atul Jain (USA), Vivek Arora (Canada), Benjamin Stocker (Switzerland), Kees Klein Goldewijk (Netherlands), Jo House (UK), Jerry Tjiputra (Norway), Scott Doney (USA), Richard A. Houghton (USA), Geun-Ha Park (USA), Peter A. Raymond (USA), Frank J. Dentener (Italy), Jean-Francois Larmarque (USA), C. Roedenbeck (Germany), P. Peylin (France), F. Chevallier (France), R. Law (USA), P. Rayner (Australia), S. Gourdji (USA), A. Jacobson (USA), W. Peters (USA), P. Patra (Japan), K. Gurney (USA), Y. Niwa (Japan), Elizabeth Holland (USA), Stephen Sitch (UK), Anders Ahlström (Sweden), Ben Poulter (France) and Mark R. Lomas (UK), Keith Lassey (New Zealand), Ning Zeng (USA), Sander Houweling, (TN), Philippe Bousquet, (France), Stefanie Kirschke (France), Marielle Saunois (France), Lori Bruhwiler (USA), Vaishali Naik (USA), Apostolos Voulgarakis (USA), Renato Spahni (Switzerland), Bruno Ringeval (France), Joe Melton (Switzerland)

Review Editors: Christoph Heinze (Norway), Pieter Tans (USA), Steven Wofsy (USA)

Date of Draft: 16 December 2011

Notes: TSU Compiled Version

Figures

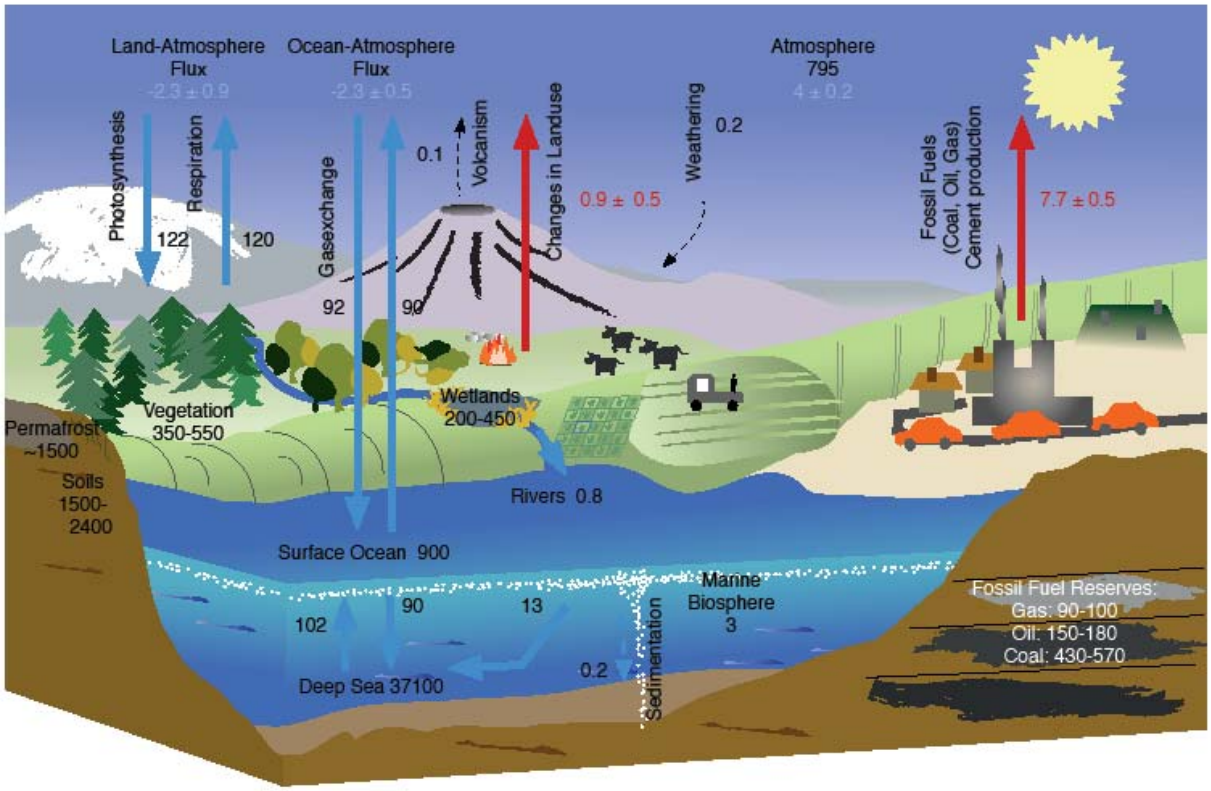

Figure 6.1: Simplified schematic of the global carbon cycle. Numbers represent reservoir sizes (in PgC), resp. carbon exchange fluxes (in PgC yr^{-1}), representing average conditions over the 2000–2009 time period.

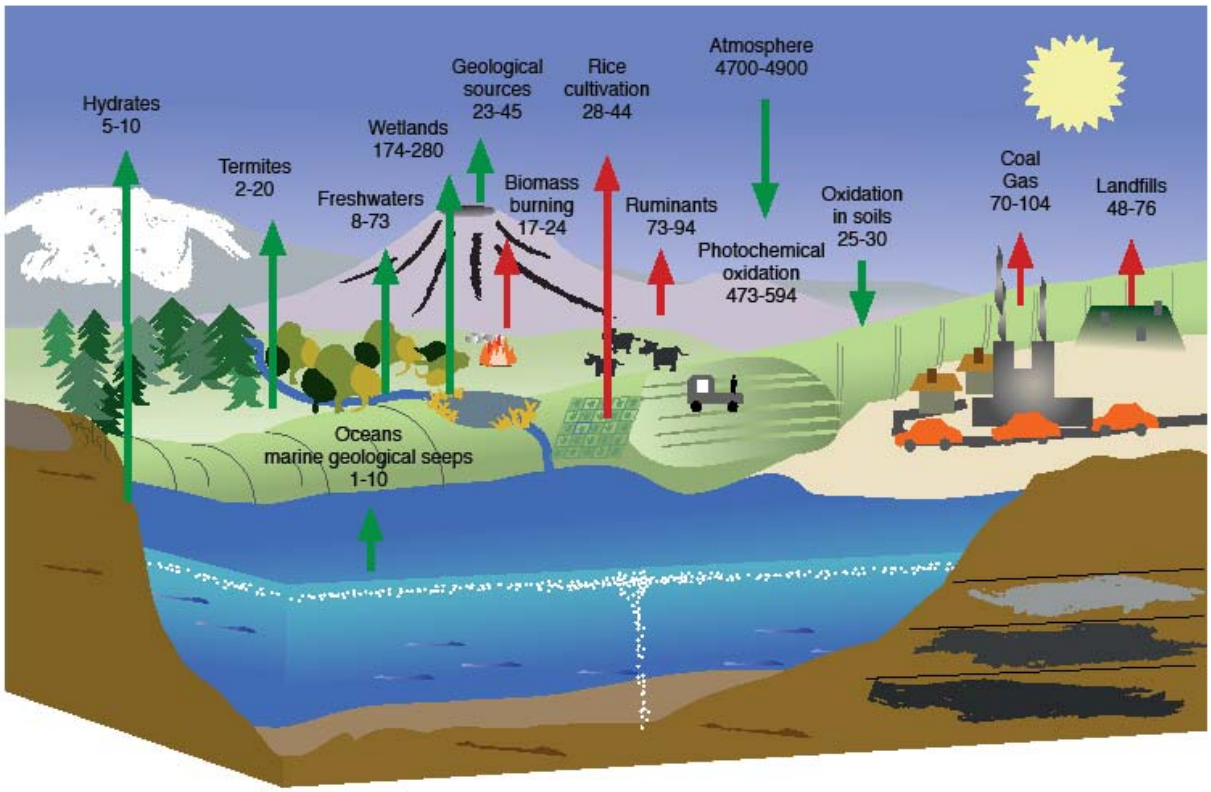

Figure 6.2: Schematic of the global cycle of CH_4. Numbers represent fluxes in $TgCH_4\ yr^{-1}$ estimated for the time period 2000–2009 (see Section 6.3.). Green arrows denote natural fluxes, red arrows anthropogenic fluxes.

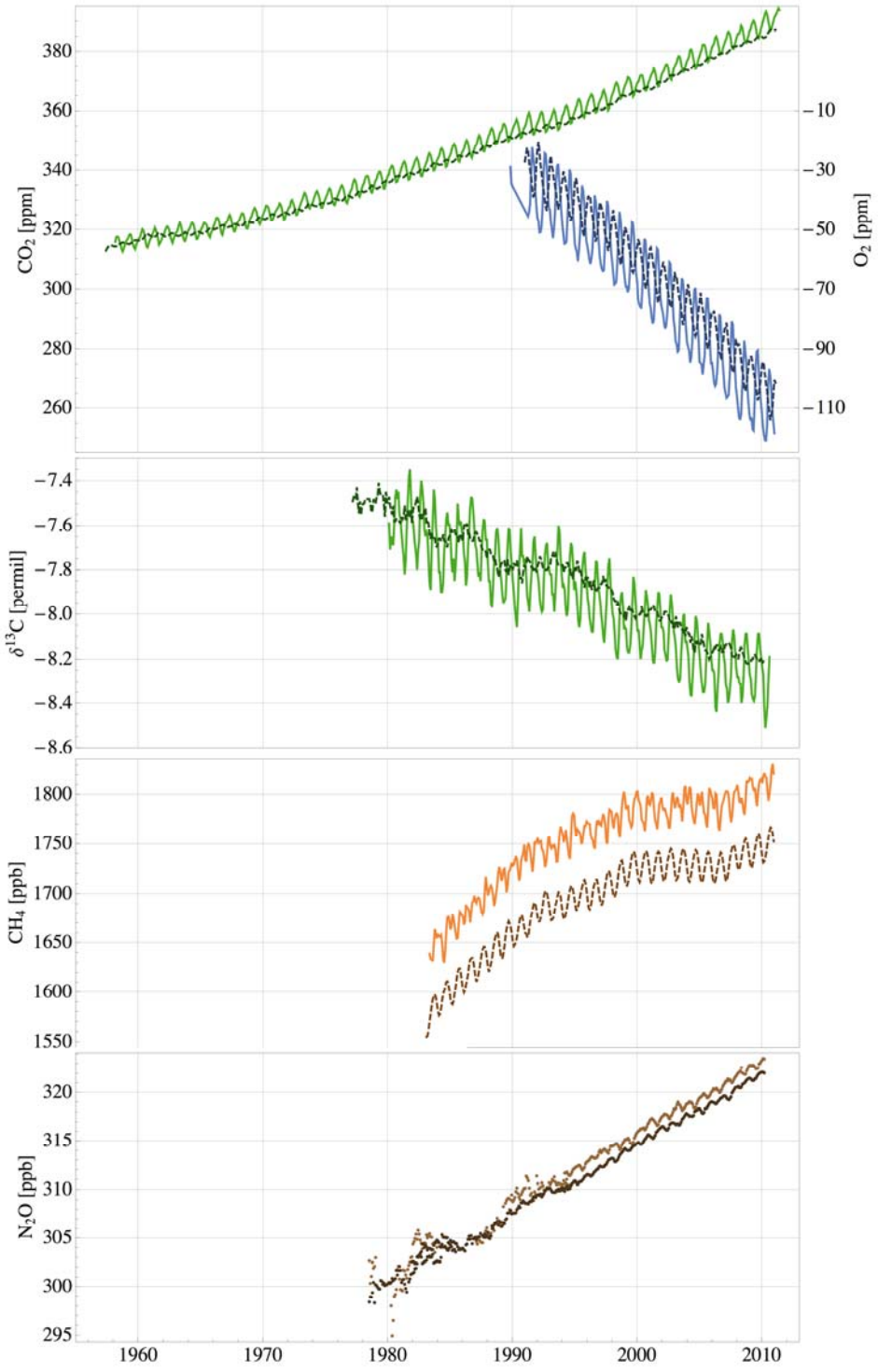

Figure 6.3: Atmospheric concentration of CO_2, oxygen, $^{13}C/^{12}C$ stable isotope ratio in CO_2, CH_4 and N_2O recorded over the last decades at representative stations in the northern (solid lines) and the southern (dashed lines) hemisphere. (a: CO_2 from Mauna Loa and South Pole (Keeling et al., 2005), O_2 from Alert and Cape Grim (http://scrippso2.ucsd.edu/ right axes), b: $^{13}C/^{12}C$: Mauna Loa, South Pole (Keeling et al., 2005), c: CH_4 from Mauna Loa and South Pole (Dlugokencky et al., 2010), d: N_2O from Adrigole and Cape Grim (Prinn et al., 2000).

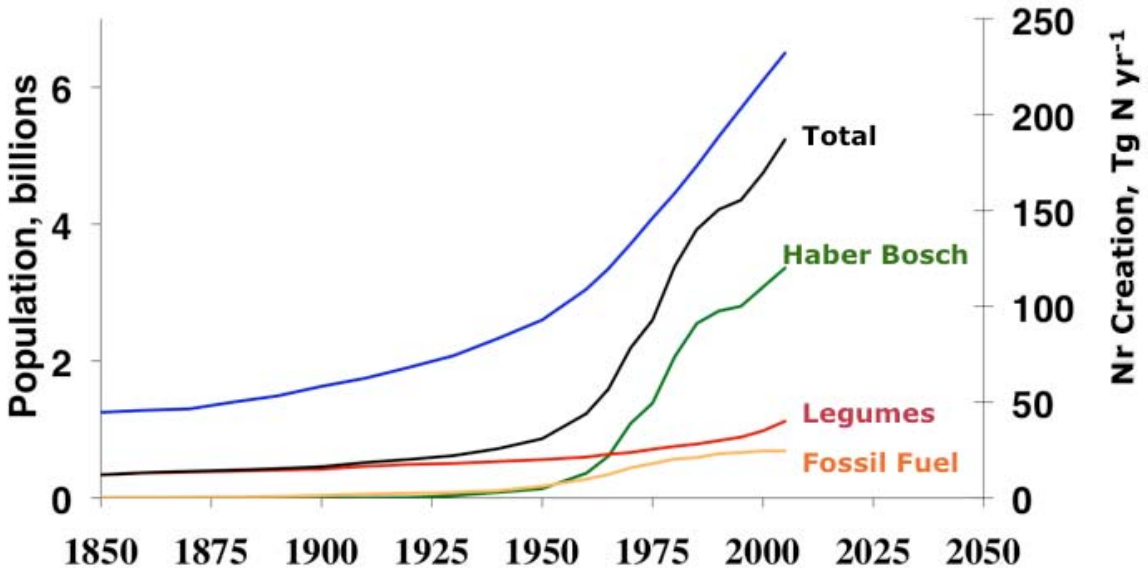

Box 6.1, Figure 1: World population (blue line) and reactive creation by the fossil fuel burning (orange line), from legumes (red line) and by the Haber-Bosch process (green line), over the last 160 years.

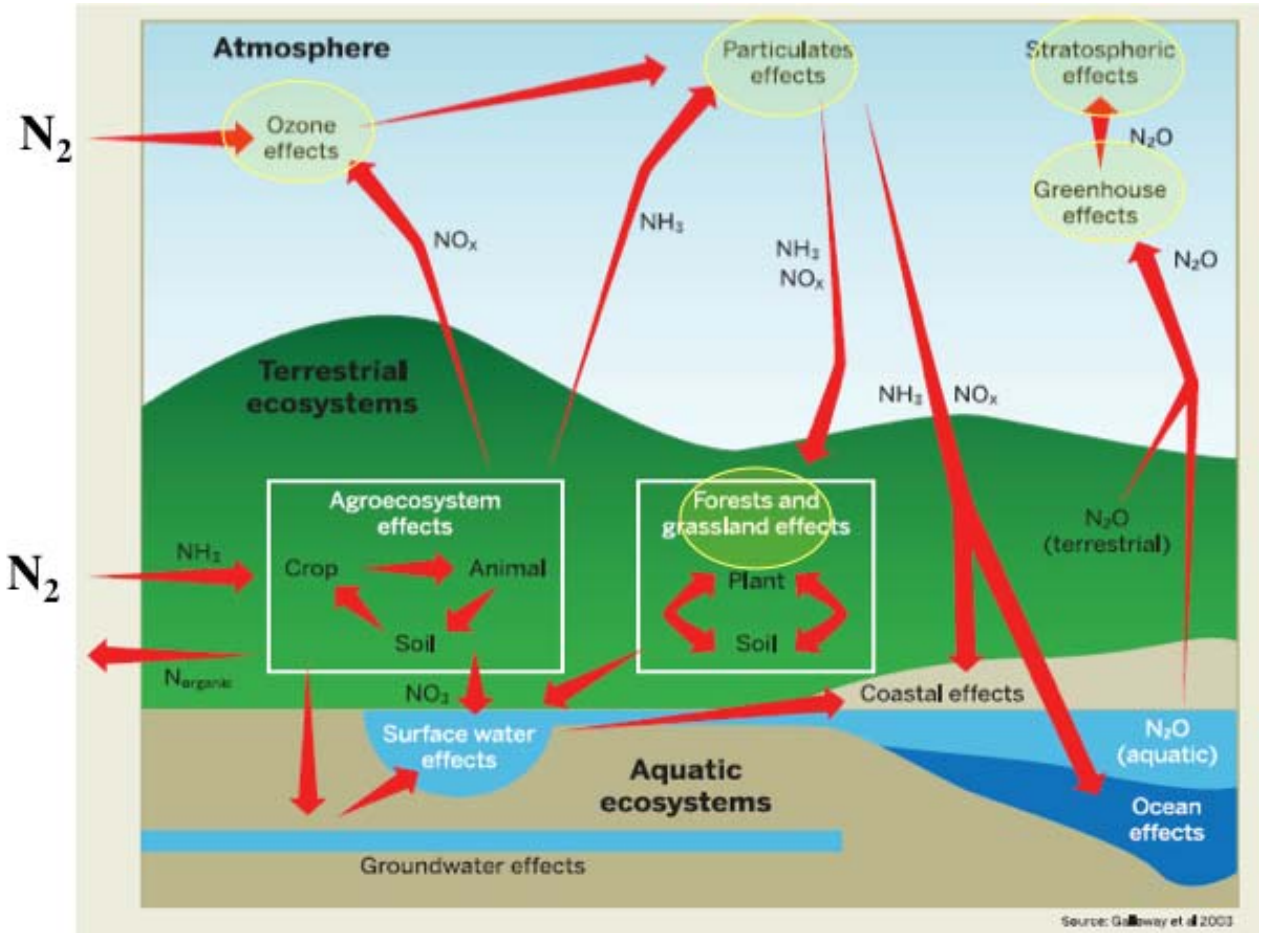

Box 6.1, Figure 2: Nitrogen cycle interactions with terrestrial and aquatic ecosystems.

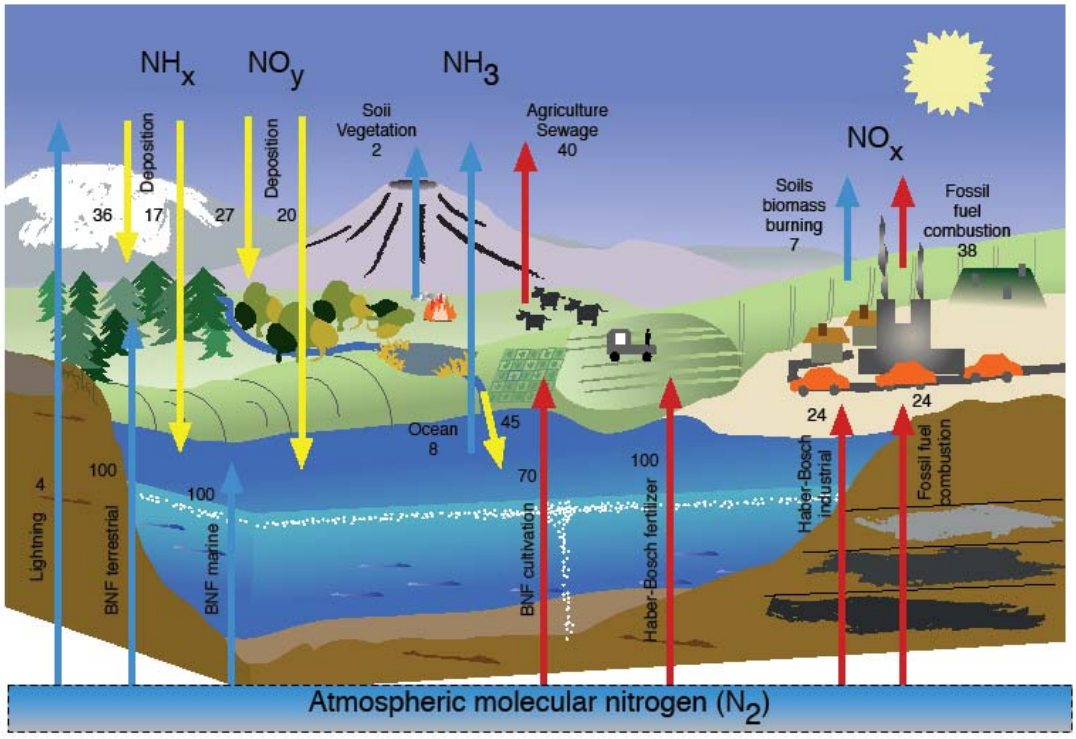

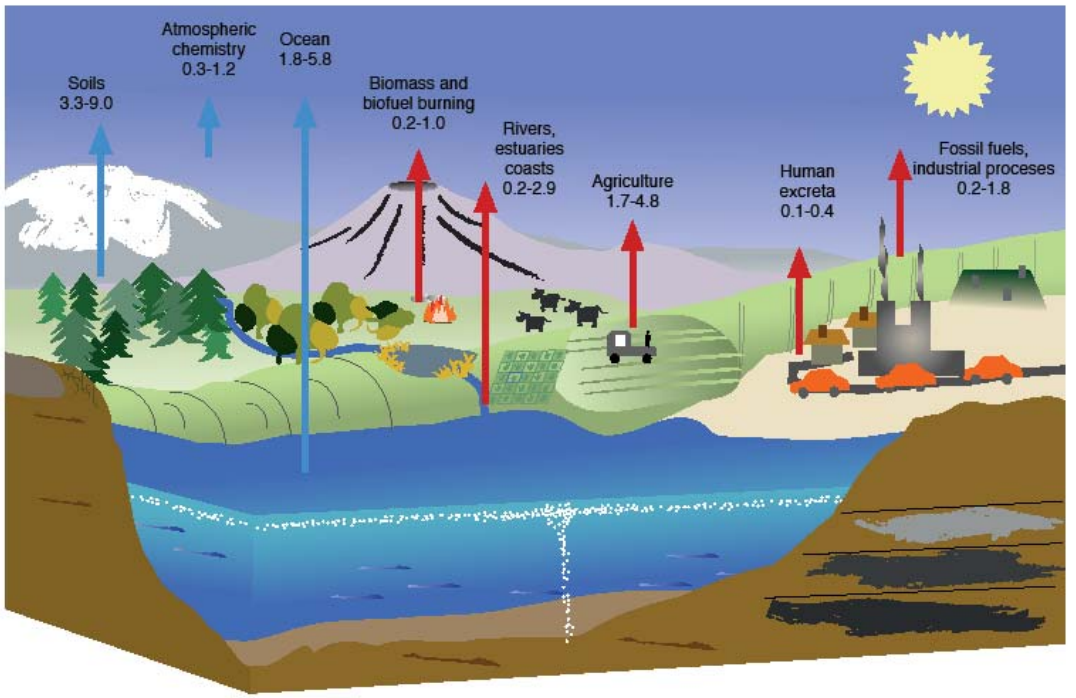

Figure 6.4: Global nitrogen cycle. In the top panel, the upper part shows the flows of reactive Nitrogen species, the lower part the processes by which atmospheric molecular nitrogen is converted to reactive nitrogen species. The bottom panel shows a schematic of the global cycle of N_2O. Blue arrows are natural, red arrows anthropogenic fluxes, and yellow arrows represent fluxes with an anthropogenic and natural component. BNF: biological nitrogen fixation. Units: TgN yr^{-1}.

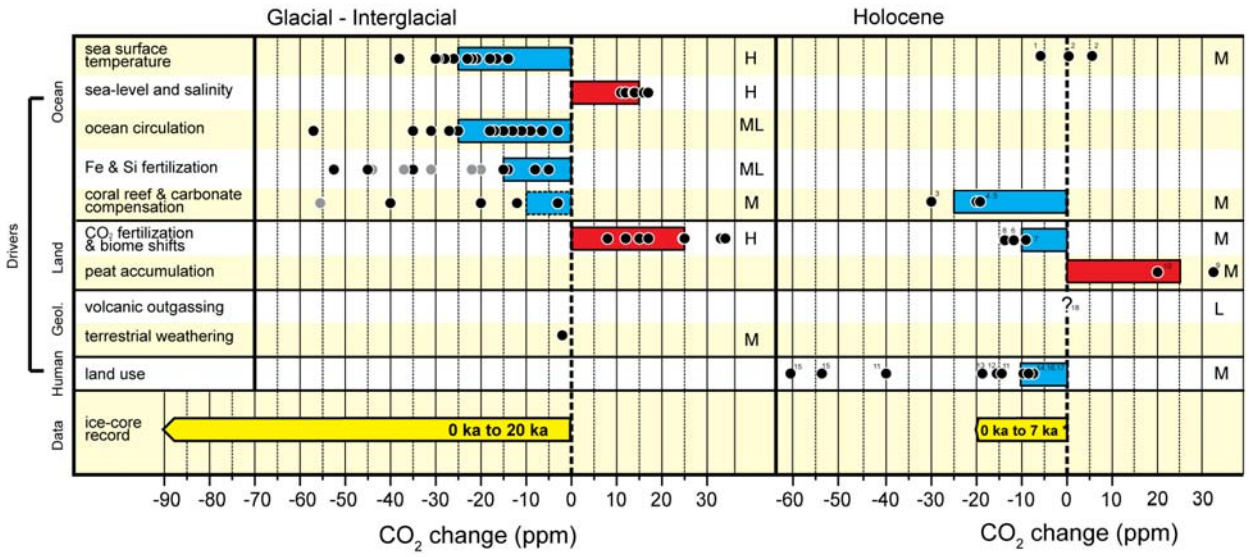

Figure 6.5: Carbon dioxide concentrations changes from late Holocene to the LGM (left) and from late Holocene to early/mid Holocene (7 ka) (right). Filled black circles represent individual model-based estimates for individual ocean, land, geological or human drivers. Solid color bars represent expert judgment (to the nearest 5 ppm) rather than a formal statistical average. References for the different model assessment used for the glacial drivers are as per (Kohfeld and Ridgwell, 2009) with excluded model projections in grey. References for the different model assessment used for the holocene drivers are 1. (Joos et al., 2004), 2. (Brovkin et al., 2008), 3. (Kleinen et al., 2010), 4. (Broecker et al., 1999), 5. (Ridgwell et al., 2003), 6. (Brovkin et al., 2002), 7. Shurgers et al. (2006), 8. (Kleinen et al., 2010), 9. (Yu, 2011), 10. (Kleinen et al., 2011), 11. (Ruddiman, 2003, 2007), 12. (Strassmann et al., 2008), 13. (Olofsson and Hickler, 2008), 14. (Pongratz et al., 2009), 15. (Kaplan et al., 2011), 16. (Lemmen, 2009), 17. (Stocker et al., 2011) and 18. (Roth and Joos, submitted).

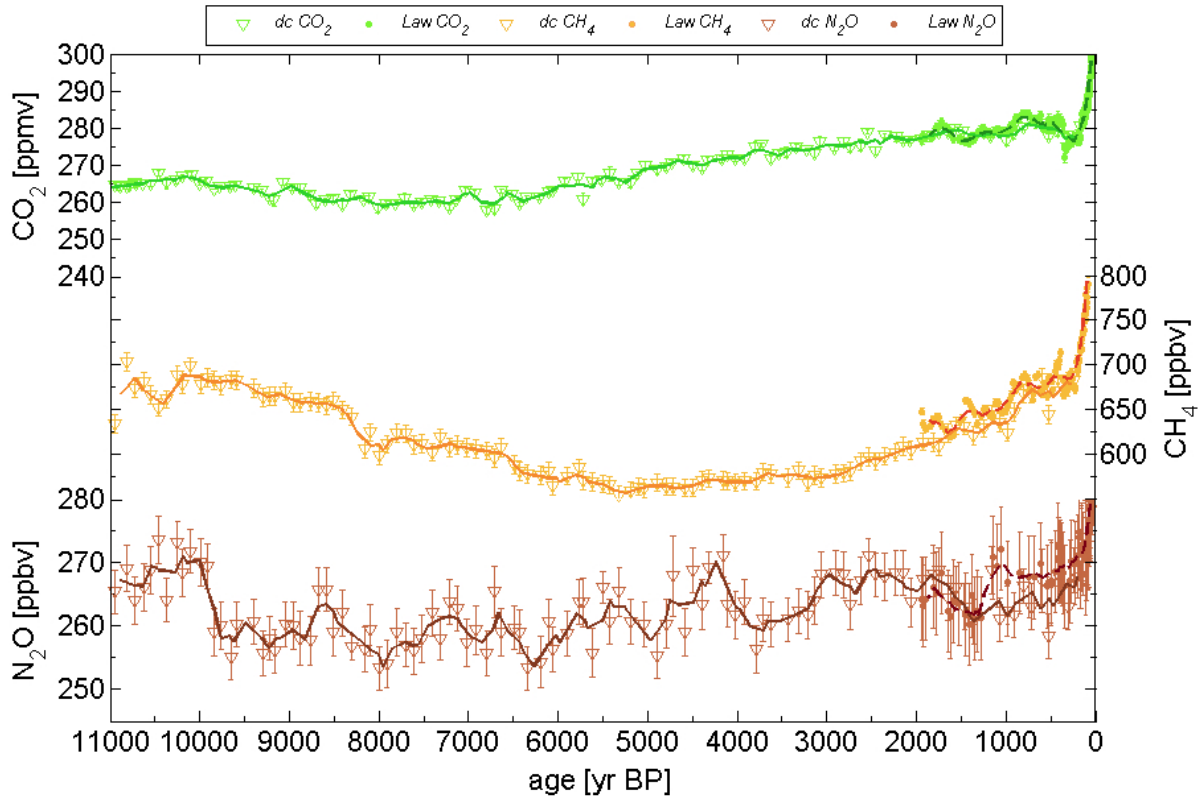

Figure 6.6: Variations of CO_2, CH_4, and N_2O concentrations during the Holocene. The data are for Antarctic ice cores (EPICA Dome C (Fluckiger et al., 2002; Monnin et al., 2004) (triangles); Law Dome, (MacFarling-Meure et al., 2006) circles), and for Greenland ice core (GRIP (Blunier et al., 1995), squares). Lines are for 200-year moving average.

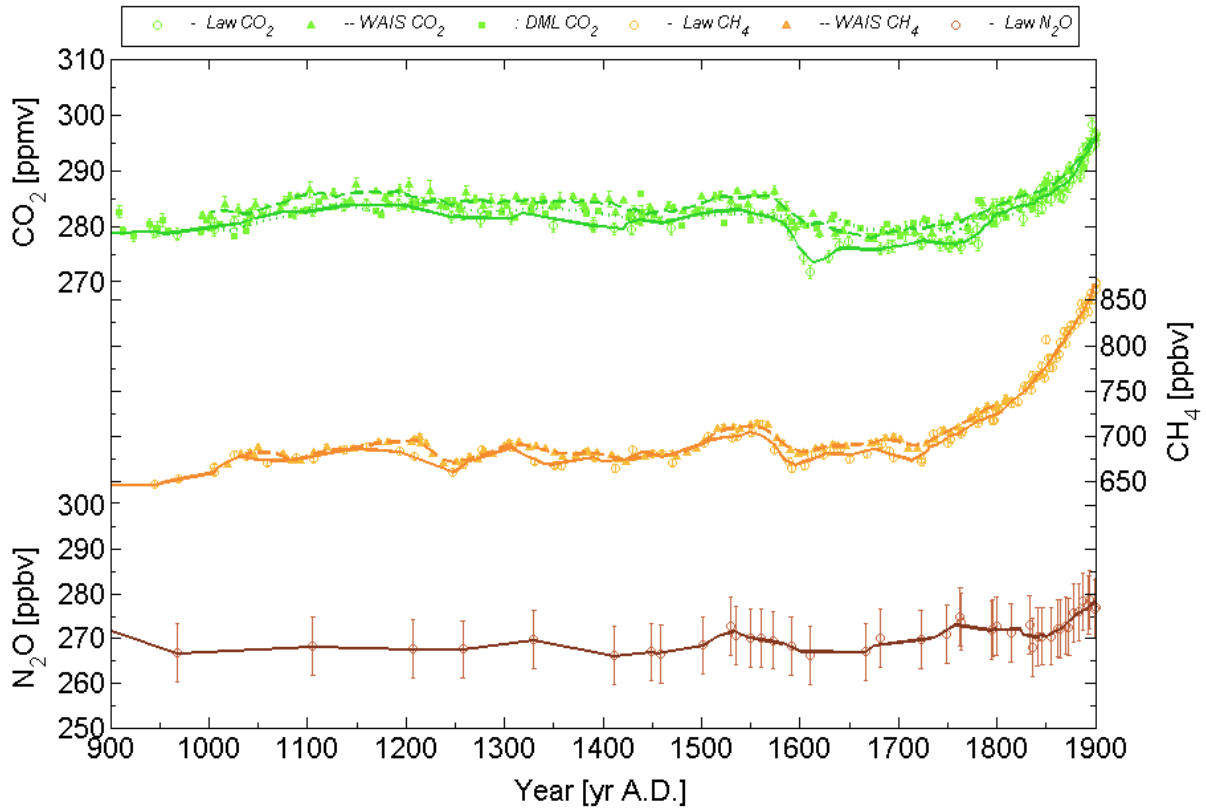

Figure 6.7: Variations of CO_2, CH_4, and N_2O during 900–1900 AD. The data are for Antarctic ice cores: (Etheridge et al., 1996; MacFarling-Meure et al., 2006), circles; West Antractic Ice Sheet (Ahn et al., submitted; Mitchell et al., 2011), triangles; Dronning Maud Land (Siegenthaler et al., 2005a), squares. Lines are for 30-year moving average.

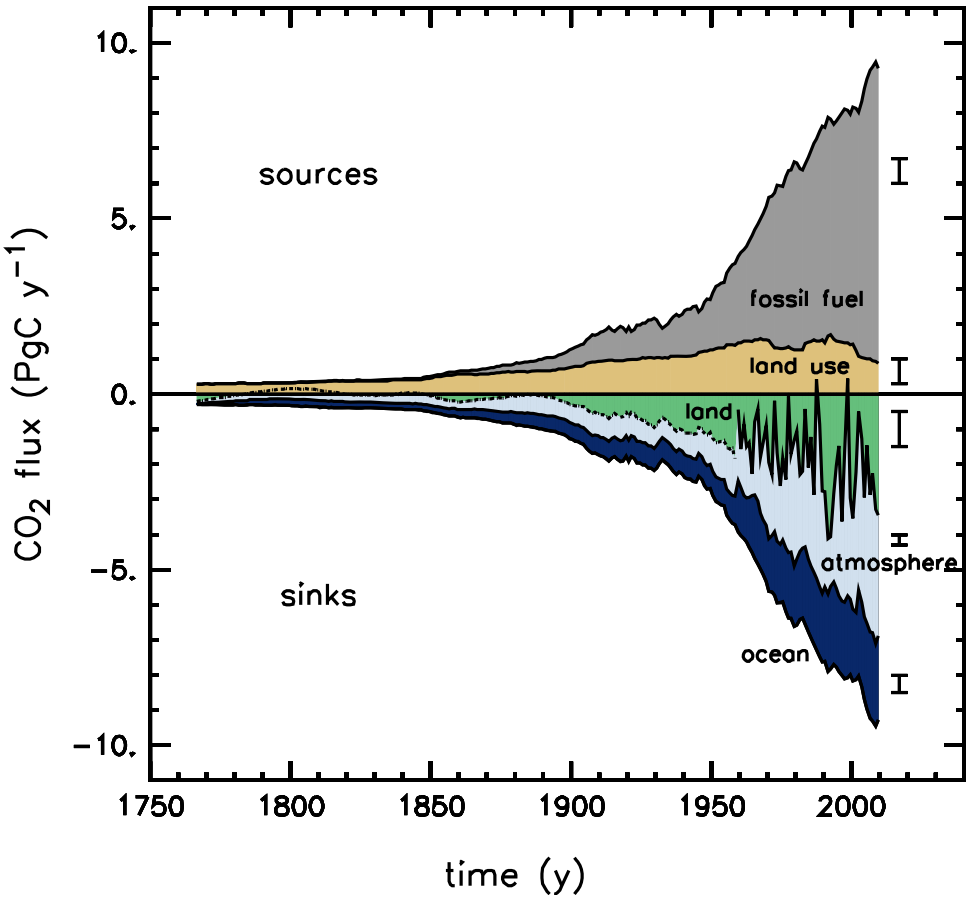

Figure 6.8: Sources and sinks fluxes (PgC yr^{-1}) for all main flux component of the global CO_2 budget from 1750 to 2010. CO_2 emissions are estimated by the Carbon Dioxide Information Analysis Center (CDIAC) based on UN energy statistics for fossil fuel combustion and US Geological Survey for cement production (Boden et al., 2011). CO_2 emissions from deforestation and other land use change prior to 1960 are from the average of three estimates (Pongratz et al., 2009; Shevliakova et al., 2009; van Minnen et al., 2009) for 1750–1959 and from (Friedlingstein et al., 2010) from 1960. The atmospheric CO_2 growth rate prior to 1960 is based on a spline fit to ice core observations (Etheridge et al., 1996; Friedli et al., 1986; Neftel et al., 1982) and a synthesis of atmospheric observations from 1960 (Conway and Tans, 2011)The fit to ice core does not capture the large interannual variability in atmospheric CO_2 and is represented with a dash line on the figure. The ocean CO_2 sink prior to 1960 is from (Khatiwala et al., 2009) and a combination of model and observations from 1960 updated (LeQuere et al., 2009).

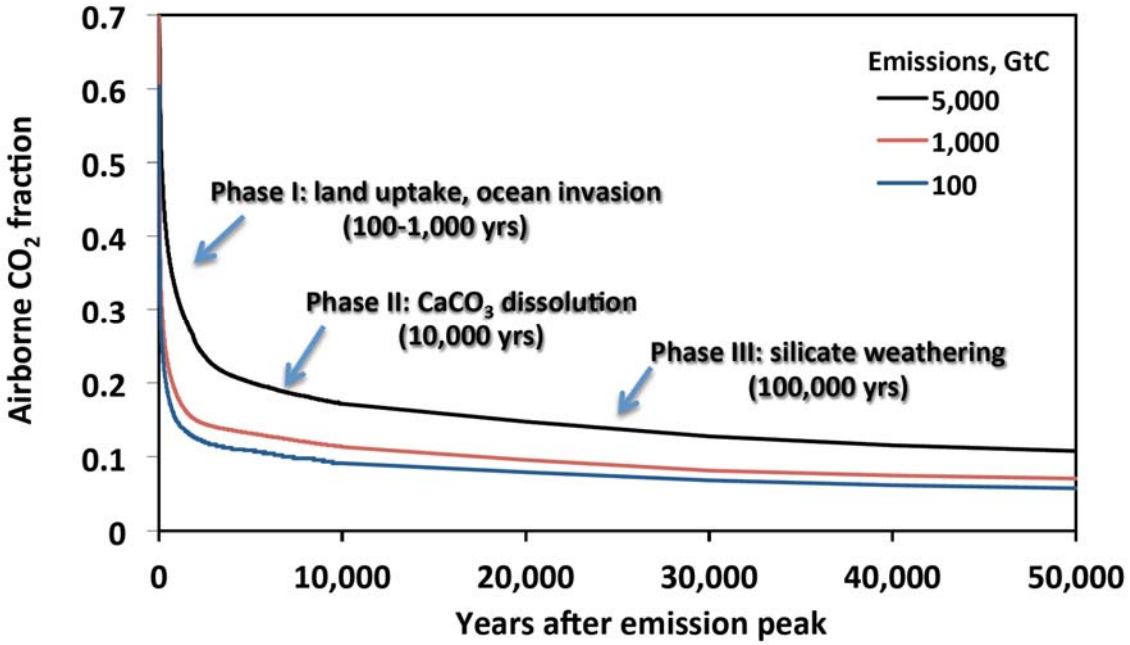

Box 6.2, Figure 1: A fraction of emitted CO_2 remaining in the atmosphere in case of total CO_2 emissions of 100 (blue), 1,000 (red), and 5,000 GtC (black line) released at once in year 0. The graph shows results of the CLIMBER model [*Archer et al.*, 2009] extended up to 50 thousand years. Arrows indicate a sequence of natural processes of CO_2 removal operating on different time scales. Note that higher CO_2 emissions lead to higher airborne CO_2 fraction due to reduced carbonate buffer capacity of the ocean and positive climate-carbon cycle feedback.

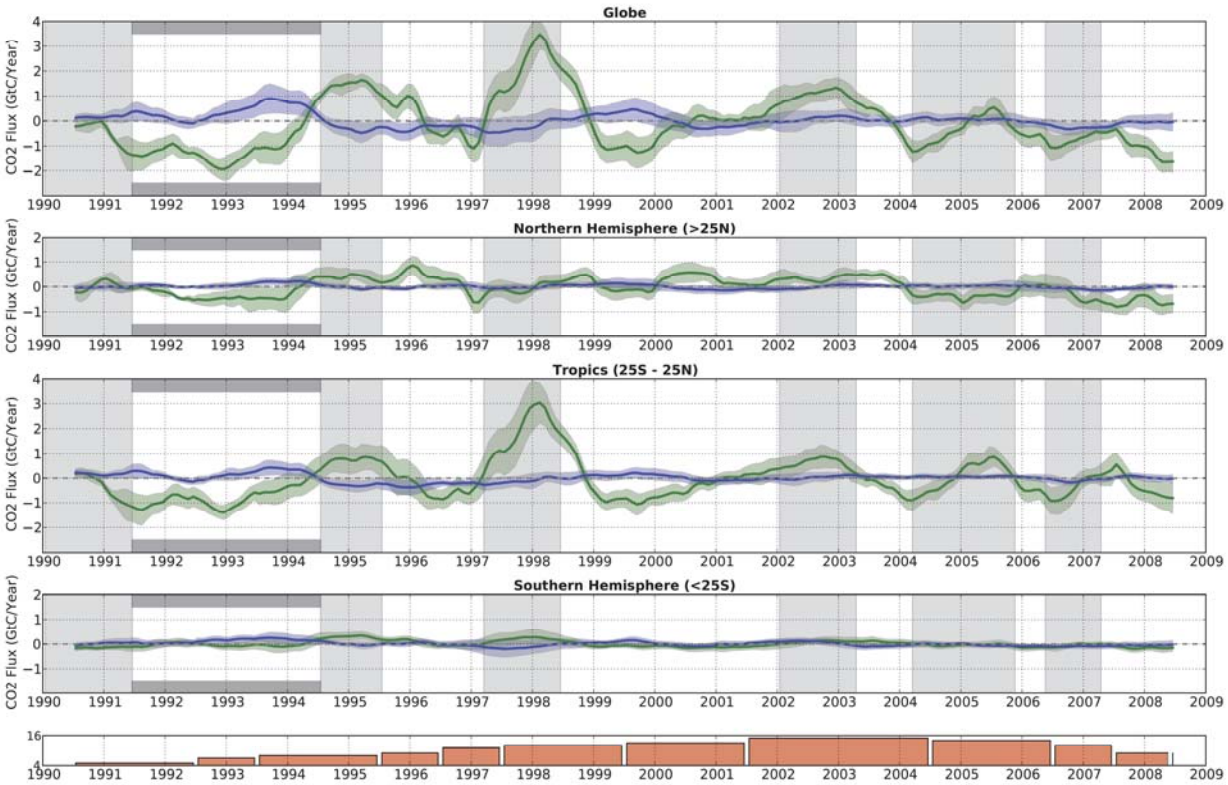

Figure 6.9: The interannual variability of surface CO_2 fluxes from inversions of the TRANSCOM project for the period of 1990–2008. The ensemble of inversion results contains up to 17-atmospheric inversion models. The ensemble mean is bounded by the 1 sigma inter-model spread in ocean-atmosphere (blue) and land-atmosphere (green) CO_2 fluxes (PgC yr^{-1}) grouped into large latitude bands, and over the globe. For each flux and each region, the CO_2 flux anomalies were obtained by subtracting the long term mean flux from each inversion and removing the seasonal signal. Grey shaded regions indicate El Niño episodes, and the back bars indicate the cooling period following the Mt. Pinatubo eruption. A positive flux means a larger than normal source of CO_2 to the atmosphere (or a smaller CO_2 sink).

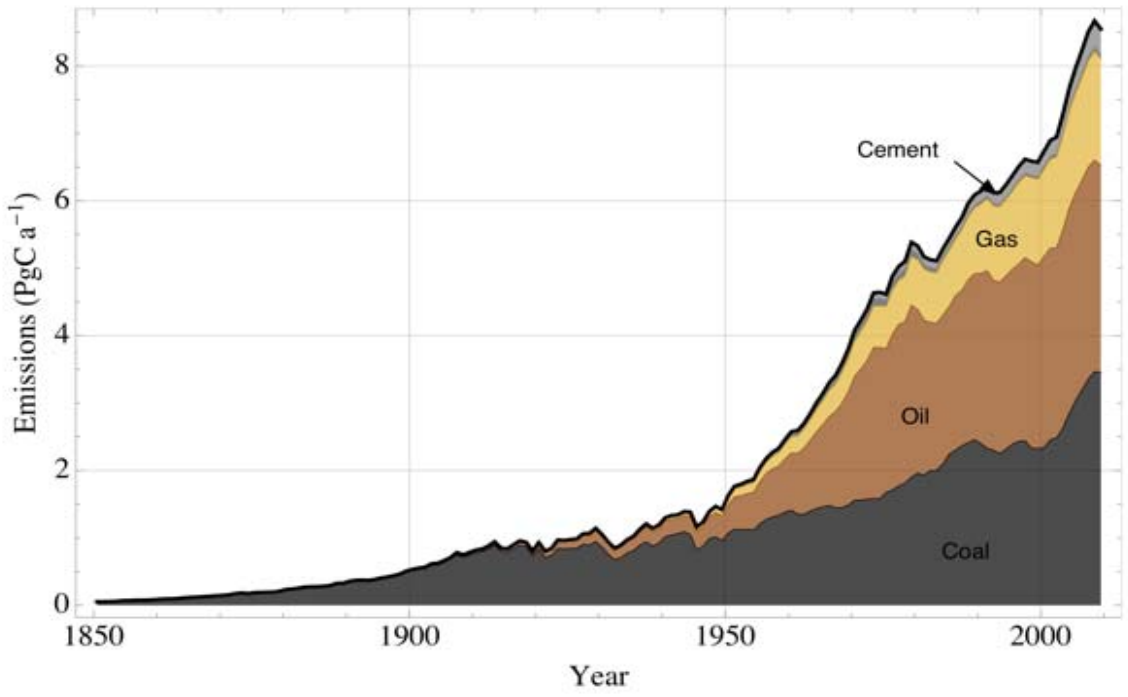

Figure 6.10: CO_2 emissions from fossil fuel combustion and cement production by fuel type (PgC yr^{-1}). CO_2 emissions are estimated by the Carbon Dioxide Information Analysis Center (CDIAC) based on UN energy statistics for fossil fuel combustion and US Geological Survey for cement production (Boden et al., 2011).

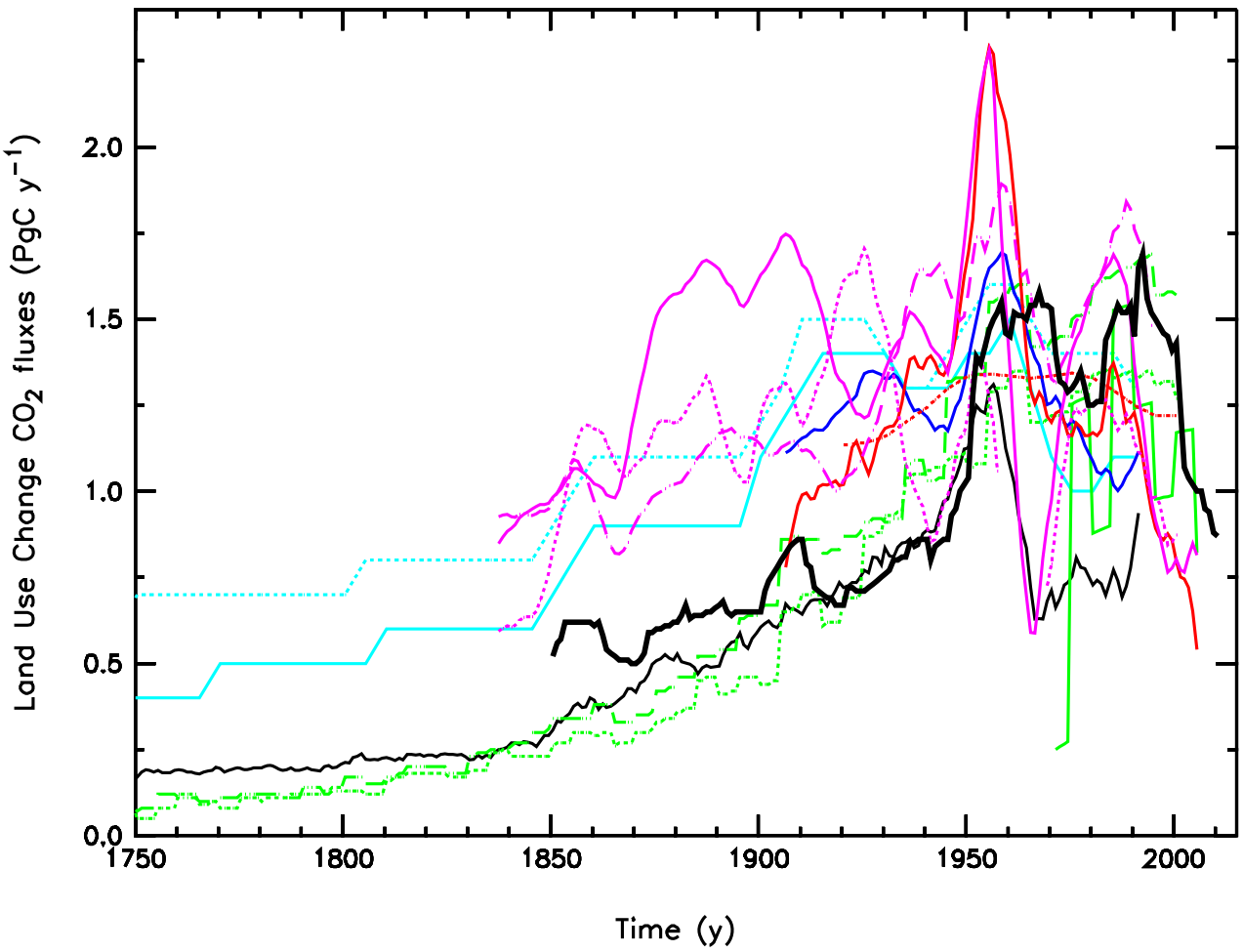

Figure 6.11: CO2 emissions from land use change from a range of methods (PgC yr–1). Estimates are from (Friedlingstein et al., 2010), thick black, (Pongratz et al., 2009), thin black, (Shevliakova et al., 2009), HYDE data: cyan full, SAGE data: cyan dotted, (vanMinnen et al., 2009), updated HYDE: green full, HYDE data: green dotted, HYDE with pastures: green dashed, (Piao et al., 2008), blue, (Strassmann et al., 2008), red dotted, (Stocker et al., 2011), red, (Yang et al., 2010) updated HYDE: purple full; FAO data: purple dash; SAGE data: purple dotted).

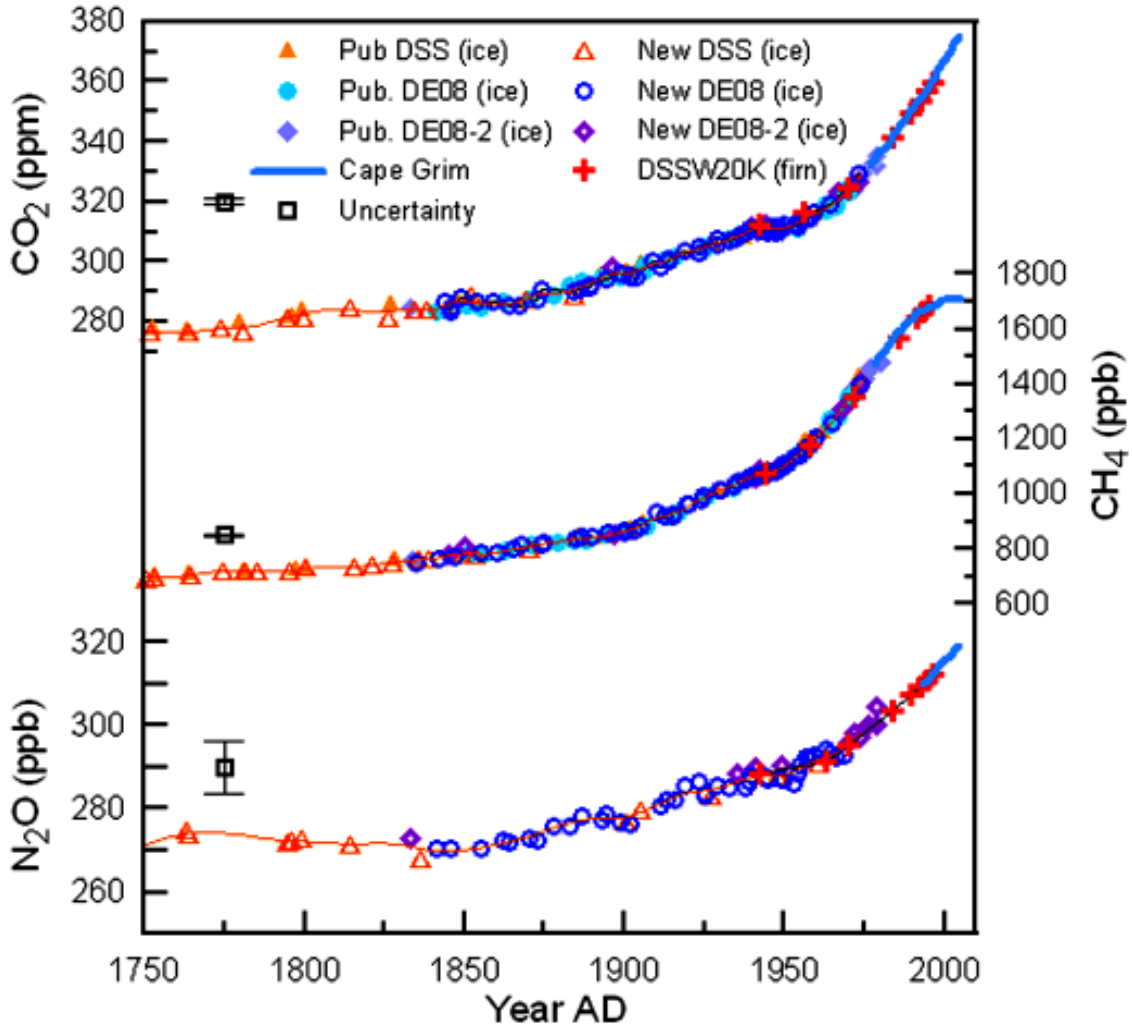

Figure 6.12: Atmospheric concentration history over the last 260 years determined from air enclosed in ice cores, firn air and direct atmospheric measurements (MacFarling-Meure et al., 2006).

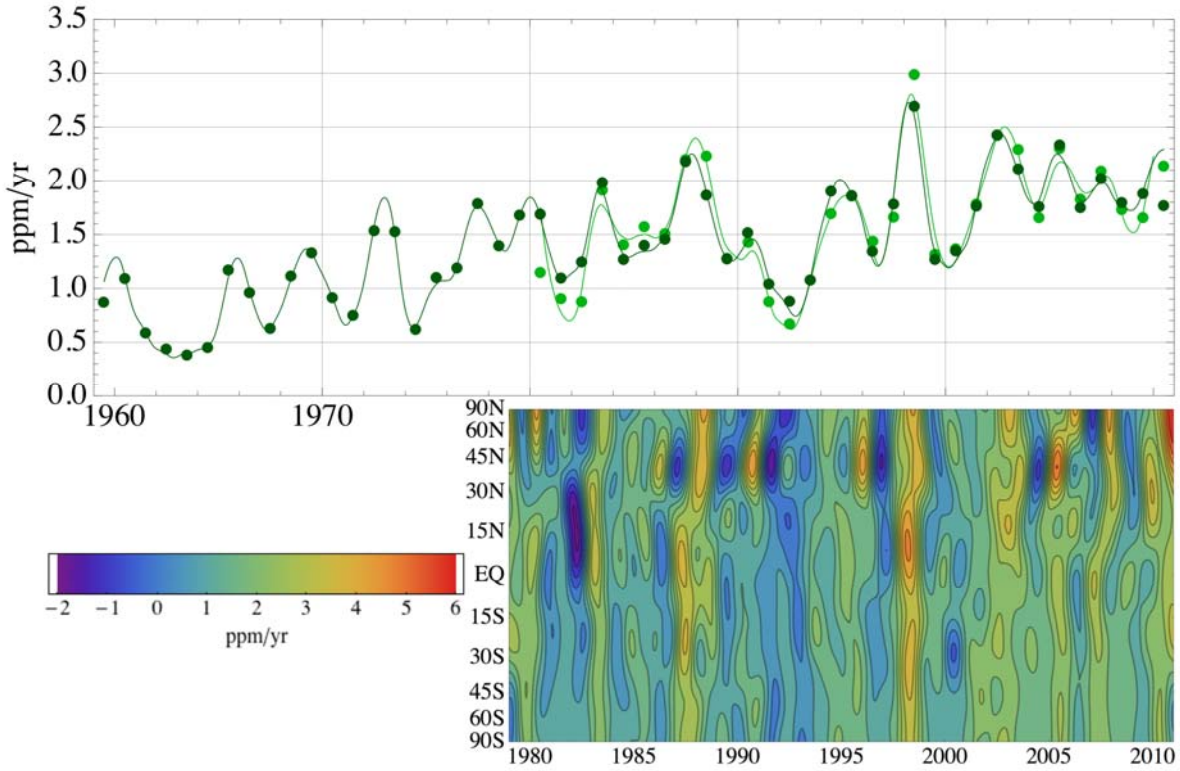

Figure 6.13: Top panel: Global average atmospheric CO_2 growth rate; symbols: annual means (Keeling et al., 2005); (Conway et al., 1994). Bottom panel: Atmospheric growth rate of CO_2 as a function of latitude determined from the GLOBALVIEW data product, representative for the marine boundary layer (Masarie and Tans, 1995).

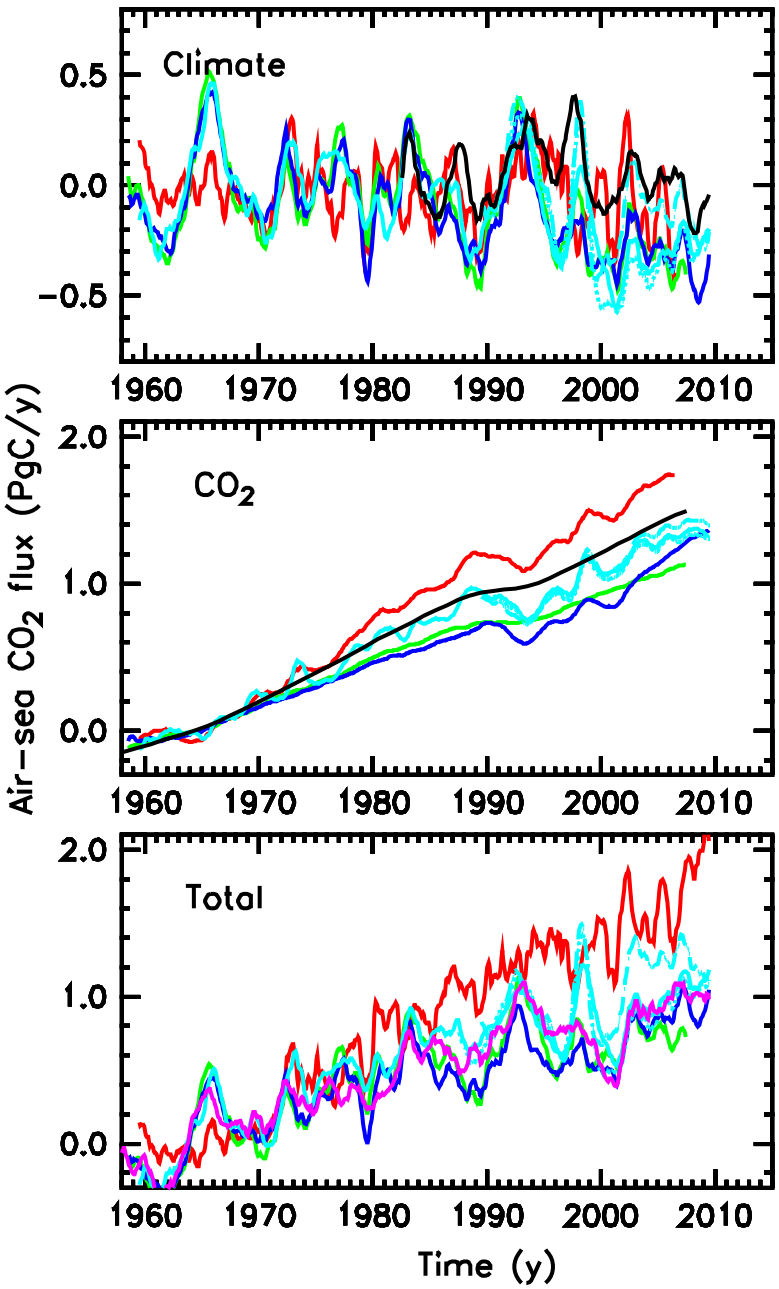

Figure 6.14: Trends in the air-sea flux of CO_2 in response to (top) variability and trends in surface climate, (middle) increasing atmospheric CO_2, and (bottom) the sum of both effects from a range of methods (PgC yr^{-1}). All estimates are normalized to zero during 1950-1960 to highlight the trends. Estimates are updates from: (Doney, 2010), dark blue for standard version, green for ETH version; (Aumont and Bopp, 2006), magenta; (LeQuere et al., 2010), cyan; (Assmann et al., 2010), red; (Park et al., 2010), top black; (Khatiwala et al., 2009), middle black.

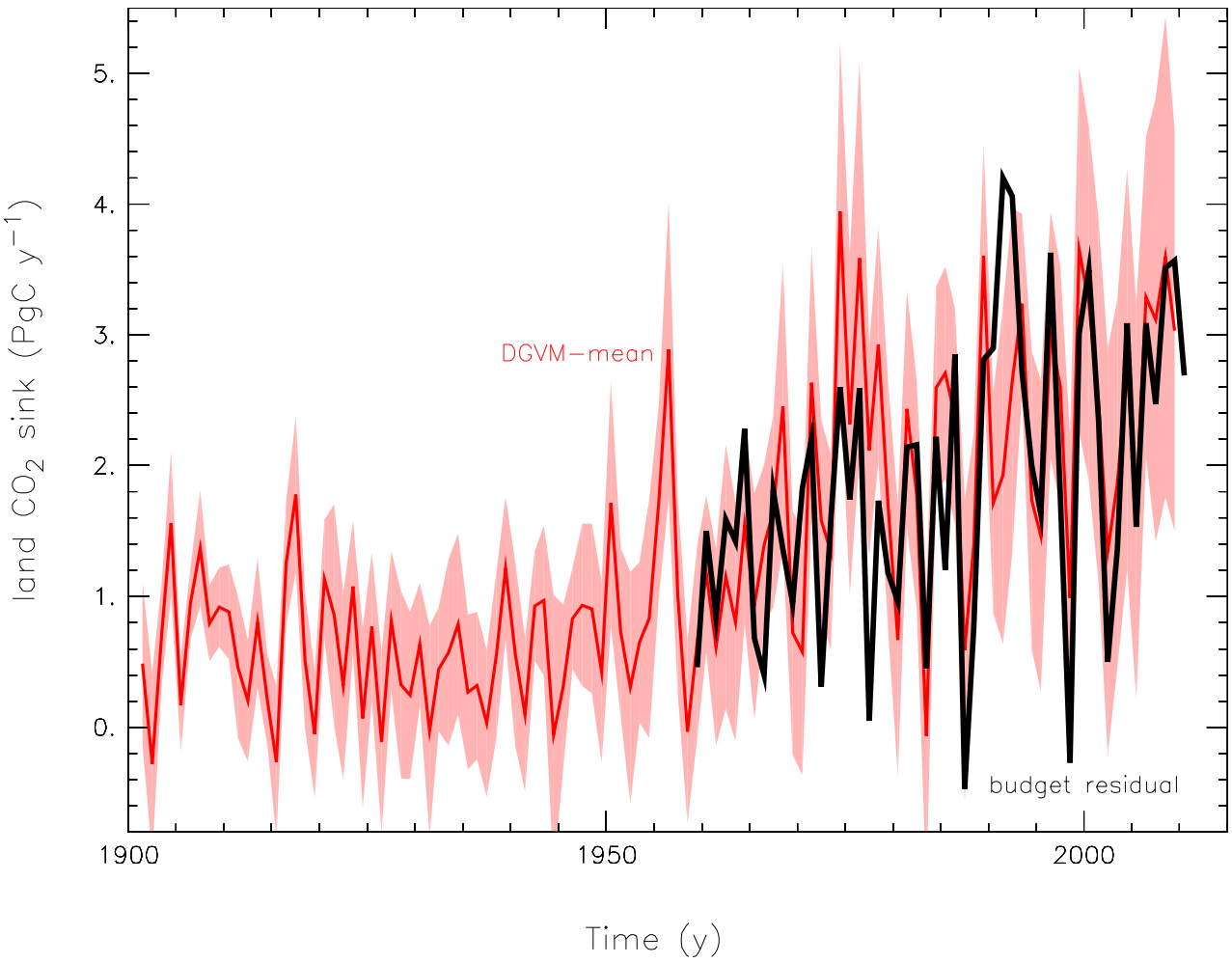

Figure 6.15: Time series for the land CO_2 sink showing the residual of the budget (emissions from fossil fuel and land use change, minus the atmospheric growth and the ocean sink; gray shading) and results from global biospheric models (see Table 6.6 for references). The gray shading shows one Mean Absolute Deviation from the mean.

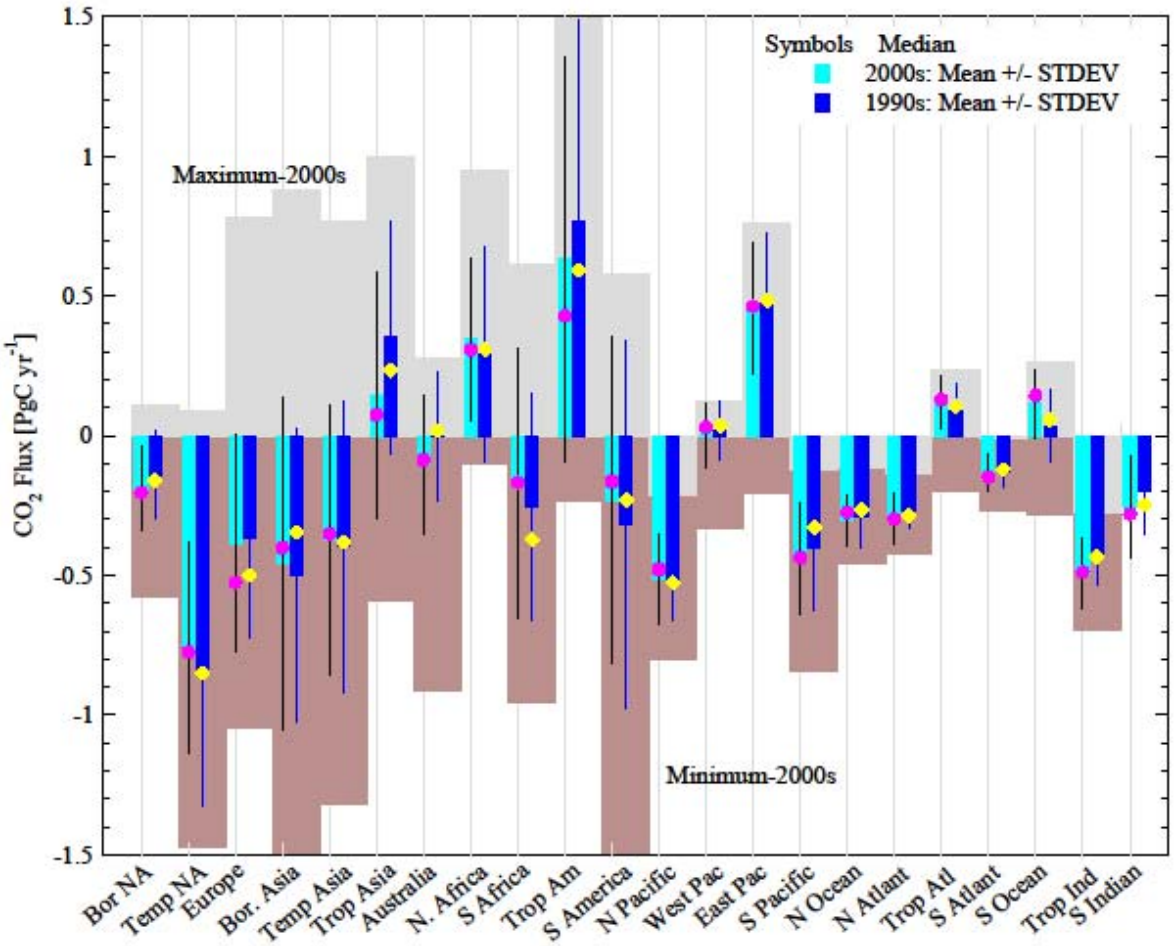

Figure 6.16: Decadal average CO_2 fluxes for 22 regions of the globe for the 1990s (blue) and 2000s (cyan). The mean values are calculated from monthly-mean fluxes from 17 inverse models of the TRANSCOM project for the period of 1990–2008,and standard deviations shown as error bars are for model-to-model differences within each decade. The minimum and maximum ranges of averages for the decade of 2000s are shown as the shaded envelope.

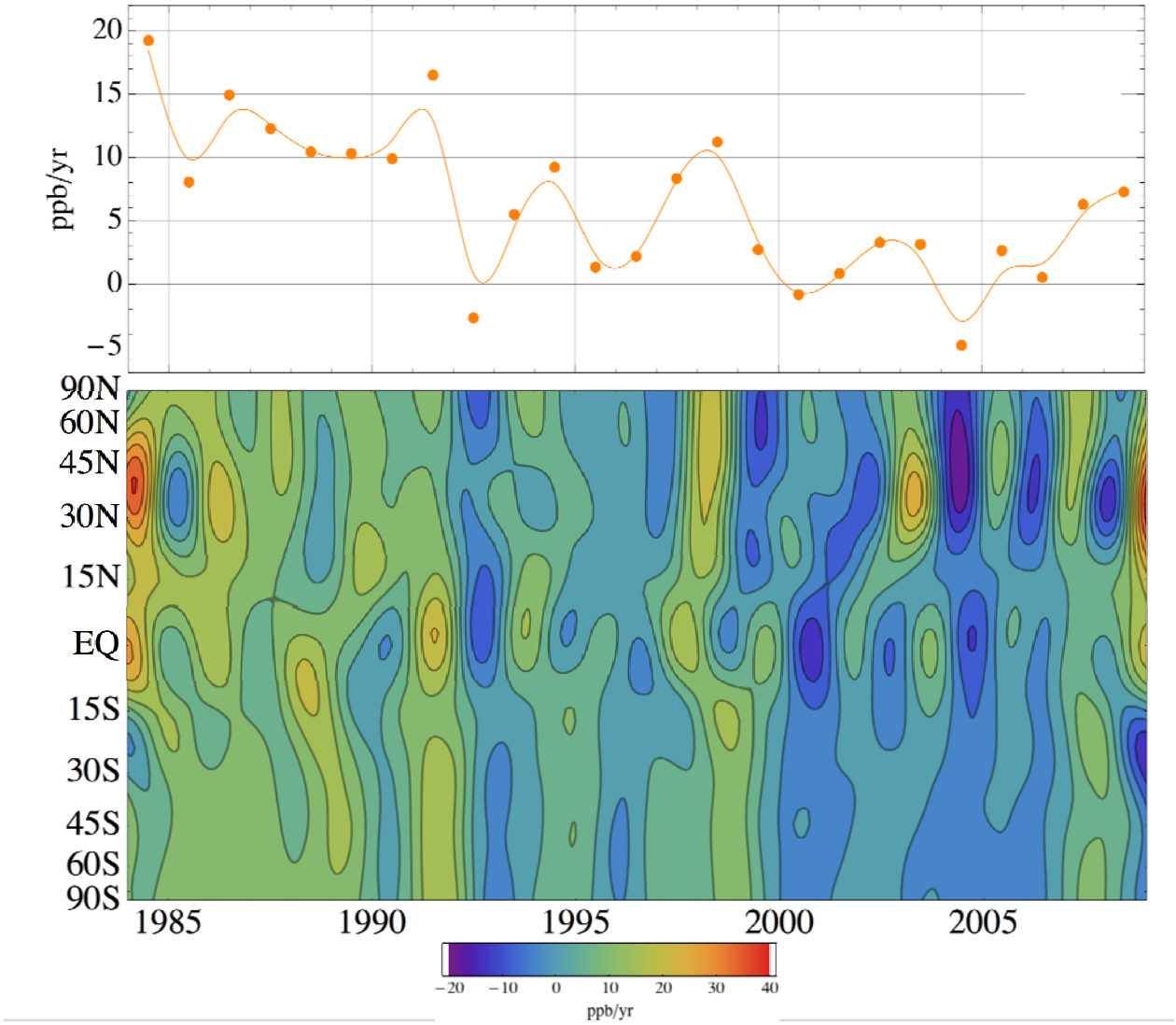

Figure 6.17: Upper panel: Globally averaged growth rate of atmospheric CH4 in ppm yr–1 determined from the GLOBALVIEW data product, representative for the marine boundary layer (Masarie and Tans, 1995). Orange dots indicate annual values augmented by a smooth line to guide the eye. Lower panel: Atmospheric growth rate of CH4 as a function of latitude determined from the GLOBALVIEW data product.

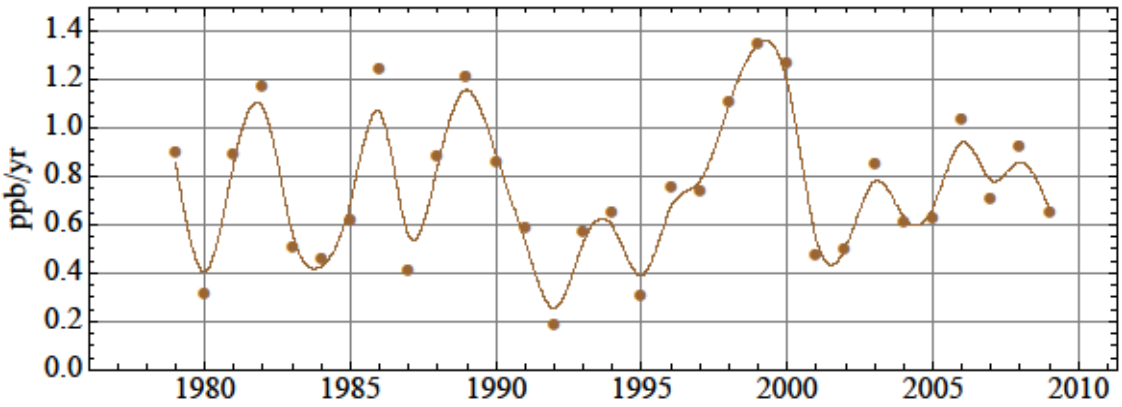

Figure 6.18: Globally averaged growth rate of N_2O in ppm yr^{-1} determined from the observations of the NOAA/ESRL halocarbons program. Brown dots indicate annual values augmented by a smoothed line to guide the eye.

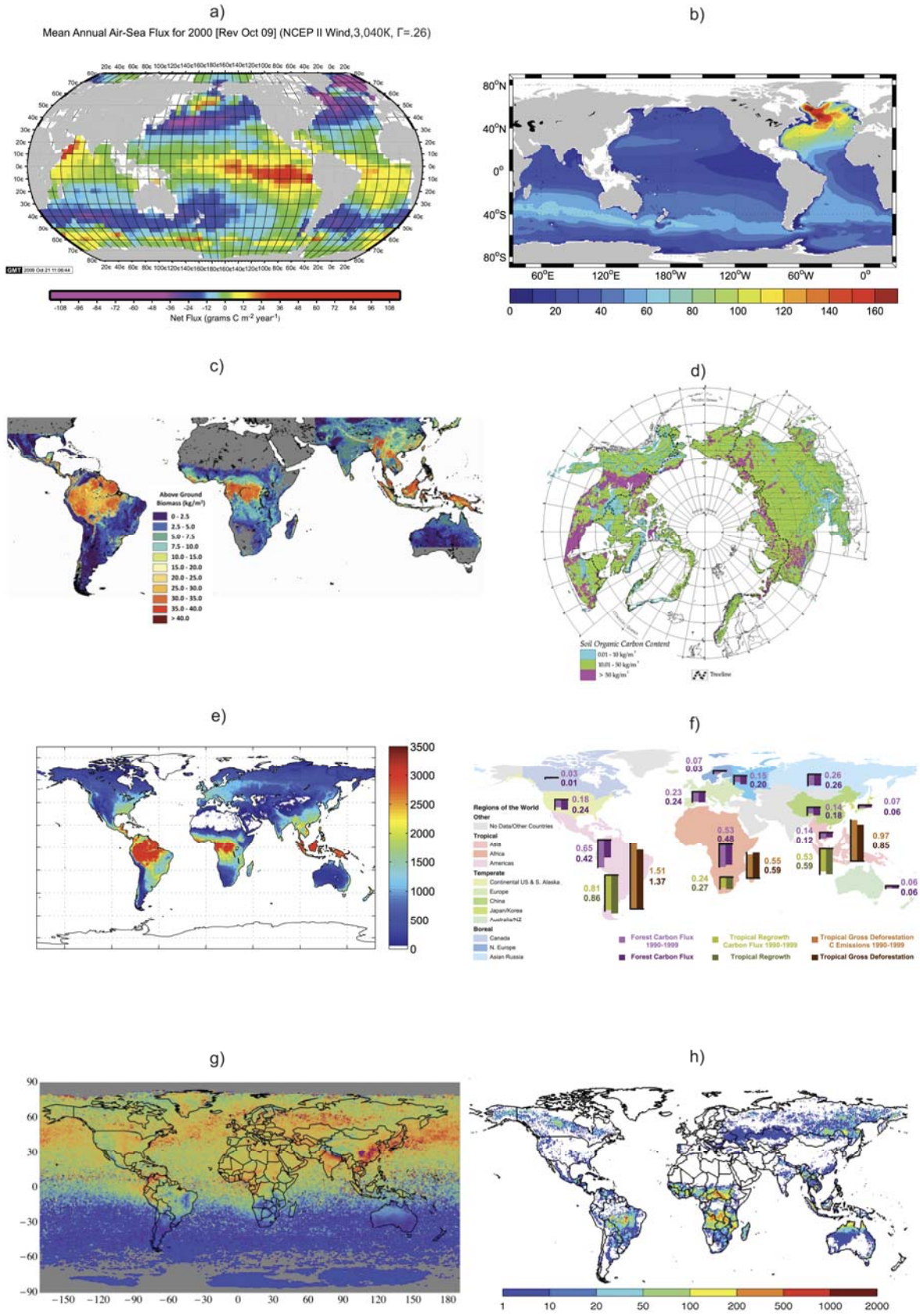

Figure 6.19: New observations since AR4: a) Climatological mean annual sea–air CO_2 flux (gC m^{-2} yr^{-1}) for the reference year 2000 (Takahashi et al., 2009); b) Column inventory of anthropogenic carbon in the ocean in 2008 (Khatiwala et al., 2009); c) Distribution of forest aboveground biomass (circa 2000) (Saatchi et al., 2011); d) Soil

organic carbon content in the northern circumpolar permafrost region (Tarnocai et al., 2009); e) Median annual GPP (gC m^{-2} yr^{-1}) (Beer et al., 2010); f) Forest fluxes and its regional attribution, PgC yr^{-1} (Pan et al. 2011); g) Column averaged CH_4 concentration retrieved by the SCIAMACHY instrument on board of the ENVISAT satellite; 7-year average 2003-2009 (Schneising et al., 2009); g) mean annual carbon emissions from biomass burning and wildfires (gC m^{-2} yr^{-1}), averaged 1997–2010 (updated from van der Werf et al., 2010).

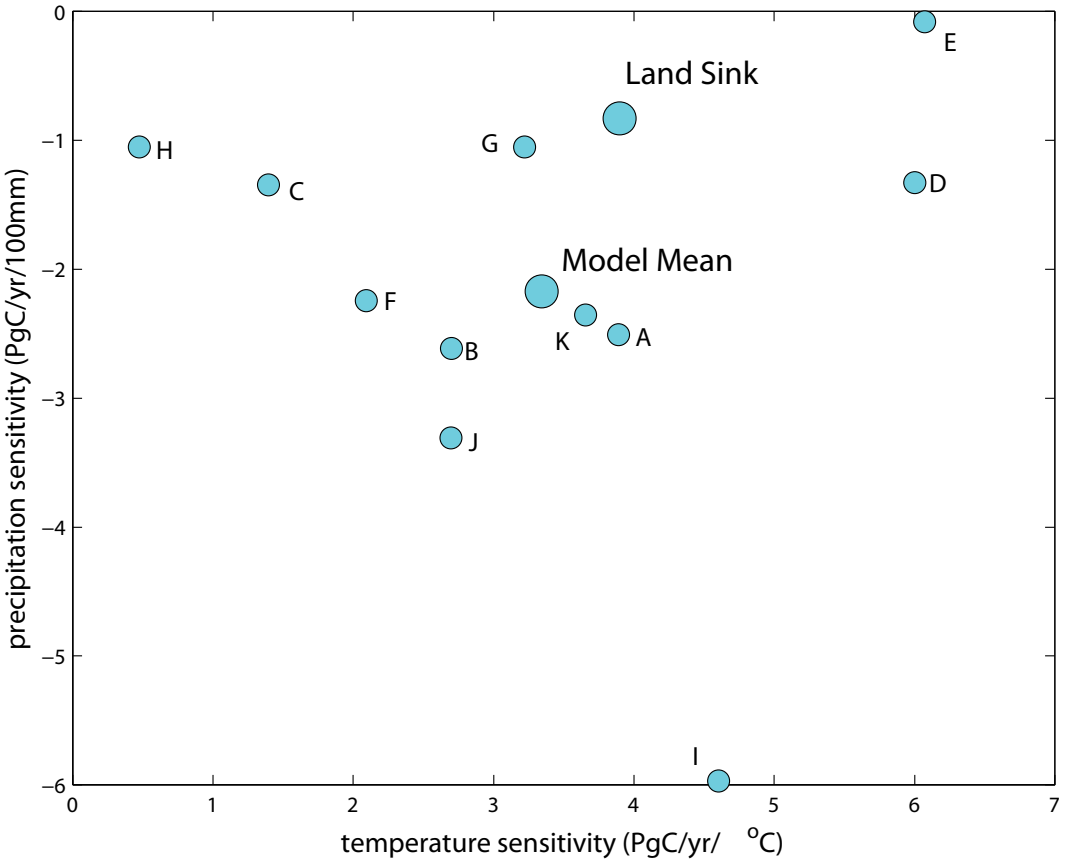

Figure 6.20: Interannual sensitivity of model estimated global Net Ecosystem Production (NEP) and residual global carbon sink to change in atmospheric CO_2 and climate during 1980–2009. The global residual land sink was estimated by the difference between the sum of fossil fuel emission and land use change emission and the sum of atmospheric growth rate and modeled ocean sink (Friedlingstein and Prentice, 2010; LeQuere et al., 2009). The sensitivities to temperature, precipitation and atmospheric CO_2 are estimated by a multiple linear regression approach with three variables (mean annual temperature, annual precipitation, and atmospheric CO_2 concentration). Negative value indicates increase in carbon sink.

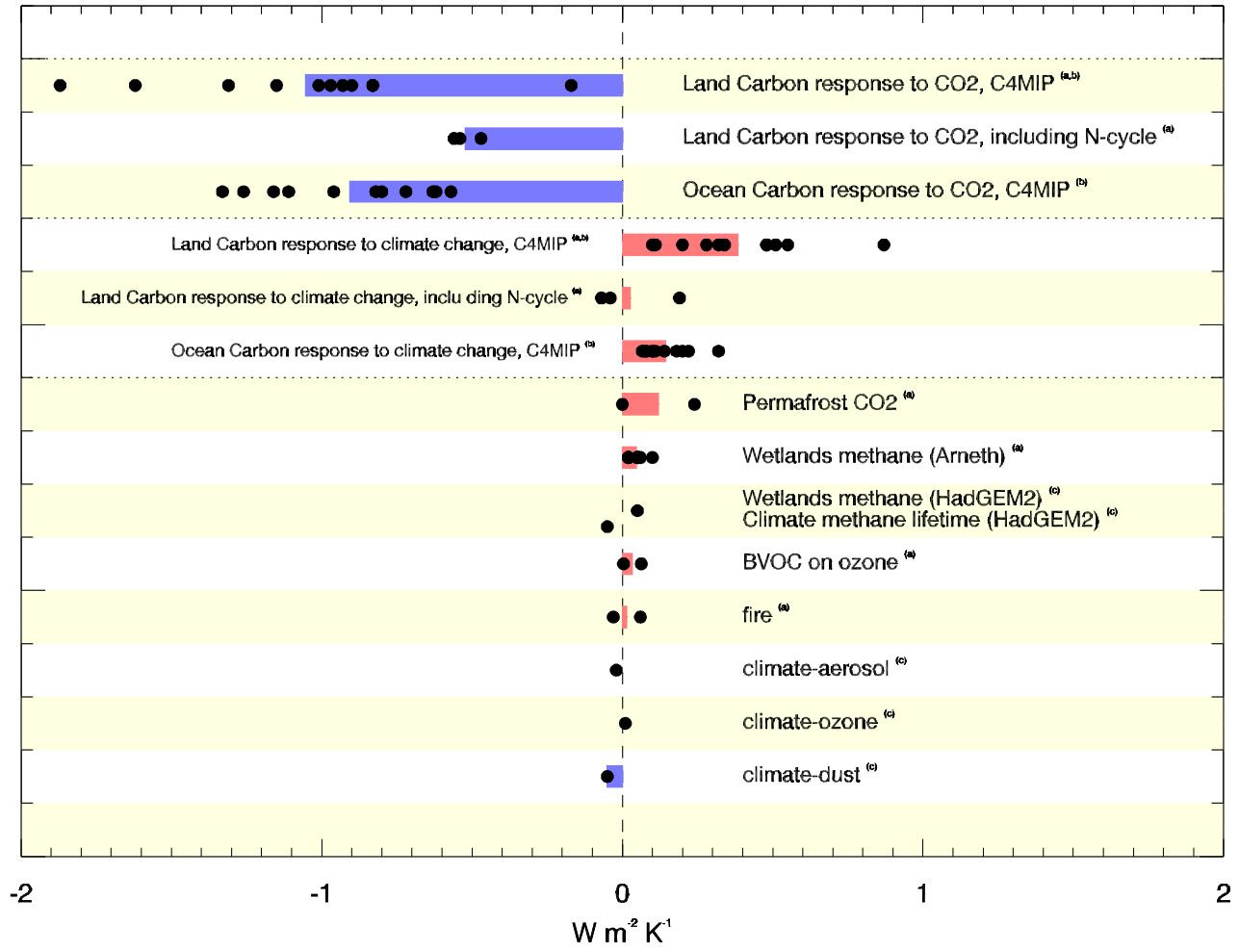

Figure 6.21: A summary of the magnitude of biogeochemical feedbacks. (Gregory et al., 2009) proposed a framework for expressing non-climate feedbacks in common units (W m^{-2} K^{-1}) with physical feedbacks, and (Arneth et al., 2010) extended this beyond carbon cycle feedbacks to other terrestrial feedbacks. The figure shows the results compiled by (Arneth et al., 2010), with ocean carbon feedbacks from C4MIP also added. Some further biogeochemical feedbacks from the HadGEM2-ES Earth System model (Collins et al., 2011a) are also shown. Black dots represent single estimates, and coloured bars denote the simple mean of the dots with no weighting or assessment being made to likelihood of any single estimate. Confidence in the magnitude of these estimates is low for feedbacks with only one, or few, dots. The role of nitrogen limitation on carbon uptake is also shown – this is not a separate feedback, but rather a modulation to the climate-carbon and concentration-carbon feedbacks. This list is not exhaustive. These feedback metrics are also likely to be state or scenario dependent and so cannot always be compared like-for-like (see Section 6.4.2.2). Results have been compiled from (a) (Arneth et al., 2010), (b) (Friedlingstein et al., 2006), (c) HadGEM2-ES (Collins et al., 2011a) simulations.

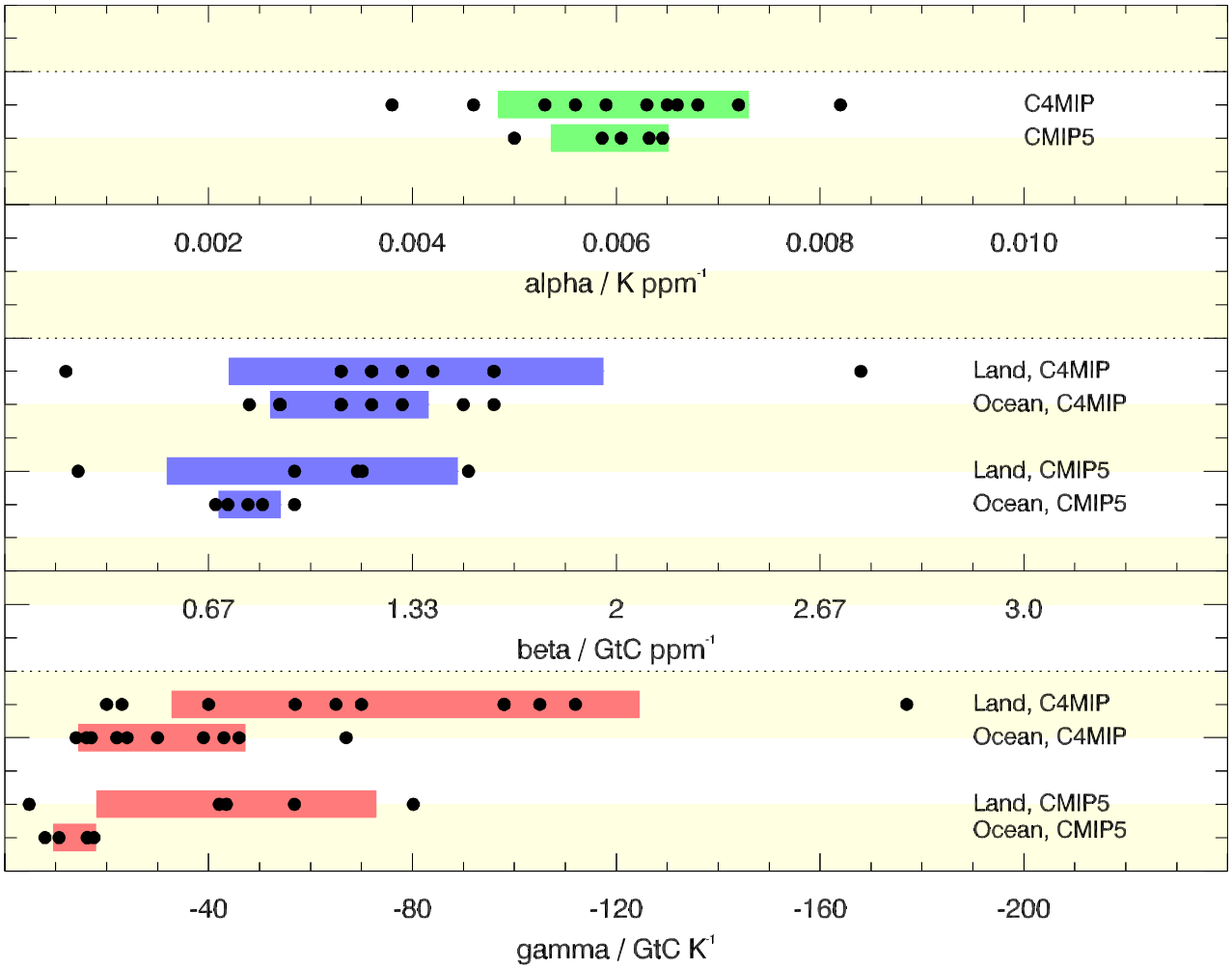

Figure 6.22: Comparison of carbon cycle feedback metrics between the C4MIP ensemble of 7 GCMs and 4 EMICs (Friedlingstein et al., 2006) and CMIP5 models (HadGEM2-ES, IPSL, CanESM, MPI-ESM). Black dots represent a single model simulation and coloured bars show the mean ±1 standard deviation of the multi-model results. The comparison with C4MIP is for context, but these metrics are known to be variable across different scenarios and rates of change (see Section 6.4.2.2). Some of the CMIP5 models are derived from models that contributed to C4MIP and some are new to this analysis. Table 6.9 lists the main attributes of each CMIP5 model used in this analysis. The SRES A2 scenario is closer in rate of change to a 0.5% yr^{-1} scenario and as such it should be expected that the CMIP5 gamma terms are comparable, but the beta terms are likely to be around 20% smaller for CMIP5 than for C4MIP. This high dependence on scenario (Section 6.4.2.2) reduces confidence in any quantitative statements of how CMIP5 carbon cycle feedbacks differ from C4MIP.

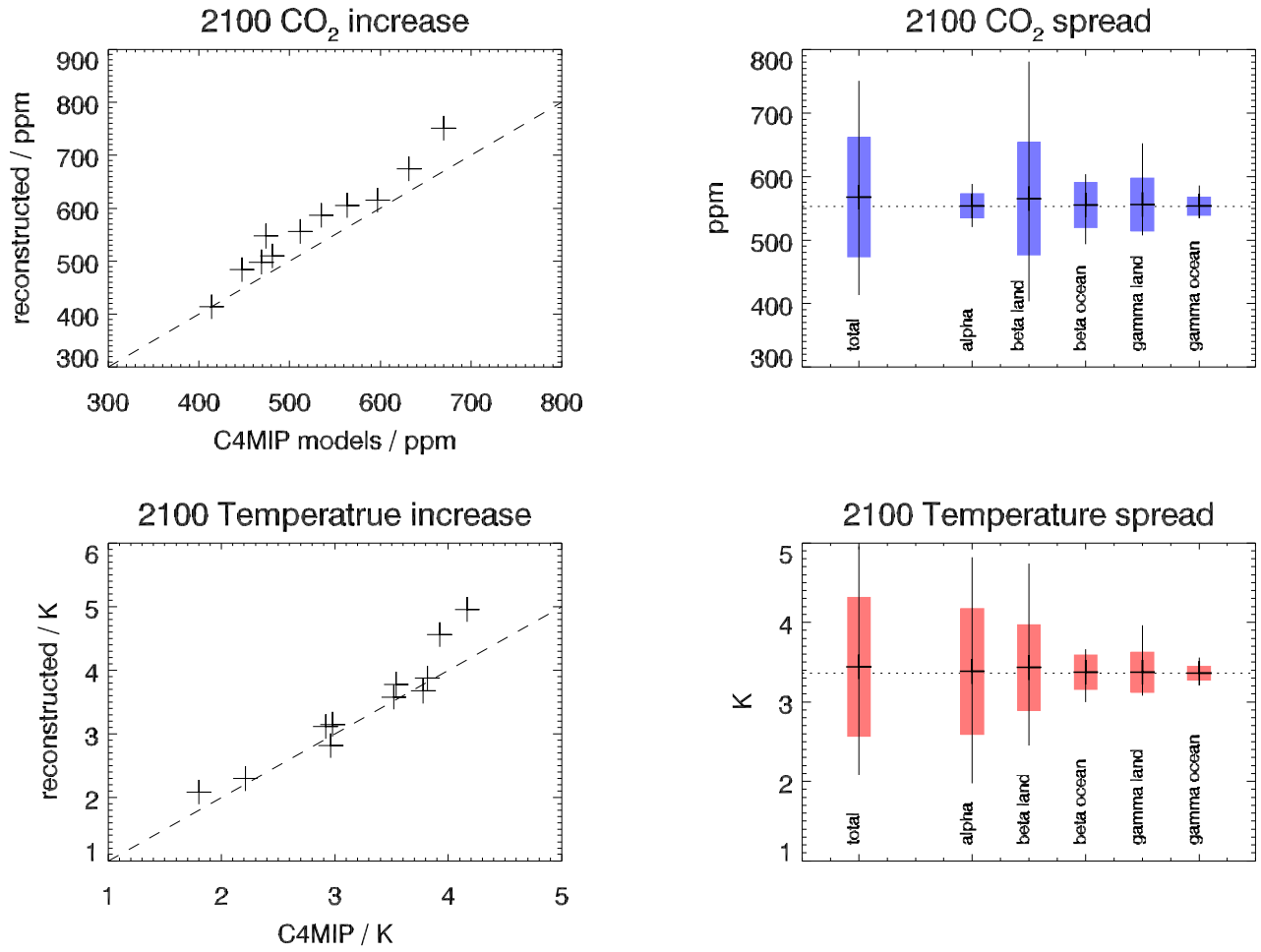

Figure 6.23: Impact of model spread in the C4MIP metrics (α, β, γ). Scatter plots show the success of the linear alpha/beta/gamma framework to estimate 2100 CO_2 and temperature change from the C4MIP models, and right panels show the relative spread that comes from each term – model spread in β_L is the dominant cause of spread in 2100 CO_2, and α for spread in 2100 ΔT.

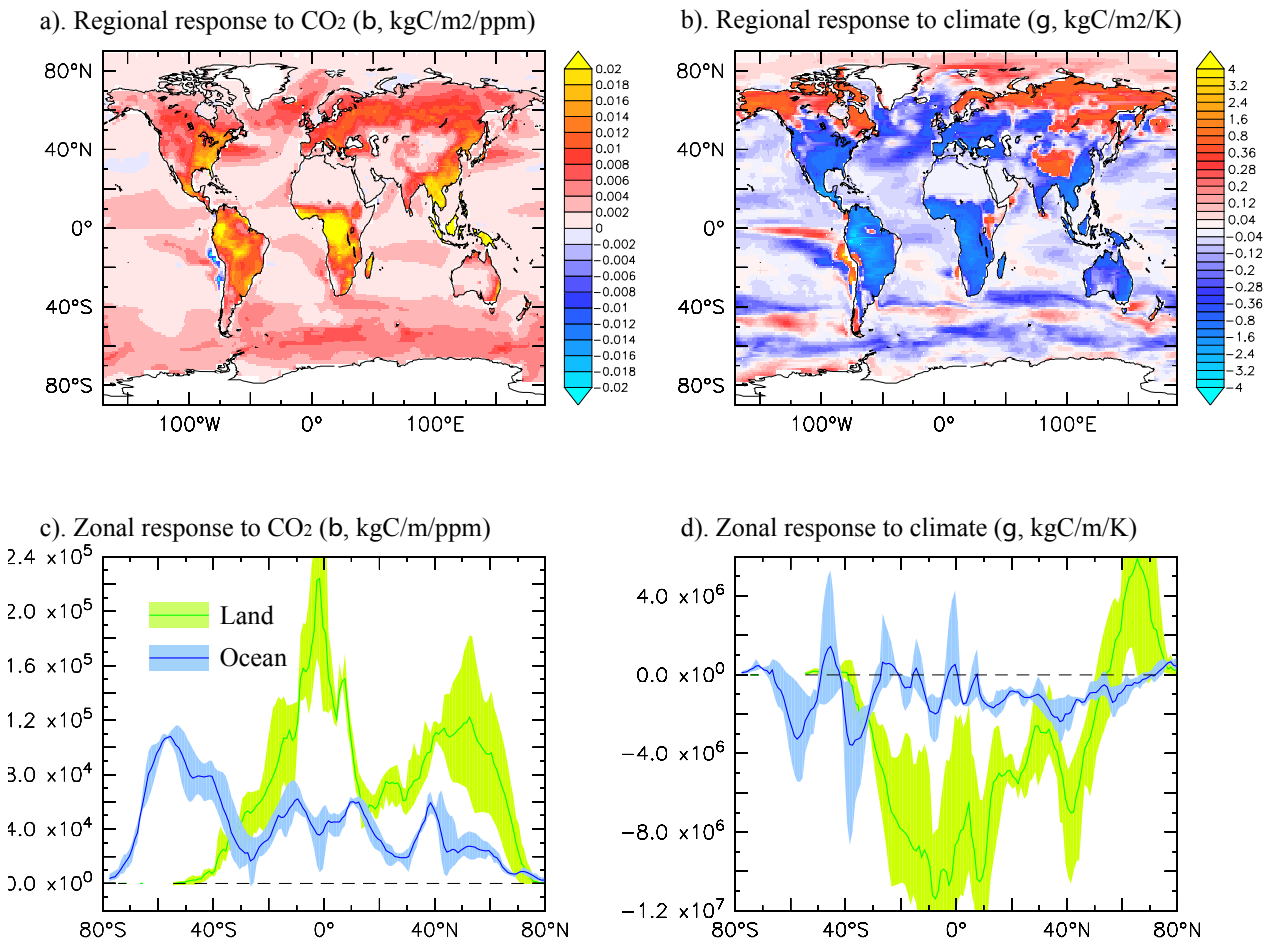

Figure 6.24: The spatial distributions of land and ocean β and γs for 3 CMIP5 models using the 1% idealised simulations. For land and ocean, β and γ are defined from changes in terrestrial carbon storage and changes in air-sea accumulated fluxes respectively, from the beginning to the end of the 1% idealised simulation relative to global (not local) CO_2 and temperature change.

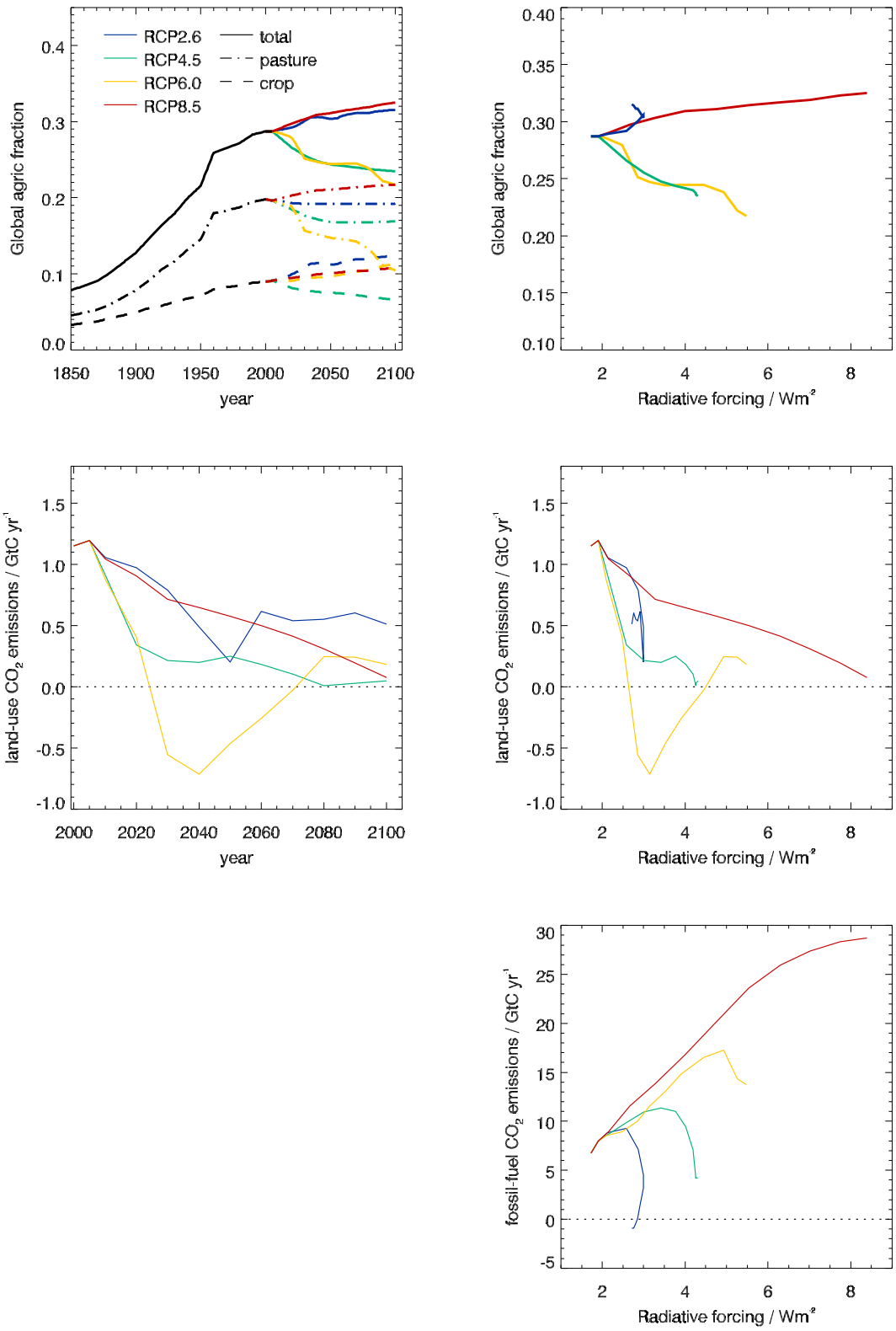

Figure 6.25: Land-use trends and emissions. Global changes in croplands and grassland from the historical record and the RCP scenarios (top panels), and associated land-use emissions of CO_2 (middle panels). Data are plotted as changes in time (left-hand side) and against the global radiative forcing for each RCP (right-hand side). There is no logical relationship (nor is there intended to be) between the land use calculated by IAMs for the RCPs and the radiative forcing level of each RCP. Bottom row shows fossil fuel emissions plotted against radiative forcing for comparison.

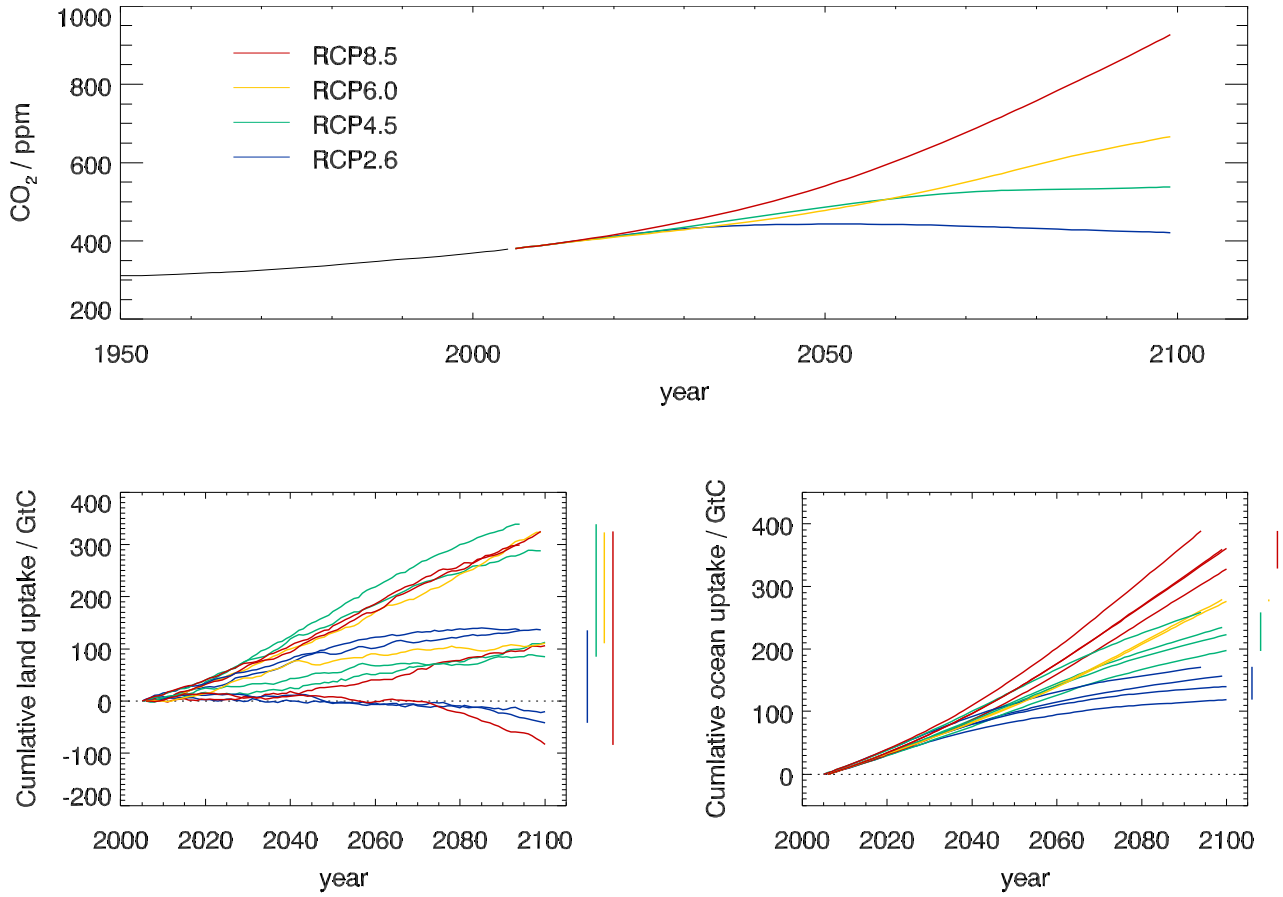

Figure 6.26: CO_2 concentration pathway in the 4 RCP scenarios (top), and the cumulative changes in land and ocean (bottom left, bottom right) carbon storage (GtC) simulated by ESMs (HadGEM2-ES, CanESM1, IPSL, MIROC – see Table 6.9) for ocean uptake the spread between models is smaller than between scenarios, but for land carbon storage the spread between models is greater than between scenarios.

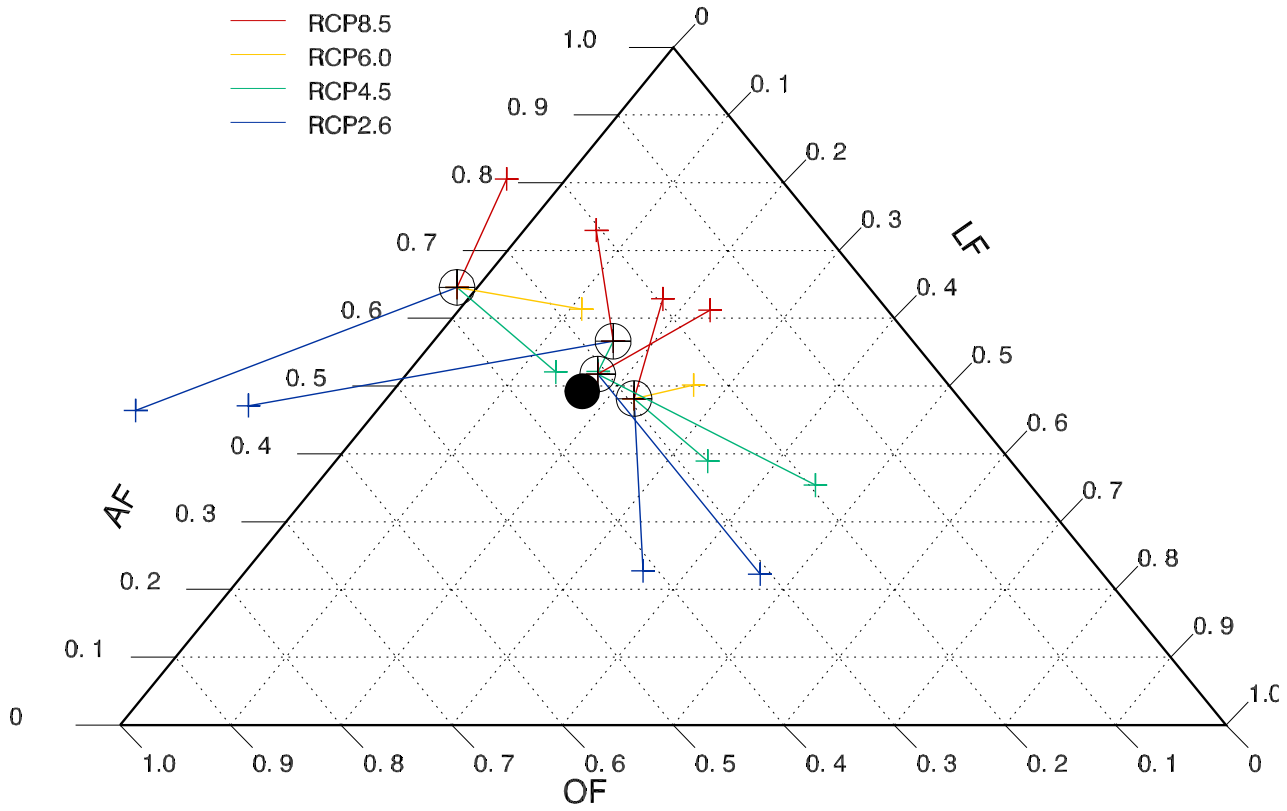

Figure 6.27: changes in airborne, land and ocean fraction of fossil fuel carbon emissions. The figure shows 3 axes whose sum is always unity – airborne fraction (AF) increases vertically, land fraction (LF) from top to bottom right, and ocean fraction (OF) from right to left. The fractions are defined as the changes in storage in each component (atmosphere, land, ocean) divided by the compatible fossil fuel emissions derived from each simulation. Open circles show model simulations for the 1990s, and the solid circle shows the observed estimate based on Table 6.10. The coloured lines and symbols denote the change in uptake fractions under the different RCP scenarios for each model, calculated using the cumulative change in carbon from 2005–2100. Due to the difficulty estimating fossil and land-use emissions from the ESMs this figure uses a fossil fuel definition of airborne fraction, rather than the preferred definition of fossil+land use emissions discussed in Section 6.3.

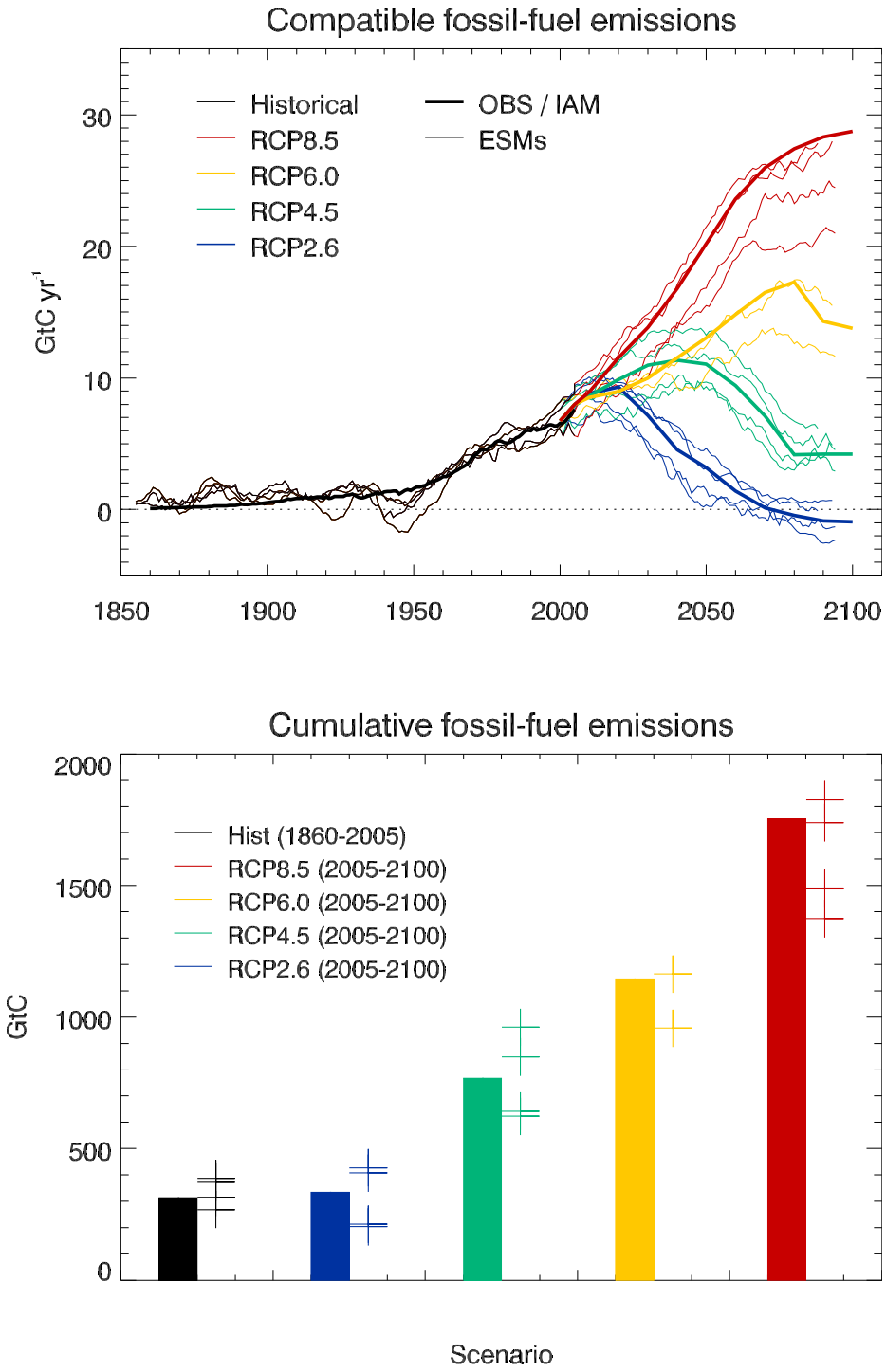

Figure 6.28: Compatible fossil fuel emissions simulated by the CMIP5 models for the 4 RCP scenarios. Top: timeseries of instantaneous emission rate. Thick lines represent the historical estimates and emissions calculated by the integrated assessment models (IAM) used to define the RCP scenarios, thin lines show results from CMIP5 ESMs. Bottom: cumulative emissions for the historical period (1860–2005) and 21st century (defined in CMIP5 as 2005–2100) for historical estimates and RCP scenarios (bars) and ESMs (symbols). In the CMIP5 model results, total carbon in the land-atmosphere-ocean system can be tracked and changes in this total must equal fossil fuel emissions to the system (see also Table 6.13). Other sources and sinks of CO_2 such as from volcanism, sedimentation or rock weathering, which are very small on centennial timescales are not considered here. Hence the compatible emissions are given by cumulative-Emissions = $\Delta C_A + \Delta C_L + \Delta C_O$ remission rate = d/dt $[C_A + C_L + C_O]$, where C_A, C_L, C_O are carbon stored in atmosphere, land and ocean respectively.

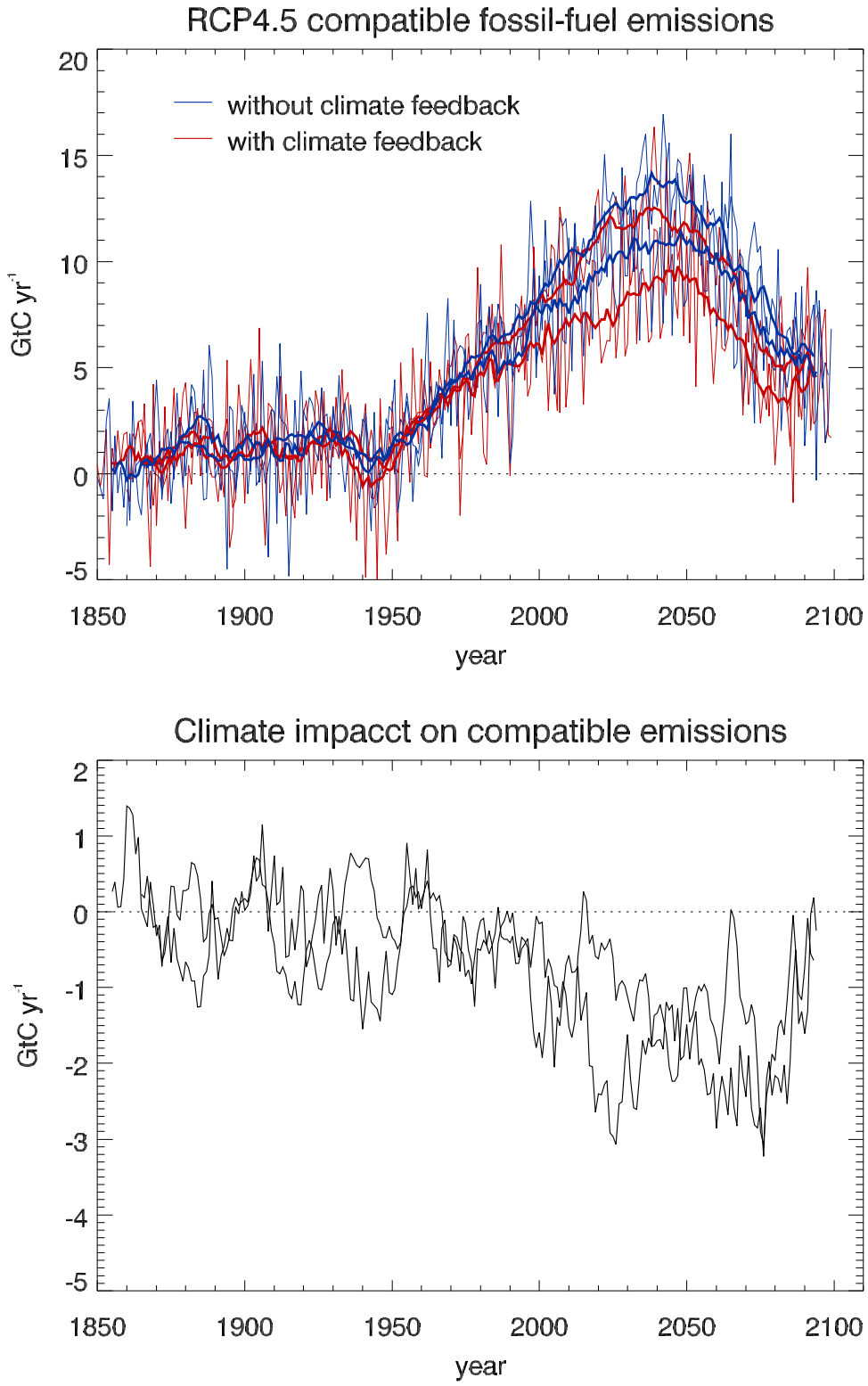

Figure 6.29: Diagnosed compatible fossil fuel emissions (top panel) in the presence (red) and absence (blue) of the climate impact on the carbon cycle for the RCP4.5 scenario, and the difference between them (bottom panel). This shows the impact of climate change on the compatible emissions to achieve the RCP4.5 CO_2 concentration pathway. HadGEM2-ES and CanESM results shown here project reductions from 977 and 891 GtC respectively to 865 and 707 GtC.

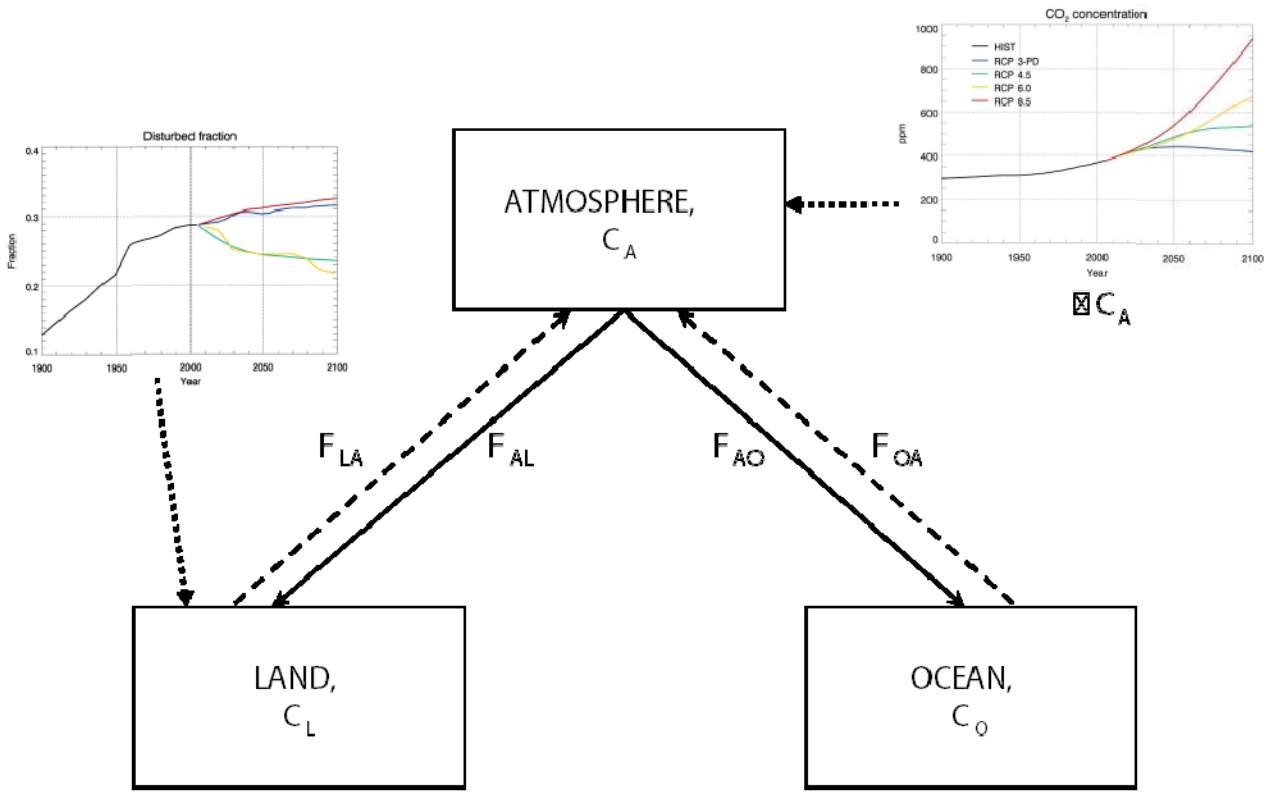

Figure 6.30: Interactions between the atmosphere, land and ocean carbon stores as simulated in ESMs. Solid arrows represent the atmosphere-to-land (F_{AL}) and atmosphere-to-ocean (F_{AO}) fluxes simulated by the ESMs. Dashed lines represent land/ocean to atmosphere fluxes (F_{LA}, F_{OA}) diagnosed in concentration-driven simulations and interactive in emission-driven simulations. The dotted arrows represent the prescribed CO_2 pathway (ΔC_A) applied in concentration-driven simulations and a scenario of land-use which may be imposed on the land carbon cycle (see Section 6.4.3.1). Associated changes in C_L caused by this land-use change may not match those implicit in the prescribed ΔC_A.

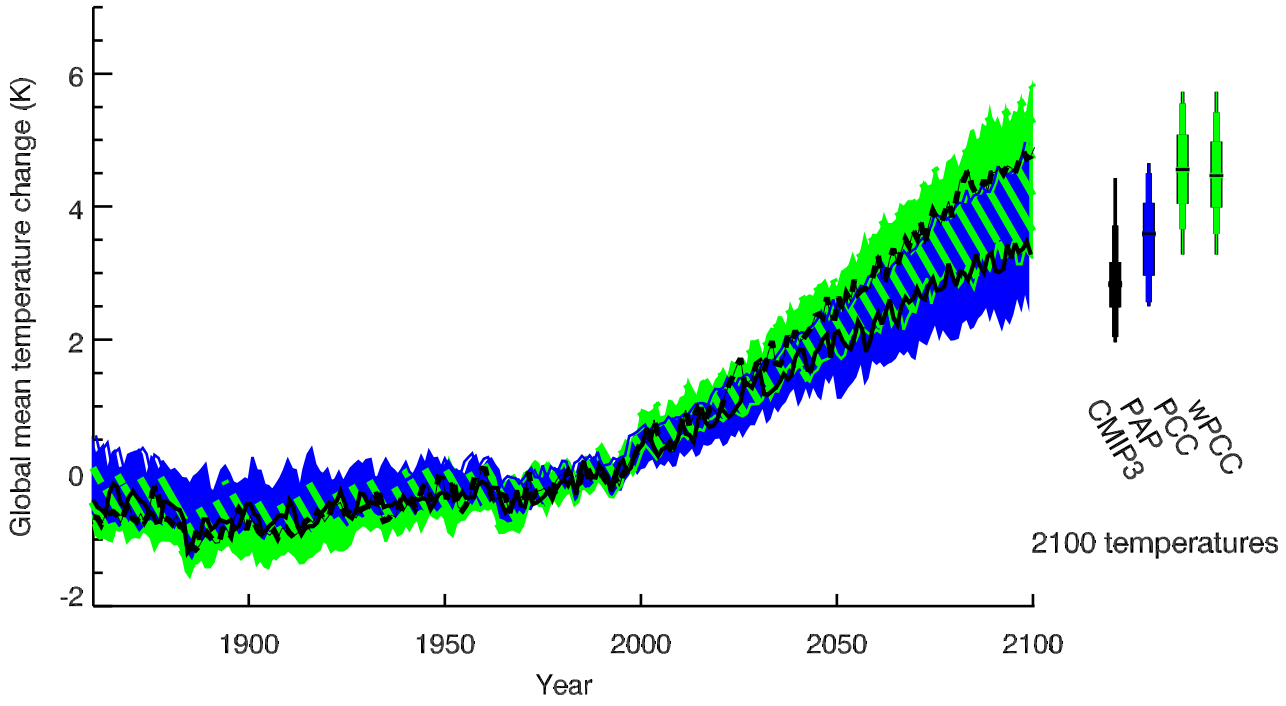

Figure 6.31: Uncertainty in global mean temperature from HadCM3 results exploring atmospheric physics and terrestrial carbon cycle parameter perturbations (Booth et al., submitted; Murphy et al., 2004). Relative uncertainties in the Perturbed Carbon Cycle (PCC, green plume) and Perturbed Atmospheric Processes (PAP, blue) on global mean anomalies of temperature (plotted with respect to the 1980–1999 period). The green/blue hatching illustrates where these two ensembles overlap. The standard simulations from the two ensembles, HadCM3 (black solid) and HadCM3C (black dashed) are also shown. Four bars are shown on the right illustrating the 2100 temperature anomalies associated with the CMIP3/AR4 ensemble (black) the PAP ensemble (blue) the land carbon cycle (PCC) and the weighted land carbon ensemble wPCC (both green). The range (thin line), 10th–90th (medium line) and 25th–75th (thick line) and 50th percentiles (central bar) are all shown.

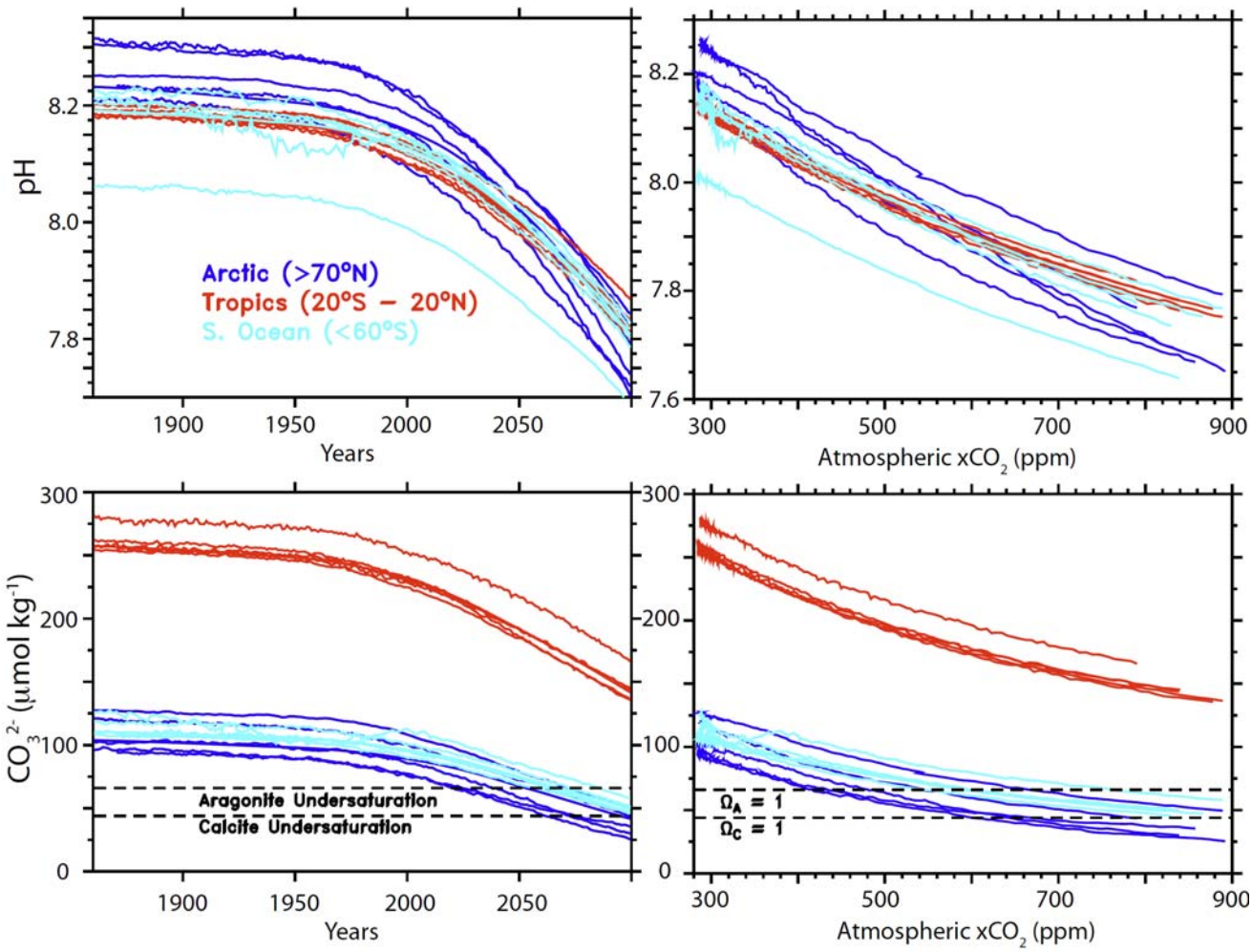

Figure 6.32: Changes in surface pH (upper panels) and surface carbonate ion concentrations (lower panels), as a function of time (left) or atmospheric CO_2 (right), simulated by 6 ESMs (IPSL-CM4-LOOP, UVIC2.8, NCAR CSM1.4, NCAR-CCSM3, BCCR-BCM, MPI-M) over the historical period and over 2000–2100 following the SRES-A2 scenarios. Three regions (discussed in the text) are shown : the Arctic Ocean (north of 70°N, dark blue), the Tropical Oceans (20°S–20°N, red) and the Southern Ocean (south of 60°S, light blue). [PLACEHOLDER FOR SECOND ORDER DRAFT: Results from the CMIP5 models].

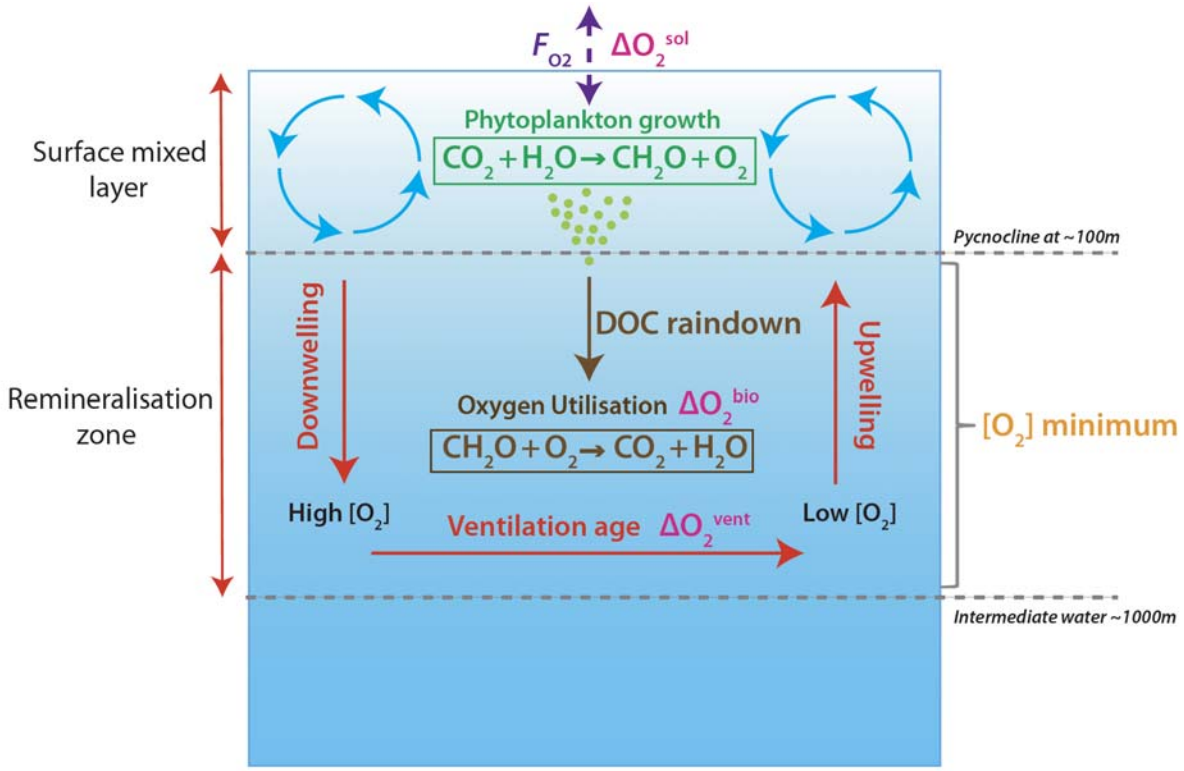

Box 6.4, Figure 1: *The ocean O_2 cycle*. The oceanic reservoir of oxygen communicates with the atmosphere via air-sea gas exchange (F_{O2}). In the ocean interior a change in dissolved O_2 concentration over time can be driven by changes in: (1) surface ocean O_2 solubility ΔO_2^{sol}, (2) the ventilation age of a water parcel advected into the subsurface (ΔO_2^{vent}) (3) biological utilisation of oxygen in remineralization of Dissolved Organic Carbon (DOC; ΔO_2^{bio}).

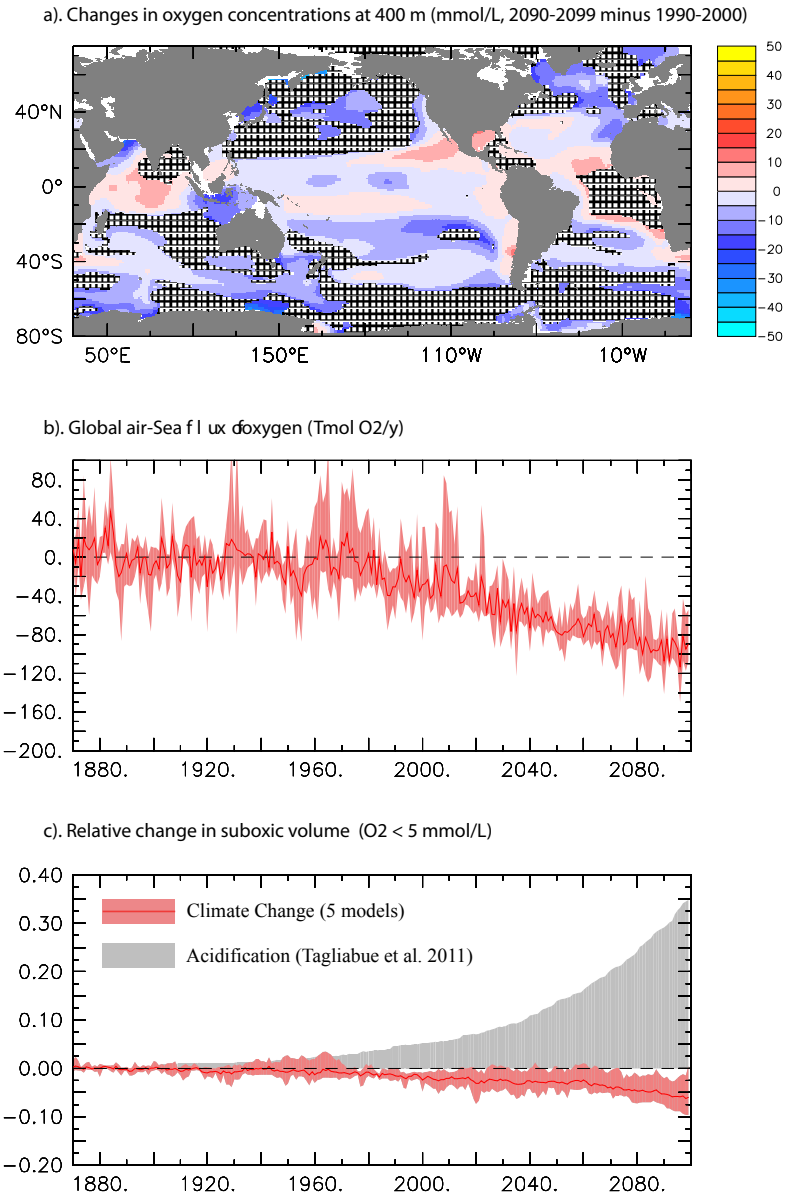

Figure 6.33: a) Model-mean (IPSL-CM4-LOOP, UVIC2.8, NCAR CSM1.4, NCAR-CCSM3, BCCR-BCM) changes in O2 concentrations (microM) at 400 m for the 2090–2100 minus 1990–2000 (SRES-A2 scenario). To indicate consistency in the sign of change, regions are stippled where at least 4 out of the 5 models agree on the sign of the mean change. b) Model range and model-mean evolution of global air-sea flux of O2 in Tmol yr–1. Negative values indicate net outgassing of O2 to the atmosphere. c) Relative change in the evolution of suboxic waters (O2 <5 micromol/L), simulated by the above mentioned 5 models (red) and by (Tagliabue et al., 2011) (grey). [PLACEHOLDER FOR SECOND ORDER DRAFT: results from the CMIP5 models].

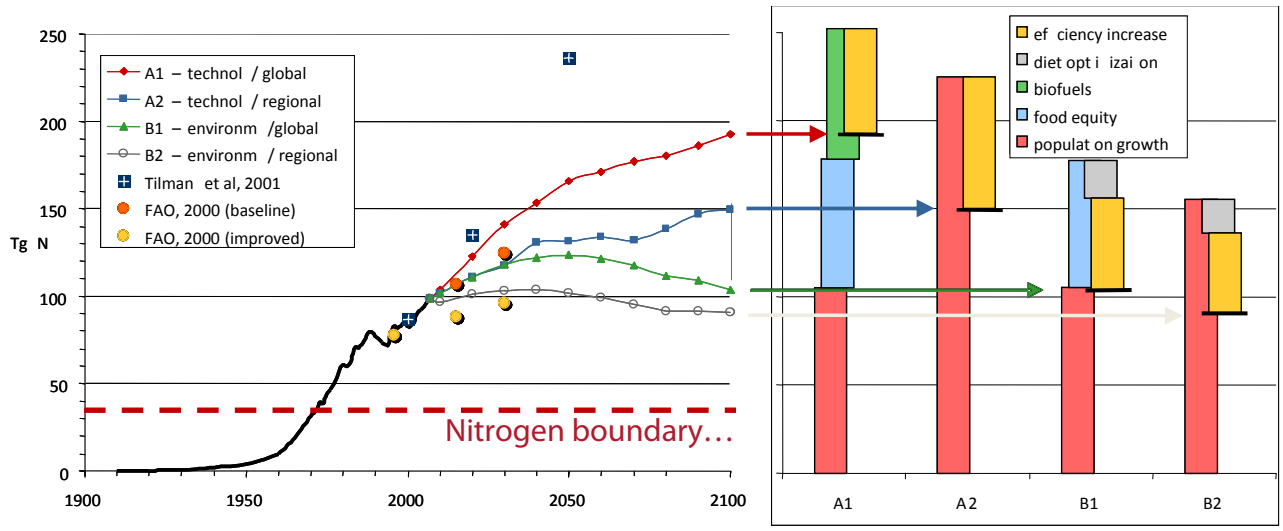

Figure 6.34: Global nitrogen fertilizer consumption scenarios (left) and the impact of individual drivers on 2100 consumption (right). This resulting consumption is always the sum (denoted at the end points of the respective arrows) of elements increasing as well as decreasing nitrogen consumption. Other relevant estimates (FAO, 2000; Tilman et al., 2001; Tubiello and Fischer, 2007) are presented for comparison (Erisman et al., 2008). The A1, B1, A2 and B2 scenarios draw from the assumptions of the IPCC Special Report Emission Scenarios (SRES) emission scenario storylines (Nakicenovic and Swart, 2000). Figure adapted from Erisman et al. (2008).

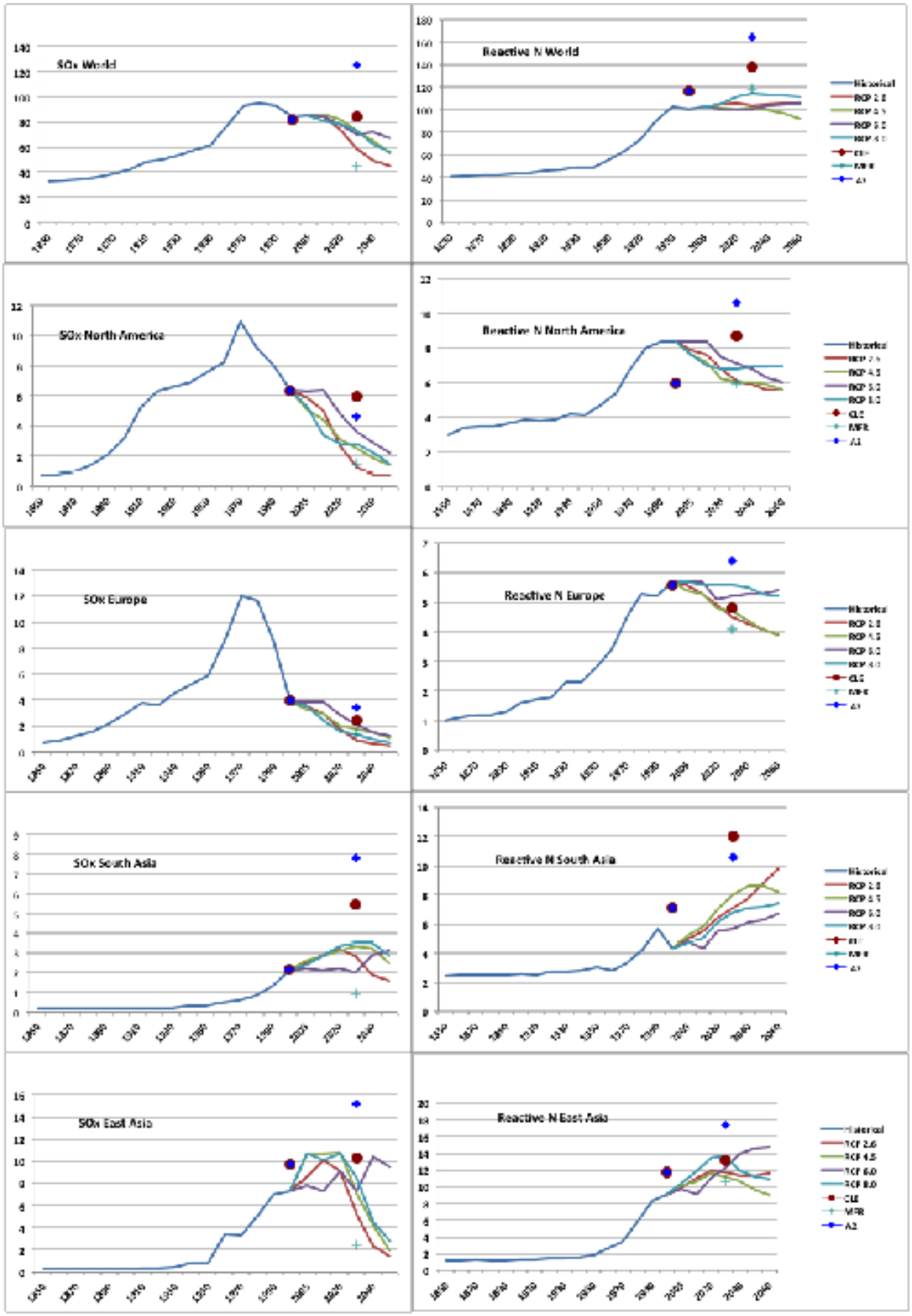

Figure 6.35: Deposition of SO_x (left panel) and reactive N (NO_y + NH_x; right panel) from 1850 to 2000 and projections of deposition to 2050 under the 4 RCP emission scenarios (Van Vuuren et al., 2011; (Lamarque et al., 2011). Also shown are the 2030 scenarios using the SRES B1/A2 energy scenario with assumed current legislation and maximum technically feasible reduction air pollutant controls (Dentener et al., 2006).

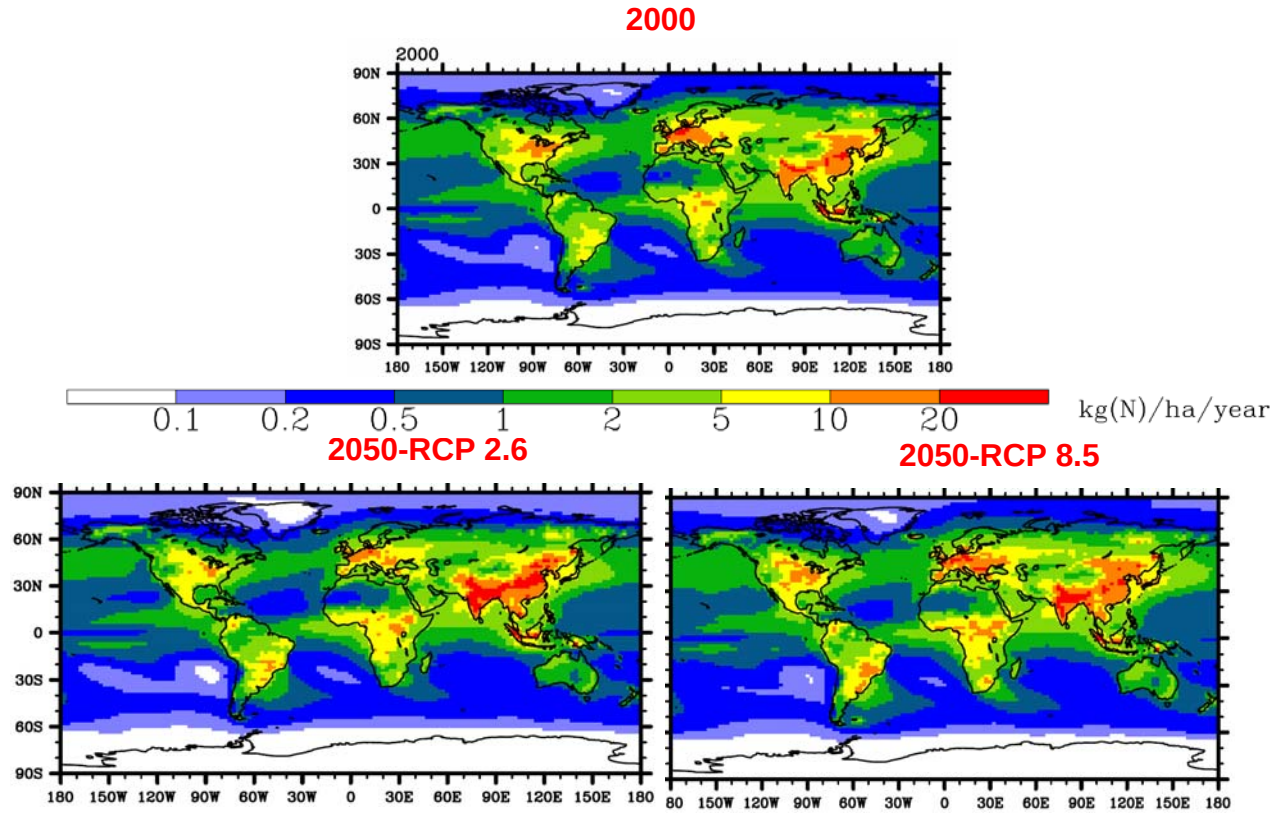

Figure 6.36: Spatial variability of N deposition in 2000 with projections for 2050, using the 2.6 and 8.5 RCP scenarios (to indicate the range), kg N ha^{-1} yr^{-1} (Lamarque et al., 2010).

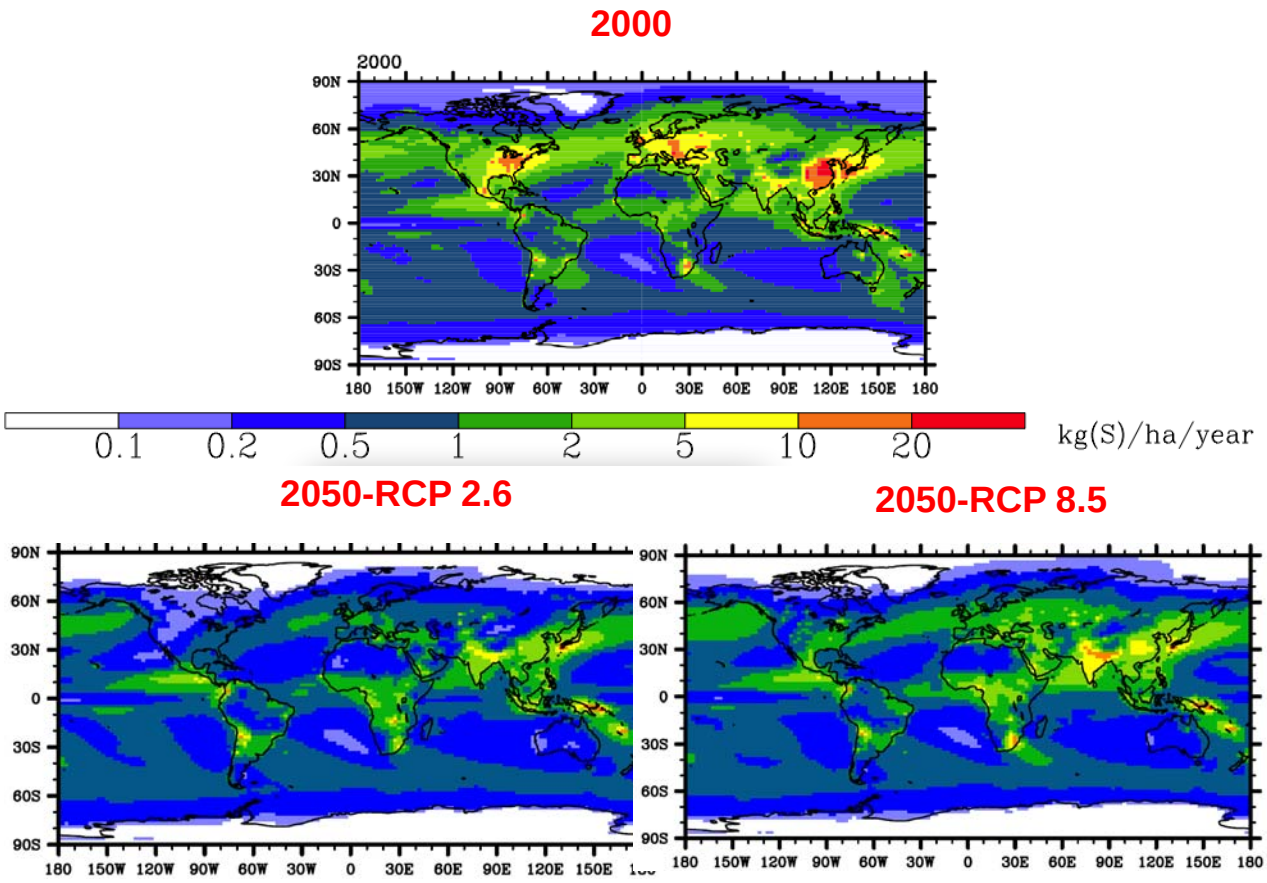

Figure 6.37: Spatial variability of S deposition in 2000 with projections for 2050, using the 2.6 and 8.5 RCP scenarios (to indicate the range), kg N ha^{-1} yr^{-1} (Lamarque et al., 2010).

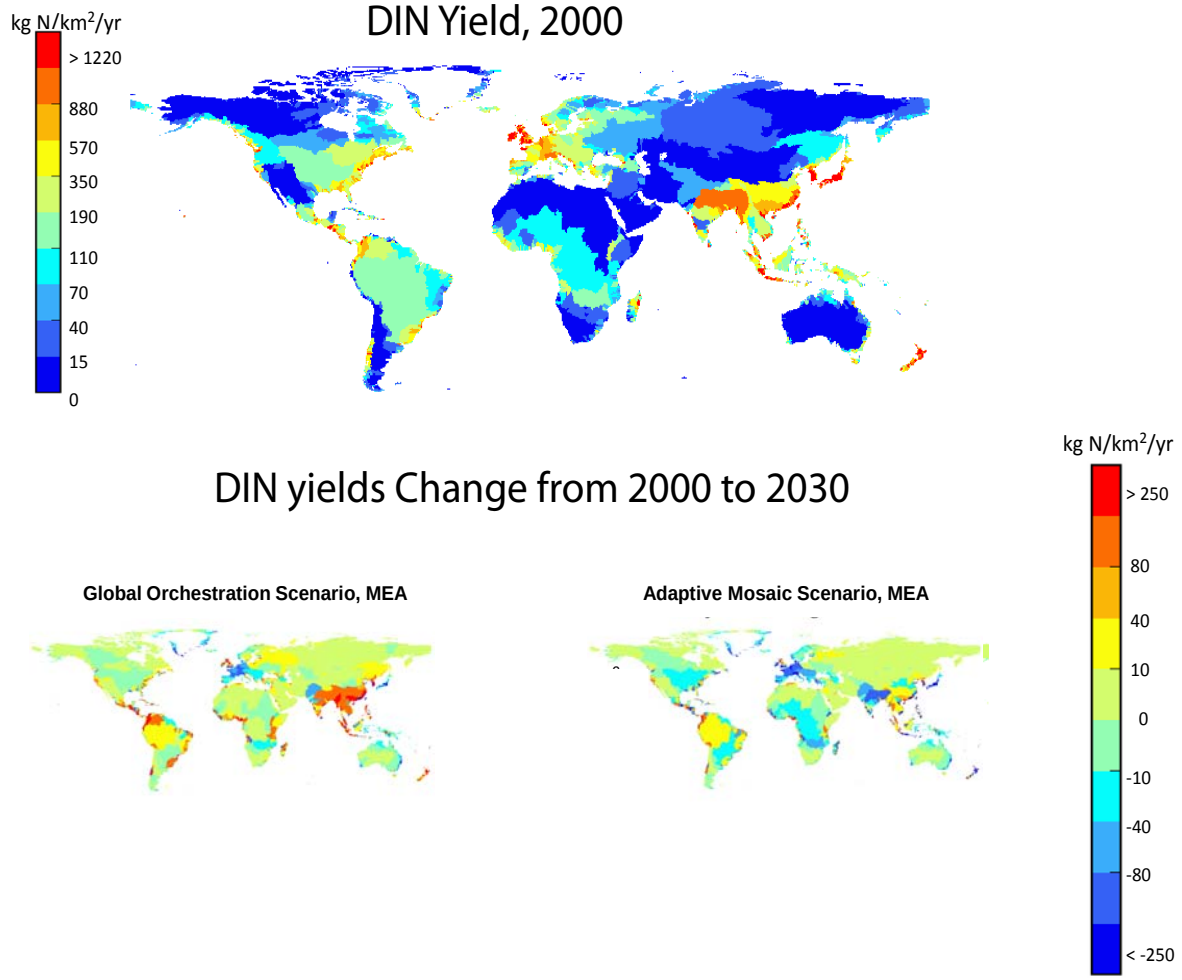

Figure 6.38: a) Dissolved inorganic nitrogen river discharge to coastal zone (mouth of rivers) in 2000, based up on Global NEWS 2 model, b) change in DIN discharge from 2000 to 2030, based upon Global Orchestration and the Adaptive Mosaic scenarios, Millennium Ecosystem Assessment, (Mayorga et al., 2010; Seitzinger et al., 2010). Units are kg N per km^2 watershed per year, as an average for each watershed.

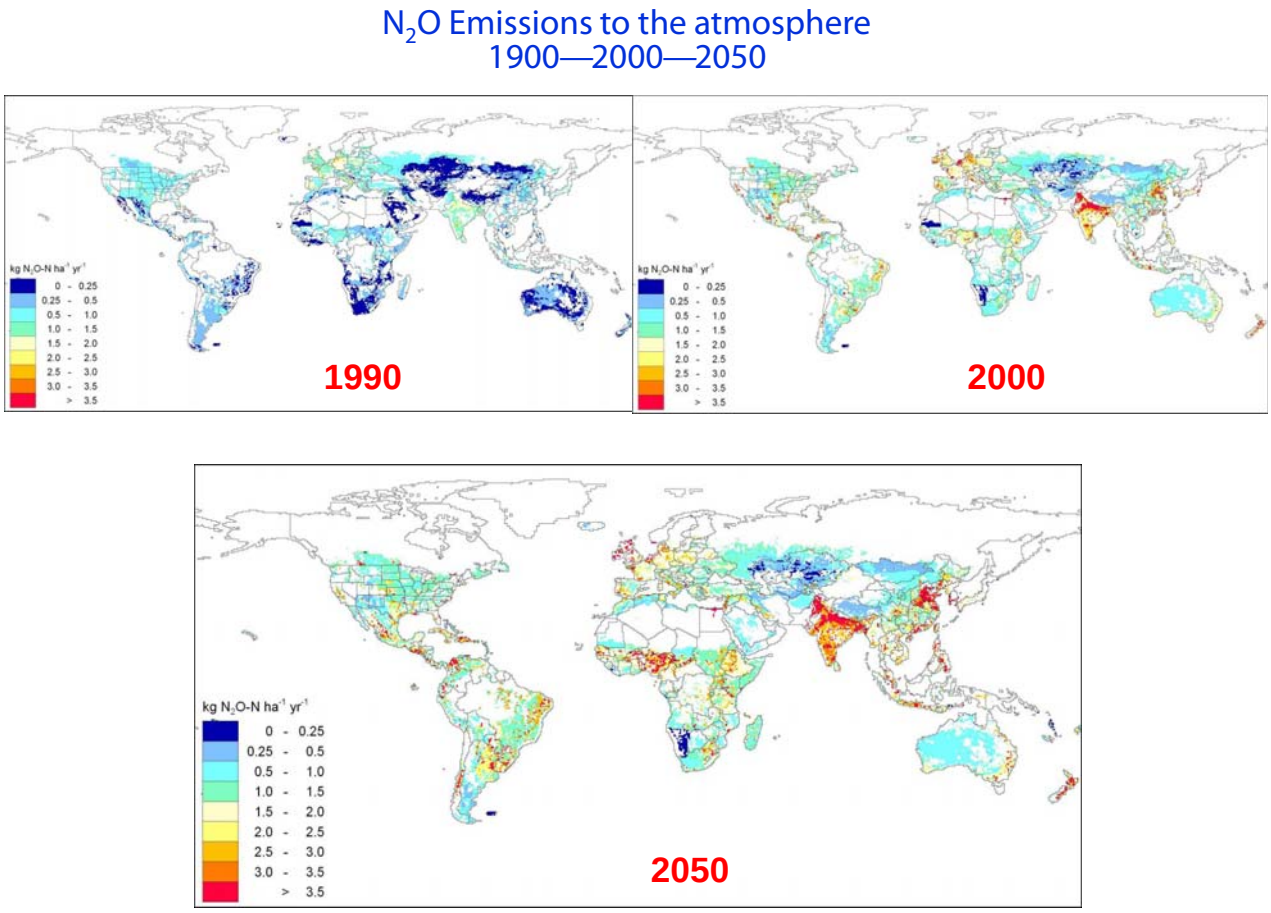

Figure 6.39: N_2O emissions in 1900, 2000 and projected to 2050 (Bouwman et al., 2011).

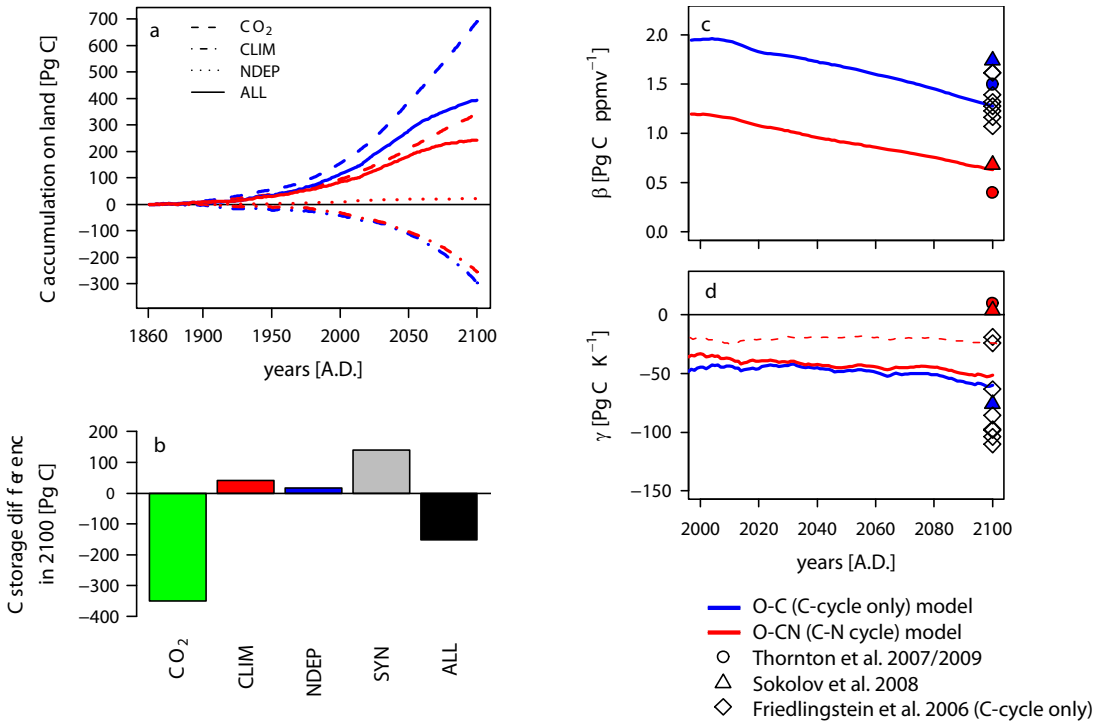

Figure 6.40: a) Projection of land C storage due to changes in atmospheric CO_2, climate, N deposition and the combination of these factors (taken from the SRES A2 scenarion using LMDz-CM4) simulated by one CN model without (blue) and with (red) nitrogen dynamics (O-CN; (Zaehle et al., 2010a)). b) Difference in projected year 2100 land C storage from a) due to nitrogen dynamics. c) Development of □$_l$ over the 21st century simulated by O-CN, compared to estimates from the carbon-cycle and carbon-nitrogen cycle simulations using CLM-CN (Thornton et al., 2007; Thornton et al., 2009), IGSM-CN (Sokolov et al., 2008), and the carbon-cycle only C4 MIP ensemble (Friedlingstein et al., 2006). d) the same for □$_l$, where the dashed lines red is accounting for the synergistic interactions between all factors in the O-CN model.

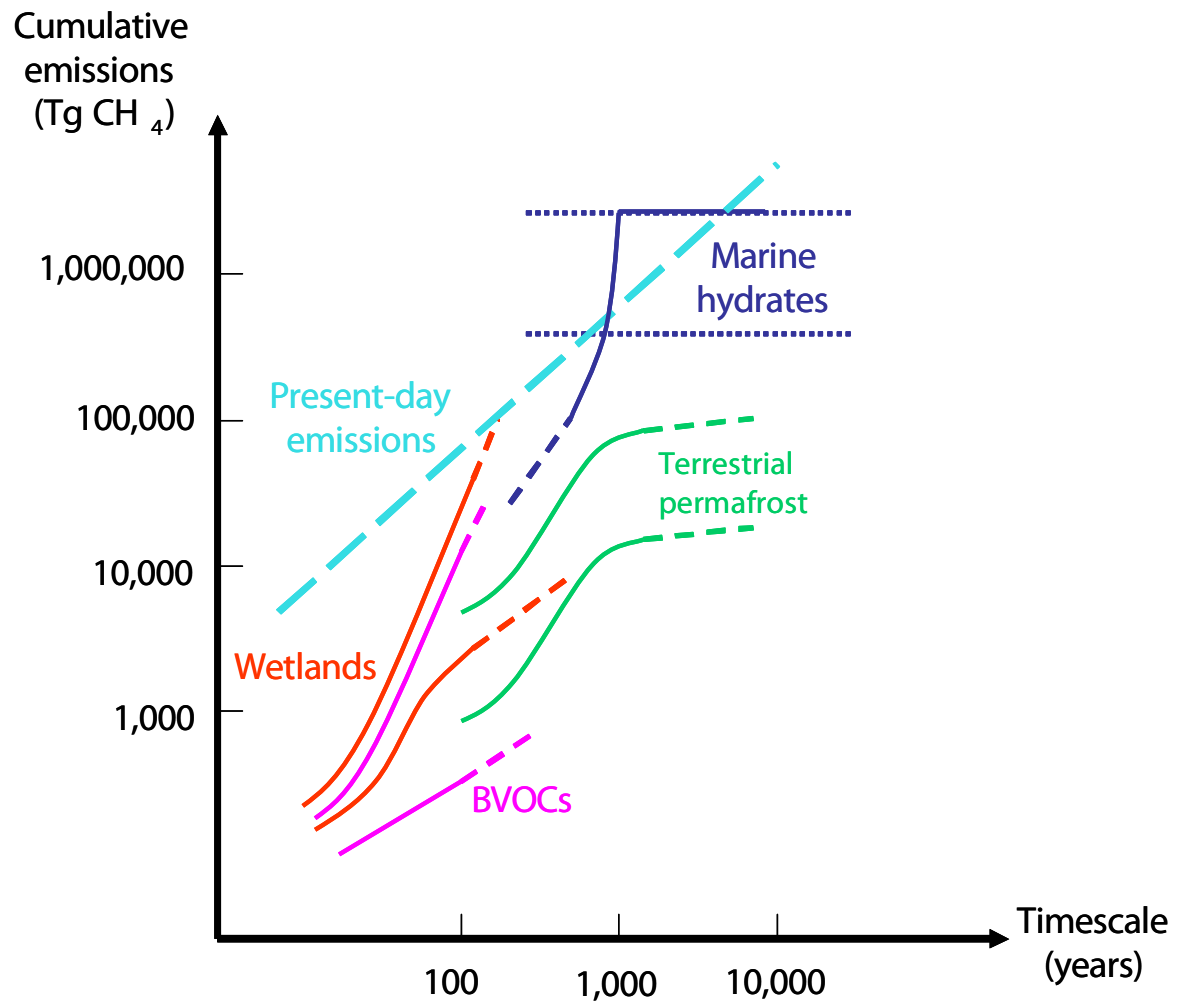

Figure 6.41: Summary diagram of the relative sizes and time scales associate with changing methane emissions (after O'Connor et al. (2010). Present day anthropogenic emissions are shown for reference, as is the effect on CH_4 from biogenic volatile organic compounds (BVOCs). BVOCs affect the atmospheric lifetime of CH_4 as they react with [OH], but are not directly emissions of CH_4. Atmospheric chemistry is not discussed further in this chapter.

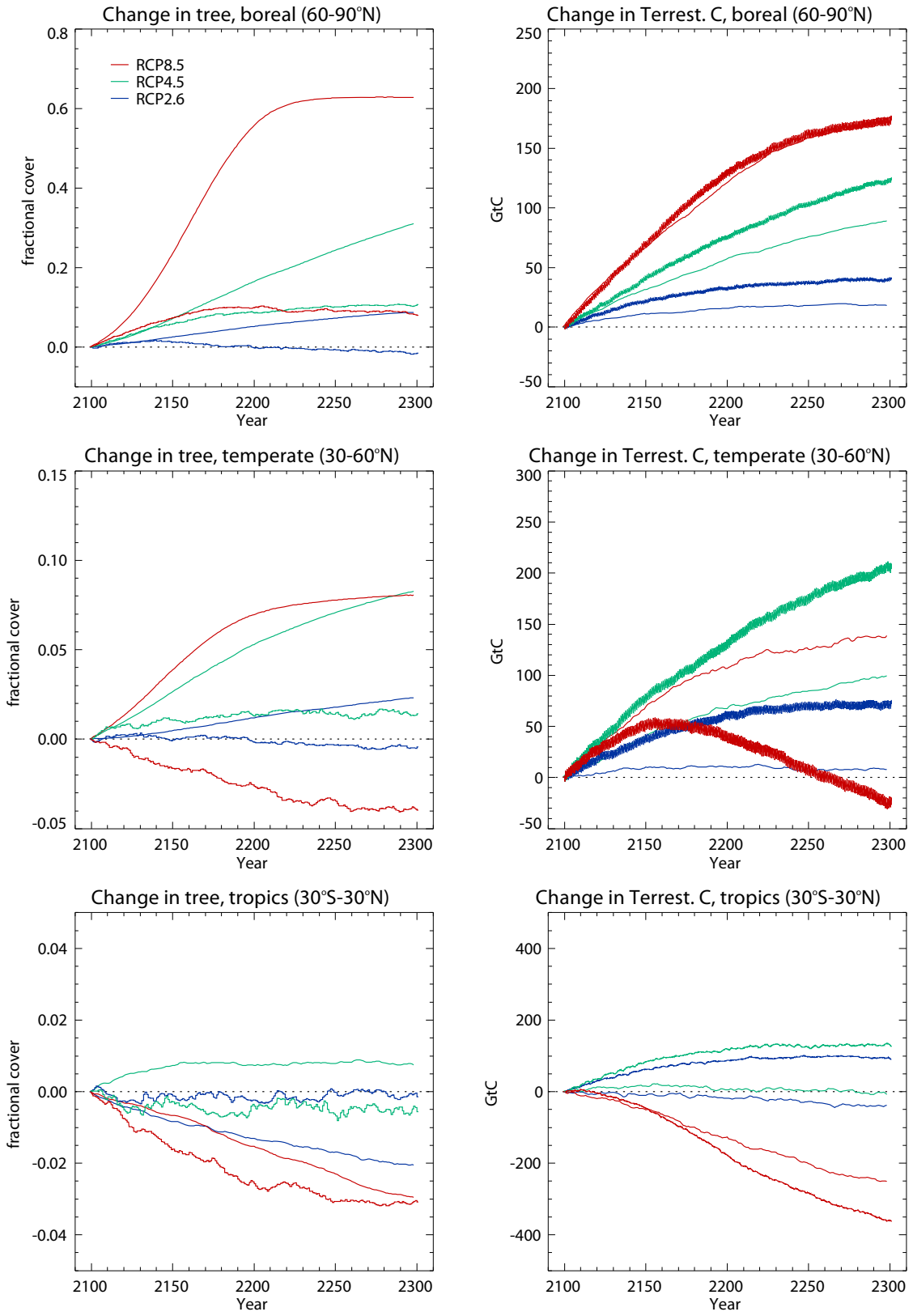

Figure 6.42: Time evolution of tree cover (left) and terrestrial carbon storage (right) for three latitude bands; boreal (60–90°N), temperate (30–60°N) and tropics (30°S–30°N) for the RCP extensions to 2300. Models shown are HadGEM2-ES and the MPI-Hamburg ESM which both simulate vegetation dynamics. Note the RCP6.0 extension was not a CMIP5 required simulation. Anthropogenic land-use in these extension scenarios is kept constant at 2100 levels, so these results show the response of natural ecosystems to the climate change.

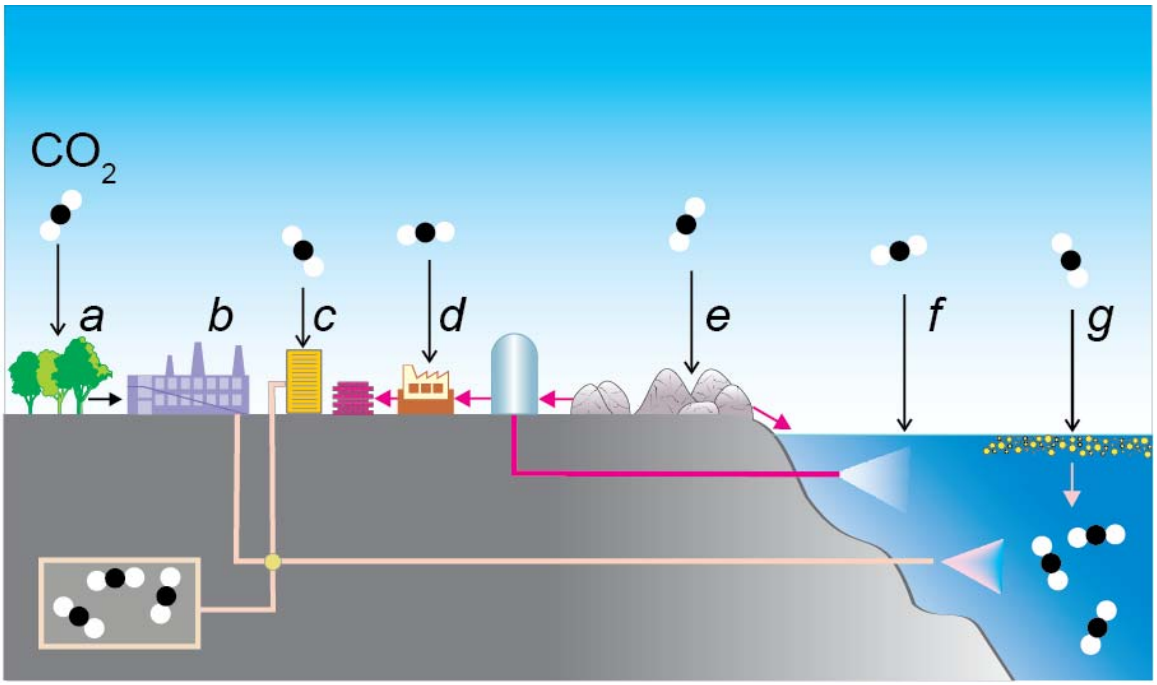

Figure 6.43: Illustration of some Carbon Dioxide Removal approaches: (a) CO_2 capture by and storage in land ecosystems, (b) combustion of biomass at an electric power plant with carbon capture and storage of CO_2 either underground or in the ocean, (c) industrialized capture of CO_2 in the atmosphere with storage either underground or in the ocean, (d) extraction of alkalinity from mined silicate rocks which are then combined with atmospheric CO_2 to produce solid carbonate minerals, (e) increasing the weathering rate of silicate rocks (some dissolved carbonate minerals are transported to the ocean), (f) alkalinity from solid minerals is added to the ocean which causes CO_2 to ingas from the atmosphere, (g) nutrients are added to the ocean, transporting carbon downward, some of which is replaced by CO_2 from the atmosphere.

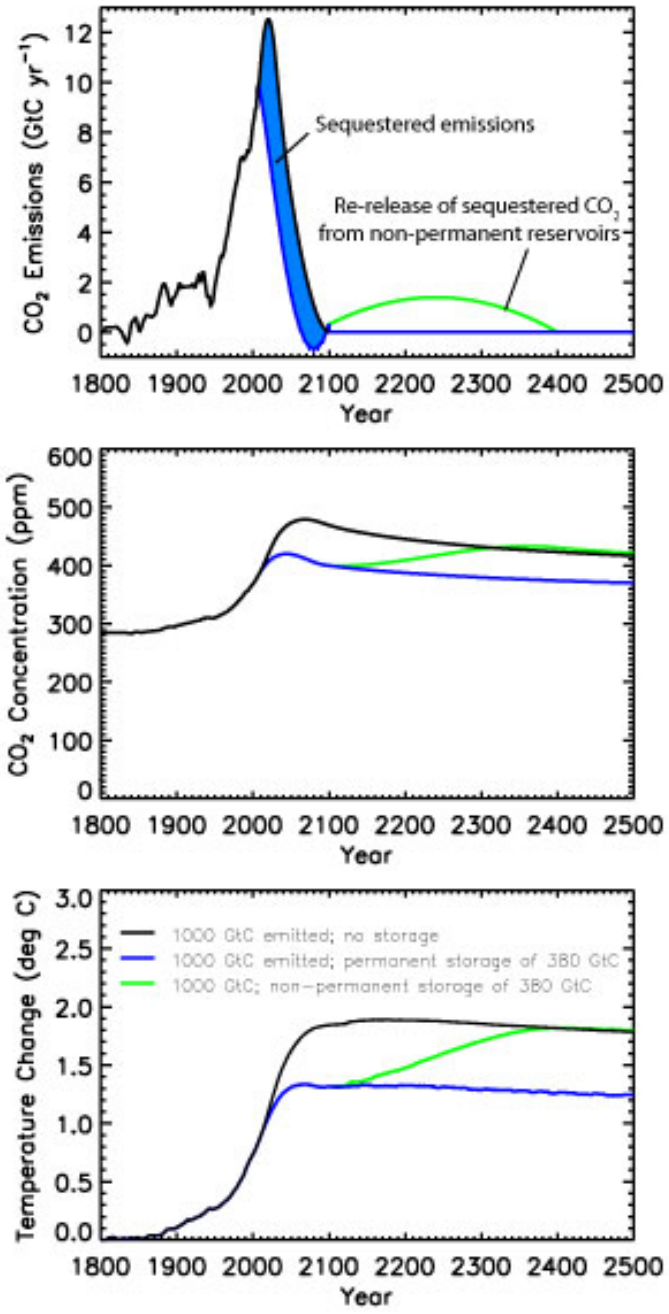

Figure 6.44: Effect of permanent and non-permanent CO_2 sequestration. Permanent sequestration of emitted CO_2 has the potential to decrease cumulative emissions and the resulting climate warming (blue line, compared to black). If the same carbon were sequestered in a non-permanent reservoir, and returned to the atmosphere over several centuries, climate change would be delayed only, and the eventual magnitude of climate change would be equivalent to the no-sequestration case (green line, compared to black). Figure modified from Figure 5 of Mathews (2010).

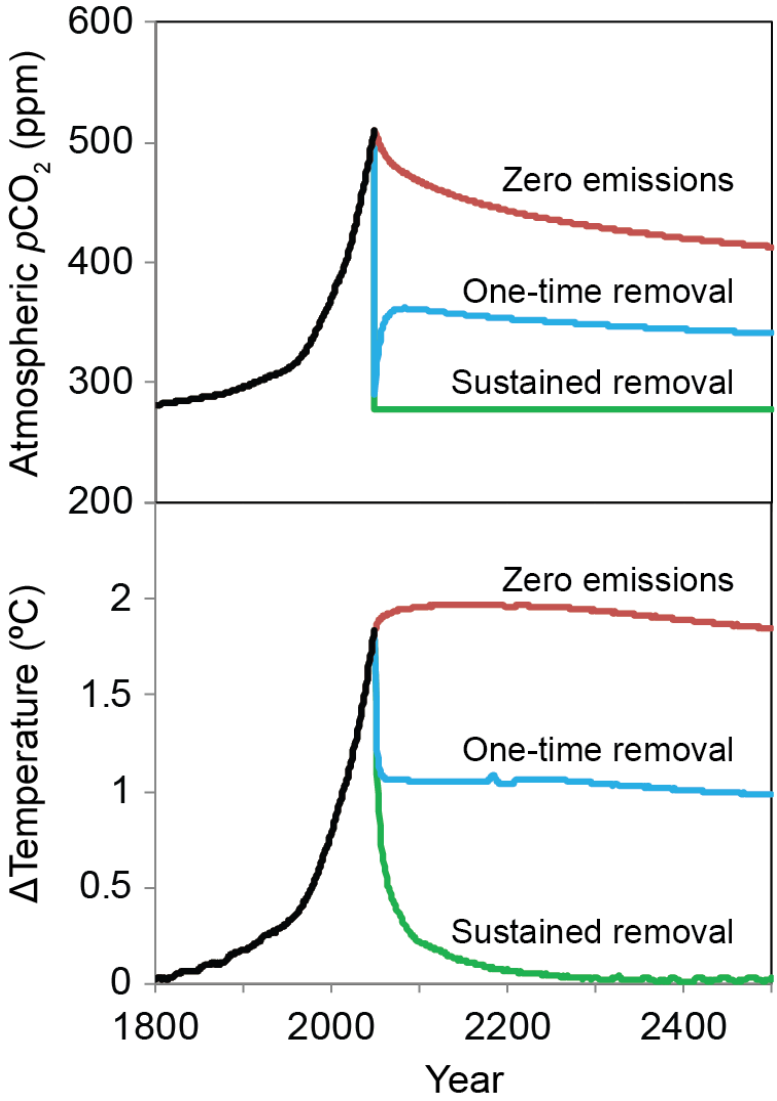

Figure 6.45: Effects of an instantaneous cessation of CO_2 emissions (amber line), one-time removal of excess atmospheric CO_2 (blue line) and removal of excess atmospheric CO_2 followed by continued removal of CO_2 that degasses from the atmosphere and ocean (green line). To a first approximation, a cessation of emissions prevents further warming but does not lead to significant cooling on the century time scale. A one-time removal of excess atmospheric CO_2 eliminates approximately half of the warming experienced at the time of the removal. To cool the planet back to pre-industrial levels requires the removal of all previously emitted CO_2, an amount equivalent to approximately twice the amount of excess CO_2 in the atmosphere. Figure adapted from (Cao and Caldeira, 2010b).

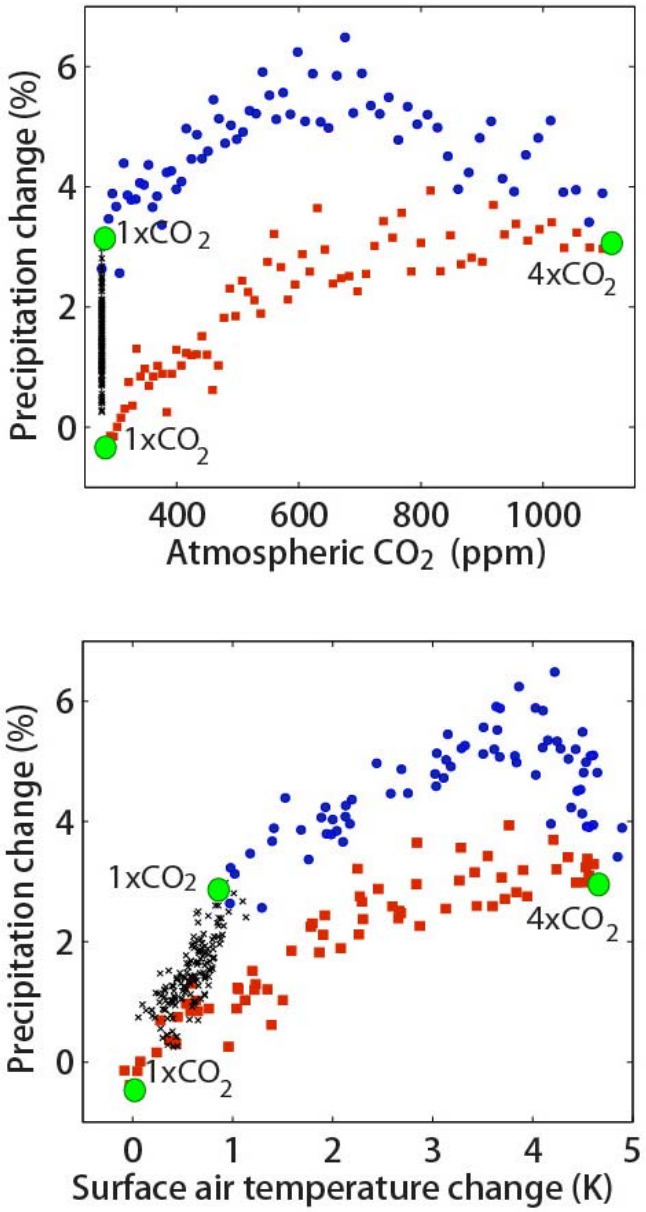

Figure 6.46: HadCM3L results from a simulation with 2% annual change in atmospheric CO_2: (a) global and annual mean changes in precipitation as a function of atmospheric CO_2; (b) global and annual mean changes in precipitation as a function of global and annual mean changes in surface temperature. Red dots represent the first 70-year simulation phase with 2% annual CO_2 increase (ramp_up) and time moves forward from the lower left to the upper right. Blue dots represent the subsequent 70-year period with 2% annual CO_2 decrease (ramp_down) and time moves forward from the upper right to the lower left. Black dots represent the following 150-years with the constant control CO_2 concentration and time moves forward from the upper right to the lower left. The simulation states when atmospheric CO_2 reaches 1 × CO_2 and 4 × CO_2 concentrations are marked with yellow circles. Due to the ocean thermal inertia one atmospheric CO_2 state corresponds to two different states of temperature and precipitation, and due to the precipitation sensitivity to atmospheric CO_2 content changes (Bala et al., 2009), one temperature state corresponds to two different precipitation states. Figure adopted from Cao et al. (2011).

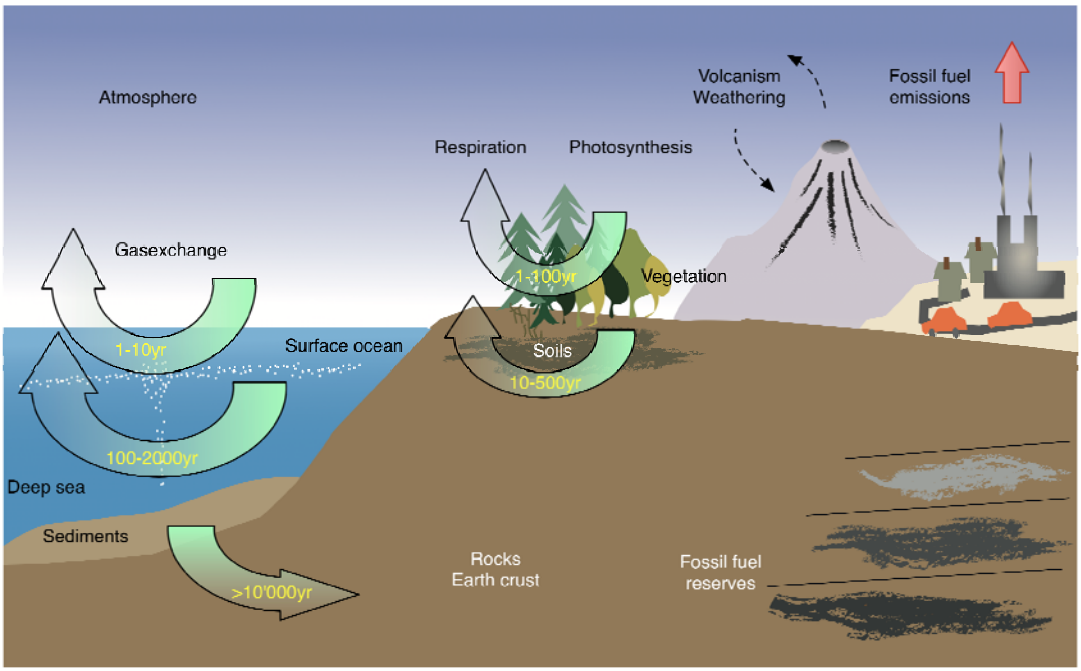

FAQ6.1, Figure 1: Simplified schematic of the global carbon cycle including its major reservoirs and turnover time scales.

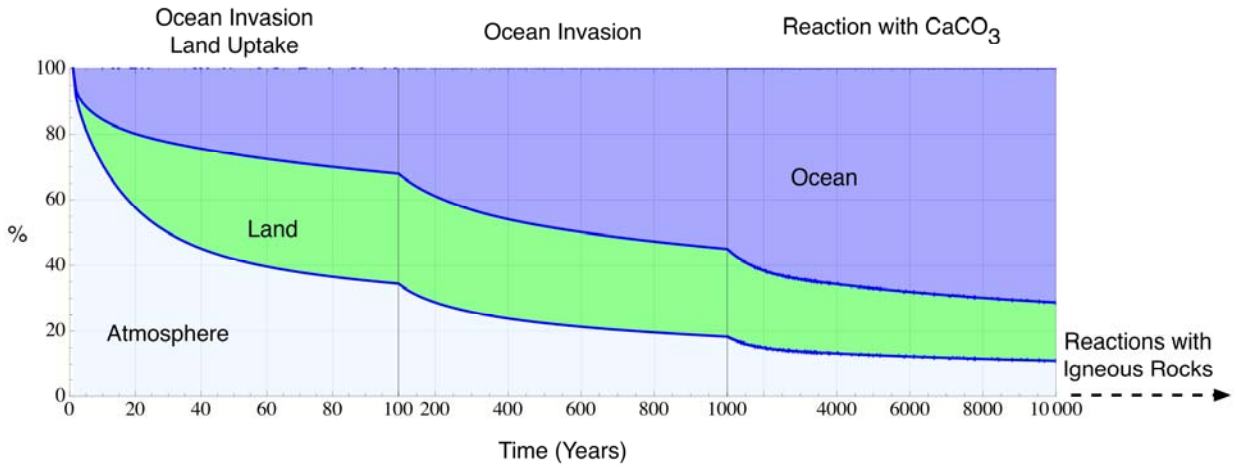

FAQ 6.1, Figure 2: Decrease of an atmospheric CO_2 pulse emission of 1000 PgC emitted at time 0 showing the different time scales of the equilibration with the different reservoirs in the global carbon cycle. Displayed is the percentage of the initial perturbation taken up by atmosphere, land and ocean (after Archer et al., 2009; the graph shows the simulation results from the CLIMBER-2 model). Note the different time scales in the three sections of the graph.

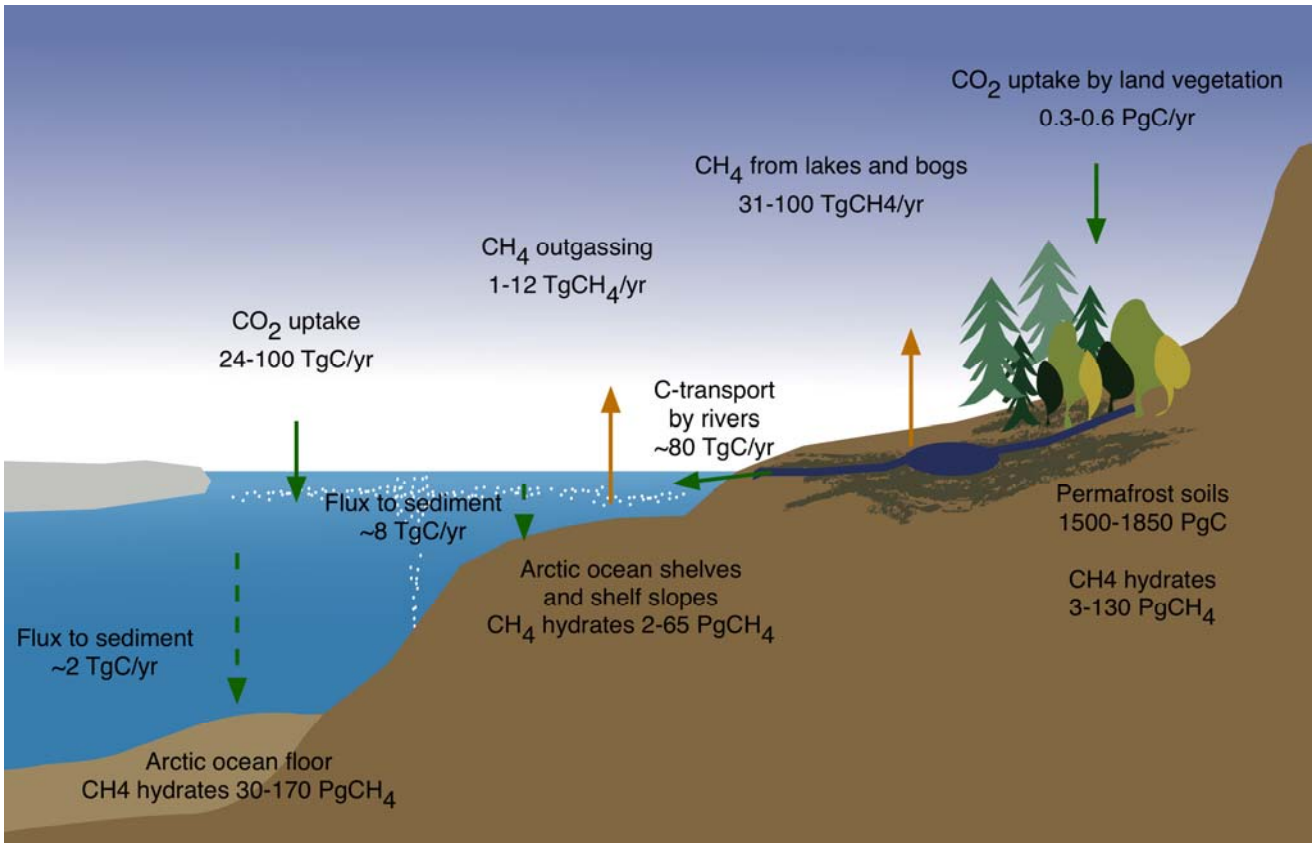

FAQ 6.2, Figure 1: Simplified graph of major carbon pools and flows in the Arctic domain, including permafrost on land, continental shelves and ocean (Adapted from McGuire et al., 2009 and Tarnocai et al., 2008).